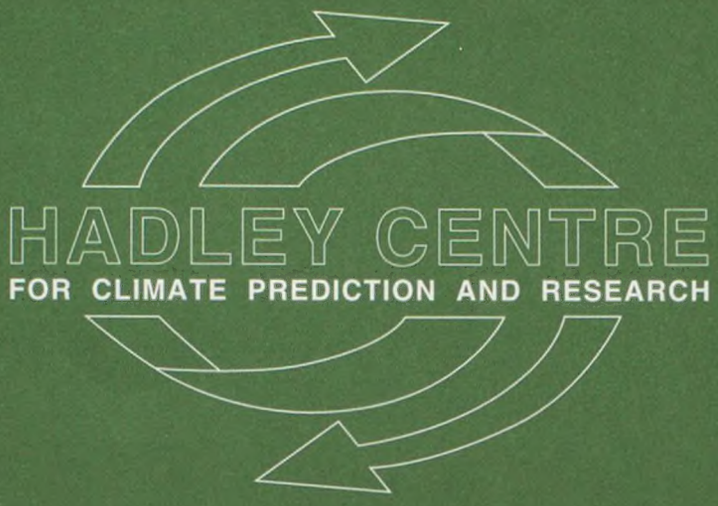

Climate simulations with the Unified Model: AMIP runs

by

C D Hall, R A Stratton and M L Gallani

CRTN 61

September 1995

CLIMATE
RESEARCH
TECHNICAL
NOTE

Hadley Centre
Meteorological Office
London Road
Bracknell
Berkshire RG12 2SY

CLIMATE RESEARCH TECHNICAL NOTE NO. 61

CLIMATE SIMULATIONS WITH THE UNIFIED MODEL: AMIP RUNS

by

C D Hall, R A Stratton and M L Gallani

Hadley Centre for Climate Prediction and Research
Meteorological Office
London Road
Bracknell
Berkshire RG12 2SY

NOTE: This paper has not been published. Permission to quote from it should be obtained from the Director of the Hadley Centre.

Climate simulations with the Unified Model: AMIP runs

September 1995

C. D. Hall, R. A. Stratton and M. L. Gallani

Summary

The Meteorological Office Unified Model has undergone continual development since it was first used for climate modelling in 1993. An updated version of the model has been developed which incorporates improvements to the representation of clouds, convection, surface and boundary layer processes, diffusion, and the specification of the drag due to sub-grid scale orography. 10-year climate simulations forced by AMIP sea surface temperatures have been performed with two model versions: the original version, which has been used for runs made available to the modelling community as part of the AMIP project, and the new version which is assessed in this Technical Note. Differences between the runs are demonstrated and a detailed comparison with published climatological means is presented. Considerable use is made of ECMWF analyses covering the AMIP period 1979-88.

The simulated fields are found in general to be realistic; in particular the air temperatures, precipitation and radiative fluxes are close to observed values, as is the variability on a wide range of time scales. Some systematic errors stand out which are not greatly affected by the changes to the model parametrization schemes described here: there is a substantial cold bias extending through much of the troposphere, the jets are too strong particularly in the southern hemisphere where there is a marked westerly bias at the surface, and the tropical easterlies are also too strong. The simulation with the new model version is judged to be better overall and the changes will be incorporated into future standard versions of the coupled ocean-atmospheric model to be used for predictions of climate change.

1. Introduction

The Unified Model (Cullen, 1993) is now used for all climate simulation work at the Meteorological Office. Unified in the sense that it is used not only for climate applications but also for operational forecasts on global to mesoscale resolution, the model has been rigorously tested on a wide range of time and space scales. In climate configuration it replaces the 11-layer model used in the first transient coupled runs (Murphy, 1995), and will be the tool for climate change evaluations that will form part of the UK contribution to future IPCC reports. The model has 19 levels in the vertical on an eta coordinate system, extending from about 25 m above the surface to a little above the 5 mb pressure level at the top. This provides a smooth transition between terrain-following model levels in the boundary layer to pressure levels in the stratosphere. The primary model variables are represented on a staggered Arakawa "B" grid having on each level in the horizontal 96x73 points at which temperature and humidity are calculated and 96x72 points for wind. A split-explicit finite difference formulation is used to solve the dynamical equations of motion. A summary of the model can be found in Phillips (1994). Successful climate simulations were achieved in 1993 with what has become known as the First Climate Version or 1CV as it will be abbreviated here. Development work since then has focused on improving the representation of clouds, convection, surface and boundary layer processes, diffusion, and the drag due to sub-grid scale orography, culminating in the Third Climate Version or 3CV. A detailed description of all the changes is provided in section 1.1 below. This note assesses the differences between the two versions and evaluates the climate simulations against published climatological means.

The primary test of a climate model is the simulation of present-day climate not only in the mean state but also in its response to changes in sea surface temperatures. A common framework for model evaluation has long been sought and Boer et. al. (1991) were the first to intercompare the simulations from a large number of different models. More recently the Atmospheric Model Intercomparison Project (AMIP; Gates, 1992) provides a more rigorous specification to achieve the same end. In this project external forcing by sea surface temperatures and sea ice is precisely defined by time-varying fields based on NMC analyses for the 10-year period 1979-88. Other prescribed parameters are the solar constant and the concentration of CO_2. 30 different models are being evaluated in the project and among the many simulations is one with the Unified Model using 1CV. The AMIP run has been repeated with 3CV and a comparison with the original run is presented here.

A large number of figures have been included in this Note in order to provide as broad a view as possible of the characteristics of the model. Many results are presented as seasonal means for December/January/February (DJF) and June/July/August (JJA) where the means of the model fields have been calculated using values at each time step within the period. The format in many cases is 3-up: the mean of the model field for 3CV, the differences between this and the field for 1CV, and at the bottom, the differences from the relevant climatological mean. The various climatologies used for comparison are listed in section 1.2 below.

1.1 Changes made for 3CV

1. *The cloud scheme*

(a) Water vapour, cloud water and cloud ice are diagnostic variables within the model and their relationship with the primary variables pressure, total water, and liquid/frozen water potential temperature must be parametrized. The scheme allows for non-zero values of the cloud condensate within the grid box even where the mean humidity is below the saturated value; in 1CV the amount of condensate is dependent on the distribution of the fluctuations of temperature within the grid box which are assumed to take a "top-hat" form. In 3CV the liquid water temperature is used as the dependent variable and its fluctuations are assumed to take a triangular distribution.

(b) The temperature range of mixed-phase clouds was modified to match observations made by the Met. Research Flight (MRF).

(c) A correction was made to the calculation of the saturation humidity mixing ratio.

2. *The parametrization of precipitation*

(a) An error in the estimation of the evaporation of falling precipitation was corrected effectively resulting in a doubling of the evaporation rate. Other modifications were made to the evaporation rate of which the main one was the inclusion of a dependence on pressure.

(b) The increments of temperature and moisture which define the initial convective mass flux were made dependent on the surface fluxes.

(c) The effective radius for water drops was determined from a MRF/UMIST parametrization using a specified aerosol value with a land-sea contrast.

(d) Precipitation rates were made dependent upon the distribution of cloud water contents within the cloudy part of the grid-box as implied by the cloud scheme.

(e) The treatment of precipitation from cloud ice was improved.

(f) Other minor changes were made to the convection scheme.

3. *The boundary layer parametrization*

Mixing in the boundary layer is calculated in terms of local turbulent fluxes, based on mixing-length theory, and a rapid-mixing term, in which the increments from the surface fluxes are distributed evenly throughout the depth of the boundary layer. A change was made to restrict rapid mixing to below the convective cloud base.

4. *The parametrization of sub-grid scale drag*

(a) The parametrization of drag due to the dissipation of gravity waves generated by mountains has been modified to include anisotropy of the orography, the effects of trapped lee waves, and a better representation of high drag states where flow blocking and hydraulic jumps occur.

(b) Roughness lengths for momentum have been redefined to include the effect of orographic form drag. The revised scheme applies more drag in the lower troposphere.

5. *Hydrology*

A 4-layer soil hydrology scheme replaced the 1-layer scheme used in 1CV giving a total soil depth of about 3 m rather than the root depth.

6. *Diffusion on eta surfaces*

(a) An operator of the form $K\nabla^{2n}$ applied on the model eta levels is used to represent dissipation by unresolved eddies and remove unwanted grid-scale noise. For 1CV n was

chosen to be 3 for wind and temperature related variables, and 2 for moisture. Fairly high levels of K gave e-folding times for the damping of 2-grid length waves of 3.7 and 6.9 hours respectively. For 3CV n was set equal to 3 for all variables and the e-folding time was increased to 12 hours, except for moisture above 150 mb where greater smoothing was achieved with n equal to 2 and an e-folding time of 4 hours.
(b) A change was made to switch off diffusion where the model surfaces are steep; it is activated principally at low levels over mountains.

7. *Filling of negative values of moisture*
The global correction scheme to fill negative values of moisture was replaced by one in which moisture is borrowed from neighbouring grid points.

8. *Albedo*
The dependence of the albedo of sea ice on temperature was changed leading to somewhat reduced values. Its effect is small in all except coupled versions of the model.

1.2 Climatological means used for validation

1. *ECMWF analyses*
Global analyses from operational numerical weather prediction systems give an accurate representation of the state of the atmosphere by using all observations available in real time. Hoskins et. al. (1989) have compiled the data from the ECMWF system into a climatology for the period 1979-88 which, since it corresponds to the AMIP period of the simulations presented here, will be used as a reference on the standard pressure levels for the main dynamical fields of geopotential height, wind and temperature, as well as the derived fields of eddy kinetic energy, eddy heat flux and eddy momentum flux. Analyses are only as good as the data on which they are based, and in the data-sparse regions of the tropics and southern hemisphere they are less accurate than in the extratropical northern hemisphere as Trenberth and Olson (1988) demonstrated in an intercomparison with similar analyses from NMC. Their characteristics also change with time as improvements are made to the analysis method. The ECMWF system in 1988 represented a major advance over the system in use 10 years earlier, and this is reflected in the quality of the analyses over the period; both the papers referred to above note the weak tropical divergent flow analysed prior to 1985 which they attribute to defects in the ECMWF model. For this reason the meridional stream function shown in section 2.2 is compared against analyses for the more recent period 1985-91.

2. *UKMO analyses*
The data assimilation system used at the UKMO is also used as a source of global numerical analyses of high quality. The data are available on the same pressure levels as the ECMWF analyses, except that the 1000 mb level is replaced by one at 950 mb. The first full year of available data is 1984 and so the early part of the AMIP period is not covered. In the results presented here, data for the 11-year period 1984-94 have been used to calculate blocking indices, standard deviations of low-pass and band-pass geopotential heights, and standard deviations of seasonal mean sea-level pressure.

3. *ERBE radiation fluxes*
Top-of-atmosphere fluxes of short and long wave radiation have been measured accurately since 1985 by the Earth Radiation Budget Experiment (ERBE, Barkstrom et. al., 1989).

Similar instruments on 3 satellites have been blended to give global coverage of both total and clear-sky fluxes (Harrison et. al., 1990).

4. *ISCCP cloud analyses*

The International Satellite Cloud Climatology Project (ISCCP) started in 1983 and provides gridded estimates of cloud cover using visible and infrared radiances from the operational geostationary and US polar orbiting satellites (Rossow and Schiffer, 1991). Only data for the total cloud cover are used here. By blending together data from several satellites problems with resolving the diurnal cycle are minimised, and agreement with the published climatologies from surface-based observations (Warren et. al., 1986 and 1988) is generally good though there are differences of detail.

5. *COADS surface data*

Merchant shipping has been a major source of meteorological observations for over 100 years, and the "Comprehensive Ocean-Atmosphere Dataset" (COADS) described in Woodruff et. al. (1987) is the main source of the data for many authors. Ward (1992) applied corrections to the wind data to ensure that the observed trends over the years 1968-88 matched the trends in the analysed pressure gradients over the same period and his data have been used here. The coverage follows the main global shipping lanes, and as a result large gaps are found in the southern hemisphere and parts of the tropics, even where observations are grouped together over several decades. Wind is either measured by a visual estimate of the sea state and reported as a Beaufort force, or, as is more frequently the case in recent times, by an anemometer sited on the mast. Anemometer heights vary greatly from ship to ship being typically in the range 10 to 30 m above the sea surface, while reports of Beaufort force are converted to a 10 m speed. The reference level is therefore imprecise; for the purposes of this note comparison has been made against the model values reduced to 10 m.

6. *Legates and Willmott precipitation and screen-level temperatures*

Mean seasonal fields of precipitation and screen-level temperature have been created by Legates and Willmott (1990a, 1990b) using surface stations over land and the COADS data over the oceans. Station reports span intervals of varying length but most fall within the period 1920-80. Over land all data have been binned to give a grid-box average. The dependence of temperature and precipitation on elevation, which is known to be strong, will not be well represented as the mean elevation of the stations used will seldom be the same as the mean orographic height of the grid box (stations are often in valleys). Differences will be largest over mountains and here the data should be treated with caution; where mean and rms differences from climatology have been calculated (Table 1) values have been excluded if the model orographic height is greater than 500 m. Precipitation data over land have been corrected for various known sources of error, of which the most important is wind. Over the oceans correlations between precipitation rates and current weather reports at coastal stations enable use to be made of the ship reports of current weather. In some instances this can give unreliable results; for instance, the large maximum in the ITCZ over the equatorial Eastern Pacific in DJF is inconsistent with satellite measurements of outgoing long wave radiation and is thought to be spurious.

7. *University of East Anglia precipitation*

A historical analysis of precipitation has been made available by the University of East Anglia (Hulme, 1992) on the 96x73 grid of the Unified Model and a climatology for the AMIP years

1979-88 has been used here. It is based on a smaller set of land stations than used by Legates and Willmott and no attempt is made to derive values over the open oceans.

8. *Oberhuber surface fluxes*
Surface fluxes of sensible and latent heat over the oceans have been estimated by Oberhuber (1988) from a subset of the COADS data covering the period 1950-79 using standard bulk formulae. He uses values of the exchange coefficients which differ a little from those used in the Unified Model, particularly in strong winds where he enhances the Charnock constant to obtain reasonable meridional transports.

9. *Hellerman surface stresses*
A global climatology of surface stress over the oceans has been created by Hellerman and Rosenstein (1983) from the complete COADS data covering the period 1870-1976. The drag coefficients used are thought to be too large (Harrison 1989) especially in low wind regimes. As with the Oberhuber fluxes sparse data coverage over the tropics and southern oceans leads to larger errors in these regions.

10. *GISST air-minus-sea temperature differences*
The Meteorological Office archive of ship observations, augmented by the COADS data, has been used to estimate air-minus-sea temperature differences (Parker et. al., 1992), and values for the period 1951-80 have been taken for the comparisons presented here. Sea surface temperatures are often measured from the engine intake and so usually represent values at a lower depth than is the case of bucket measurements. As air temperatures are usually recorded on the bridge spurious effects due to heating of the ship structure are avoided by only using night-time observations in the creation of the averages.

11. *Radiosonde observations*
Analyses of relative humidity from numerical data assimilation systems are not as reliable as those of wind or temperature. Global observations of moisture are sparse and numerical analyses of relative humidity will depend strongly on the numerical model and will be contaminated by model-related errors. The direct use of observations for validation purposes is therefore preferable. The climatology of radiosonde humidity observations used here has been generated at the Hadley Centre from CLIMAT reports received for the period 1971-90. It covers some 350 stations worldwide which have been binned into 3 regions for comparison: 30-90°N, 30°S-30°N, and 90-30°S. In the northern hemisphere the data are reasonably evenly spread across the land areas, but in the tropics and southern hemisphere the data are few and the values should be treated with caution.

2. Systematic errors

2.1 Mean sea-level pressure

Figure 1a shows the simulated mean sea-level pressure from 3CV for December/January/ February (DJF). Differences from 1CV are shown in Figure 1b, and from a climatology based on ECMWF analyses in Figure 1c. Similar fields for March/April/May(MAM), June/July/ August (JJA) and September/October/November (SON) are shown in Figures 2a-c,

Objective Validation

	(a)		(b)	
	1CV	3CV	1CV	3CV
DJF	-0.1/2.61	0.3/2.81	-0.29/1.97	0.14/1.58
MAM	-0.3/2.78	0.1/2.49	-0.28/1.92	0.20/1.60
JJA	-0.4/2.69	0.1/2.46	-0.65/2.54	0.06/1.91
SON	-0.1/2.92	0.3/2.58	-0.55/1.72	0.00/1.46

(c)

	1CV	3CV
DJF	-1.72/3.98	-2.30/4.66
MAM	-0.47/2.76	-0.92/2.61
JJA	0.80/2.90	-0.44/2.60
SON	-0.69/3.15	-1.67/3.25

Table 1. Mean/rms differences from climatology where the model surface height is less than 500 m; (a) mean sea level differences from ECMWF climatology 1979-88, (b) precipitation differences over land from University of East Anglia climatology 1979-88, and (c) 1.5 m temperature differences over land from Legates and Willmott climatology.

3a-c and 4a-c respectively. Errors are largest in the northern hemisphere in DJF; the Atlantic low has about the right depth at around 1000 mb but the pattern is shifted southward with too much troughing in mid ocean and pressure too high over Iceland and the Norwegian Sea. In the North Pacific the errors are rather different; here the Aleutian Low is too deep and the pattern is shifted eastward from its true position giving large negative anomalies over Alaska and the west coast of North America and corresponding positive anomalies centred over Japan. The Siberian high is of about the right intensity but the large positive error over the Russian Arctic region gives rise to an easterly pressure gradient in the error field with consequences for the temperature errors which will be seen in section 2.5. A similar error pattern in the northern hemisphere is seen in MAM but the amplitude is generally smaller. In JJA and SON the simulated pressure field is closer to observation and differences from climatology, which are mostly positive at high latitudes, are in general less than 4 mb. In the southern hemisphere there is a common pattern to the pressure errors which spans all seasons of the year: pressure in the sub-tropical anticyclones is too high by 2-4 mb while the low pressure belt around the Antarctic continent is to deep by 2-6 mb. As a result there is an excessive westerly gradient over a wide band in middle latitudes. Errors in the tropics are small and mostly negative particularly in the Pacific equatorial trough.

One general characteristic of the differences between the simulations with 3CV and 1CV which is apparent to a varying degree in all 4 seasons, is an increase in pressure over middle and high latitudes and a decrease in the tropics. A similar signal was found when the revised schemes for orographic and gravity-wave drag were tested. The net effect is to improve the simulation in the southern hemisphere by reducing the excessive westerly gradients, while

having an overall negative impact elsewhere by adding to existing systematic errors. Superimposed on this planetary-scale impact are regional changes: the errors in the Atlantic and Aleutian lows in DJF are greater in 3CV, while from India to the tropical North West Pacific pressure is higher in JJA, and to a lesser extent in SON, associated with a much better simulation of the summer monsoon flow over Asia. A net improvement in the simulation in MAM, JJA and SON and a deterioration in DJF is confirmed in the objective validation against the analyses presented in Table 1(a).

2.2 Upper-air winds

Zonal mean westerly winds for 3CV and the differences from 1CV and a climatology based on ECMWF analyses are shown in Figures 5a-c for DJF. The ECMWF data only extend to 30 mb so validation at the uppermost model levels has not been made. The strength of the northern jet at just over 40 ms^{-1} is some 4ms^{-1} greater than observed and is shifted slightly upward and poleward. In the southern hemisphere the excessive westerly gradient, which was noted at the surface in the pressure pattern, extends throughout the atmosphere; westerly wind errors increase with height to reach 6-8 ms^{-1} at the level of the jet and exceed 10 ms^{-1} in the stratosphere. In the tropics there is a marked westerly wind error centred on the equator at 300 mb with easterly errors in the upper troposphere and lower stratosphere. Very similar tropical wind errors are seen not only in JJA (Figures 6a-c) but also in MAM and SON (not shown); similarly, the westerly error in the southern hemisphere is present in all seasons. At high latitudes above 100 mb there is an easterly error in both hemispheres in winter which increases with height. In DJF these errors are larger in 3CV, while in JJA, however, the impact is quite different and in many respects beneficial; the equatorial westerly error is reduced, as is the easterly error at 100 mb, while changes elsewhere are quite small.

The wind field at 250 mb in DJF (Figures 7a-c) shows good agreement with ECMWF analyses; winter jets in the northern hemisphere reach just over 60 ms^{-1} in the Pacific and 40 ms^{-1} over the Atlantic in both model versions and in the observations. Similar agreement is found in JJA (Figures 8a-c). Differences between 1CV and 3CV are small except in the North East Pacific in DJF where the pattern in 3CV is excessively anticyclonic. In the southern hemisphere the simulated jets are stronger than in the analyses and there is only a hint of the observed double structure over the Pacific. At 850 mb the subtropical easterlies in DJF (Figure 9a-c) and JJA (Figure 10a-c) in the simulations with both 1CV and 3CV exceed 10 ms^{-1} in many places, which is considerably stronger than in the analyses, and this is consistent with the stronger easterly surface pressure gradients noted above on the equatorial side of the subtropical highs. The main difference between the two versions of the model occurs in JJA over South East Asia where the strength of the low-level monsoon jet is considerably reduced in 3CV and agrees much more closely with the observations; in particular the spurious westward extension into the equatorial West Pacific is eliminated and the strength over India and the Bay of Bengal is reduced. In middle latitudes the wind errors are largest in DJF and reflect the errors in the pressure pattern already noted.

The zonal mean meridional circulation is shown in Figures 11a-c and 12a-c as a stream function. The dominant feature, the Hadley circulation, is positioned well in both DJF and JJA. It is considerably too strong in 1CV compared with a climatology based on ECMWF analyses for the years 1985-91. Some sensitivity to the convection scheme and the level of

diffusion has been found, and the changes introduced for 3CV have led to a weaker and more realistic circulation, particularly in JJA.

2.3 Upper-air temperature and humidity

Zonal mean temperature for 3CV and the differences from 1CV and a climatology based on ECMWF analyses are shown in Figures 13a-c for DJF and Figures 14a-c for JJA. A tropospheric cold bias is evident increasing in magnitude from around -1 K near the surface to as much as -6 or -7 K at the tropopause. Errors are slightly smaller in 3CV in DJF, especially around 30°N, but in JJA there is little overall difference between the runs. Temperature errors are largest in the polar lower stratosphere in summer and reach -17 K at 150-200 mb in the southern hemisphere, a characteristic common to many general circulation models (Boer et. al., 1991). This aspect is noticeably worse in 3CV than it was in 1CV, and appears to be related to the changes in the moisture field arising from the local method for correcting for negative humidity (Hall, 1994). Specific humidity has increased in these regions together with the relative humidity (Figures 15a-c and 16a-c) and the resulting adjustments to the long-wave radiative fluxes may well account for the lower temperatures. With the exception of the equatorial regions below 500 mb, relative humidity in the troposphere is lower in 3CV than 1CV. Differences are particularly large where the relative humidity itself is lowest, typically in the dry descending air in anticyclones; this is largely due to the lower values of the diffusion coefficient and the higher order of the diffusion operator in the later version (see Hall and Stratton, 1994). In the boundary layer, which is dominated by the turbulent mixing of moisture, the changes in relative humidity between 1CV and 3CV are less. Comparison against radiosonde observations is provided in Figure 17 for DJF (left) and JJA (right), and this shows a marked positive bias of between 15 and 20 percent in the simulated fields. Even allowing for systematic errors in the measurements of moisture, which can be large in the upper troposphere, the differences are too large to dismiss. The reduction in relative humidity noted in the change to 3CV is therefore confirmed as an improvement.

2.4 Precipitation and soil moisture

For both versions of the model, 1CV and 3CV, the simulated global patterns of precipitation are very realistic and bear close resemblance to the climatology of Legates and Willmott (1990a). In DJF (Figures 19a-c) the main differences between the two runs are found in the tropics and most can be attributed to the effects of reduced diffusion in 3CV. This leads to higher and more realistic amounts over the tropical land masses of Africa and South America, and smoother fields where there are mountains or differential land-sea forcing around resolved islands or narrow peninsulars. The absence of large grid-point maxima over the Andes is due to the change which eliminates all horizontal diffusion where orographic surfaces are steep. Disagreement with climatology is small and only two aspects seem significant; the spurious rainfall minimum over Indonesia, which has improved to some extent in 3CV, and the large precipitation amounts over the southern Indian Ocean, though in the latter case confidence in the climatological values is not high. As was remarked earlier, the maximum of over 20 mm day^{-1} in the equatorial East Pacific in the climatology is almost certainly excessive and the model values are probably realistic; the representation of the ITCZ in the simulation is good with the precipitation maxima lying in a narrow band to the north of the equator and

in the broader region of the SPCZ. In JJA (Figures 20a-c) very good agreement is again achieved with climatological values. Improvements in the tropical precipitation noted in DJF over land and mountains are also present in this season. A marked improvement in the rainfall associated with the summer monsoon flow over South East Asia can be seen in the run with 3CV. The excessively strong low-level jet which was noted to extend too far into the tropical West Pacific is associated with unrealistically high rainfall totals in this region in 1CV. This aspect is greatly improved at 3CV, and there are also higher totals over Indonesia, though the spurious minimum similar to the one found in DJF is not eliminated. At high latitudes precipitation totals which had been in closer agreement with climatology at 1CV, are generally too large at 3CV especially over Alaska and northern Siberia. On a regional scale the area around the Black Sea and the Caspian Sea is significantly drier than observed in both runs. Objective measures of the fit to the climatology generated by the University of East Anglia (Hulme, 1992) are provided in Table 1(b). This is heavily weighted towards land points and confirms the markedly better simulation with 3CV even though the contributions from the spuriously large grid-point accumulations over mountains have been excluded.

Soil moisture, defined as a total within the root zone, is a much smoother field with the introduction of a multi-layer hydrology scheme in 3CV, particularly in the tropics where very large grid-point to grid-point variability is present in 1CV: see Figures 21a-b for DJF and Figures 22a-b for JJA. In middle latitudes overall levels of soil moisture are similar in the two runs, while at high latitudes in JJA slightly more soil moisture is found in 3CV in regions where higher precipitation was noted above. Largest differences are found over the Amazon basin, a region which has uniformly high values throughout the year with the multi-layer scheme, but which dried out considerably in JJA when a scheme with only one layer was used in 1CV.

2.5 Near surface fields

Over land areas the climatology of screen-level temperatures of Legates and Willmott (1990b) is used to validate the derived 1.5 m temperatures from the model simulations. In DJF (Figures 23a-c), apart from the large differences to be expected over high ground, the only major discrepancy is over northern Russia where there is a cold bias as large as -10 K in places. This is no doubt related to the excessive surface pressure around the Arctic coast and the easterly gradient in the error field which implies a failure of maritime westerlies to reach this area as often as observed. In JJA (Figures 24a-c) differences from climatology over low ground are generally very small, the only notable warm bias being in the region of the Black Sea which was where low precipitation and soil moisture had been identified in the preceding section. Over eastern USA and South America temperatures are between 2 and 6 K lower in 3CV than in 1CV and fit the observed values better. In the Amazon Basin higher soil moisture at this time of year is no doubt the critical factor leading to the lower screen temperatures. Large mean errors in DJF and to a lesser extent in SON are confirmed in objective validation scores in Table 1(c).

Over the oceans sea-minus-air temperature differences are crucial values entering the equations for local stability and the flux of sensible heat; they are compared with GISST analyses derived from observations made by merchant ships in records going back over many years. Figures 25a-c show the comparison for DJF and Figures 26a-c for JJA. Errors are

almost uniformly positive, or equivalently, the simulated sea-minus-air temperature differences are too large; model values in the tropics of 1.5-2.0 K are typically 0.4-0.8 K larger than observed, while in DJF to the east of cold northern continental land masses values as large as 6-8 K associated with cold-air outbreaks over a warm sea are some 2 K greater than in the GISST fields. Errors in 3CV are generally smaller in the tropics than in 1CV, but larger in middle latitudes.

Relative humidity at 1.5 m in DJF (Figures 18a-b) is almost universally lower in 3CV over the oceans, and this change is largely due to the corrected evaporation of falling precipitation. Difference charts for JJA (not shown) are very similar. The values over the oceans show general agreement with the climatology based on COADS observations published by Wright (1988); relative humidity is around 80% in the equatorial regions falling to nearer 75% in the subtropical highs. Model humidity greater than 90% over the Southern Ocean cannot be widely verified, but at the few grid points where Wright has sufficient data to obtain a mean observed value it seems that they are too high.

Model values of the derived wind at 10 m are compared with a climatology based on COADS ship winds in Figures 27a-c (DJF) and Figures 28a-c (JJA). The excessive strength of the mean wind in the Pacific in DJF and the southward shift in the pattern in the Atlantic in the same season reflect errors in the pressure gradients already noted. The trade winds both north and south of the equator are too strong, but not by as much as the apparent error in the 850 mb winds. The south west monsoon over Asia in JJA is too intense, but the errors are reduced in the run with 3CV as was noted in the fields of precipitation and 850 mb wind. Over land a decrease in the magnitude of the wind can be seen, and this can be directly attributed to the increased parametrized drag in 3CV.

2.6 Surface fluxes

Surface fluxes such as those provided by Oberhuber (1988) depend on parametrized relationships with the observed variables in much the same way that the model fluxes are derived from the basic model variables. Differences between the two will be due in part to differences in the parametrizations used. A comparison of the simulated fluxes of latent heat from the AMIP run with Oberhuber's values for DJF (Figures 29a-c) and JJA (Figures 30a-c) show that the model values are almost universally larger in the tropics and sub tropics by typically 20-50 Wm^{-2}. Gordon and Wright (1995) noted similar differences in their study of a coupled version of the Unified Model in which a strong relaxation to climatological sea surface temperatures was imposed; they attributed the larger tropical fluxes to the larger exchange coefficients assumed in the model parametrization in light winds and unstable conditions (the "free convective limit"). Some of the differences are probably also related to the excessive surface winds and sea-minus-air temperature differences (which will increase instability and the exchange coefficients) noted in the previous section. In middle latitudes latent heat fluxes are small both in the model and in the climatology and in the North Atlantic errors are mostly negative. Changes introduced between 1CV and 3CV have generally made the errors larger in DJF particularly in the tropical North Pacific where local differences from the Oberhuber climatology approach 100 Wm^{-2} in places. In JJA the main impact of the changes at 3CV is to reduce the excessive fluxes associated with the Asian summer monsoon.

Sensible heat fluxes (Figures 31a-c and 32a-c) are larger than the estimates of Oberhuber almost everywhere, and the main cause is likely to be the larger than observed sea-minus-air temperature differences. In DJF the large fluxes in the West Atlantic associated with cold-air outbreaks, which reach a maximum value of around 100 Wm^{-2}, are well simulated in the model, while the large fluxes in the North West Pacific generated under similar conditions are overestimated.

Wind stress over the oceans (Figures 33a-c and 34a-c) is closely related to the surface wind and where its magnitude is overestimated, such as in the trade wind regions, the North Pacific and the Indian summer monsoon as was noted in the previous section, similar errors in the wind stress are to be expected. The Hellerman climatology is generally accepted to overestimate the true values and should just be taken as a guide to the actual pattern. Over land large differences between 1CV and 3CV are related to the revised orographic and gravity wave drag schemes; wind stresses with the new scheme are much larger over mountains and this is particularly noticeable over Antarctica, the Andes, and the Himalayas. The increases are generally matched by decreases in the drag due to gravity wave dissipation so that the net stress on the atmosphere at any latitude remains little changed.

2.7 Cloud and radiative fluxes

Radiative fluxes in a climate model are highly dependent on the schemes for parametrizing the sub-grid scale cloud physics, and a great deal of variability from model to model is to be expected; indeed the systematic errors reported by Hurrell (1995) and Barker et. al. (1994) bear no resemblance to each other nor to the errors presented here. Cloud in the model is identified as either layer type, occupying a fraction of a grid box on any model level, or convective type in which case it occupies a vertical column. Measurements of the three-dimensional distribution are not reliable as some cloud is obscured when observed from the ground or from space, so comparisons here are only presented between the two model versions; zonal mean amounts of layer cloud are shown in Figures 35a-b for DJF and Figures 36a-b for JJA. The two model changes having most effect on cloud amount are the modifications to the cloud scheme and in the definition of the mixed phase relationship (see section 1.1). In general terms there is a reduction in amounts of high cloud above 500 mb and in stratus and/or fog in the few model levels closest to the surface, while amounts in many of the levels in between become greater; the increase is largest for boundary-layer cloud in the summer hemisphere at middle and high latitudes. Amounts of convective cloud (Figures 37a-c and 38a-c) are smaller than for layer cloud; differences between the two model simulations are small except in regions of tropical ascent where a reduction is found in 3CV associated with the weaker Hadley circulation. Total cloud amounts presented here (Figures 39a-c and 40a-c) are calculated as the sum of the convective cloud and an integrated effect of the layer cloud where a maximum/random overlap assumption has been used along the lines of Geleyn and Hollingsworth (1979). These amounts represent the cloud used in the calculation of the long wave fluxes; the short wave fluxes are calculated using a simplified cloud distribution, which is an undesirable inconsistency introduced for computational efficiency. Globally averaged cloud cover is 0.55 in DJF and 0.53 in JJA which compare with a value of 0.62 from the ISCCP climatology in both seasons. The deficit is largest over the mid-latitudes oceans at all times of the year; model values reach 0.7 in the North Atlantic, North Pacific and Southern Oceans where ISCCP estimates are as high as 0.9. Some increase between 1CV and 3CV can be noted in these regions in the summer months in each

hemisphere. Other regions of cloud deficit lie in the subtropics where sheets of marine stratocumulus, capped by the trade wind inversion, persist over the cold seas bordering the western coasts of southern Africa, South America and North America. Model cloud amounts are up to 0.5 less than observed, which is a characteristic of many numerical models, and has been attributed to insufficient vertical resolution in the boundary layer. Small improvements can be noted in 3CV particularly at some of the coastal grid points. In other parts of the tropics, where deep convection is dominant, cloud amounts are generally closer to observed values. Much of this cloud in the model is thin cirrus. The large changes in mountainous regions which vary greatly in magnitude from grid point to grid point are due to the smoother fields obtained with the reduced values of diffusion.

It is not possible to catalogue the separate effects of all the changes listed in section 1.1 and reference is only made to those that have a major impact. The change in cloud scheme outlined in 1.1(a) falls into this category and its effect on a 10-year simulation was discussed by Gallani (1994). It is found to lead to albedo over all middle and high latitude regions which is considerably higher than the measurements from ERBE, the errors being particularly large over land in JJA. With increased cloud in summer there is a consequential lowering of temperature over land, not only at the surface, but through much of the lower troposphere. The small changes between 1CV and 3CV noted here in the cloud cover and tropospheric temperatures reflects the impact of the other changes made to the cloud physics, particularly to the specification of mixed-phase clouds (section 1.1(b)), which have offset some the adverse effects of the change in cloud scheme. The new cloud scheme was introduced to reduce the unrealistically large cloud liquid water paths found in simulations with 1CV as Figures 41a-b and 42a-b demonstrate. Differences are particularly large over the middle latitude oceans in summer, which are regions of extensive cloud cover and where grid-box mean liquid water is close to the in-cloud value. Estimates based on SSM/I data made by Greenwald et. al. (1993) suggest that values in these regions should be around 0.1 Kg m^{-2} which is much closer to what is obtained in the simulation with 3CV than 1CV. The differences in the tropics, which are also large in places, cannot be validated in the same way as the retrieval algorithm applied to the satellite measurements is not thought to be valid in these regions. Cloud ice paths (Figures 43a-b and 44a-b) show fewer differences between the two runs though there is a general tendency towards lower values in simulation with 3CV. No reliable measurements of cloud ice paths exist for comparison.

Top-of-atmosphere albedo in both DJF (Figures 45a-c) and JJA (Figures 46a-c) agrees well with the observations from ERBE, the differences being less than 0.05 in most locations. Over middle latitude oceans there is no overall tendency for negative albedo errors showing that, in spite of a substantial lack of cloud indicated by the ISCCP data, the average radiative fluxes are close to observation. In the regions of subtropical marine stratocumulus the lack of cloud in the model is evident from the low albedos compared with ERBE, errors which are particularly large in JJA and SON (not shown). In JJA tropical albedos are too low in the ITCZ and the errors, which are somewhat larger in 3CV than in 1CV, reach 0.1 in places. The change to 3CV has the greatest impact over the equatorial West Pacific where lower rainfall is associated with lower albedo. Improvements in the rainfall pattern are generally matched by improvements in the albedo and the main error in both fields is in the Indonesian region which is too dry and radiatively too dark. Over land areas in all seasons systematic errors are not large, though over the Sahara albedos less than 0.3 suggest that the underlying surface is insufficiently reflective.

Global Radiation Budget

	1CV				3CV			
	isw	osw	olw	net	isw	osw	olw	net
DJF	351.6	108.6	234.0	+9.0	351.6	104.1	237.5	+10.0
MAM	339.2	102.4	235.7	+1.1	339.2	97.9	239.6	+1.6
JJA	331.5	97.8	241.2	-7.5	331.5	95.0	243.8	-7.3
SON	343.4	103.1	237.9	+2.4	343.4	98.6	240.6	+4.1

Top-of-atmosphere radiation versus ERBE
(mean/rms differences)

	1CV		3CV	
	osw	olr	osw	olr
DJF	2.1/18.3	1.4/11.7	-2.6/18.9	4.9/12.4
MAM	2.8/18.2	1.7/11.9	-1.7/16.3	5.6/12.1
JJA	1.2/22.3	2.3/12.4	-1.7/18.5	4.9/11.7
SON	1.5/19.3	2.4/12.1	-3.0/17.0	5.1/12.6

Table 2. Validation of the radiative fluxes: incoming short wave (isw), outgoing short wave (osw), and outgoing long wave (olr).

In middle latitudes top-of-atmosphere outgoing long wave radiation is in good agreement with ERBE in both DJF (Figures 47a-c) and JJA (Figures(48a-c). In the tropics differences are mostly positive in the ITCZ confirming that there is insufficient optically thick high cloud in areas of deep convection. Differences are particularly large in the Pacific warm pool region and in JJA the error has become markedly greater with the change to 3CV.

A valuable test of the climate simulation is provided by the global integral of the top-of-atmosphere radiation which in reality should be zero over long periods of time as the earth is in thermal equilibrium with its surroundings. Where sea-surface temperatures are prescribed, as is the case here, the ocean can act as an unregulated source or sink of heat in the model; this integral therefore represents the imbalance in the thermal exchange between the atmosphere and the underlying sea surface. Table 2 presents the global radiation budget for each of the four seasons and it is clear that the annual imbalance of around +2 Wm^{-2} is small both in absolute magnitude and compared with an imbalance of 5 W m^{-2} in the ERBE observations. There is little difference between 1CV and 3CV which reflects the importance placed on this parameter during the development stages of both model versions. Values of rms differences from ERBE data show a generally improved fit in the outgoing short wave, but a slightly worse fit in the outgoing long wave.

2.8 Eddy fluxes

The covariances uv and vT define respectively the northward fluxes of westerly momentum and heat; they may be broken up into their stationary and transient components in the normal way, which for momentum is:

$$\overline{u^* v^*} = (\bar{u} - [\bar{u}])\,(\bar{v} - [\bar{v}])$$

$$\overline{u' v'} = \overline{uv} - \bar{u}\,\bar{v}$$

The square brackets denote a zonal mean and the overbar denotes a time mean using data at every time step over all days within the season in question (DJF or JJA) and all 10 years of the AMIP period (i.e. transients are calculated with respect to the 10-year mean).

The transient northward momentum fluxes for DJF are shown in Figures 49a-c and for JJA in Figures 50a-c. The positions of the maxima in each hemisphere at the jet stream level are well captured in both seasons, but the magnitude of the fluxes is in all instances too large, especially in the southern winter hemisphere when a model maximum of 88 m^2s^{-2} is found where the ECMWF analyses have 55 m^2s^{-2} and UKMO analyses (not shown) have 56 m^2s^{-2}. Errors become slightly greater with the change from 1CV to 3CV. A maximum flux at 150 mb, which is southward in DJF and northward in JJA, is found over the equator in the model simulations but barely, if at all, in the analyses. The feature is even more pronounced in the stationary fluxes (Figures 51a-c and 52a-c) where a marked reduction is evident in the change to 3CV. A large part of the stationary flux at this level is found over the equatorial Indian Ocean which is a region of few observations and where confidence in the analyses is low. The model flow here in JJA is northeasterly forming part of the outflow from the Pacific warm pool region, which in turn is driven by low level convergence from the Asian monsoon. This monsoon flow is far too strong in 1CV and this is no doubt a primary factor leading to the excessive upper level cross equatorial momentum flux; the improved, though still over strong monsoon flow in 3CV is therefore associated with the improved momentum fluxes seen here. The stationary fluxes of momentum outside the tropics are only significant in the winter northern hemisphere where they are associated with the stationary troughs on a planetary scale maintained by the large land-sea temperature contrasts. As with the transient fluxes in this hemisphere, the model values are close to, but a little larger than, the fluxes in the analyses.

Northward eddy heat fluxes in DJF (Figures 53a-c) and JJA (Figures 54a-c) simulated by the model show many of the features found in the analyses. Errors are largest at in the southern hemisphere in both seasons where southward fluxes are considerably greater than observed, though this difference may in part reflect errors in analyses. Overall there is little difference between 1CV and 3CV in the poleward fluxes of heat in either season.

2.9 Variability and blocking

Lack of variability was a characteristic of the previous 11-layer version of the UK Meteorological Office model (Hall et. al., 1994) and indeed of several other general circulation models (e.g. Boer and Lazare, 1988) though Roeckner et. al. (1992) report realistic values from a model with T42 resolution. In this respect the Unified Model is quite different

from the 11-layer version, showing values of transient eddy kinetic energy in both DJF (Figures 55a-c) and JJA (Figures 56a-c) which are on the whole somewhat higher than found in the ECMWF analyses. The maxima around 250-300 mb in the middle latitudes of both hemispheres are well positioned, and in the northern hemisphere are close to the observed values, but there is too much energy in the flow at 150 mb and more generally in the southern hemisphere. Some reduction in the transient eddy kinetic energy in equatorial regions and an improved agreement with climatology is found in the change from 1CV to 3CV, otherwise there is little noticeable different between the two simulations. Above 100 mb the model demonstrates a lack of variability in the tropics due to a failure to simulate a quasi-biennial oscillation.

The validation of variability on different time scales is investigated by applying specific numerical filters to time series of daily fields of 500 mb geopotential height in an identical manner to Blackmon et. al. (1977). The standard deviations of the band-pass filtered fields, which represent variability on synoptic time scales of between 2.5 and 6 days, are shown for DJF (Figure 57) and JJA (Figure 58). In the northern hemisphere in winter the main storm tracks across the oceans are well represented, though values are a little lower than observed in the North Atlantic, more especially in the east, where a failure of lows to move sufficiently frequently towards Iceland and the Norwegian Sea is suggested. It was noted that the simulated mean sea-level pressure is too high in these regions. In the North Pacific the agreement with analyses is good. A tendency to underestimate oceanic values is also present in JJA particularly in the run with 3CV. In the southern hemisphere the model simulation correctly positions the maximum storm track region in the southern Indian Ocean in both DJF and JJA, though values are generally too large in the winter season. The change to 3CV has led to somewhat higher values overall. The standard deviations of the low-pass filtered fields, which represent variability on time scales of 10 to 90 days, are shown for DJF (Figure 59) and JJA (Figure 60). Agreement with the pattern and magnitudes shown in the analyses is good in both hemispheres and seasons; the main regions where blocking is found in the winter northern hemisphere, Northern Europe and the North East Pacific, are well captured as is the maxima in the Southern Pacific at high latitudes. In 3CV there is, however, a lack of variability in DJF over an area extending across Alaska and the Arctic Ocean.

A blocking index devised by Tibaldi and Molteni (1990) is used widely in model verification and values of the percent of days blocked at each longitude in the northern hemisphere in the 4 seasons DJF, MAM, JJA and SON are presented in Figure 61. The incidence of blocking both as observed and as simulated by the model varies a good deal from year to year and the 10-year period used is rather short to obtain an accurate estimate of the long-term mean value. In the European region there is a tendency for longitude of maximum blocking to be displaced to the east of its observed position and for the frequency to be underestimated in DJF and MAM. More severe underestimation in these two seasons is found in the Pacific region with 3CV where the simulated occurrence of blocking is less than half that shown in the analyses. Apart from sampling differences to be expected from a short simulation period, there is no obvious explanation for the marked deterioration between 1CV and 3CV in DJF.

The ability of the model to simulate variability on the longest timescales is demonstrated by the standard deviation of the 10 seasonal means of mean sea-level pressure which make up the AMIP period (Figures 62a-c and 63a-c). Overall values are in good agreement with the analyses and are as close as can be expected from such a small sample of years. Maxima in

the North Atlantic and North Pacific are well represented as is the maximum in the southern Pacific Ocean close to the Antarctic continent.

3. Conclusions

The AMIP experiment provides the framework for stringent tests of climate simulations with general circulation models, not only of the time mean fields but also of the variability over a wide range of time scales. The validation of 10-year integrations with the Unified Model presented here focuses on the global scale and on the main model fields and parametrized fluxes, and in this context the simulated climate appears realistic when compared with observational data. Perhaps the most satisfactory features are:

- Precipitation distributions which are in close agreement with observed climatological means in all seasons.
- 1.5 m temperatures over non-mountainous land which are, with the exception of a cold bias in DJF, in good agreement with observations.
- A generally realistic simulation of variability on a wide range of time scales as measured by transient eddy kinetic energy, the standard deviation of band-pass and low pass filtered 500 mb geopotential heights, blocking indices, and the standard deviation of seasonal mean sea-level pressure.
- Fluxes of long and short wave radiation at the top of the atmosphere which are in good agreement with observed fluxes from ERBE.
- On a regional scale, a good simulation of the summer monsoon flow over South East Asia.

A wide range of systematic errors have been identified of which the most important are:

- A cold bias throughout the whole of the troposphere increasing with height and reaching 6-7 K at the tropopause.
- A cold bias of 10-15 K in the lower stratosphere over the summer pole.
- A simulation of the flow in middle and high latitudes of the northern hemisphere in DJF, which by no measure poor, is less satisfactory than in the other 3 seasons. It has many inter-related characteristics: a southward shift in the position of the Atlantic low, excessive westerly flow in the Pacific, an Aleutian low that is too deep and shifted eastward, a high pressure anomaly centred over northern Russia and covering much of the Arctic region, strong jets which are shifted poleward and upward, and a cold bias over land at high latitudes.
- A westerly error in the southern hemisphere in all seasons extending up to jet stream levels.
- Stratospheric easterly winds in the tropics which are too strong above 200 mb.
- A westerly bias centred on the equator in mid troposphere.
- A poor simulation in an area centred on Indonesia and extending to parts of the equatorial Pacific and Indian Oceans; rainfall, cloud amount and albedo are too low, while outgoing long wave radiation is too high.
- Too little marine stratocumulus in those parts of the tropics to the east of continents where the trade wind boundary layer is relatively shallow.
- A positive bias in the relative humidity, perhaps as large as 15 percent, in much of the troposphere above the boundary layer in middle latitudes.
- Sea-minus-air temperature differences which are too large over almost all ocean areas.

The current version of the Unified Model, the third climate version (3CV), incorporates many improvements to the parametrization schemes over the first version (1CV) and their combined

impact on the simulation has been assessed here. Of the number of significant changes that have been identified many, but not all, are beneficial:

- Precipitation is closer to observations over the tropical regions of Africa and South America, but the fit is less good over high latitudes of the northern hemisphere in JJA. The large grid-point maxima over mountains have been eliminated.
- A major improvement has been achieved in the simulation of the summer monsoon flow over South East Asia; its strength is weaker, it no longer erroneously extends into the tropical North West Pacific, and precipitation amounts and top-of-atmosphere albedo are more realistic. The improvement has, however, been achieved at the expense of a worse fit to ERBE observations of outgoing long wave radiation.
- The strength of the Hadley circulation is weaker, particularly in JJA, and is now close to observed values.
- There has been a small reduction in the moist bias.
- A number of the errors in the winter circulation in the northern hemisphere identified above have become a little larger.
- Pressure has built in middle and high latitudes and dropped in the tropics. This has had the beneficial effect of reducing by a small amount the westerly bias in the southern hemisphere while increasing errors in some other areas.
- Temperature and wind errors in the stratosphere have become larger overall.
- Cloud liquid water paths are much lower in middle latitudes and are in much better agreement with SSM/I observations.

The overall impact of the changes may be judged to be beneficial and this is largely borne out by the objective scores for the rms fit to the climatological values of certain key variables presented in Tables 1 and 2.

4. References

Barker, H.W., Li, Z. and Blanchet, J.-P., 1994. Radiative characteristics of the Canadian Climate Centre second-generation general circulation model. J. Clim., 7, 1070-1091.

Barkstrom, B., Harrison, E., Smith, G., Green, R., Kibler, J. and Cess, R., 1989: Earth Radiation Budget Experiment (ERBE) archival and April 1985 results. Bull. Am. Met. Soc., 70, 1254-1262.

Blackmon, M.L., Wallace, J.M., Lau, N.-C. and Mullen, S.L., 1977. An observational study of the northern hemisphere wintertime circulation. J. Atm. Sci., 34, 1040-1053.

Boer, G.J., Arpe, K., Blackburn, M., Déqué, M. Gates, W.L., Hart, T.L., le Treut, H., Roeckner, E., Sheinin, D.A., Simmons, I., Smith, R.N.B., Tokiola, T., Wetherald, R.T. and Williamson, D., 1991. An intercomparison of the climates simulated by 14 atmospheric general circulation models. CAS/WGNE Rep. No. 15, WMO/TD No. 425.

Boer, G.J. and Lazare, M., 1988. Some results concerning the effect of horizontal resolution and gravity-wave drag on simulated climate. J. Clim., 1, 789-806.

Cullen, M.J.P., 1993: The unified forecast/climate model. Meteorol. Mag., 122, 81-94.

Gallani, M.L., 1994. Comparisons between 1st and 2nd versions of the climate model. Hadley Centre Internal Note No. 58.

Gates, W.L., 1992. AMIP: the atmospheric model intercomparison project. Bull. Amer. Meteor. Soc., 73, 1962-1970.

Geleyn, J.-F., and Hollingsworth, A., 1979. An economical analytical method for the computation of the interaction between scattering and line absorption of radiation. Beitr. Phys. Atmos., 52, 1-16.

Gordon, C. and Wright, D.K., 1995. A comparison of modelled surface fluxes with climatological estimates. Meteorological Office, Hadley Centre CRTN No. 53.

Greenwald, T.J., Stephens, G.L., Vonder Haar, T.H. and Jackson, D.L., 1993. A physical retrieval of cloud liquid water over the global oceans using Special Sensor Microwave/Imager (SSM/I) observations. J. Geophys. Res., 98, 18471-18488.

Hall, C.D., 1994. Stratospheric moisture in the climate model. Meteorological Office, Hadley Centre Internal Note No. 61.

Hall, C.D. and Stratton, R.A., 1994. The effect of changing horizontal diffusion in the atmospheric version of the Unified Climate Model. Meteorological Office, Hadley Centre CRTN No. 44.

Hall, N.M.J., Hoskins, B.J., Valdes, P.J. and Senior, C.A., 1994. Storm tracks in a high-resolution GCM with doubled carbon dioxide. Q. J. R. Meteorol. Soc., 120, 1209-1230.

Harrison, D.E., 1989. On climatological monthly mean wind stress and wind stress curl fields over the world ocean. J. Clim., 2, 57-70.

Harrison, E.F., Minnis, P., Barkstrom, B.R., Ramanathan, V., Cess, R.D., and Gibson, G.G., 1990. Seasonal variation of cloud radiative forcing derived from the Earth Radiation Budget Experiment. J. Geophys. Res., 95, 18687-18703.

Hellerman, S. and Rosenstein, M., 1983. Normal wind stress over the world ocean with error estimates. J. Oceanog., 13, 1043-1104.

Hoskins, B.J., Hsu, H.H., James, I.N., Masutani, M., Sardeshmukh, P.D. and White, G.H., 1989. Diagnostics of the global atmospheric circulation based on ECMWF analyses 1979-1989. WCRP-27, WMO/TD No. 326.

Hulme, M., 1992. A 1951-80 global land precipitation climatology for the evaluation of general circulation models. Clim. Dyn., 7, 57-72.

Hurrell, J.W., 1995. Comparison of NCAR Community Climate Model (CCM) climates. Clim. Dyn., 11, 25-50.

Legates, D.R. and Willmott, C.J., 1990a. Mean seasonal and spatial variability in gauge-corrected global precipitation. Int. J. Climatology, 10, 111-127.

Legates, D.R. and Willmott, C.J., 1990b. Mean seasonal and spatial variability in global surface air temperature. Theor. and Appl. Clim., 41, 11-21.

Murphy, J.M., 1995. Transient response of the Hadley Centre coupled ocean-atmosphere model to increasing carbon dioxide. Part I: control climate and flux adjustment. J. Clim., 8, 36-56.

Oberhuber, J.M., 1988. An atlas based on the 'COADS' data set: the budgets of heat,buoyancy and turbulent kinetic energy at the surface of the global ocean. Max-Plank-Institut fur Meteorogie Report No. 15.

Parker, D.E., Folland, C.K., Bevan, A., Ward, M.N., Jackson, M. and Maskell, K., 1992. Marine surface data for analysis of climate fluctuations of interannual to century timescales. National Research Council (National Academy of Sciences) paper presented at the Workshop on Climate Variability on Decade-to-Century Timescales. Irvine, California, USA.

Phillips, T.J., 1994. A summary documentation of the AMIP models. PCMDI Report No. 18.

Roeckner, E., Arpe, K., Bengtsson, L., Brinkop, S., Dümenil, L., Esch, M., Kirk, E., Lunkeit, F., Ponater, M., Rockel, B., Sausen, R., Schlese, U., Schubert, S. and Windelband, M., 1992. Simulation of the present-day climate with the ECHAM model: impact of model physics and resolution. Max-Plank-Institut für Meteorologie Report No. 93.

Rossow, W.B. and Schiffer, R.A., 1991. ISCCP cloud data products. Bull. Amer. Met. Soc., 72, 2-20.

Tibaldi, S. and Molteni, F., 1990. On the operational predictability of blocking. Tellus, 42A, 343-365.

Trenberth, K.E. and Olson, J.G., 1998. An evaluation and intercomparison of global analyses from the National Meteorological Center and the European Centre for Medium Range Forecasts. Bull. Amer. Meteor. Soc., 69, 1047-1057.

Ward, M.N., 1992. Provisionally corrected surface wind data, worldwide ocean-atmosphere surface fields and Sahelian rainfall variability. J. Clim., 5, 454-475.

Warren, S.G., Hahn, C.J., London, J., Cherrin, R.M. and Jeene, R.L., 1986. Global distribution of total cloud cover and cloud type amounts over land. NCAR/TN-273.

Warren, S.G., Hahn, C.J., London, J., Cherrin, R.M. and Jenne, R.L., 1988. Global distribution of total cloud cover and cloud type amounts over the ocean. NCAR/TN-317.

Woodruff, S.D., Slutz, R.J., Jenne, R.L. and Steurer, P.M., 1987. A comprehensive ocean-atmosphere data set. Bull. Amer. Meteor. Soc., 68, 1239-1250.

Wright, P.B., 1988. An atlas based on the COADS data set: fields of mean wind, cloudiness and humidity at the surface of the global ocean. Max-Plank-Institut für Meteorologie Report No. 14.

5. Figure captions

Figure 1 Mean sea-level pressure; Dec/Jan/Feb; (a) 3CV, (b) 3CV - 1CV, (c) 3CV - ECMWF 1979-88.

Figure 2 Mean sea-level pressure; Mar/Apr/May; (a) 3CV, (b) 3CV - 1CV, (c) 3CV - ECMWF 1979-88.

Figure 3 Mean sea-level pressure; Jun/Jul/Aug; (a) 3CV, (b) 3CV - 1CV, (c) 3CV - ECMWF 1979-88.

Figure 4 Mean sea-level pressure; Sep/Oct/Nov; (a) 3CV, (b) 3CV - 1CV, (c) 3CV - ECMWF 1979-88.

Figure 5 Zonal mean westerly wind; Dec/Jan/Feb; (a) 3CV, (b) 3CV - 1CV, (c) 3CV - ECMWF 1979-88.

Figure 6 Zonal mean westerly wind; Jun/Jul/Aug; (a) 3CV, (b) 3CV - 1CV, (c) 3CV - ECMWF 1979-88.

Figure 7 Vector wind and isotachs at 250 mb; Dec/Jan/Feb; (a) 3CV, (b) 3CV - 1CV, (c) 3CV - ECMWF 1979-88.

Figure 8 Vector wind and isotachs at 250 mb; Jun/Jul/Aug; (a) 3CV, (b) 3CV - 1CV, (c) 3CV - ECMWF 1979-88.

Figure 9 Vector wind and isotachs at 850 mb; Dec/Jan/Feb; (a) 3CV, (b) 3CV - 1CV, (c) 3CV - ECMWF 1979-88.

Figure 10 Vector wind and isotachs at 850 mb; Jun/Jul/Aug; (a) 3CV, (b) 3CV - 1CV, (c) 3CV - ECMWF 1979-88.

Figure 11 Zonal mean meridional stream function; Dec/Jan/Feb; (a) 3CV, (b) 3CV - 1CV, (c) 3CV - ECMWF 1985-91.

Figure 12 Zonal mean meridional stream function; Jun/Jul/Aug; (a) 3CV, (b) 3CV - 1CV, (c) 3CV - ECMWF 1985-91.

Figure 13 Zonal mean temperature; Dec/Jan/Feb; (a) 3CV, (b) 3CV - 1CV, (c) 3CV - ECMWF 1979-88.

Figure 14 Zonal mean temperature; Jun/Jul/Aug; (a) 3CV, (b) 3CV - 1CV, (c) 3CV - ECMWF 1979-88.

Figure 15 Zonal mean relative humidity; Dec/Jan/Feb; (a) 3CV, (b) 3CV - 1CV.

Figure 16 Zonal mean relative humidity; Jun/Jul/Aug; (a) 3CV, (b) 3CV - 1CV.

Figure 17 Relative humidity, mean differences from radiosondes 1971-90; Dec/Jan/Feb and Jun/Jul/Aug; 90N-30N, 30N-30S and 30S-90S.

Figure 18 Relative humidity at 1.5 m; Dec/Jan/Feb; (a) 3CV, (b) 3CV - 1CV.

Figure 19 Total precipitation; Dec/Jan/Feb; (a) 3CV, (b) 1CV, (c) Legates and Willmott.

Figure 20 Total precipitation; Jun/Jul/Aug; (a) 3CV, (b) 1CV, (c) Legates and Willmott.

Figure 21 Soil moisture content; Dec/Jan/Feb; (a) 3CV, (b) 1CV.

Figure 22 Soil moisture content; Jun/Jul/Aug; (a) 3CV, (b) 1CV.

Figure 23 Temperature at 1.5 m; Dec/Jan/Feb; (a) 3CV, (b) 3CV - 1CV, (c) 3CV - Legates and Willmott.

Figure 24 Temperature at 1.5 m; Jun/Jul/Aug; (a) 3CV, (b) 3CV - 1CV, (c) 3CV - Legates and Willmott.

Figure 25 Air-minus-sea temperature differences; Dec/Jan/Feb; (a) 3CV, (b) 3CV - 1CV, (c) 3CV - GISST.

Figure 26 Air-minus-sea temperature differences; Jun/Jul/Aug; (a) 3CV, (b) 3CV - 1CV, (c) 3CV - GISST.

Figure 27 Vector winds and isotachs at 10 m; Dec/Jan/Feb; (a) 3CV, (b) 1CV, (c) COADS.

Figure 28 Vector winds and isotachs at 10 m; Jun/Jul/Aug; (a) 3CV, (b) 1CV, (c) COADS.
Figure 29 Surface latent heat flux; Dec/Jan/Feb; (a) 3CV, (b) 3CV - 1CV, (c) 3CV - Oberhuber.
Figure 30 Surface latent heat flux; Jun/Jul/Aug; (a) 3CV, (b) 3CV - 1CV, (c) 3CV - Oberhuber.
Figure 31 Surface sensible heat flux; Dec/Jan/Feb; (a) 3CV, (b) 3CV - 1CV, (c) 3CV - Oberhuber.
Figure 32 Surface sensible heat flux; Jun/Jul/Aug; (a) 3CV, (b) 3CV - 1CV, (c) 3CV - Oberhuber.
Figure 33 Surface wind stress; Dec/Jan/Feb; (a) 3CV, (b) 1CV, (c) Hellerman
Figure 34 Surface wind stress; Jun/Jul/Aug; (a) 3CV, (b) 1CV, (c) Hellerman
Figure 35 Zonal mean layer cloud; Dec/Jan/Feb; (a) 3CV, (b) 1CV.
Figure 36 Zonal mean layer cloud; Jun/Jul/Aug; (a) 3CV, (b) 1CV.
Figure 37 Zonal mean convective cloud; Dec/Jan/Feb; (a) 3CV, (b) 1CV.
Figure 38 Zonal mean convective cloud; Jun/Jul/Aug; (a) 3CV, (b) 1CV.
Figure 39 Total cloud amount; Dec/Jan/Feb; (a) 3CV, (b) 3CV - 1CV, (c) 3CV - ISCCP.
Figure 40 Total cloud amount; Jun/Jul/Aug; (a) 3CV, (b) 3CV - 1CV, (c) 3CV - ISCCP.
Figure 41 Vertically integrated cloud liquid water; Dec/Jan/Feb; (a) 3CV, (b) 1CV.
Figure 42 Vertically integrated cloud liquid water; Jun/Jul/Aug; (a) 3CV, (b) 1CV.
Figure 43 Vertically integrated cloud ice; Dec/Jan/Feb; (a) 3CV, (b) 1CV.
Figure 44 Vertically integrated cloud ice; Jun/Jul/Aug; (a) 3CV, (b) 1CV.
Figure 45 Albedo at top of atmosphere; Dec/Jan/Feb; (a) 3CV, (b) 3CV - 1CV, (c) 3CV - ERBE 1985-88.
Figure 46 Albedo at top of atmosphere; Jun/Jul/Aug; (a) 3CV, (b) 3CV - 1CV, (c) 3CV - ERBE 1985-88.
Figure 47 Outgoing longwave radiation at top of atmosphere; Dec/Jan/Feb; (a) 3CV, (b) 3CV - 1CV, (c) 3CV - ERBE 1985-88.
Figure 48 Outgoing longwave radiation at top of atmosphere; Jun/Jul/Aug; (a) 3CV, (b) 3CV - 1CV, (c) 3CV - ERBE 1985-88.
Figure 49 Zonal mean northward flux of momentum by transient eddies; Dec/Jan/Feb; (a) 3CV, (b) 1CV, (c) ECMWF 1979-88.
Figure 50 Zonal mean northward flux of momentum by transient eddies; Jun/Jul/Aug; (a) 3CV, (b) 1CV, (c) ECMWF 1979-88.
Figure 51 Zonal mean northward flux of momentum by stationary eddies; Dec/Jan/Feb; (a) 3CV, (b) 1CV, (c) ECMWF 1979-88.
Figure 52 Zonal mean northward flux of momentum by stationary eddies; Jun/Jul/Aug; (a) 3CV, (b) 1CV, (c) ECMWF 1979-88.
Figure 53 Zonal mean northward flux of sensible heat by transient eddies; Dec/Jan/Feb; (a) 3CV, (b) 1CV, (c) ECMWF 1979-88.
Figure 54 Zonal mean northward flux of sensible heat by transient eddies; Jun/Jul/Aug; (a) 3CV, (b) 1CV, (c) ECMWF 1979-88.
Figure 55 Zonal mean transient eddy kinetic energy; Dec/Jan/Feb; (a) 3CV, (b) 3CV - 1CV, (c) 3CV - ECMWF 1979-88.
Figure 56 Zonal mean transient eddy kinetic energy; Jun/Jul/Aug; (a) 3CV, (b) 3CV - 1CV, (c) 3CV - ECMWF 1979-88.
Figure 57 Standard deviation of band pass filtered 500 mb heights; Dec/Jan/Feb; (a) 3CV, (b) 1CV, (c) UKMO 1984-94.

Figure 58 Standard deviation of band pass filtered 500 mb heights; Jun/Jul/Aug; (a) 3CV, (b) 1CV; (c) UKMO 1984-94.

Figure 59 Standard deviation of low pass filtered 500 mb heights; Dec/Jan/Feb; (a) 3CV, (b) 1CV, (c) UKMO 1984-94.

Figure 60 Standard deviation of low pass filtered 500 mb heights; Jun/Jul/Aug; (a) 3CV, (b) 1CV, (c) UKMO 1984-94.

Figure 61 Blocking index northern hemisphere; 3CV, 1CV, UKMO 1984-94; (a) Dec/Jan/Feb, (b) Mar/Apr/May, (c) Jun/Jul/Aug, (d) Sep/Oct/Nov.

Figure 62 Standard deviation of seasonal mean sea-level pressure; Dec/Jan/Feb; (a) 3CV, (b) 1CV, (c) UKMO 1984-94.

Figure 63 Standard deviation of seasonal mean sea-level pressure; Jun/Jul/Aug; (a) 3CV, (b) 1CV, (c) UKMO 1984-94.

Figure 1(a) AMIP: 3rd Climate Version. 10-year Dec/Jan/Feb
Mean sea-level pressure
From 1/ 1/1979 to 1/ 1/1989

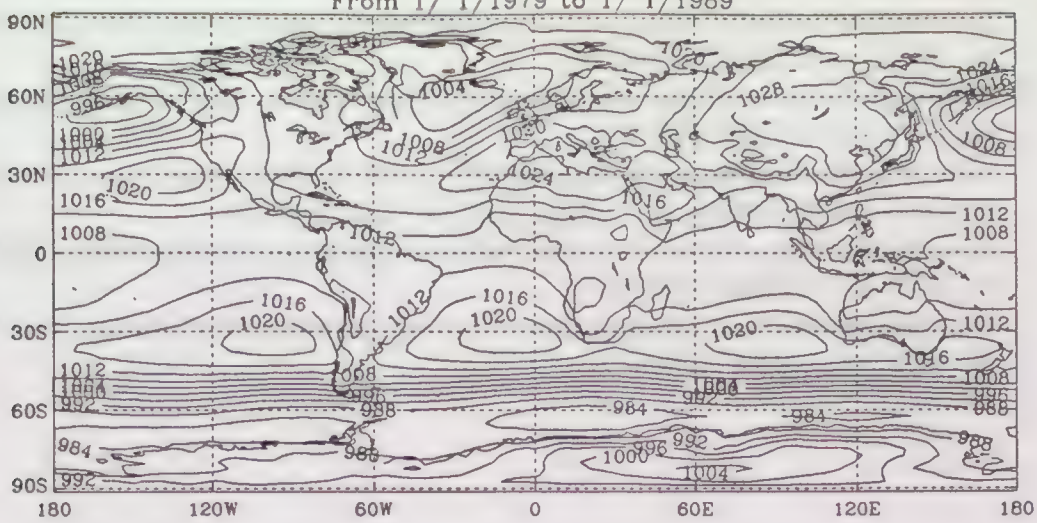

(b) AMIP: 3rd Climate Version. 10-year Dec/Jan/Feb minus
AMIP: 1st Climate Version. 10-year Dec/Jan/Feb
Mean sea-level pressure

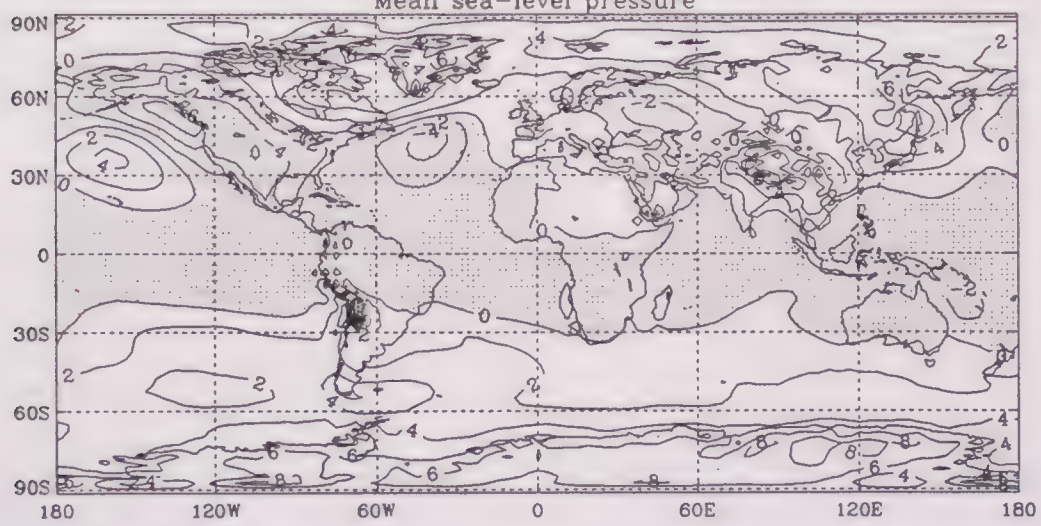

(c) AMIP: 3rd Climate Version. 10-year Dec/Jan/Feb minus
ECMWF climatology. Dec/Jan/Feb 1979-88
Mean sea-level pressure

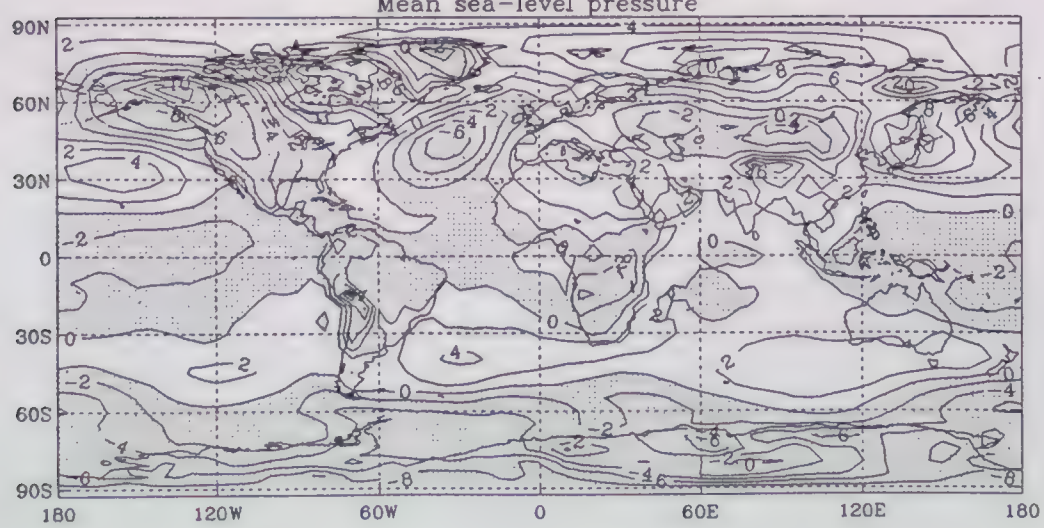

Area-weighted rms difference = 3.00

Figure 2(a) AMIP: 3rd Climate Version. 10-year Mar/Apr/May
Mean sea-level pressure
From 1/ 3/1979 to 1/ 6/1988

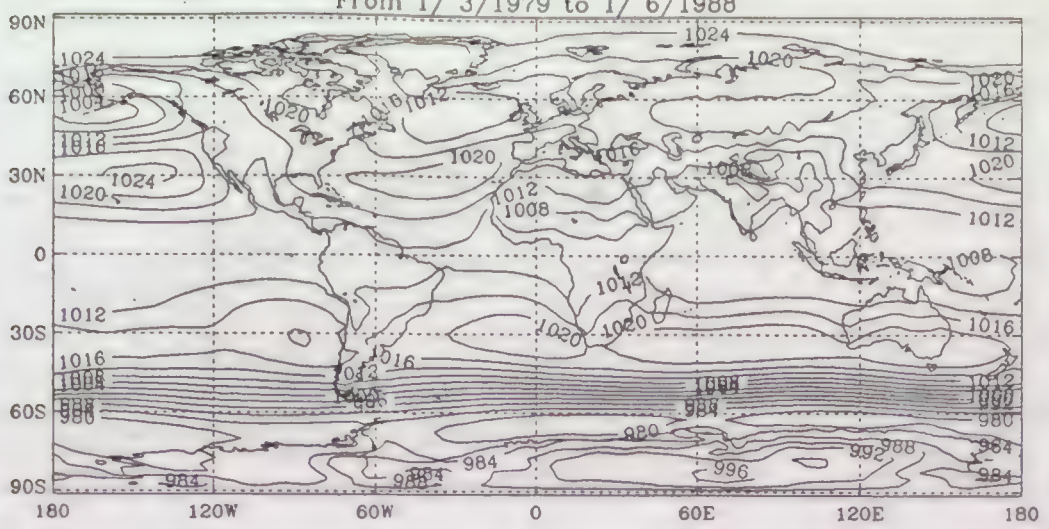

(b) AMIP: 3rd Climate Version. 10-year Mar/Apr/May minus
AMIP: 1st Climate Version. 10-year Mar/Apr/May
Mean sea-level pressure

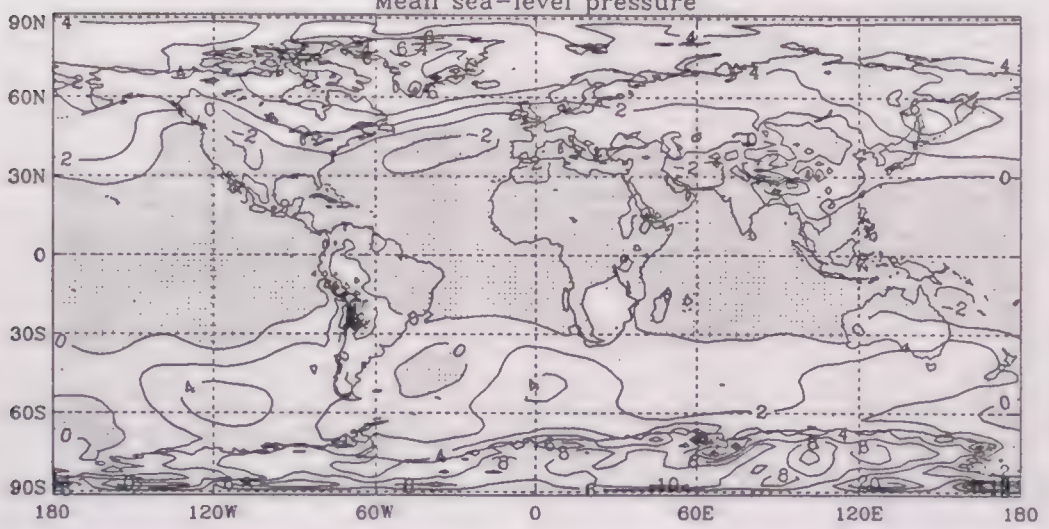

(c) AMIP: 3rd Climate Version. 10-year Mar/Apr/May minus
ECMWF climatology. Mar/Apr/May 1979-88
Mean sea-level pressure

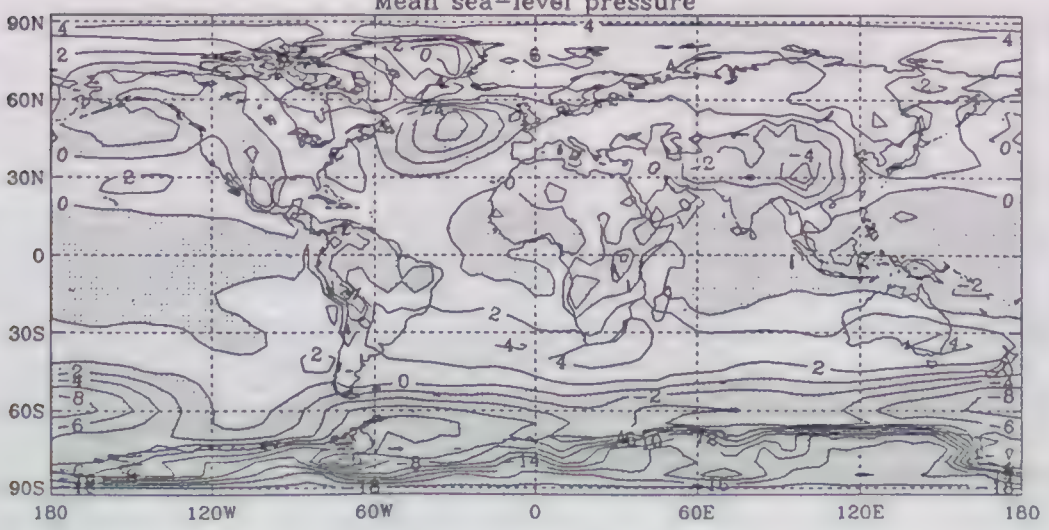

Area-weighted rms difference = 3.05

Figure 3(a) AMIP: 3rd Climate Version. 10-year Jun/Jul/Aug
Mean sea-level pressure
From 1/ 6/1979 to 1/ 9/1988

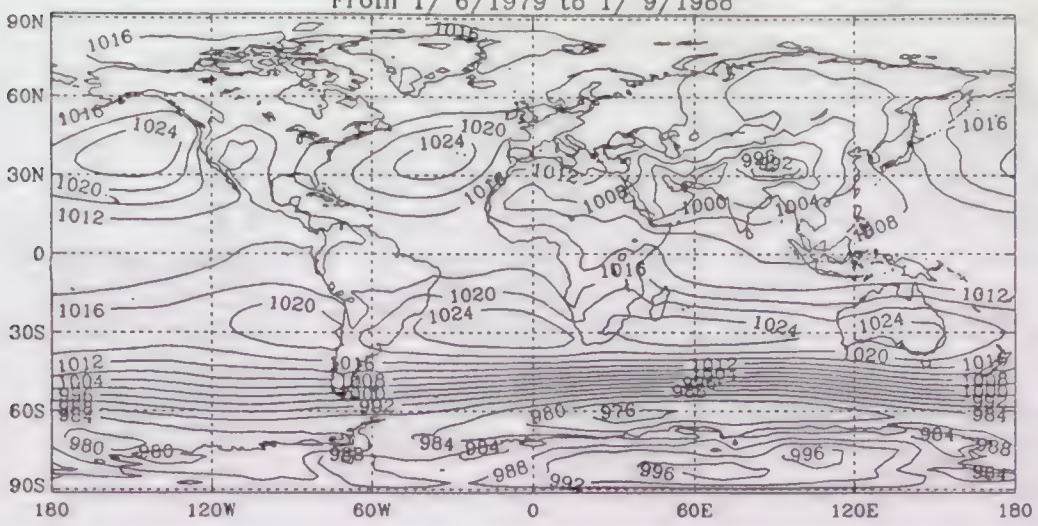

(b) AMIP: 3rd Climate Version. 10-year Jun/Jul/Aug minus
AMIP: 1st Climate Version. 10-year Jun/Jul/Aug
Mean sea-level pressure

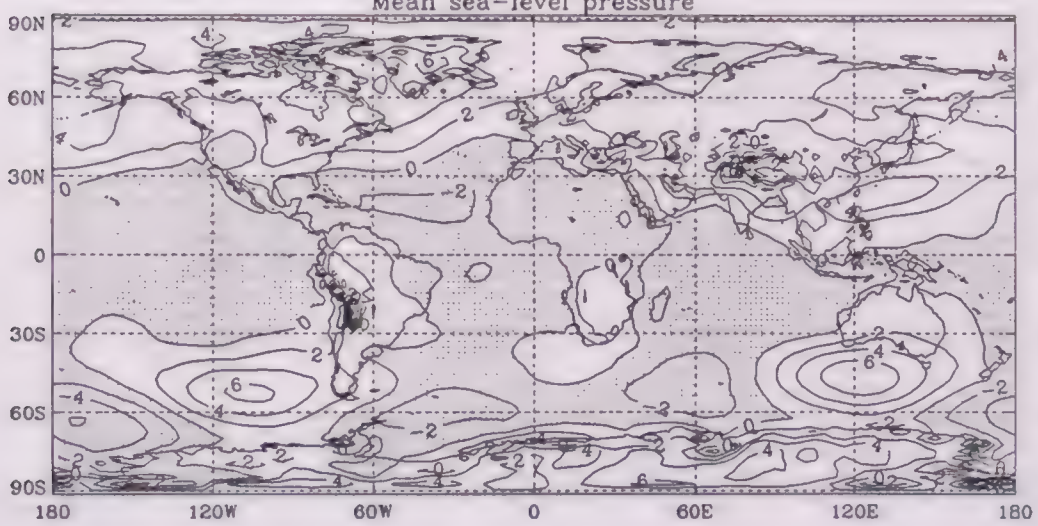

(c) AMIP: 3rd Climate Version. 10-year Jun/Jul/Aug minus
ECMWF climatology. Jun/Jul/Aug 1979-88
Mean sea-level pressure

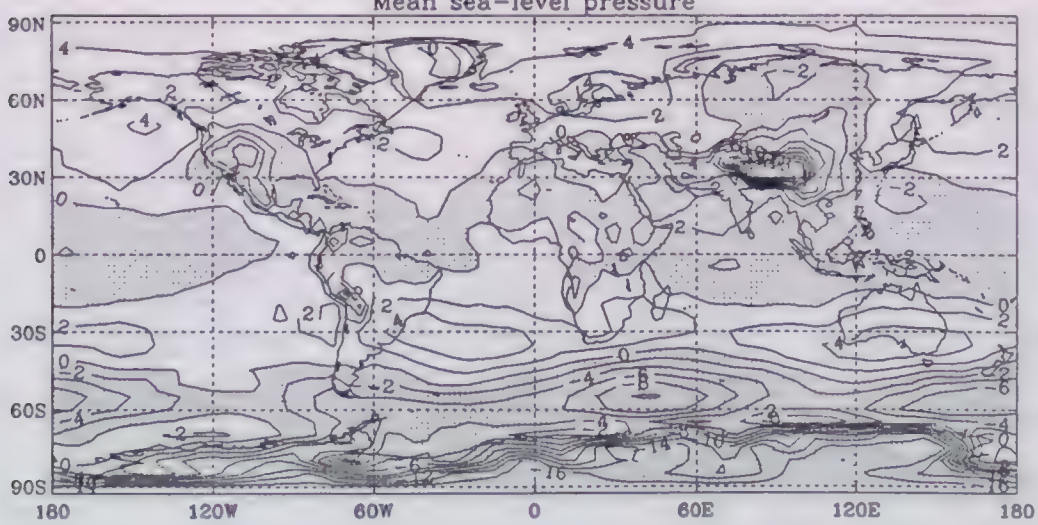

Area-weighted rms difference = 3.35

Figure 4(a) AMIP: 3rd Climate Version. 10-year Sep/Oct/Nov
Mean sea-level pressure
From 1/ 9/1979 to 1/12/1988

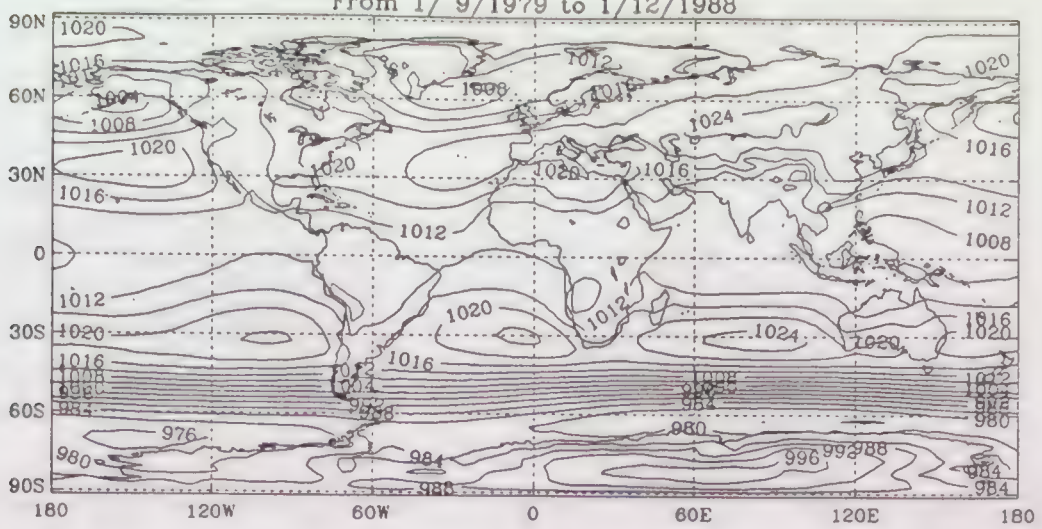

(b) AMIP: 3rd Climate Version. 10-year Sep/Oct/Nov minus
AMIP: 1st Climate Version. 10-year Sep/Oct/Nov
Mean sea-level pressure

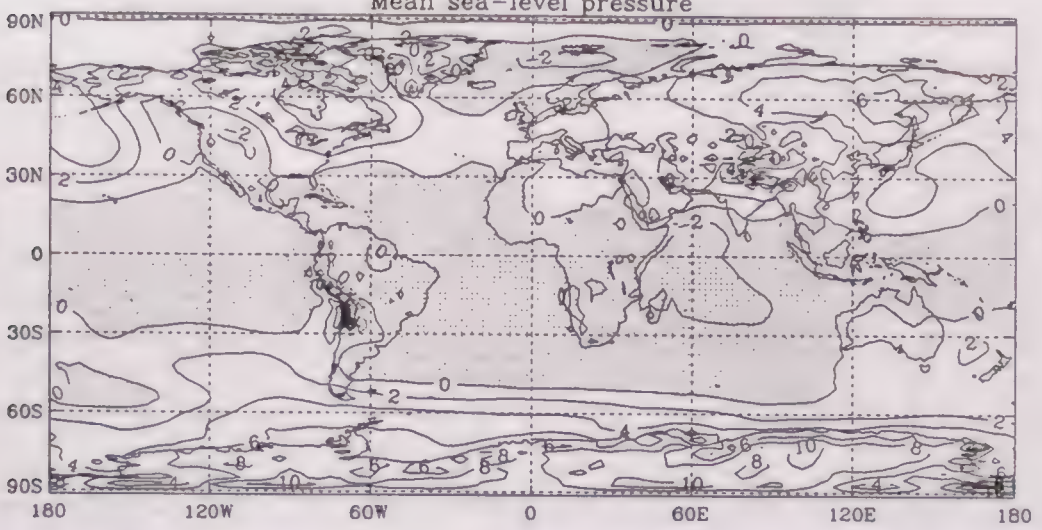

(c) AMIP: 3rd Climate Version. 10-year Sep/Oct/Nov minus
ECMWF climatology. Sep/Oct/Nov 1979-88
Mean sea-level pressure

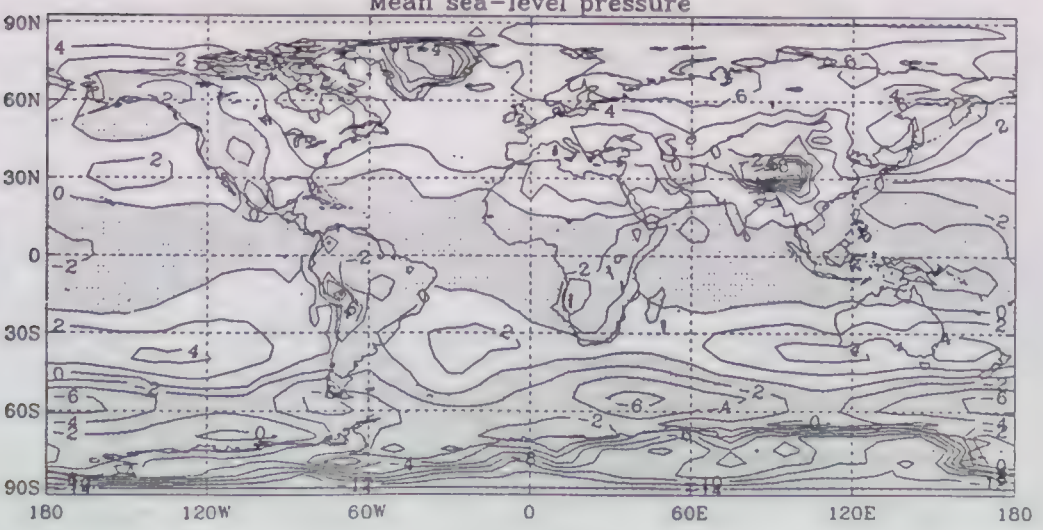

Area-weighted rms difference = 2.86

Figure 5(a) AMIP: 3rd Climate Version 10-year Dec/Jan/Feb
Zonal mean westerly component of wind
From 1/ 1/1979 to 1/ 1/1989

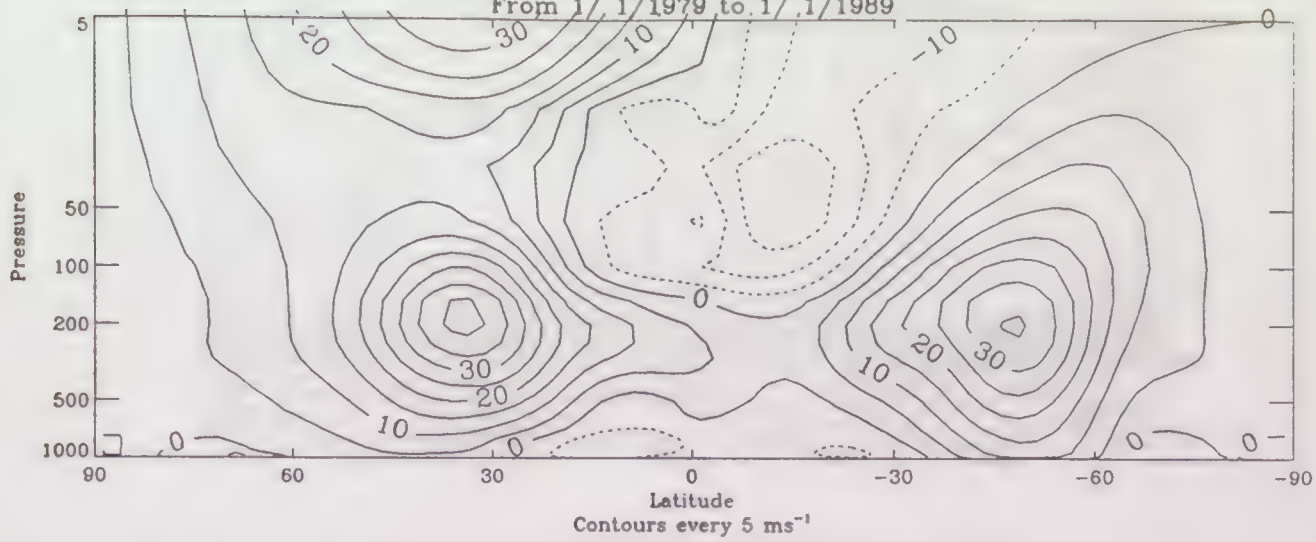

(b) AMIP: 3rd Climate Version. 10-year Dec/Jan/Feb minus
AMIP: 1st Climate Version. 10-year Dec/Jan/Feb
Zonal mean westerly component of wind

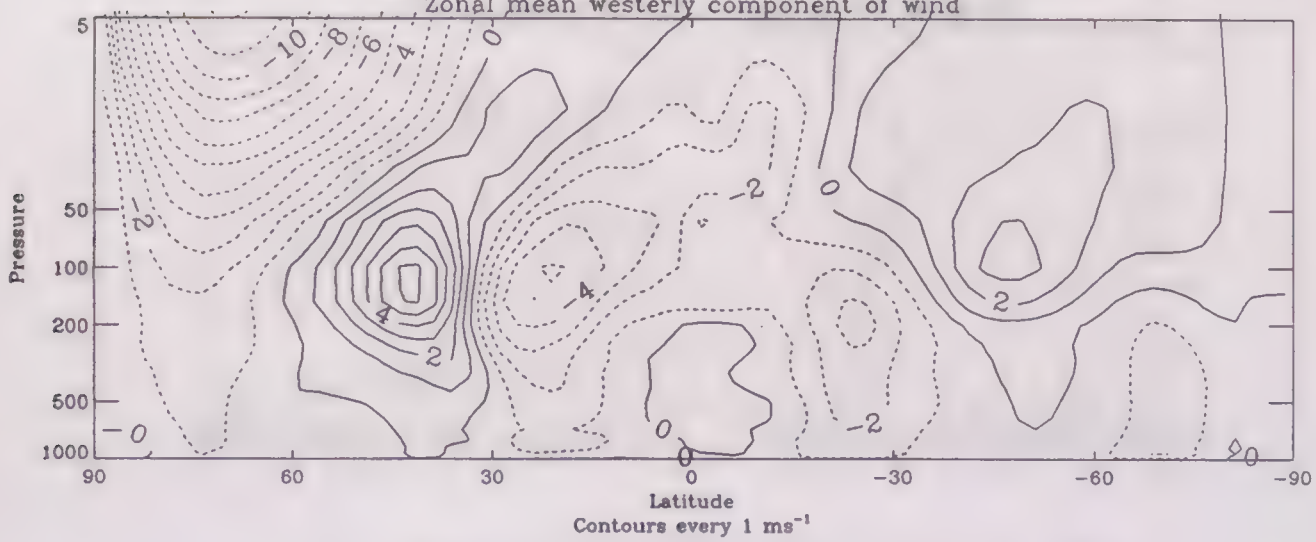

(c) AMIP: 3rd Climate Version. 10-year Dec/Jan/Feb minus
ECMWF climatology. Dec/Jan/Feb 1979-88
Zonal mean westerly component of wind

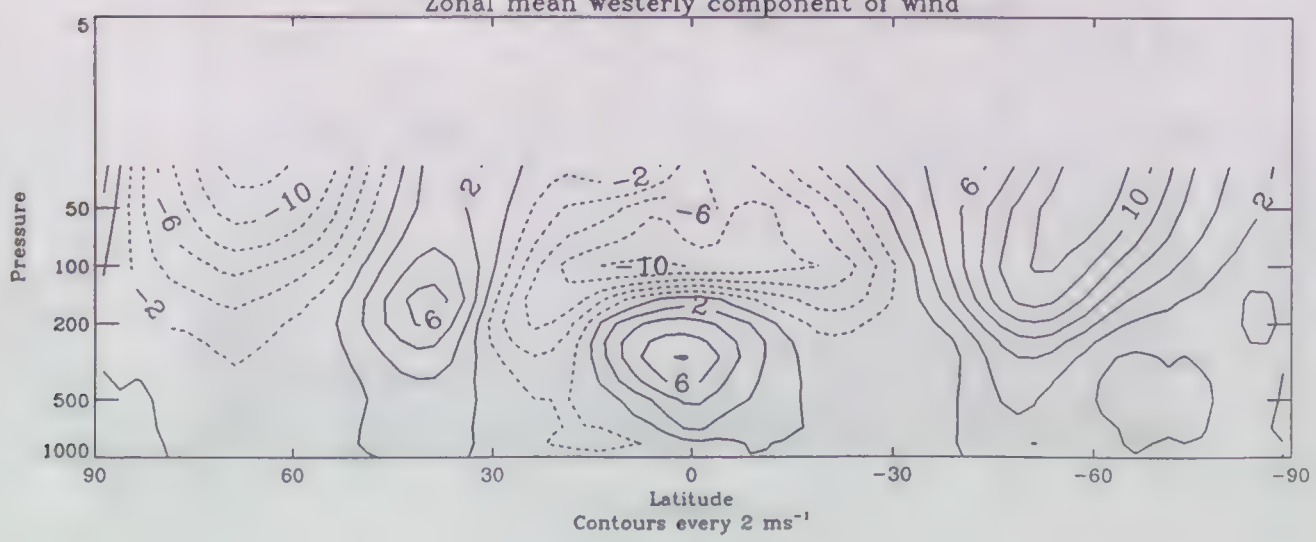

Figure 6(a) AMIP: 3rd Climate Version. 10-year Jun/Jul/Aug
Zonal mean westerly component of wind
From 1/ 6/1979 to 1/ 9/1988

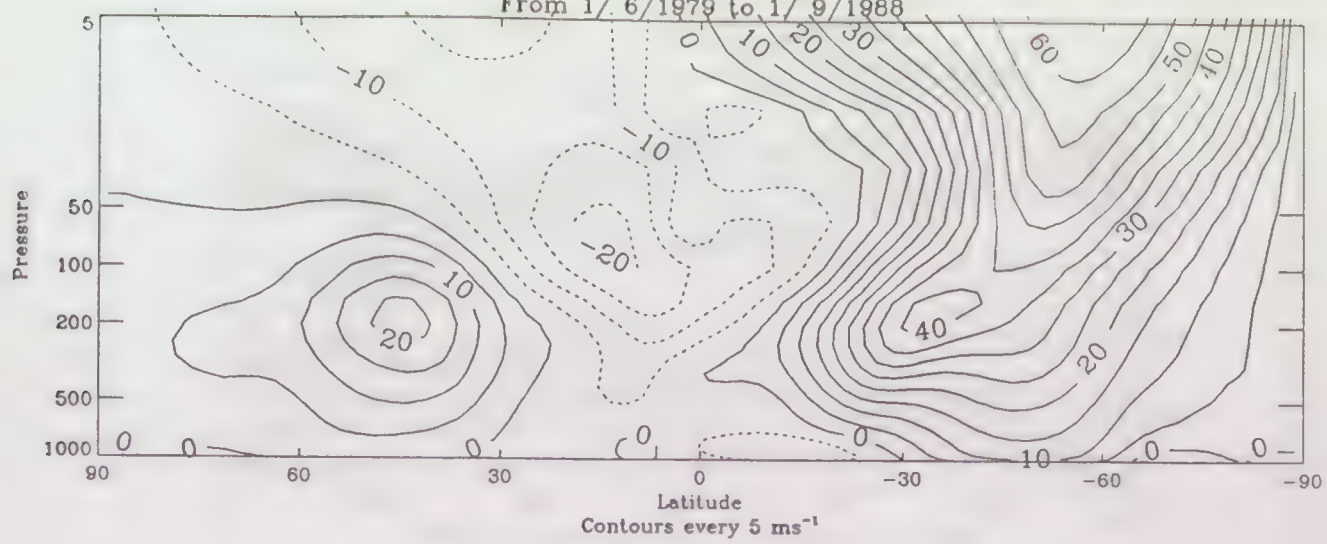

(b) AMIP: 3rd Climate Version. 10-year Jun/Jul/Aug minus
AMIP: 1st Climate Version. 10-year Jun/Jul/Aug
Zonal mean westerly component of wind

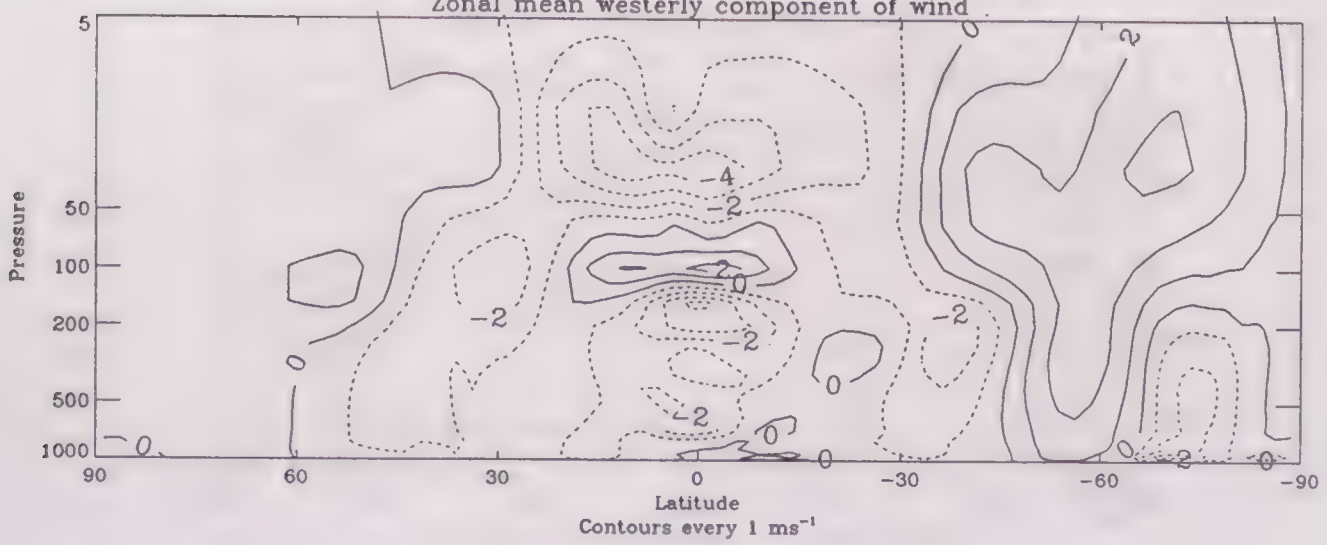

(c) AMIP: 3rd Climate Version. 10-year Jun/Jul/Aug minus
ECMWF climatology. Jun/Jul/Aug 1979-88
Zonal mean westerly component of wind

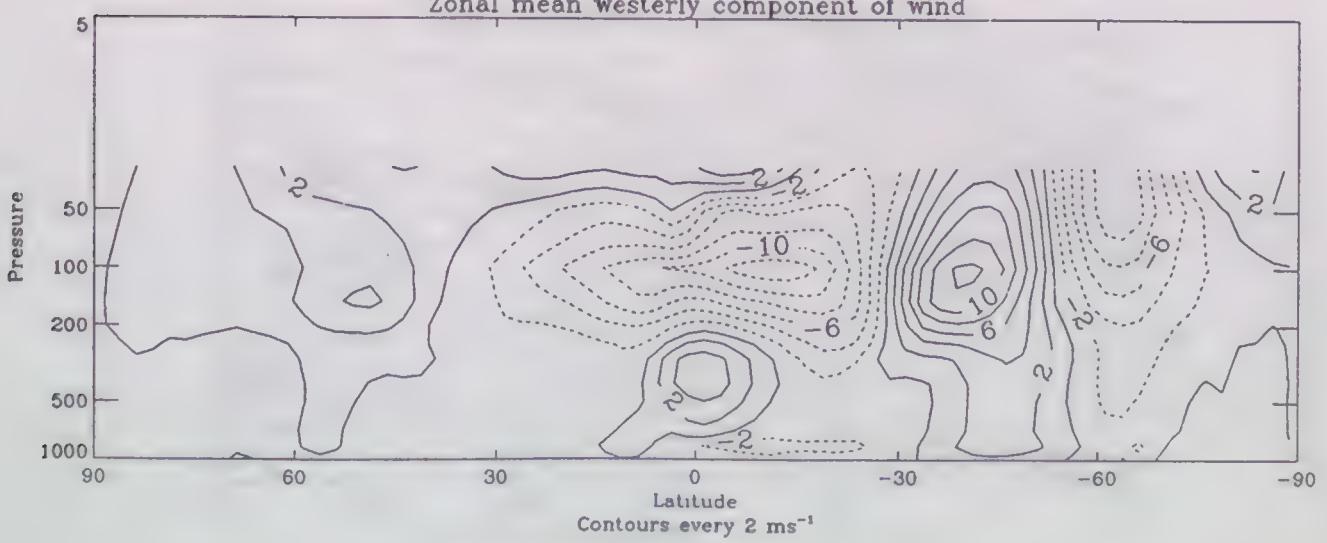

Figure 7(a) Amip: 3rd Climate Version. 10-year Dec/Jan/Feb
Vector wind and isotachs at 250 mb
From 1/ 1/1979 to 1/ 1/1989

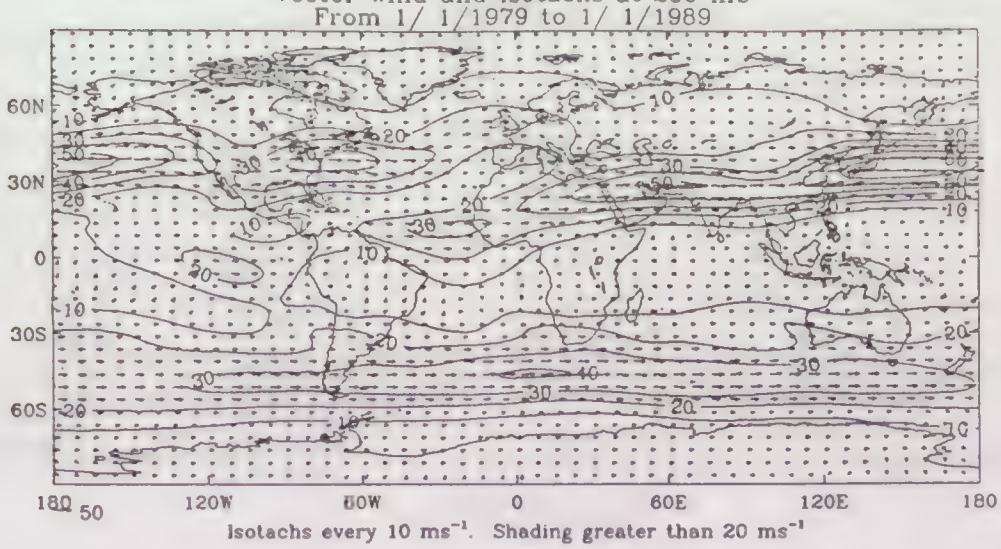

Isotachs every 10 ms^{-1}. Shading greater than 20 ms^{-1}

(b) Amip: 3rd Climate Version. 10-year Dec/Jan/Feb minus
AMIP: 1st Climate Version. 10-year Dec/Jan/Feb
Vector wind and isotachs at 250 mb

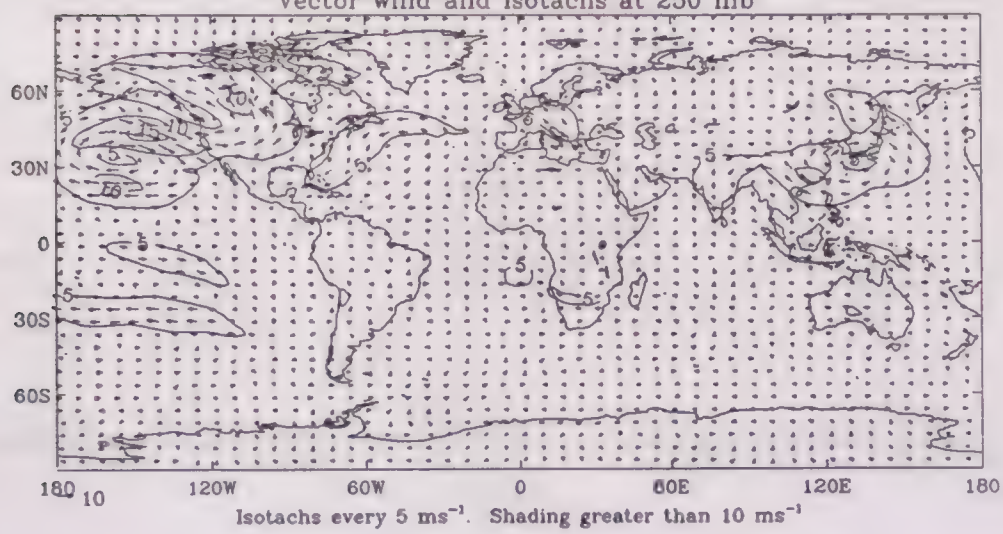

Isotachs every 5 ms^{-1}. Shading greater than 10 ms^{-1}

(c) Amip: 3rd Climate Version. 10-year Dec/Jan/Feb minus
ECMWF climatology. Dec/Jan/Feb 1979-88
Vector wind and isotachs at 250 mb

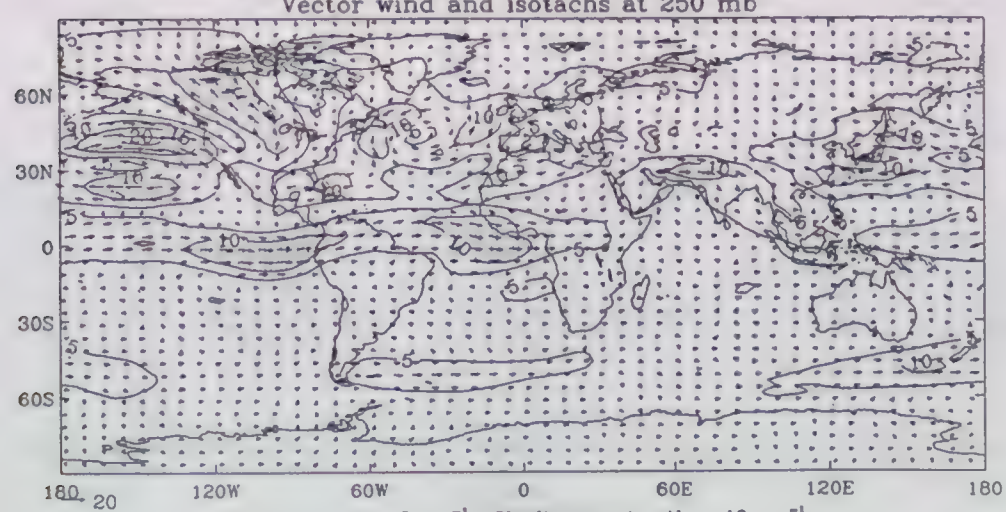

Isotachs every 5 ms^{-1}. Shading greater than 10 ms^{-1}

Figure 8(a) Amip: 3rd Climate Version. 10-year Jun/Jul/Aug
Vector wind and isotachs at 250 mb
From 1/ 6/1979 to 1/ 9/1988

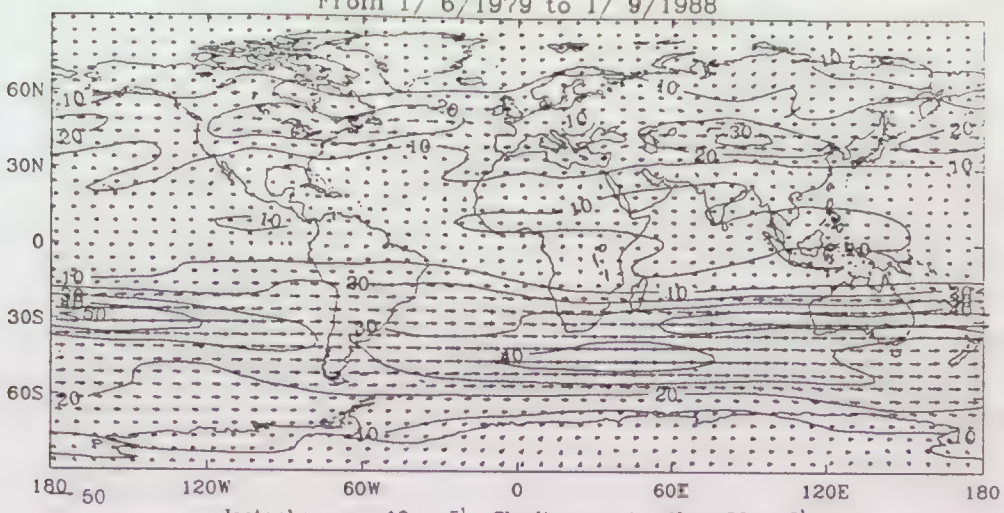

Isotachs every 10 ms^{-1}. Shading greater than 20 ms^{-1}

(b) Amip: 3rd Climate Version. 10-year Jun/Jul/Aug minus
AMIP: 1st Climate Version. 10-year Jun/Jul/Aug
Vector wind and isotachs at 250 mb

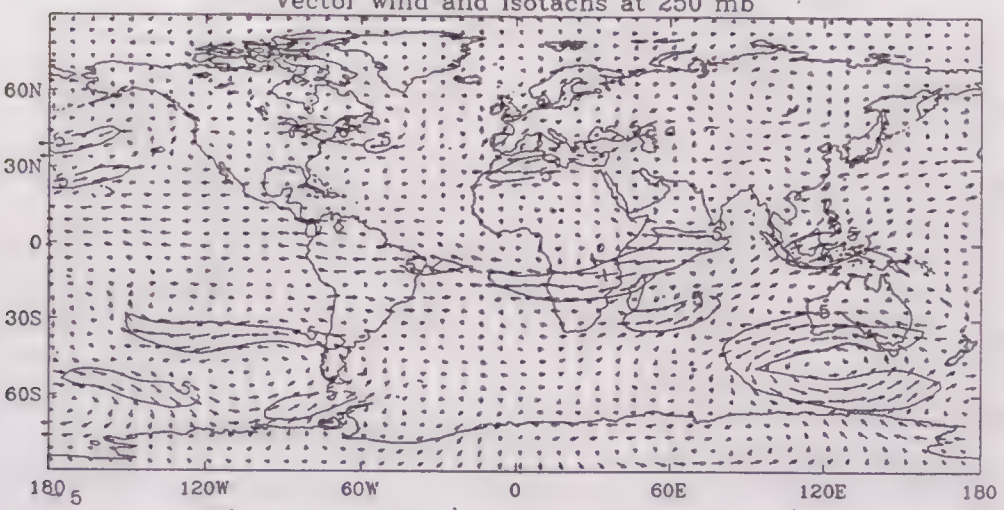

Isotachs every 5 ms^{-1}. Shading greater than 10 ms^{-1}

(c) Amip: 3rd Climate Version. 10-year Jun/Jul/Aug minus
ECMWF climatology. Jun/Jul/Aug 1979-88
Vector wind and isotachs at 250 mb

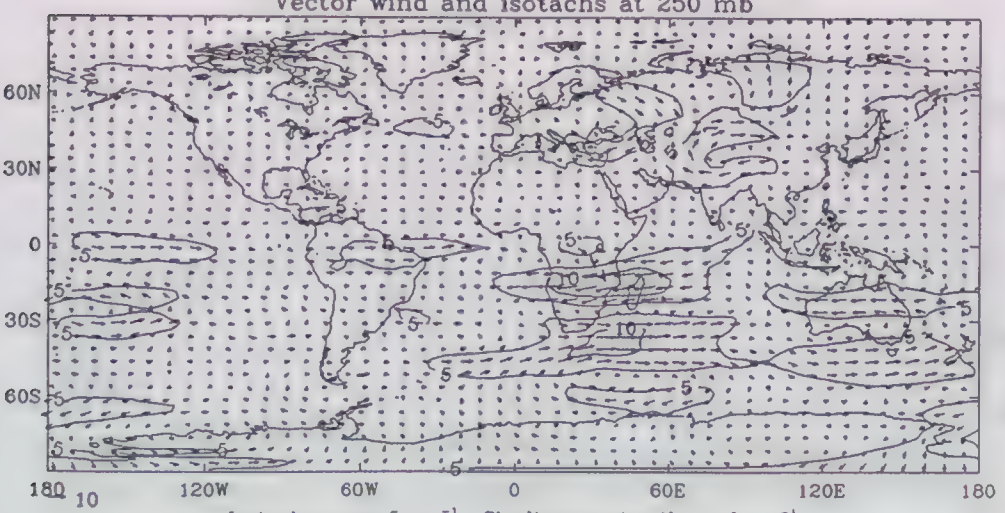

Isotachs every 5 ms^{-1}. Shading greater than 10 ms^{-1}

Figure 9(a) AMIP: 3rd Climate Version. 10-year Dec/Jan/Feb
Vector wind and isotachs at 850 mb
From 1/ 1/1979 to 1/ 1/1989

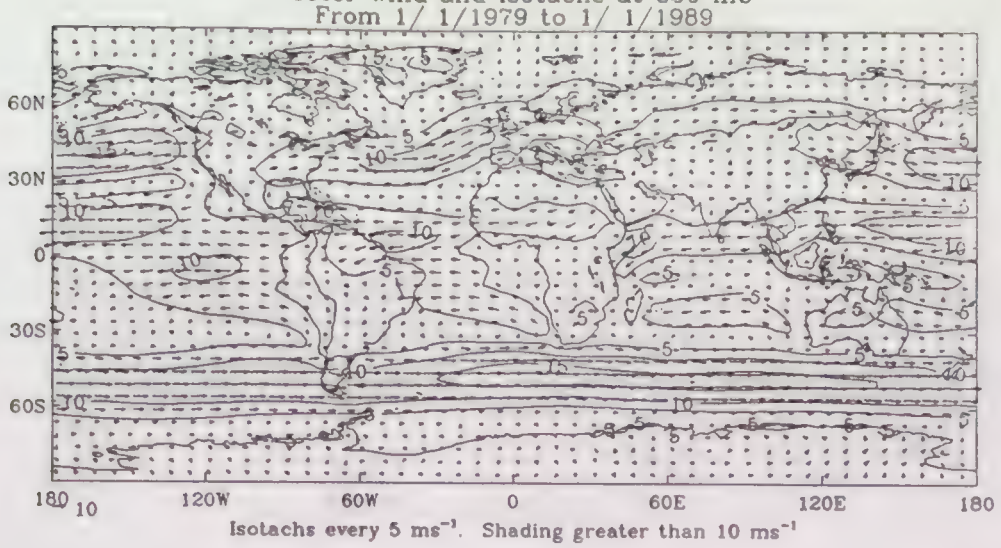

Isotachs every 5 ms^{-1}. Shading greater than 10 ms^{-1}

(b) AMIP: 3rd Climate Version. 10-year Dec/Jan/Feb minus
AMIP: 1st Climate Version. 10-year Dec/Jan/Feb
Vector wind and isotachs at 850 mb

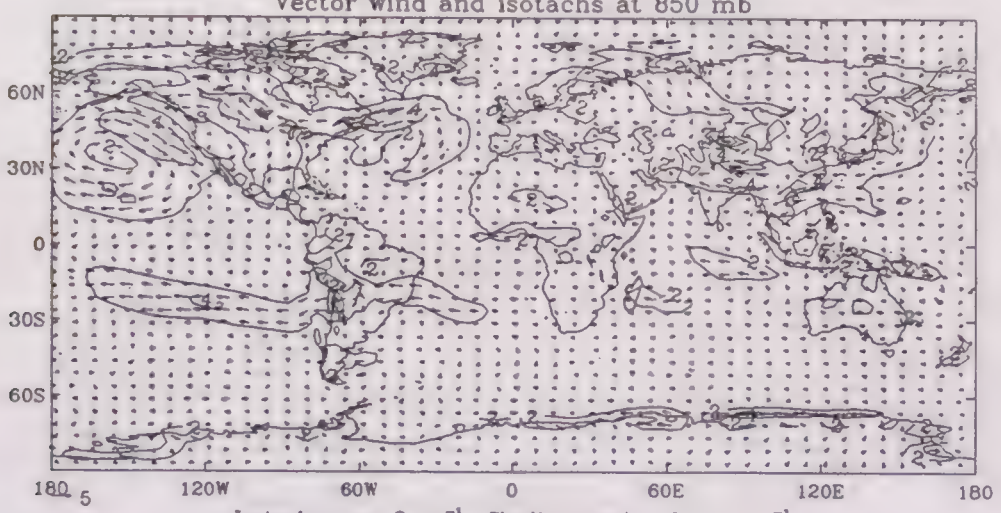

Isotachs every 2 ms^{-1}. Shading greater than 4 ms^{-1}

(c) AMIP: 3rd Climate Version. 10-year Dec/Jan/Feb minus
ECMWF climatology. Dec/Jan/Feb 1979-88
Vector wind and isotachs at 850 mb

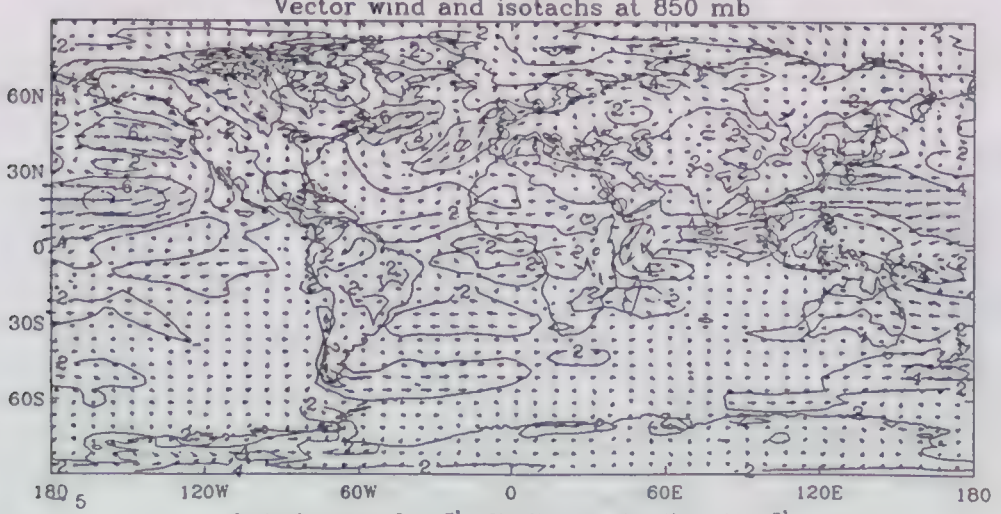

Isotachs every 2 ms^{-1}. Shading greater than 4 ms^{-1}

Figure 10(a) AMIP: 3rd Climate Version 10-year Jun/Jul/Aug
Vector wind and isotachs at 850 mb
From 1/ 6/1979 to 1/ 9/1988

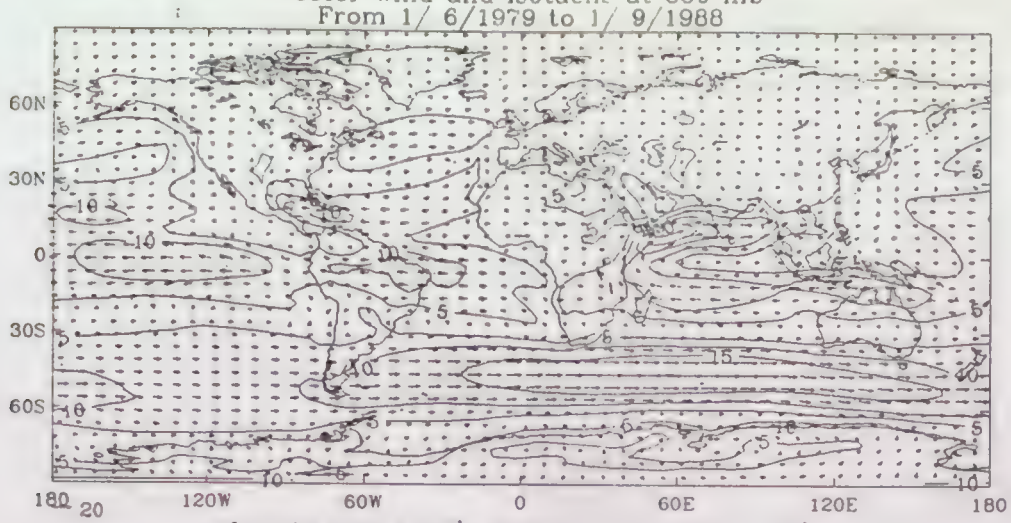

Isotachs every 5 ms^{-1}. Shading greater than 10 ms^{-1}

(b) AMIP: 3rd Climate Version. 10-year Jun/Jul/Aug minus
AMIP: 1st Climate Version. 10-year Jun/Jul/Aug
Vector wind and isotachs at 850 mb

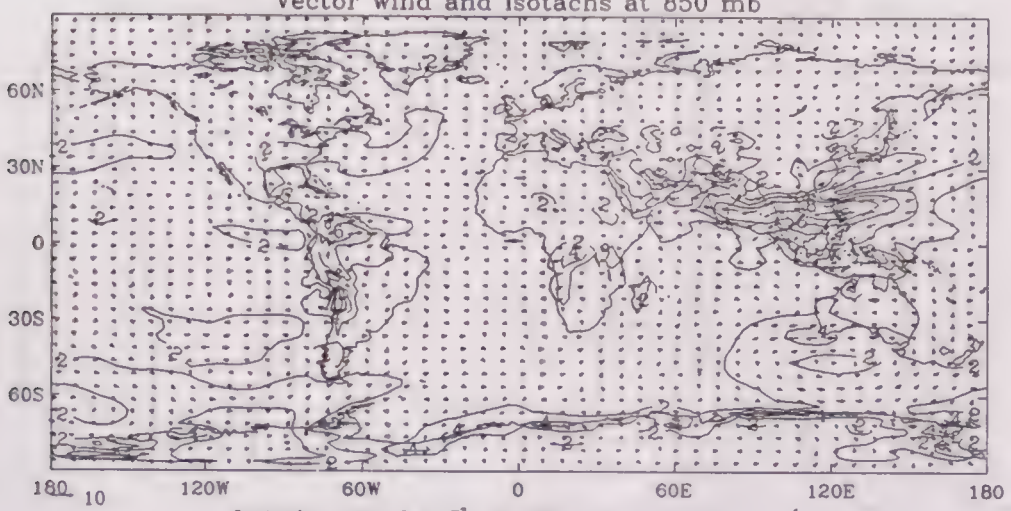

Isotachs every 2 ms^{-1}. Shading greater than 4 ms^{-1}

(c) AMIP: 3rd Climate Version. 10-year Jun/Jul/Aug minus
ECMWF climatology. Jun/Jul/Aug 1979-88
Vector wind and isotachs at 850 mb

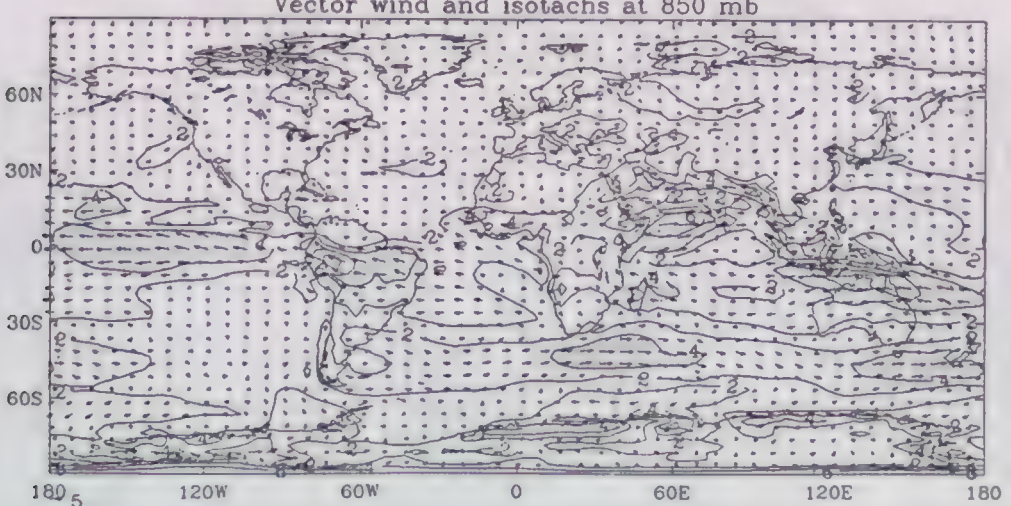

Isotachs every 2 ms^{-1}. Shading greater than 4 ms^{-1}

Figure 11(a) AMIP: 3rd Climate Version. 10-year Dec/Jan/Feb
Zonal mean stream function
From 1/ 1/1979 to 1/ 1/1989

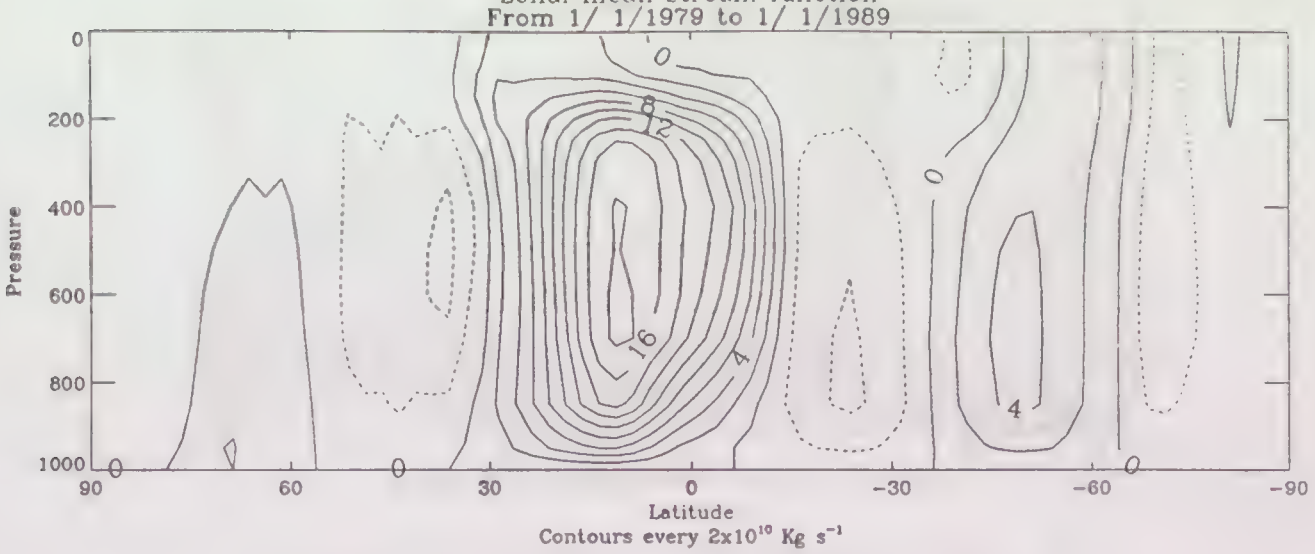

(b) AMIP: 3rd Climate Version. 10-year Dec/Jan/Feb minus
AMIP: 1st Climate Version. 10-year Dec/Jan/Feb
Zonal mean stream function

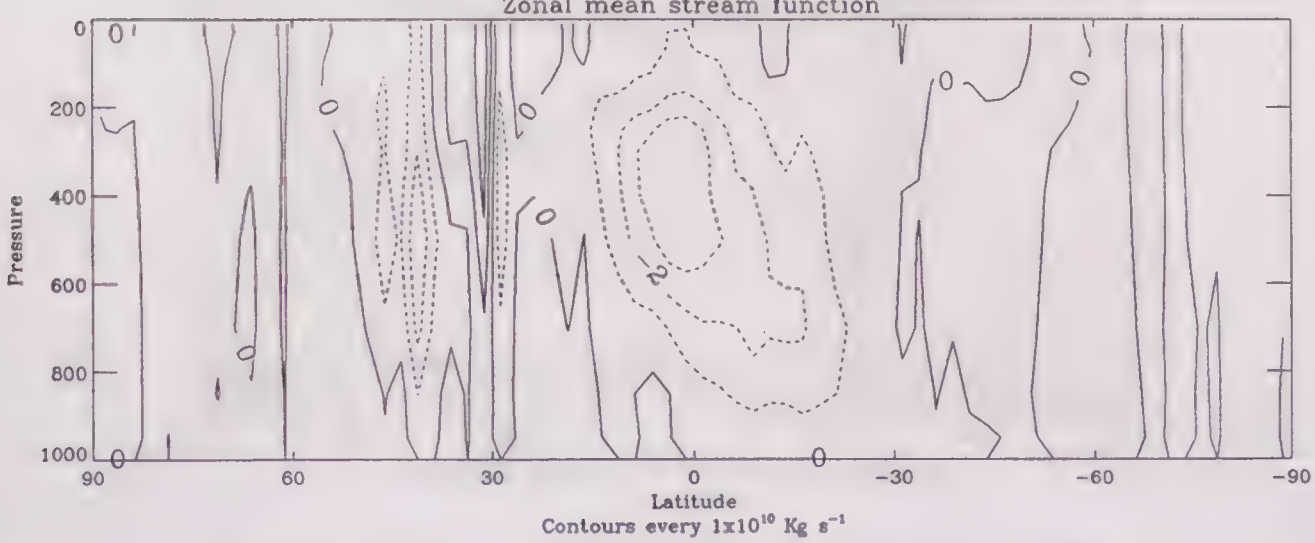

(c) AMIP: 3rd Climate Version. 10-year Dec/Jan/Feb minus
ECMWF climatology. Dec/Jan/Feb 1985-91
Zonal mean stream function

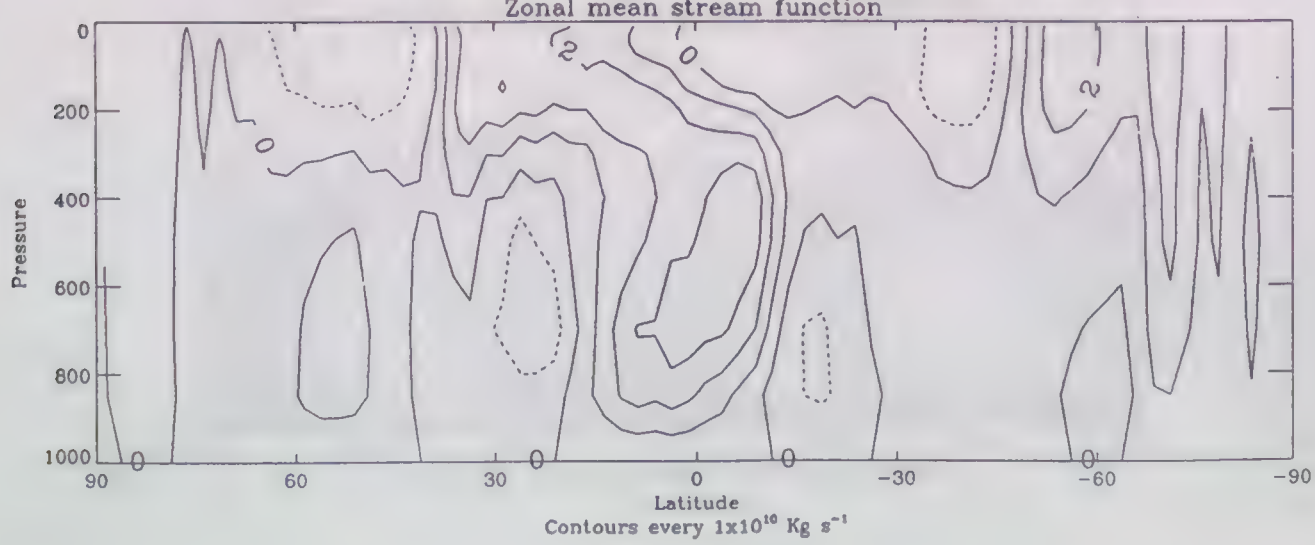

Figure 12(a) AMIP: 3rd Climate Version. 10-year Jun/Jul/Aug
Zonal mean stream function
From 1/ 6/1979 to 1/ 9/1988

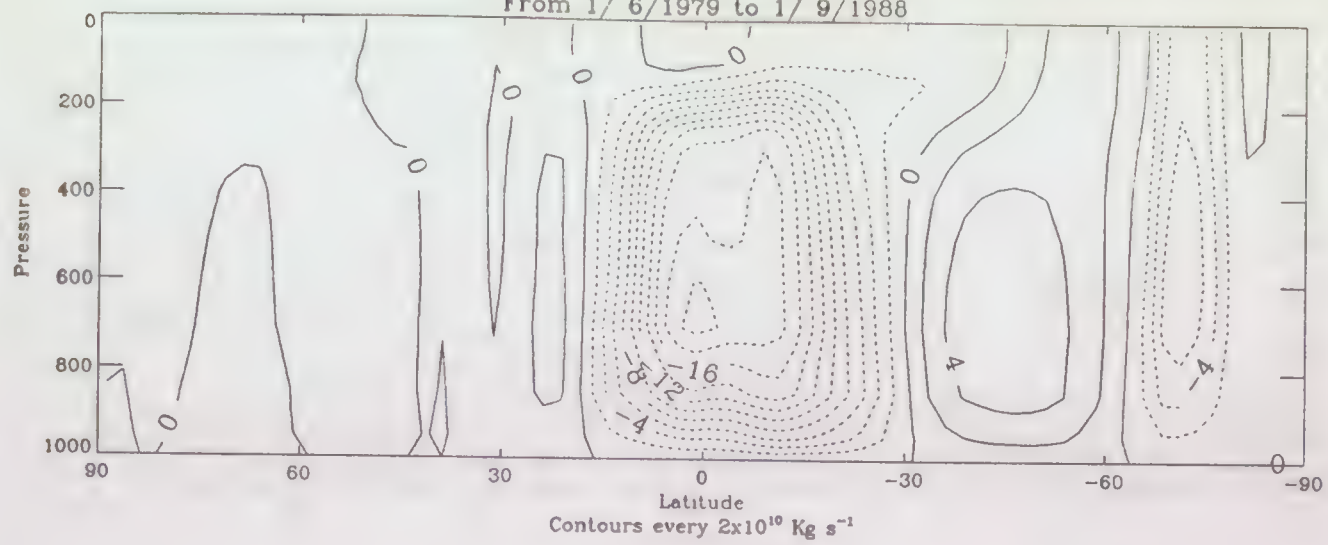

(b) AMIP: 3rd Climate Version. 10-year Jun/Jul/Aug minus
AMIP: 1st Climate Version. 10-year Jun/Jul/Aug
Zonal mean stream function

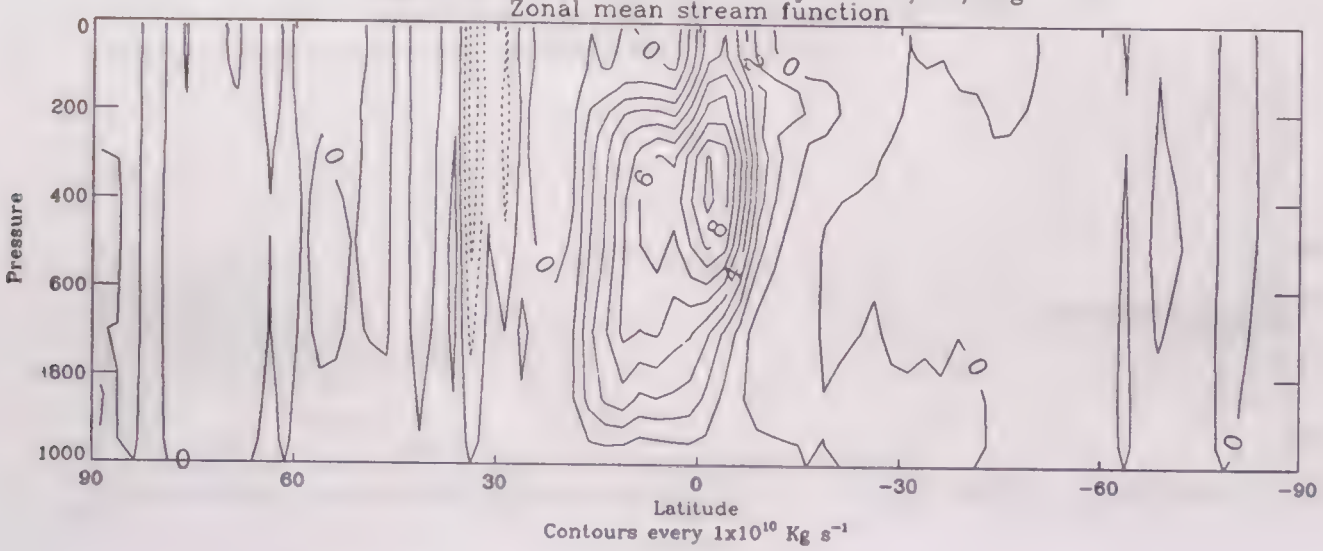

(c) AMIP: 3rd Climate Version. 10-year Jun/Jul/Aug minus
ECMWF climatology. Jun/Jul/Aug 1985-91
Zonal mean stream function

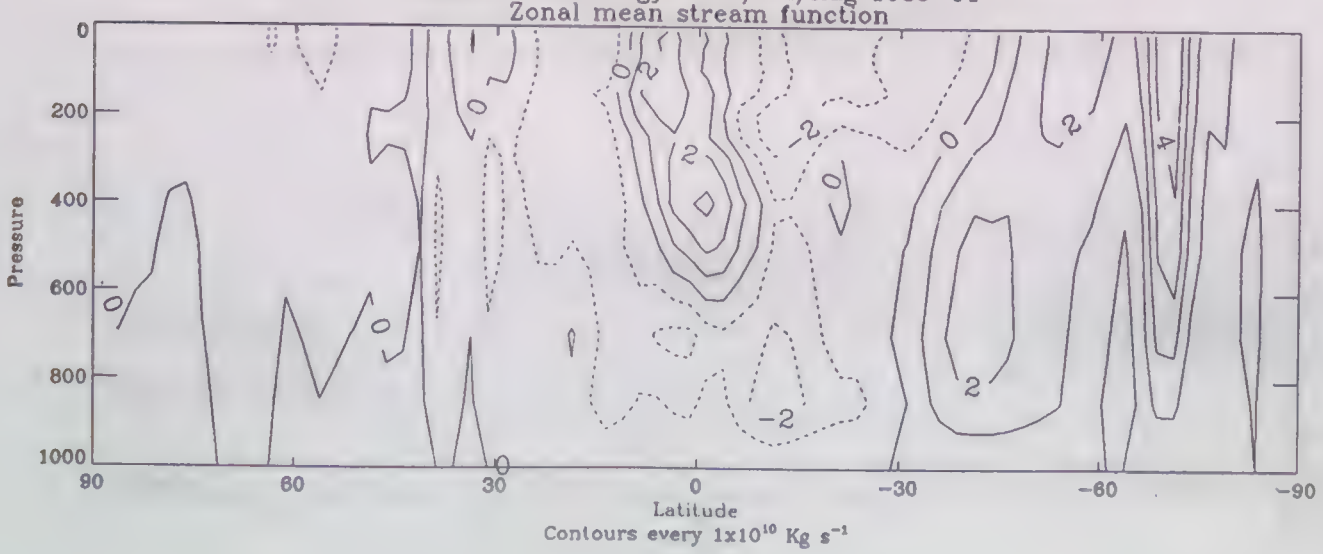

Figure 13(a) AMIP: 3rd Climate Version. 10-year Dec/Jan/Feb
Zonal mean temperature
From 1/ 1/1979 to 1/ 1/1989

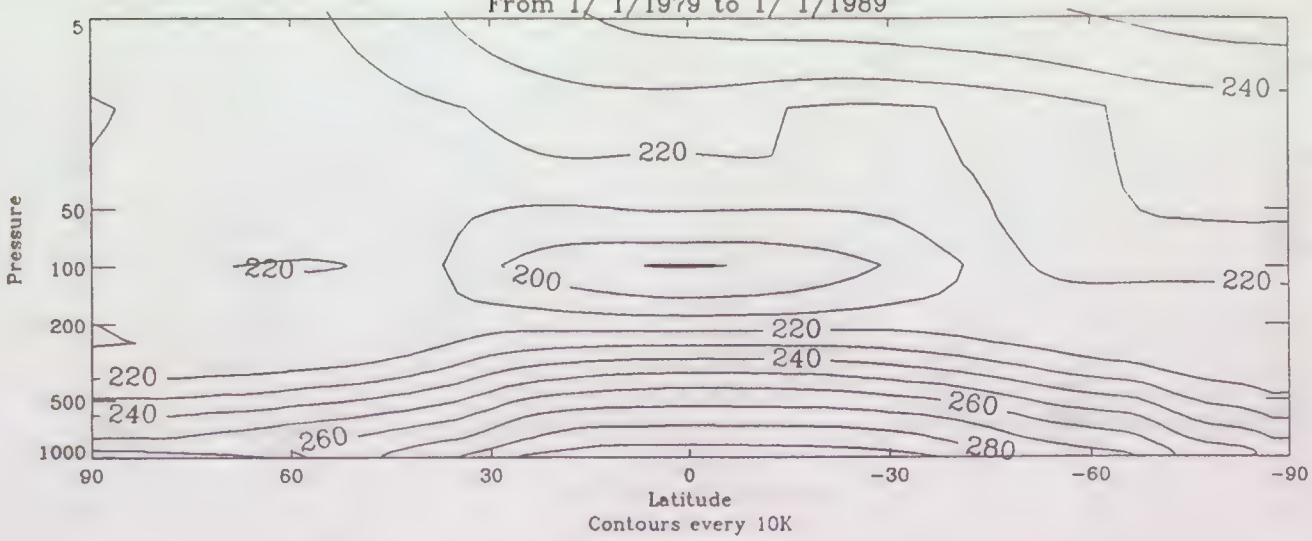

(b) AMIP: 3rd Climate Version. 10-year Dec/Jan/Feb minus
AMIP: 1st Climate Version. 10-year Dec/Jan/Feb
Zonal mean temperature

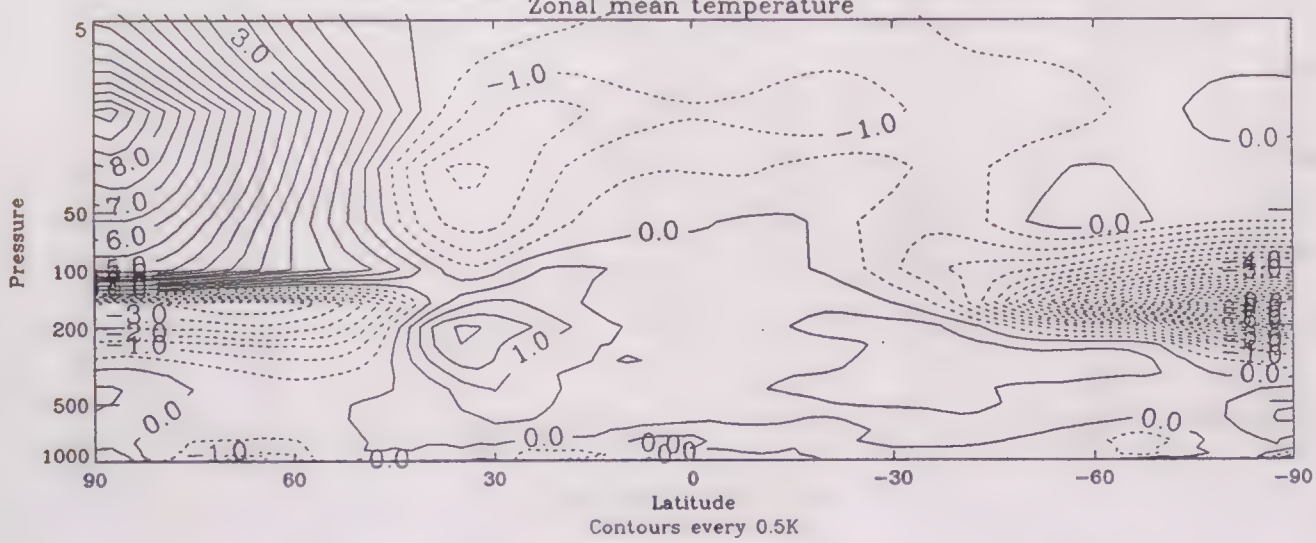

(c) AMIP: 3rd Climate Version. 10-year Dec/Jan/Feb minus
ECMWF climatology. Dec/Jan/Feb 1979-88
Zonal mean temperature

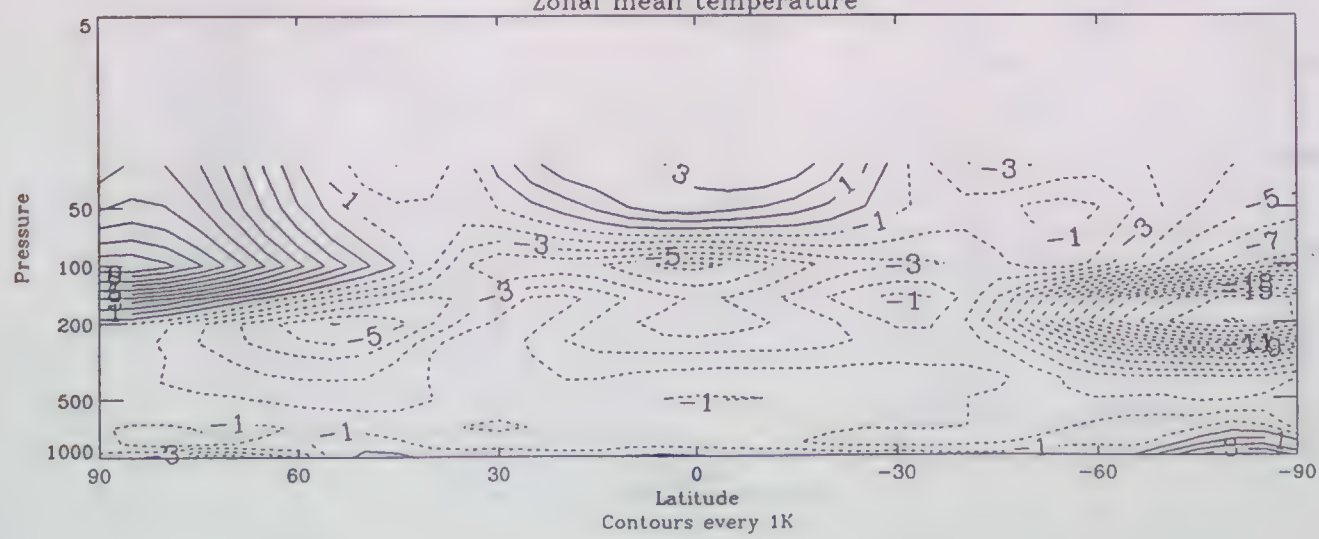

Figure 14(a) AMIP: 3rd Climate Version 10-year Jun/Jul/Aug
Zonal mean temperature
From 1/ 6/1979 to 1/ 9/1988

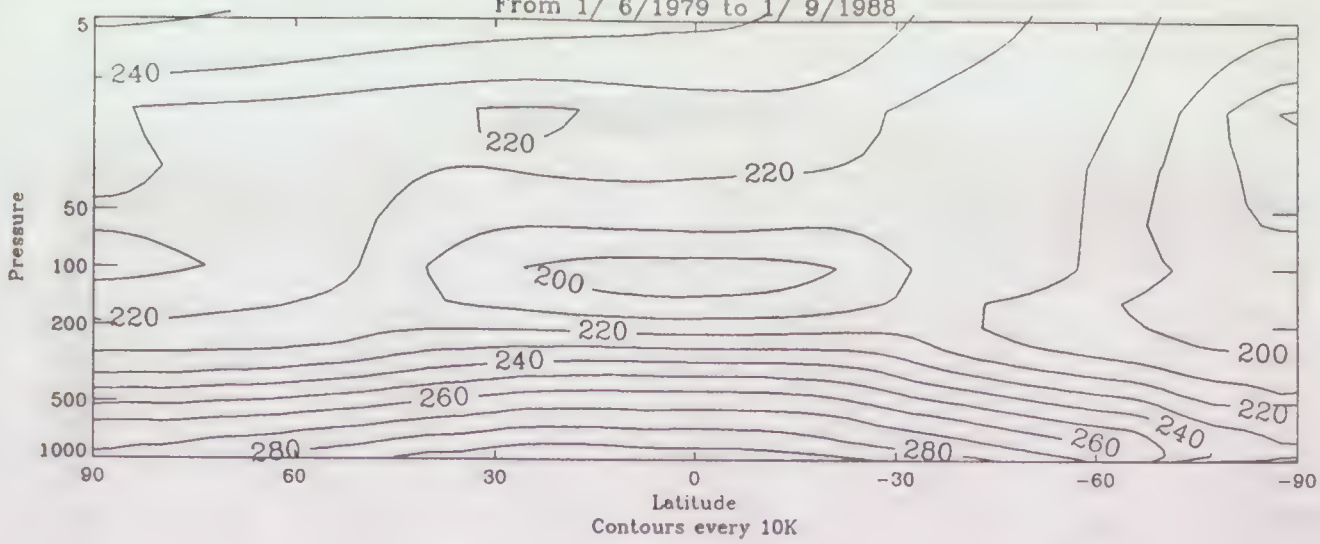

(b) AMIP: 3rd Climate Version. 10-year Jun/Jul/Aug minus
AMIP: 1st Climate Version. 10-year Jun/Jul/Aug
Zonal mean temperature

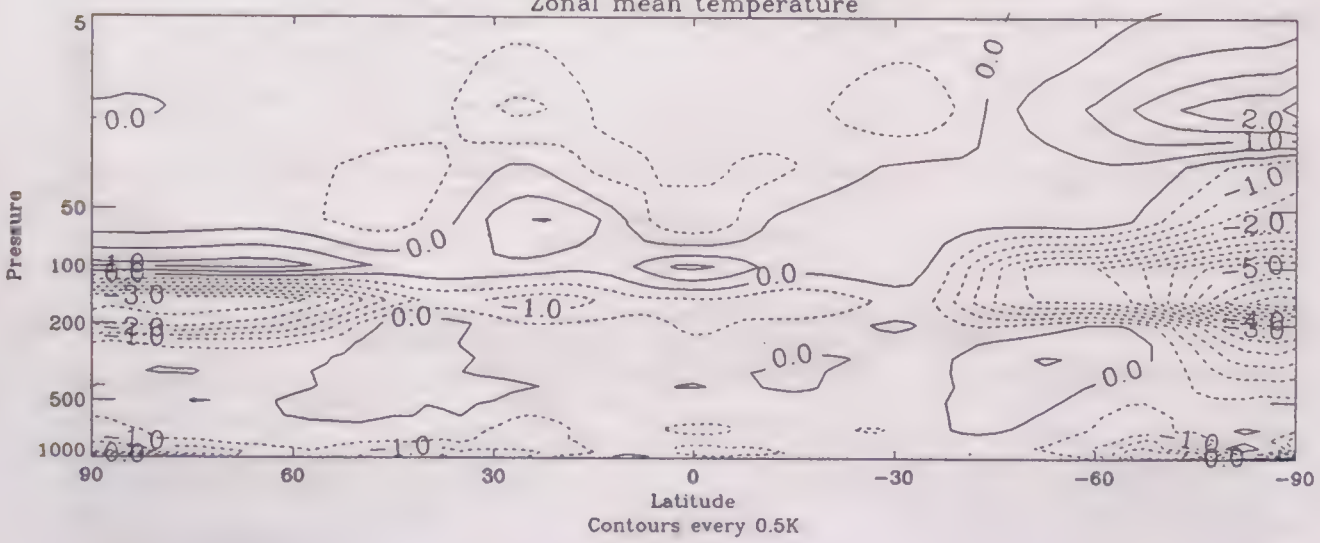

(c) AMIP: 3rd Climate Version. 10-year Jun/Jul/Aug minus
ECMWF climatology. Jun/Jul/Aug 1979-88
Zonal mean temperature

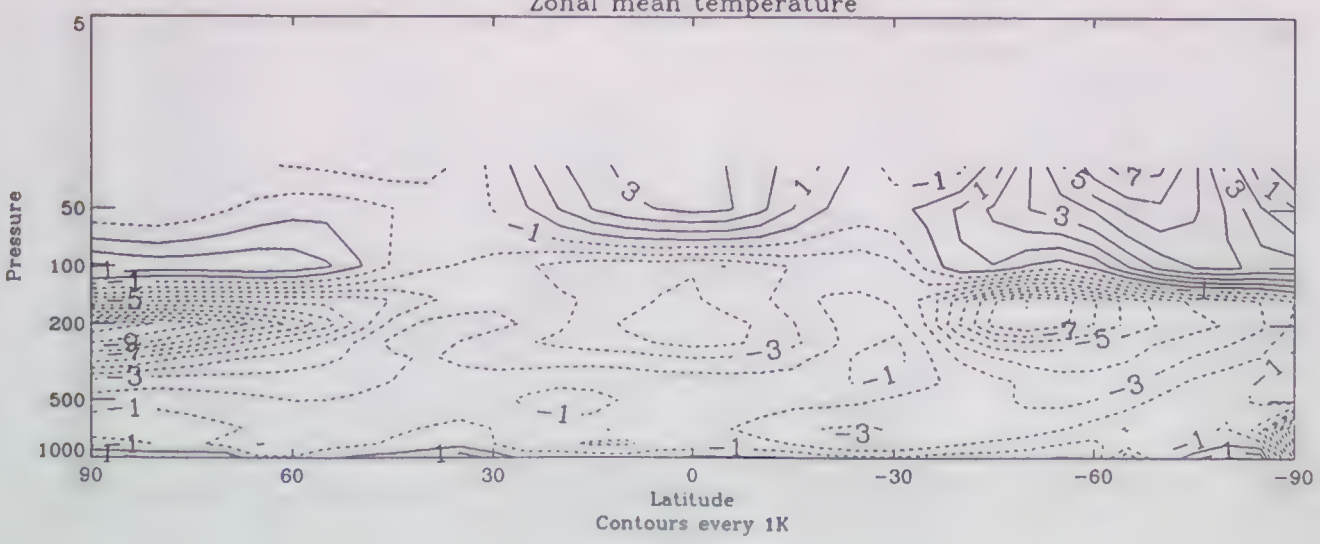

Figure 15(a) AMIP: 3rd Climate Version. 10-year Dec/Jan/Feb
Zonal mean relative humidity
From 1/ 1/1979 to 1/ 1/1989

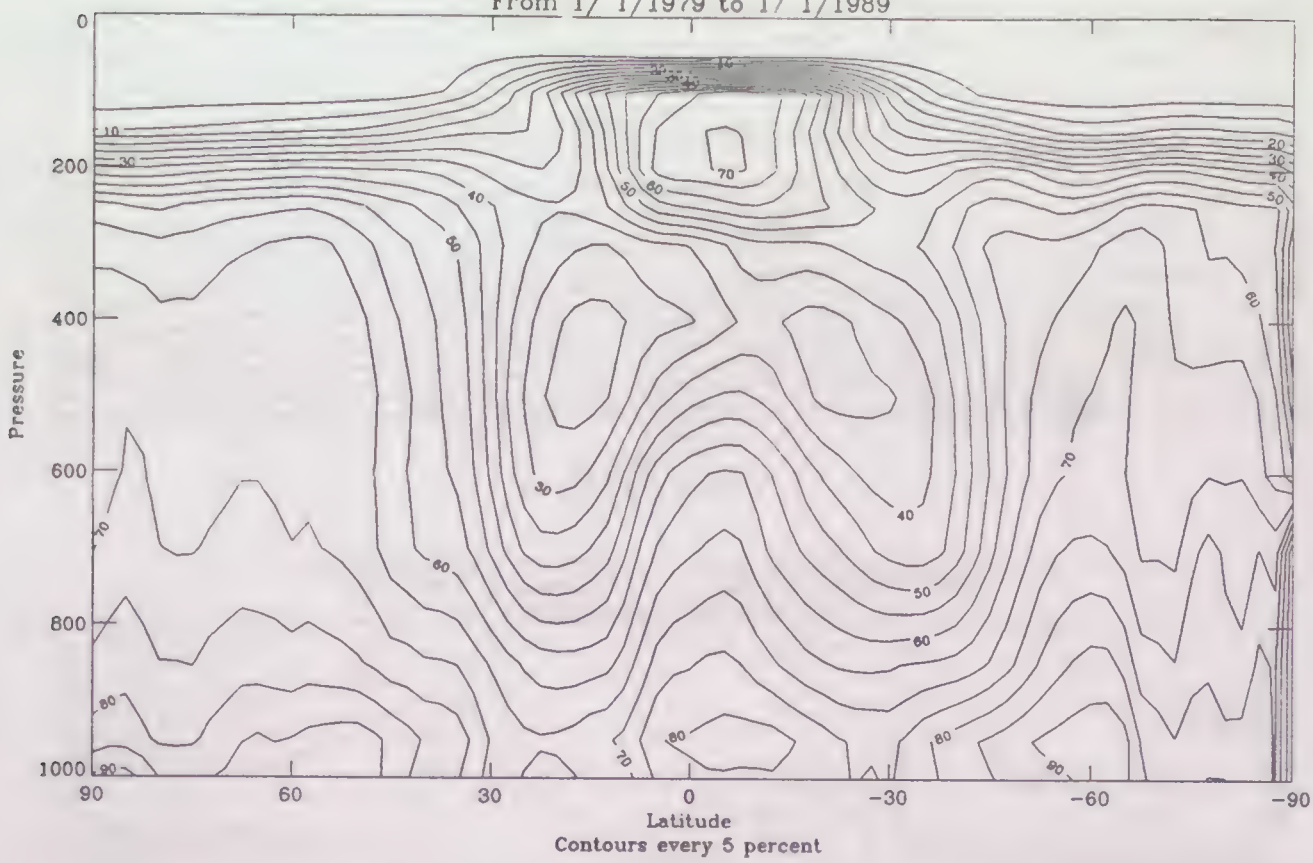

(b) AMIP: 3rd Climate Version. 10-year Dec/Jan/Feb minus
AMIP: 1st Climate Version. 10-year Dec/Jan/Feb
Zonal mean relative humidity

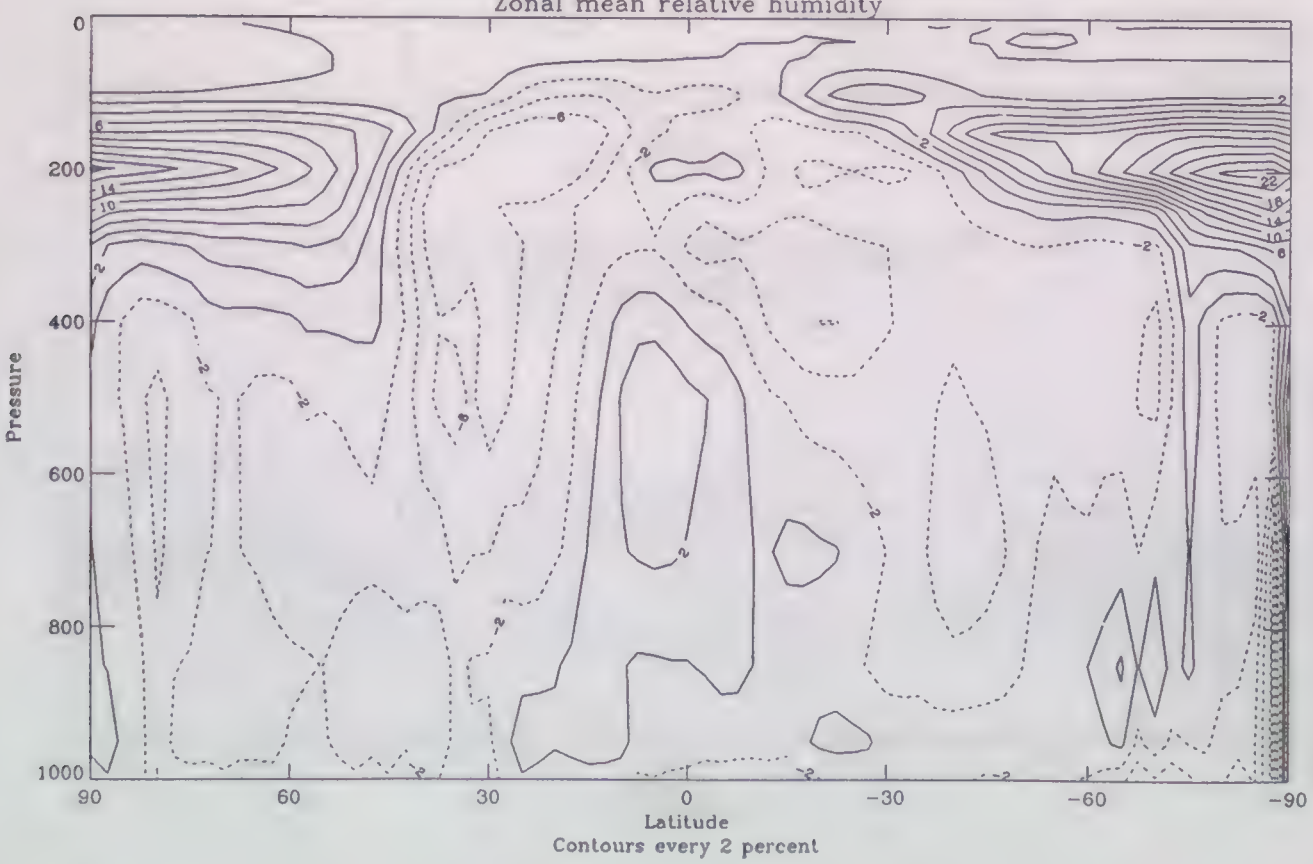

Figure 16(a) AMIP: 3rd Climate Version. 10-year Jun/Jul/Aug
Zonal mean relative humidity
From 1/ 6/1979 to 1/ 9/1988

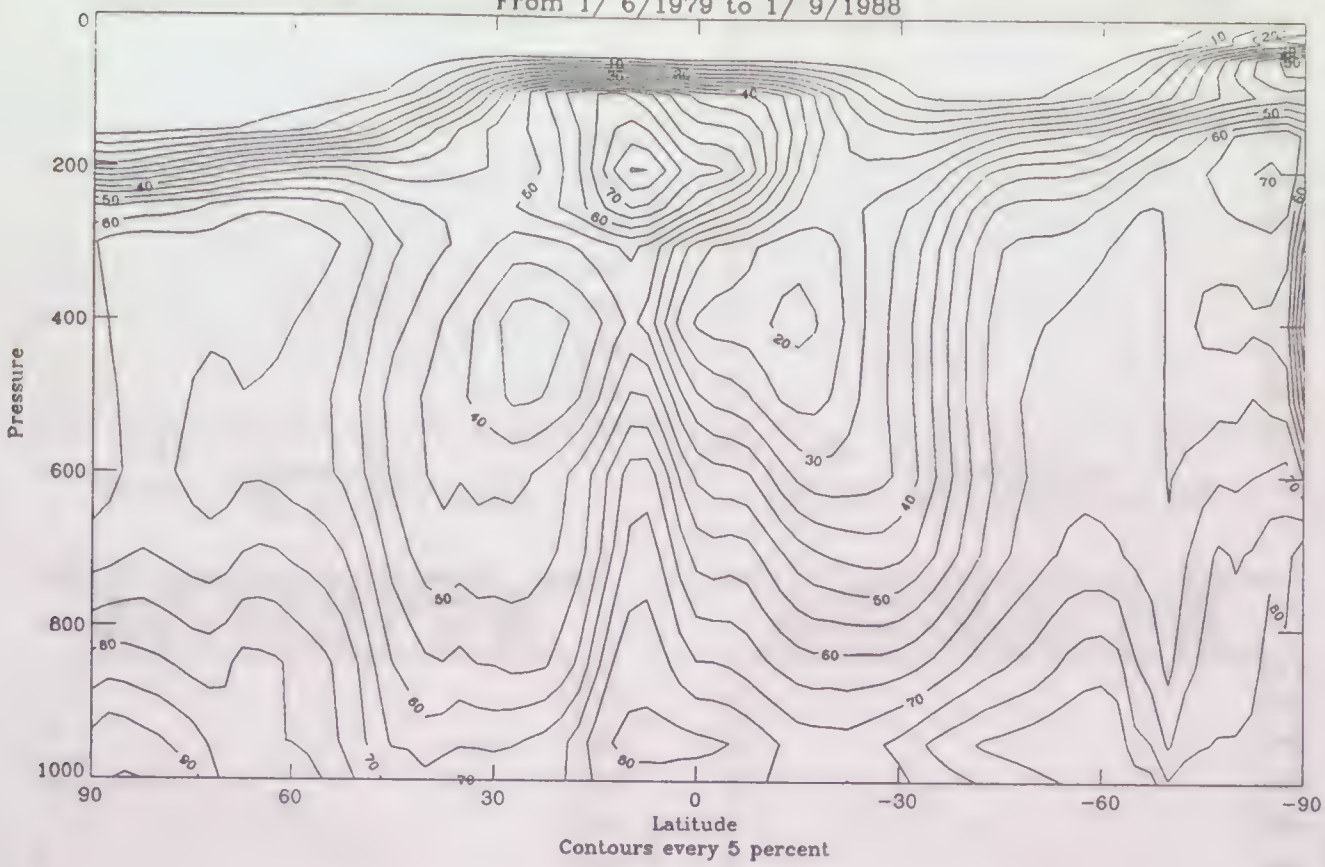

(b) AMIP: 3rd Climate Version. 10-year Jun/Jul/Aug minus
AMIP: 1st Climate Version. 10-year Jun/Jul/Aug
Zonal mean relative humidity

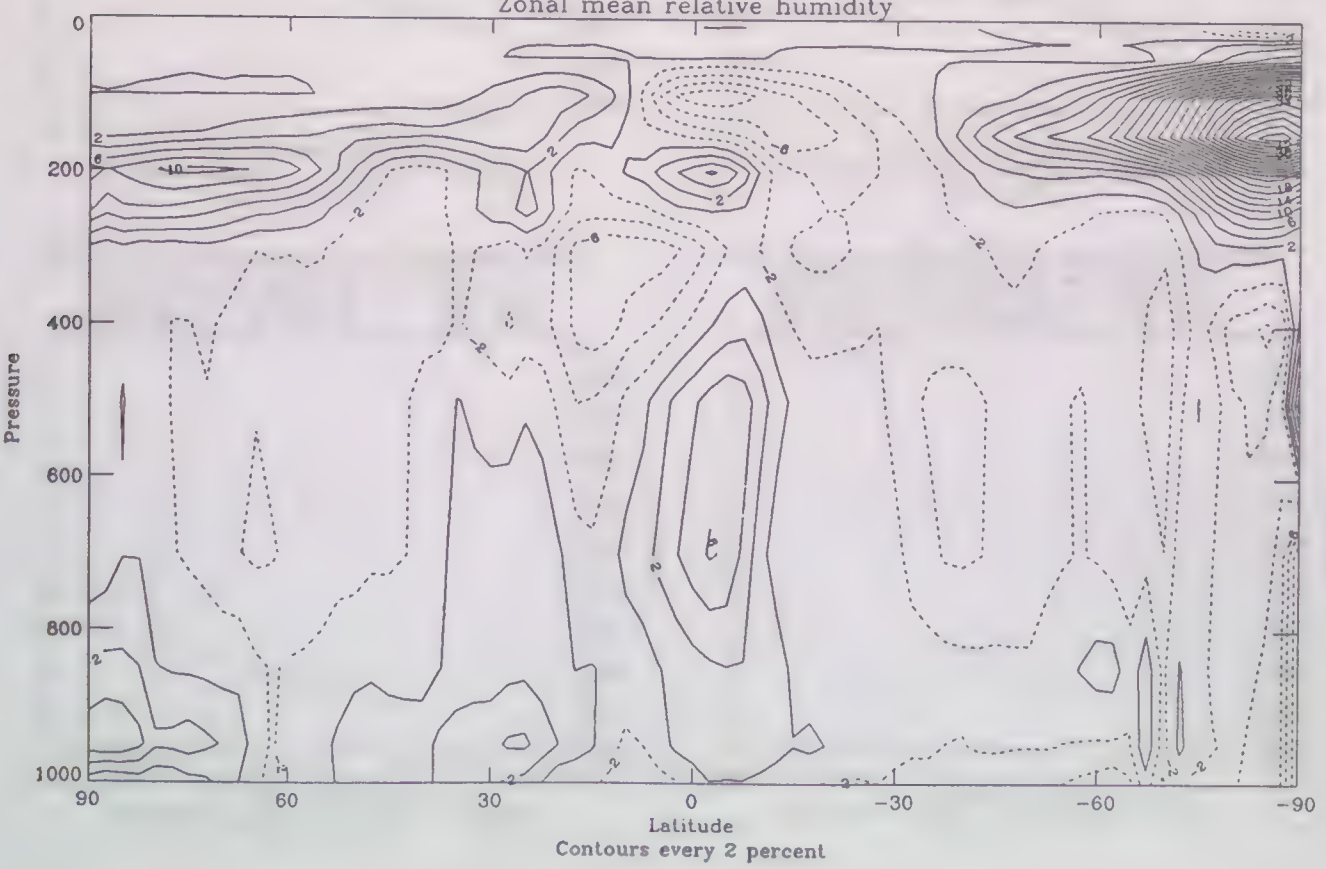

Figure 17

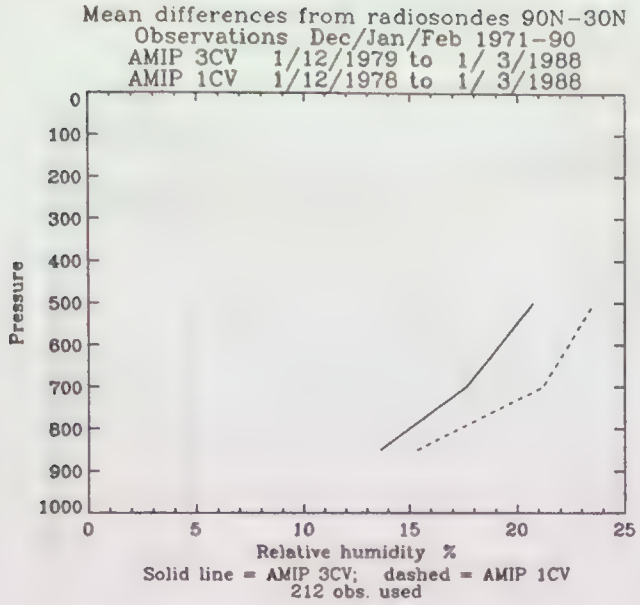
Mean differences from radiosondes 90N-30N
Observations Dec/Jan/Feb 1971-90
AMIP 3CV 1/12/1979 to 1/ 3/1988
AMIP 1CV 1/12/1978 to 1/ 3/1988
Pressure
Relative humidity %
Solid line = AMIP 3CV; dashed = AMIP 1CV
212 obs. used

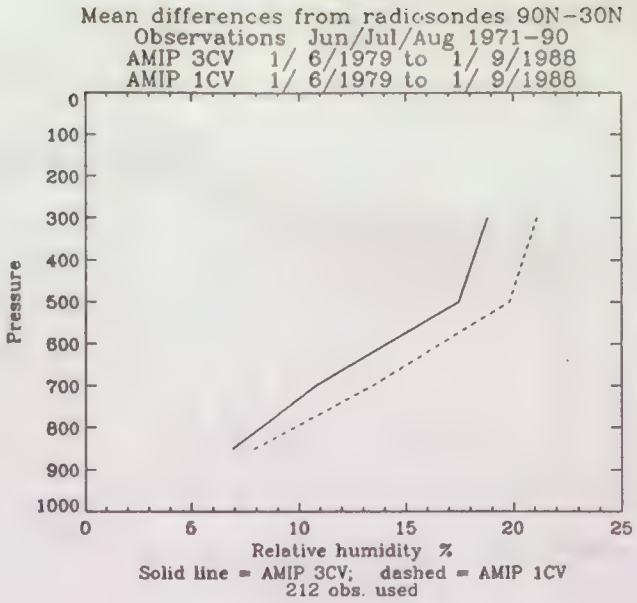
Mean differences from radiosondes 90N-30N
Observations Jun/Jul/Aug 1971-90
AMIP 3CV 1/ 6/1979 to 1/ 9/1988
AMIP 1CV 1/ 6/1979 to 1/ 9/1988
Pressure
Relative humidity %
Solid line = AMIP 3CV; dashed = AMIP 1CV
212 obs. used

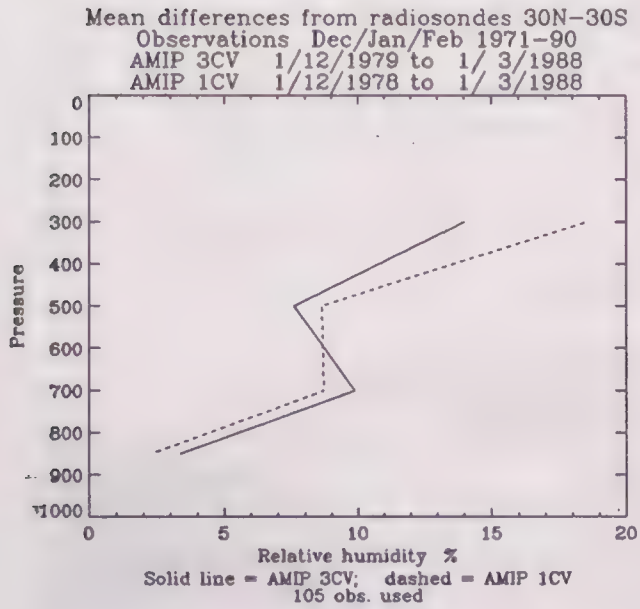
Mean differences from radiosondes 30N-30S
Observations Dec/Jan/Feb 1971-90
AMIP 3CV 1/12/1979 to 1/ 3/1988
AMIP 1CV 1/12/1978 to 1/ 3/1988
Pressure
Relative humidity %
Solid line = AMIP 3CV; dashed = AMIP 1CV
105 obs. used

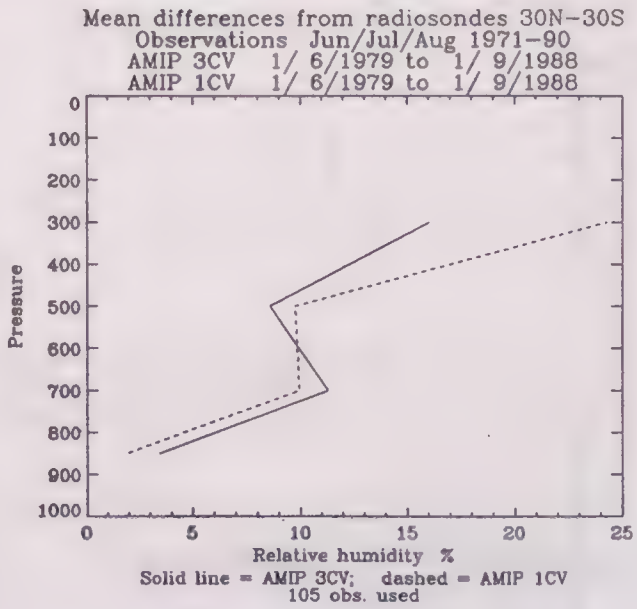
Mean differences from radiosondes 30N-30S
Observations Jun/Jul/Aug 1971-90
AMIP 3CV 1/ 6/1979 to 1/ 9/1988
AMIP 1CV 1/ 6/1979 to 1/ 9/1988
Pressure
Relative humidity %
Solid line = AMIP 3CV; dashed = AMIP 1CV
105 obs. used

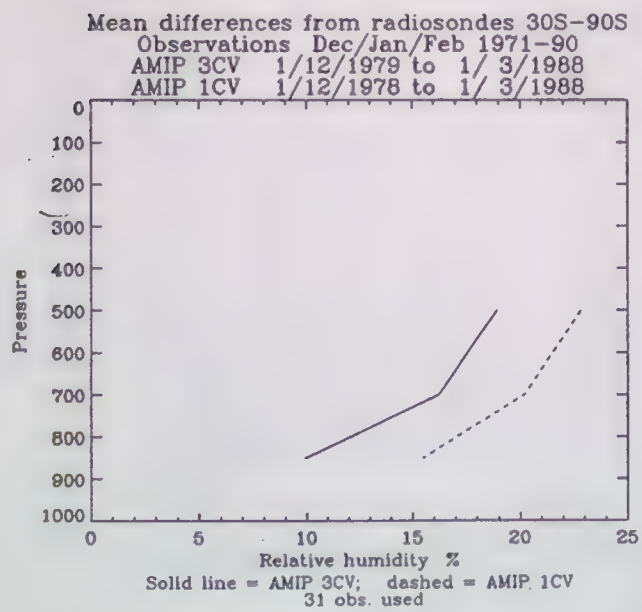
Mean differences from radiosondes 30S-90S
Observations Dec/Jan/Feb 1971-90
AMIP 3CV 1/12/1979 to 1/ 3/1988
AMIP 1CV 1/12/1978 to 1/ 3/1988
Pressure
Relative humidity %
Solid line = AMIP 3CV; dashed = AMIP 1CV
31 obs. used

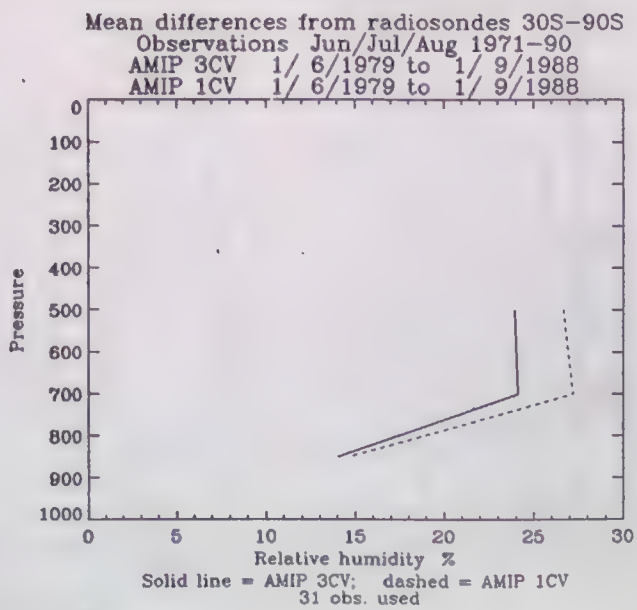
Mean differences from radiosondes 30S-90S
Observations Jun/Jul/Aug 1971-90
AMIP 3CV 1/ 6/1979 to 1/ 9/1988
AMIP 1CV 1/ 6/1979 to 1/ 9/1988
Pressure
Relative humidity %
Solid line = AMIP 3CV; dashed = AMIP 1CV
31 obs. used

Figure 18(a) AMIP: 3rd Climate Version. 10-year Dec/Jan/Feb
1.5 m Relative Humidity
From 1/ 1/1979 to 1/ 1/1989

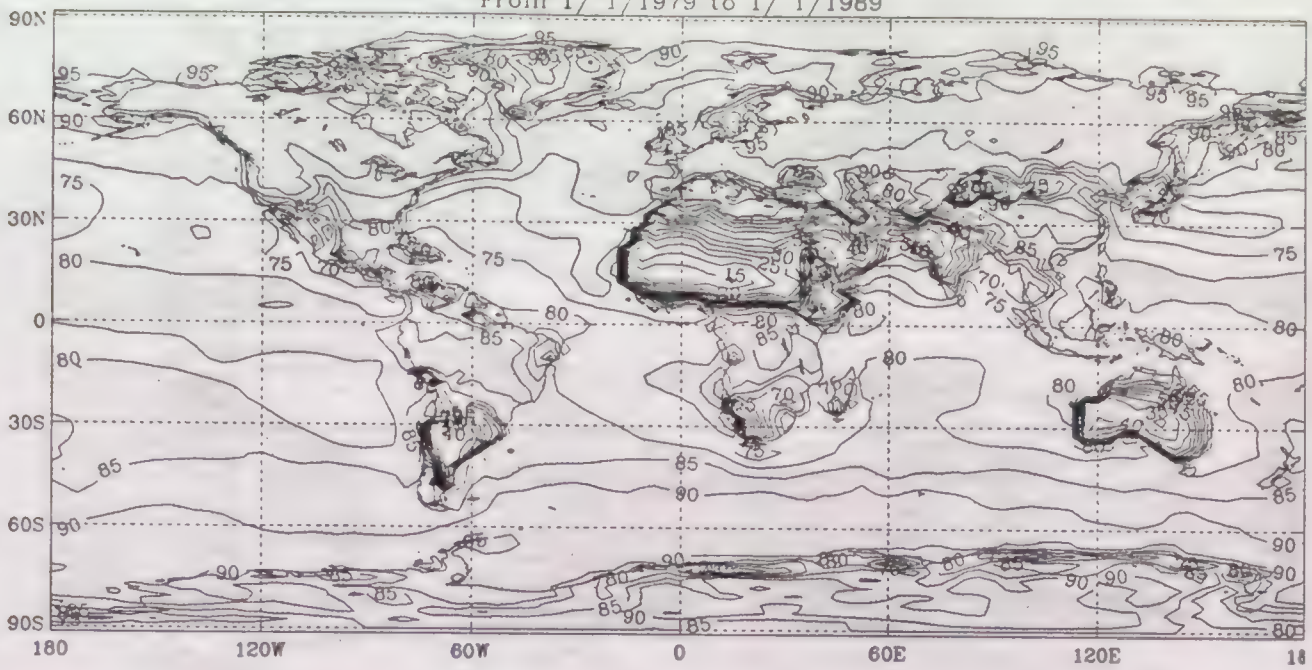

Contours every 5 percent. Shading greater than 80

(b) AMIP: 3rd Climate Version. 10-year Dec/Jan/Feb minus
AMIP: 1st Climate Version. 10-year Dec/Jan/Feb
1.5 m Relative Humidity

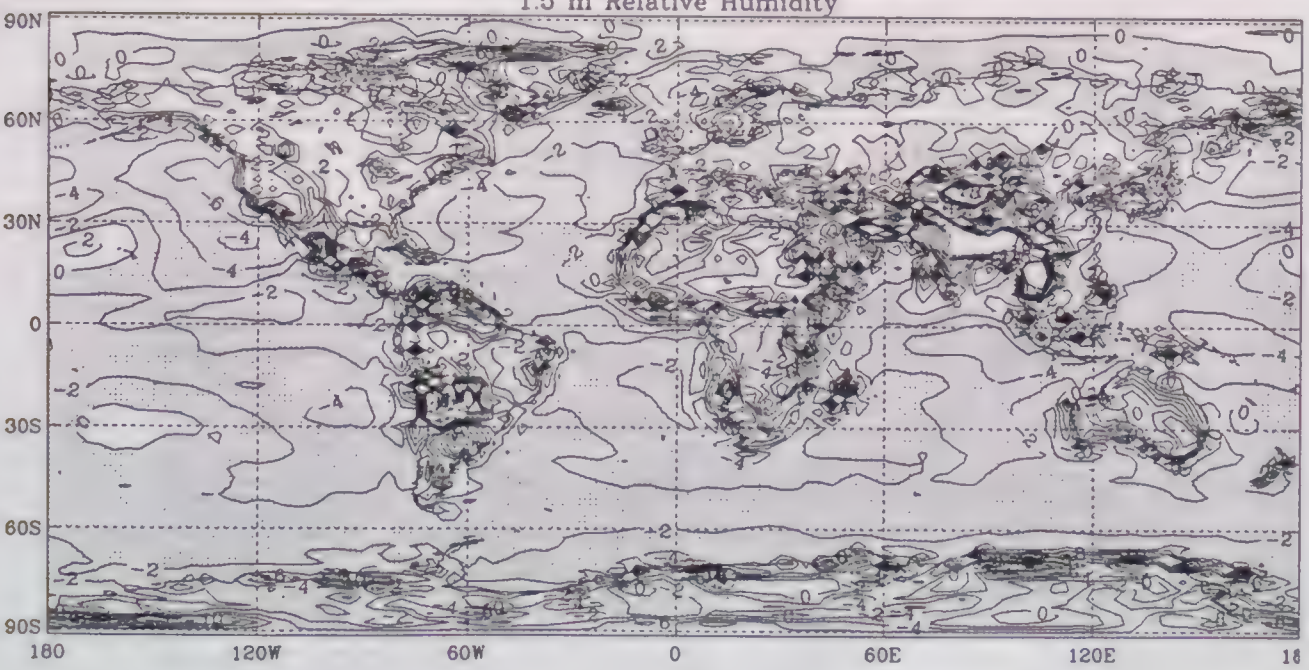

Contours every 2. Shading less than 0

Figure 19(a) AMIP: 3rd Climate Version. 10-year Dec/Jan/Feb
Total precipitation
From 1/ 1/1979 to 1/ 1/1989

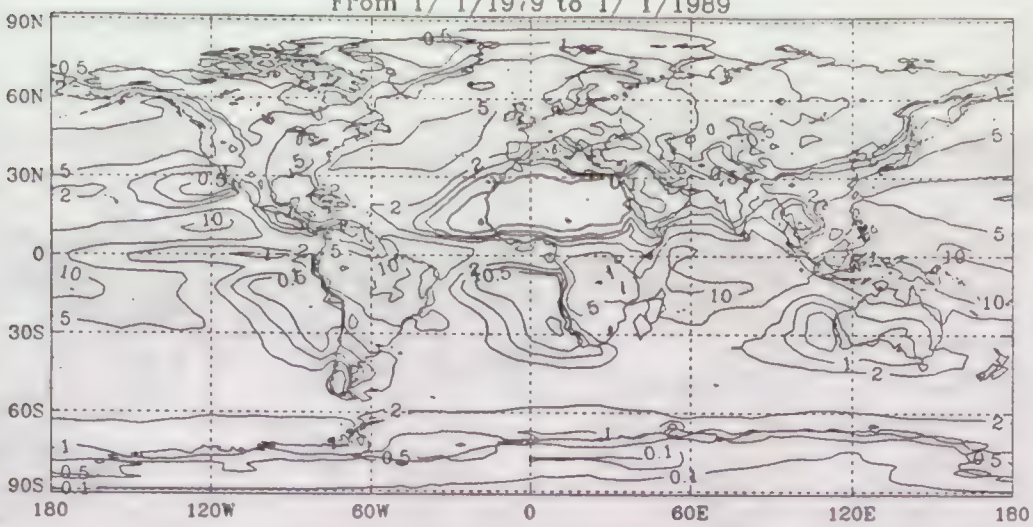

Contours every 0.1, 0.5, 1, 2, 5, 10 and 20 mm. Shading greater than 5
Area-weighted mean value = 3.18

(b) AMIP: 1st Climate Version. 10-year Dec/Jan/Feb
Total precipitation
From 1/12/1978 to 1/ 3/1988

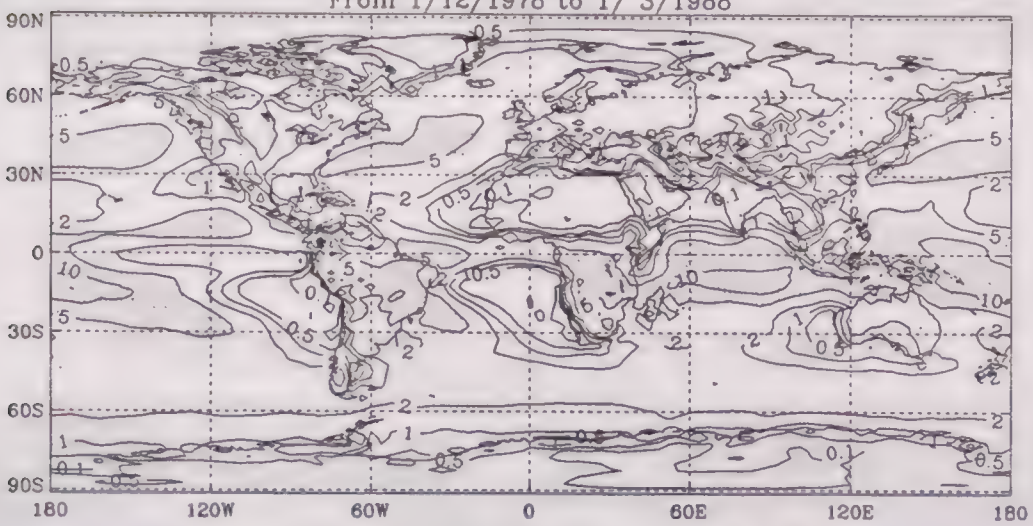

Contours every 0.1, 0.5, 1, 2, 5, 10 and 20 mm. Shading greater than 5
Area-weighted mean value = 2.98

(c) Legates & Willmott climatology. Dec/Jan/Feb
Total precipitation

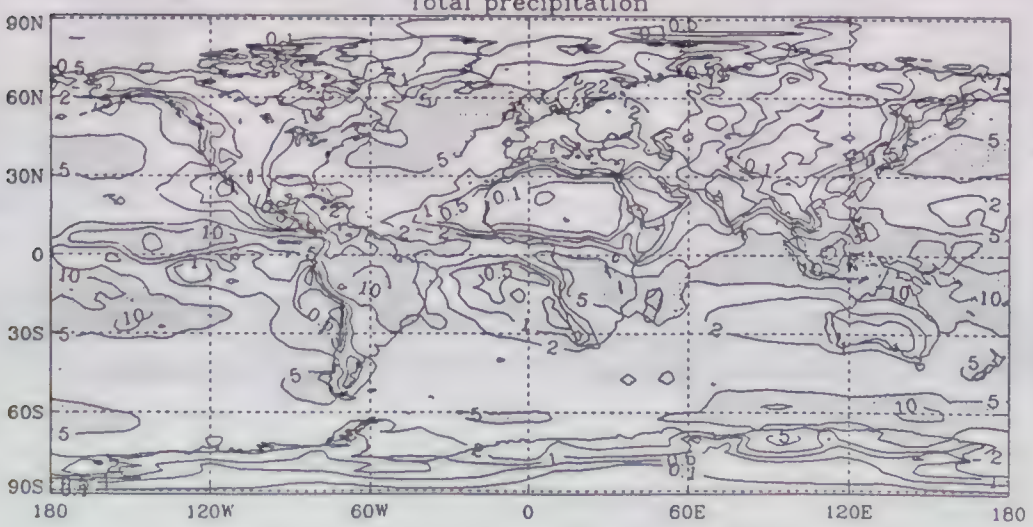

Contours every 0.1, 0.5, 1, 2, 5, 10 and 20 mm. Shading greater than 5
Area-weighted mean value = 3.54

Figure 20(a) AMIP 3rd Climate Version 10-year Jun/Jul/Aug
Total precipitation
From 1/ 6/1979 to 1/ 9/1988

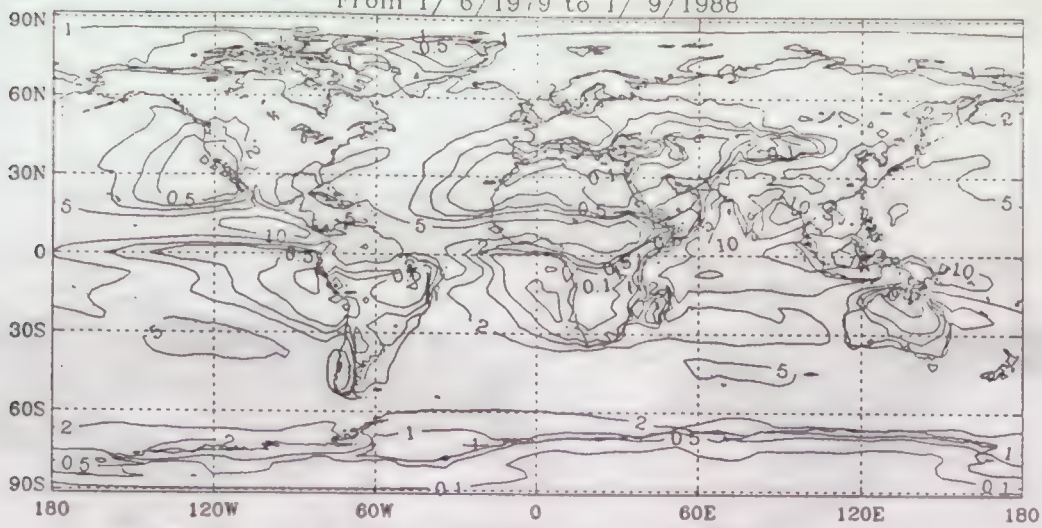

Contours every 0.1, 0.5, 1, 2, 5, 10 and 20 mm. Shading greater than 5
Area-weighted mean value = 3.28

(b) AMIP: 1st Climate Version. 10-year Jun/Jul/Aug
Total precipitation
From 1/ 6/1979 to 1/ 9/1988

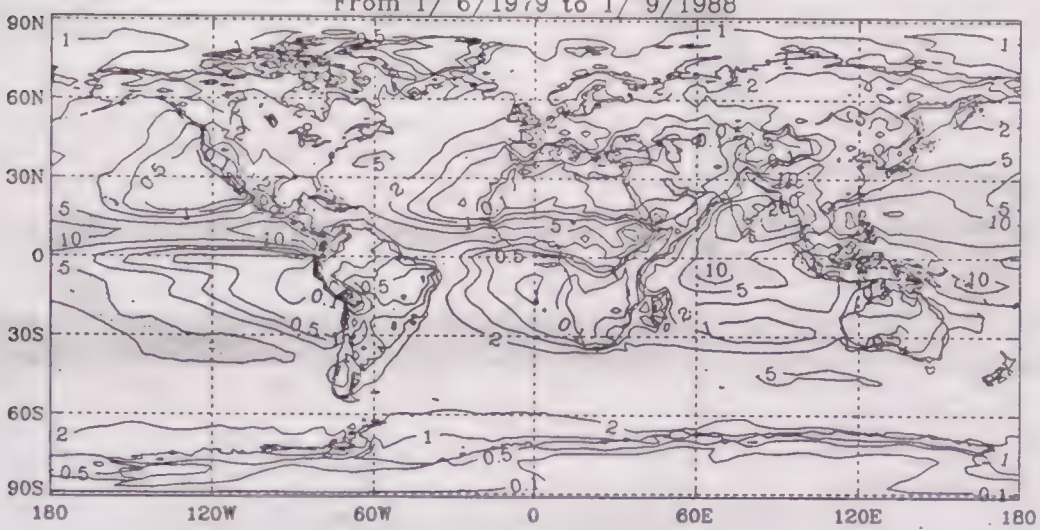

Contours every 0.1, 0.5, 1, 2, 5, 10 and 20 mm. Shading greater than 5
Area-weighted mean value = 3.08

(c) Legates & Willmott climatology. Jun/Jul/Aug
Total precipitation

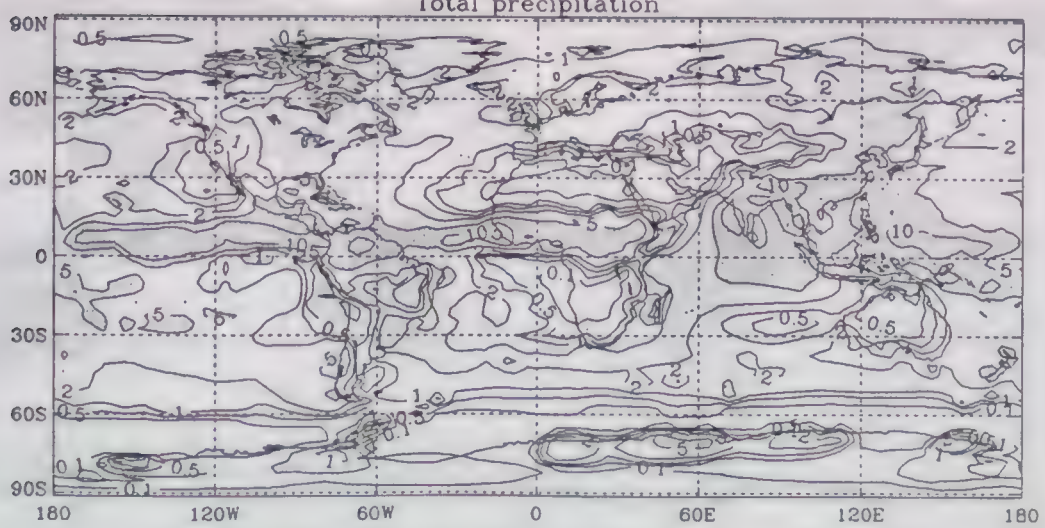

Contours every 0.1, 0.5, 1, 2, 5, 10 and 20 mm. Shading greater than 5
Area-weighted mean value = 2.89

Figure 21(a) AMIP: 3rd Climate Version. 10-year Dec/Jan/Feb
Total soil moisture content
From 1/ 1/1979 to 1/ 1/1989

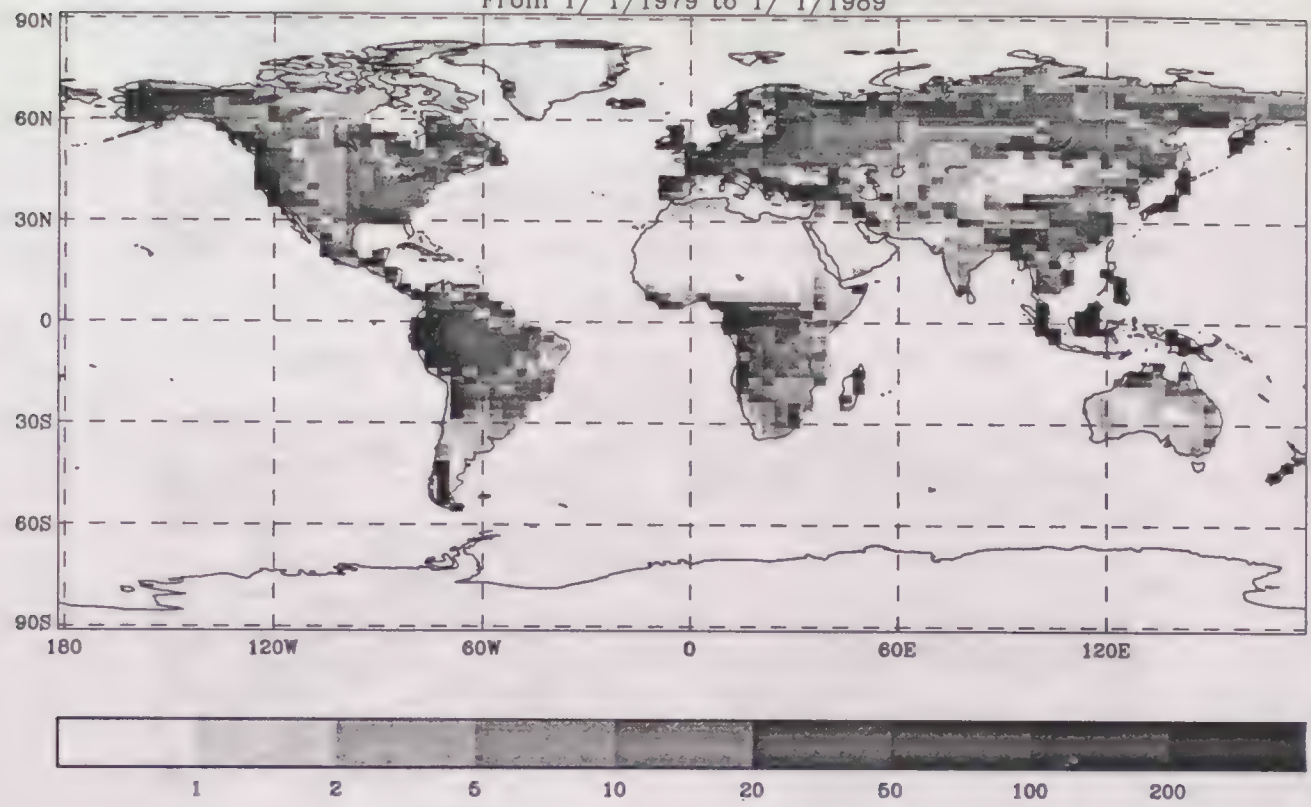

(b) AMIP: 1st Climate Version. 10-year Dec/Jan/Feb
Total soil moisture content
From 1/12/1978 to 1/ 3/1988

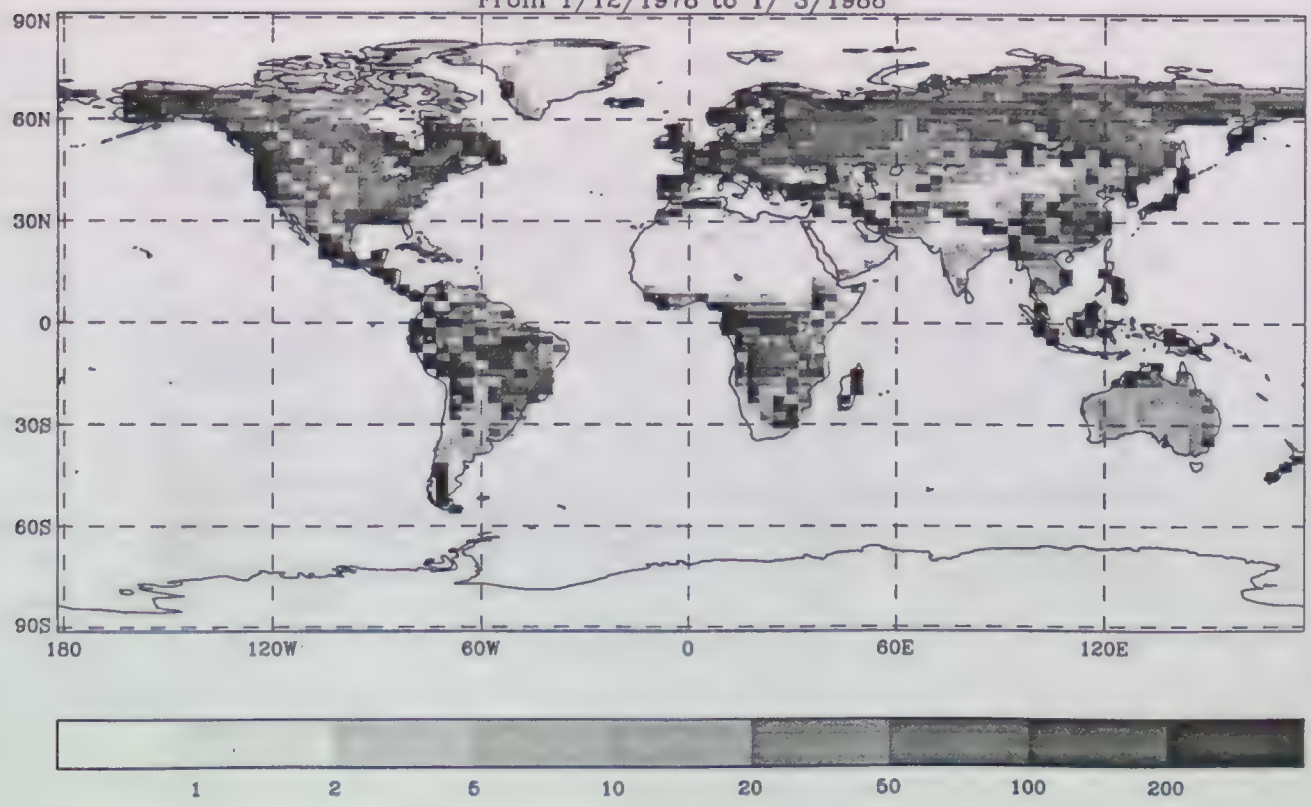

Figure 22(a) AMIP: 3rd Climate Version. 10-year Jun/Jul/Aug
Total soil moisture content
From 1/ 6/1979 to 1/ 9/1988

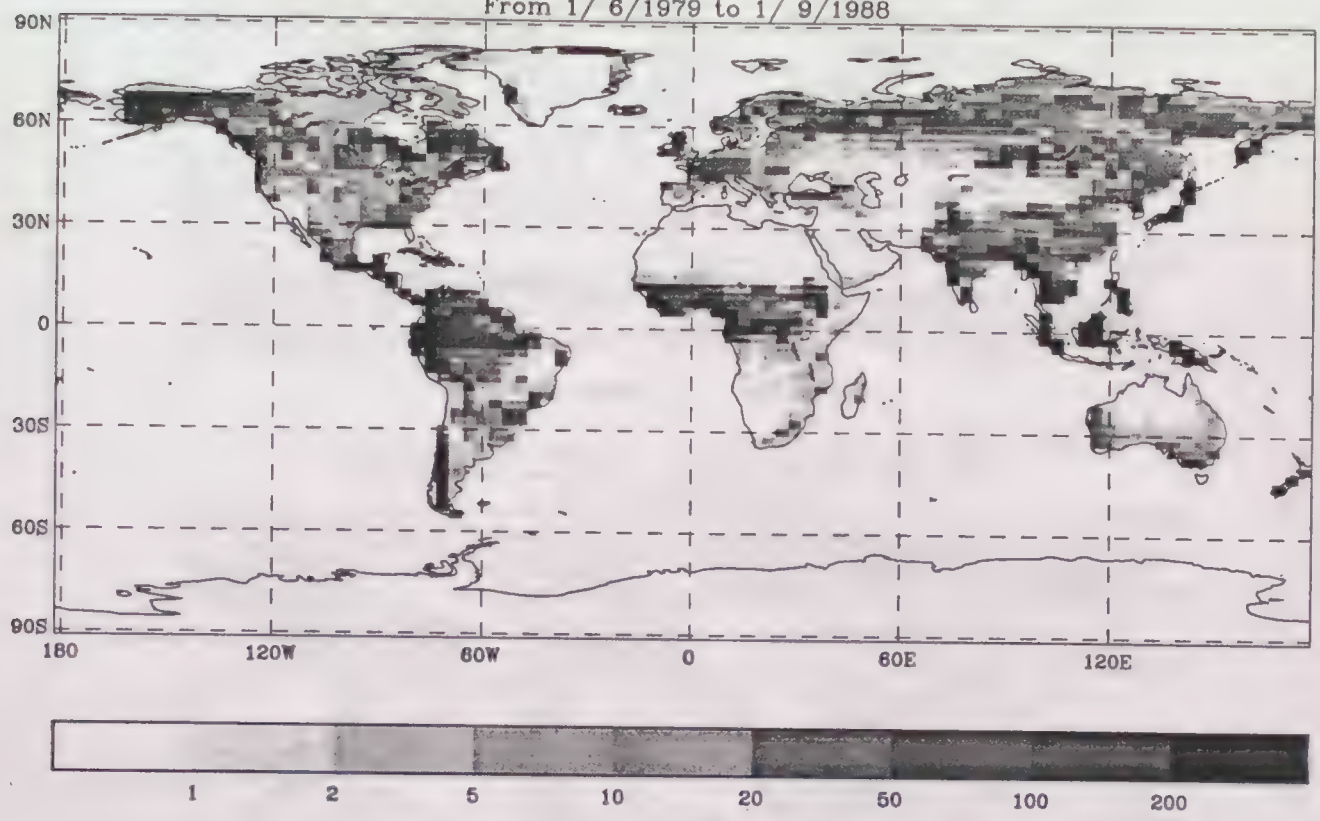

(b) AMIP: 1st Climate Version. 10-year Jun/Jul/Aug
Total soil moisture content
From 1/ 6/1979 to 1/ 9/1988

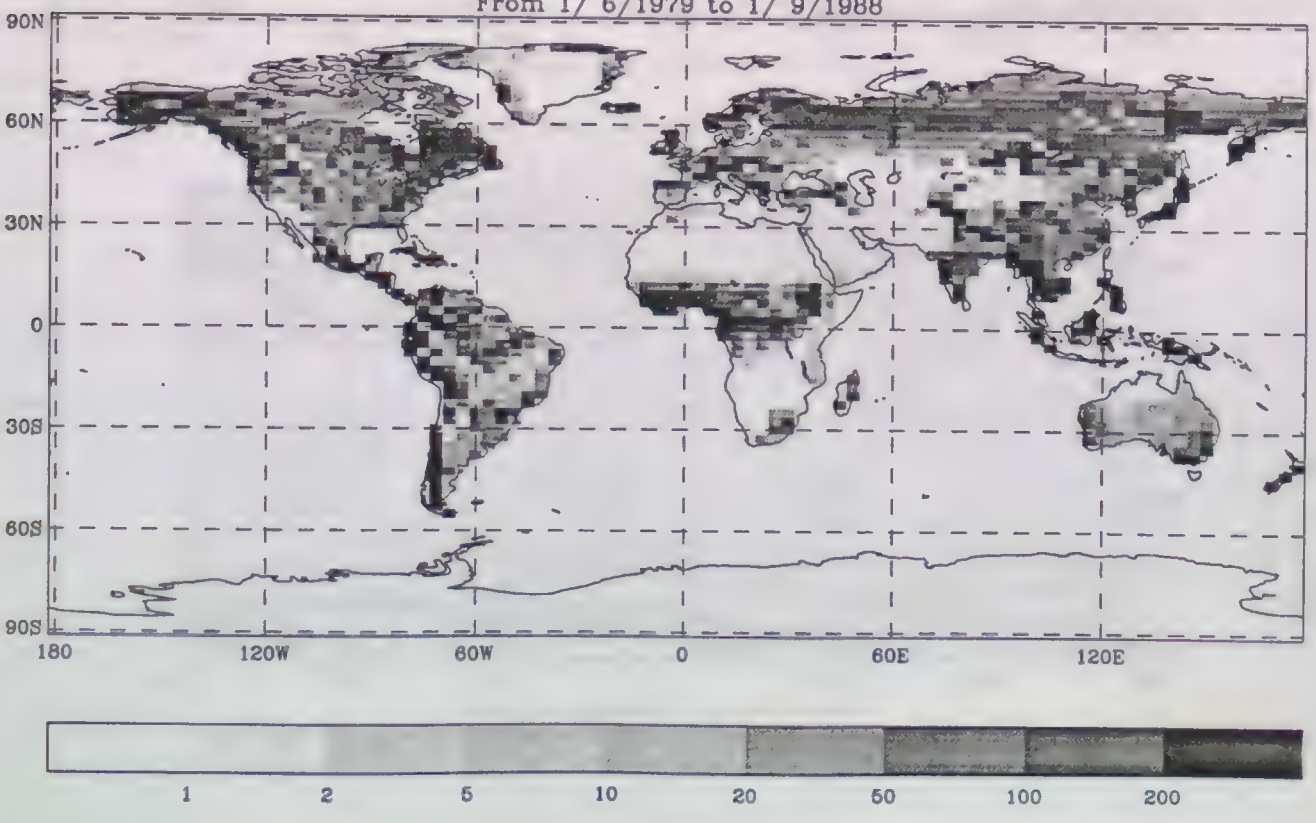

Figure 23(a) AMIP: 3rd Climate Version. 10-year Dec/Jan/Feb
Temperature at 1.5 m
From 1/ 1/1979 to 1/ 1/1989

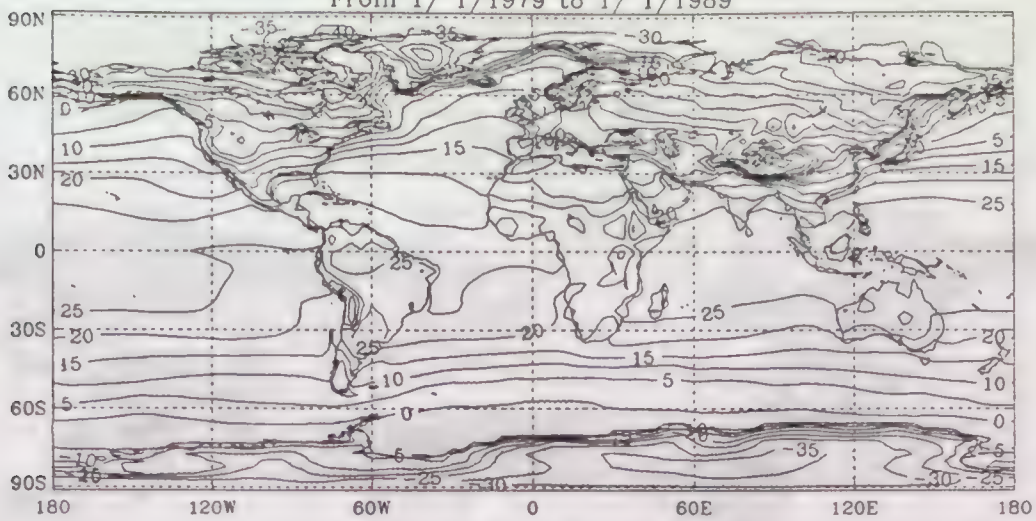

Contours every 5°C. Shading less than 0

(b) AMIP: 3rd Climate Version. 10-year Dec/Jan/Feb minus
AMIP: 1st Climate Version. 10-year Dec/Jan/Feb
Temperature at 1.5 m

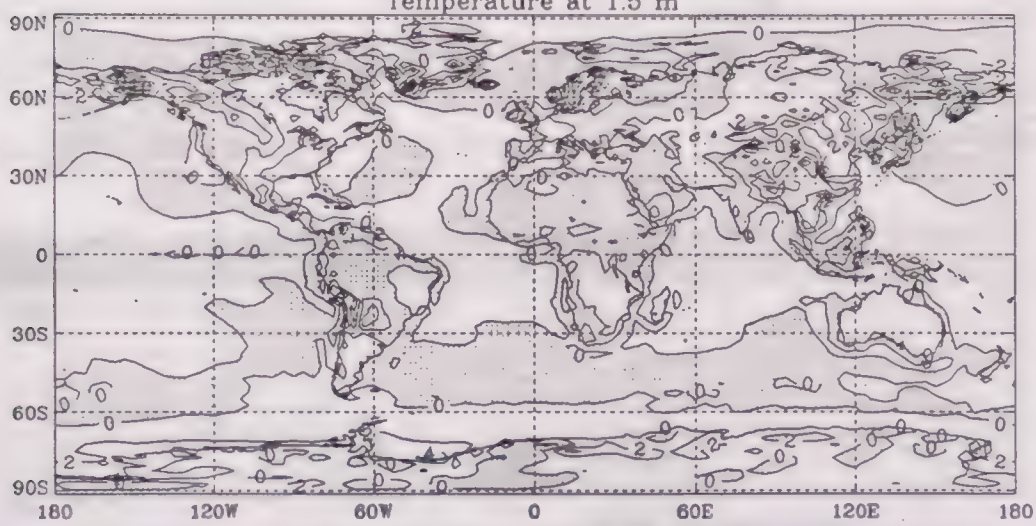

Contours every 2. Shading less than 0

(c) AMIP: 3rd Climate Version. 10-year Dec/Jan/Feb minus
Legates & Willmott climatology. Dec/Jan/Feb
Temperature at 1.5 m

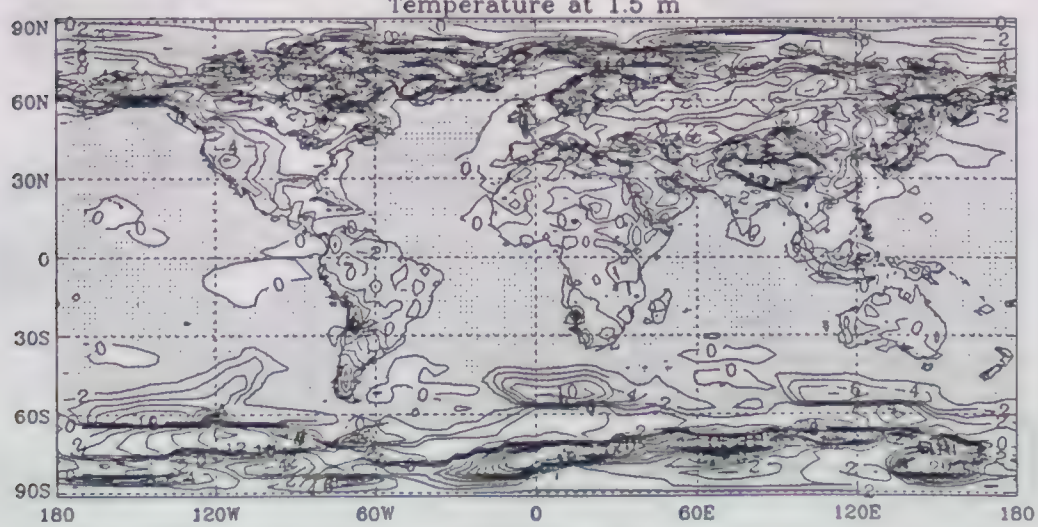

Contours every 2. Shading less than 0

Figure 24(a) AMIP: 3rd Climate Version. 10-year Jun/Jul/Aug
Temperature at 1.5 m
From 1/ 6/1979 to 1/ 9/1988

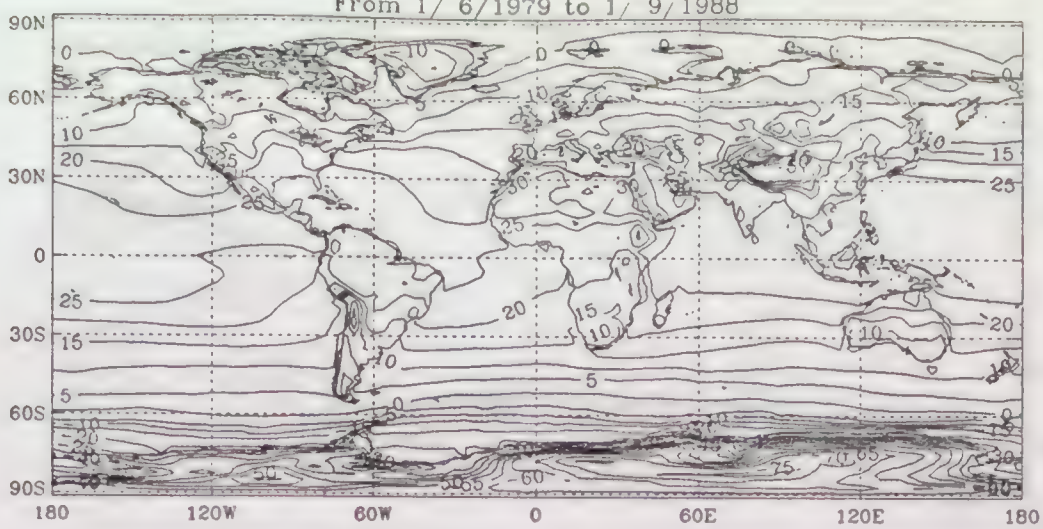

Contours every 5°C. Shading less than 0

(b) AMIP: 3rd Climate Version. 10-year Jun/Jul/Aug minus
AMIP: 1st Climate Version. 10-year Jun/Jul/Aug
Temperature at 1.5 m

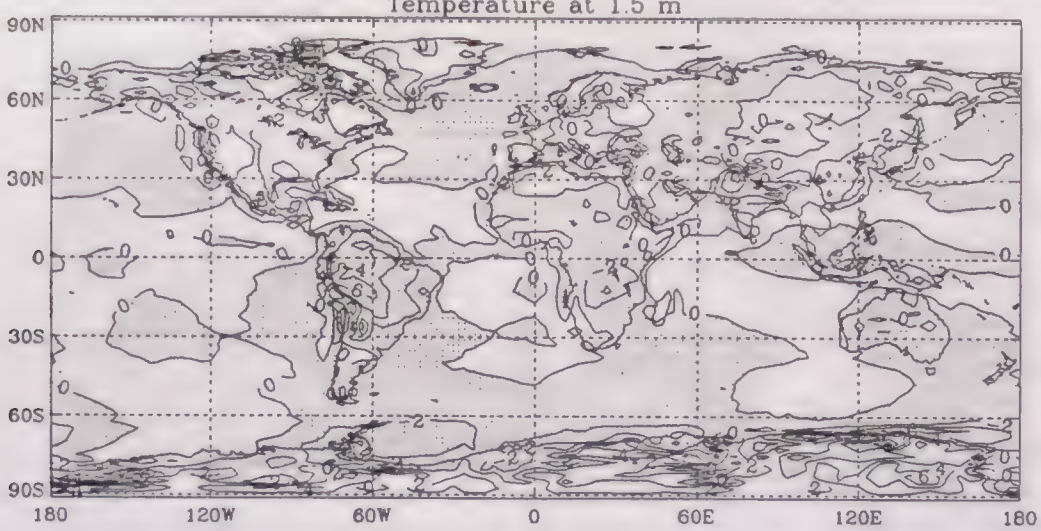

Contours every 2. Shading less than 0

(c) AMIP: 3rd Climate Version. 10-year Jun/Jul/Aug minus
Legates & Willmott climatology. Jun/Jul/Aug
Temperature at 1.5 m

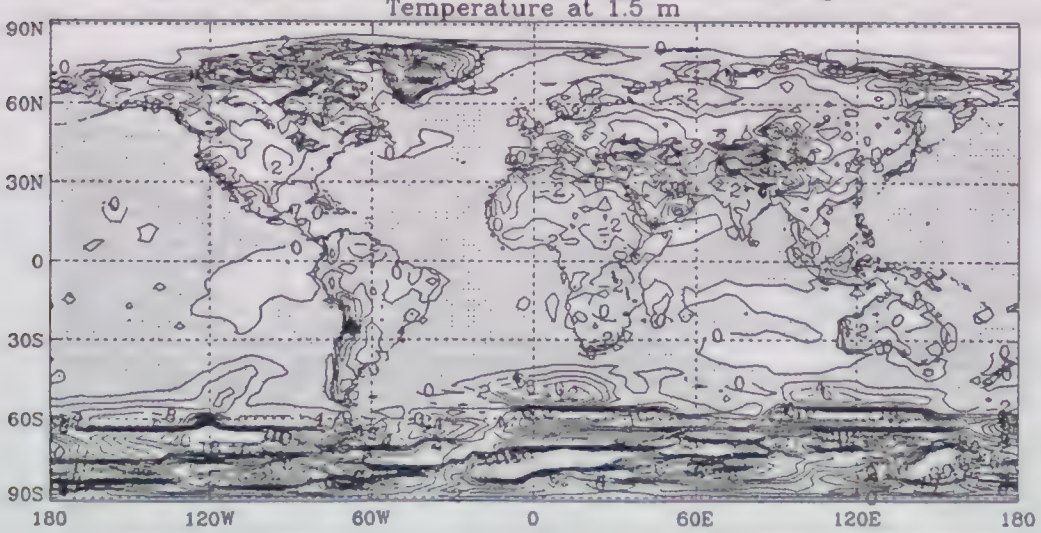

Contours every 2. Shading less than 0

Figure 25(a) AMIP: 3rd Climate Version. 10-year Dec/Jan/Feb
Sea-minus-air temperature differences
From 1/ 1/1979 to 1/ 1/1989

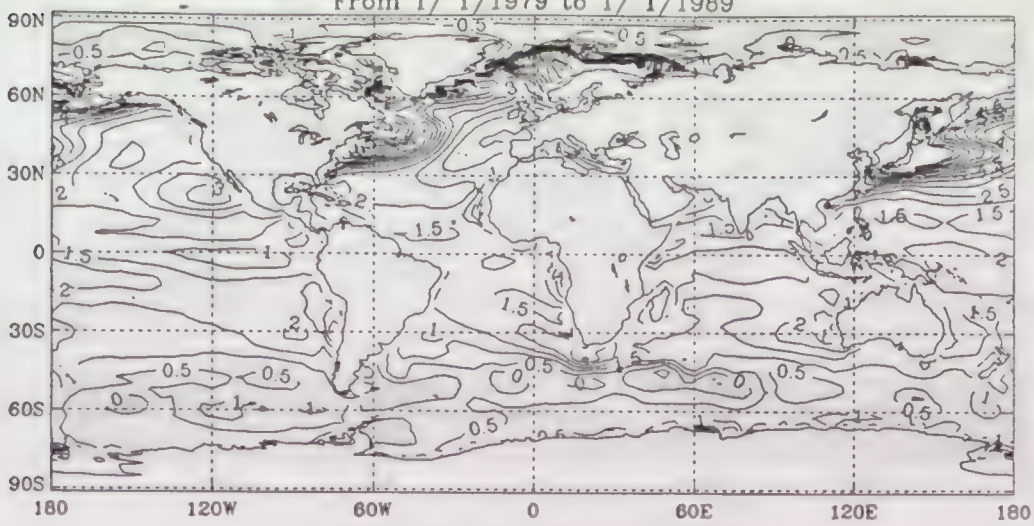

Contours every 0.5 K. Shading less than 0

(b) AMIP: 3rd Climate Version. 10-year Dec/Jan/Feb minus
AMIP: 1st Climate Version. 10-year Dec/Jan/Feb
Sea-minus-air temperature differences

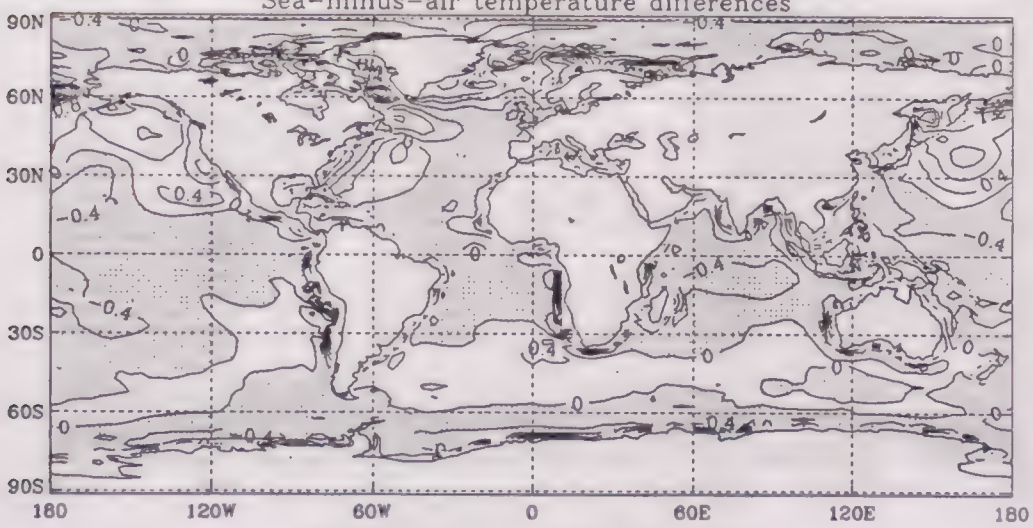

Contours every 0.4 K. Shading less than 0

(c) AMIP: 3rd Climate Version. 10-year Dec/Jan/Feb minus
GISST 5° x 5° climatology. Dec/Jan/Feb 1951-80. Night-time observations only
Sea-minus-air temperature differences

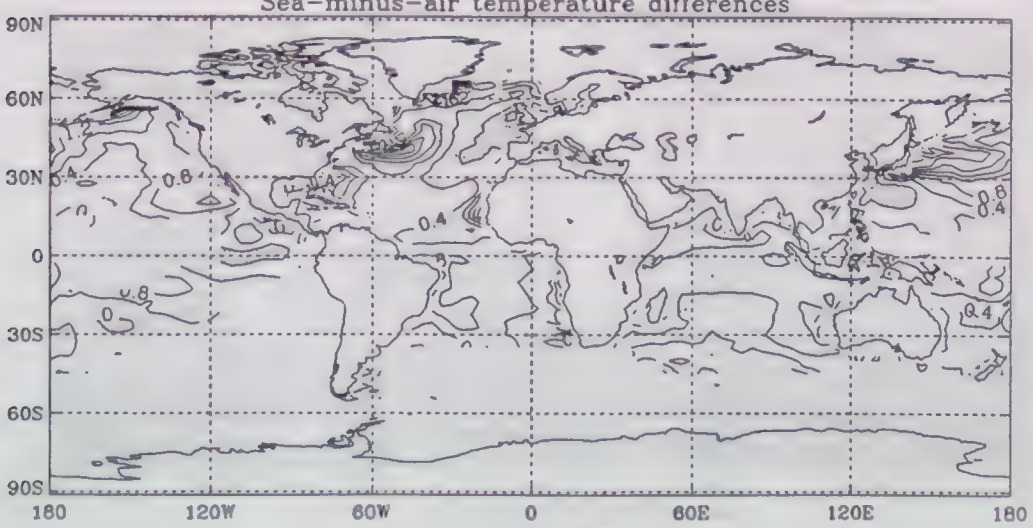

Contours every 0.4 K. Shading less than 0

Figure 26(a) AMIP: 3rd Climate Version 10-year Jun/Jul/Aug
Sea-minus-air temperature differences
From 1/ 6/1979 to 1/ 9/1988

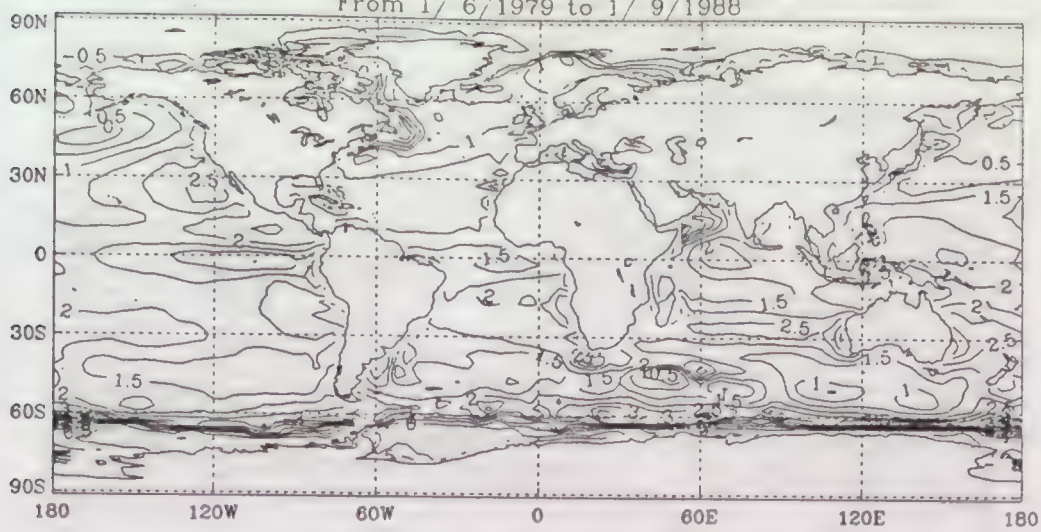

Contours every 0.5 K. Shading less than 0

(b) AMIP: 3rd Climate Version. 10-year Jun/Jul/Aug minus
AMIP: 1st Climate Version. 10-year Jun/Jul/Aug
Sea-minus-air temperature differences

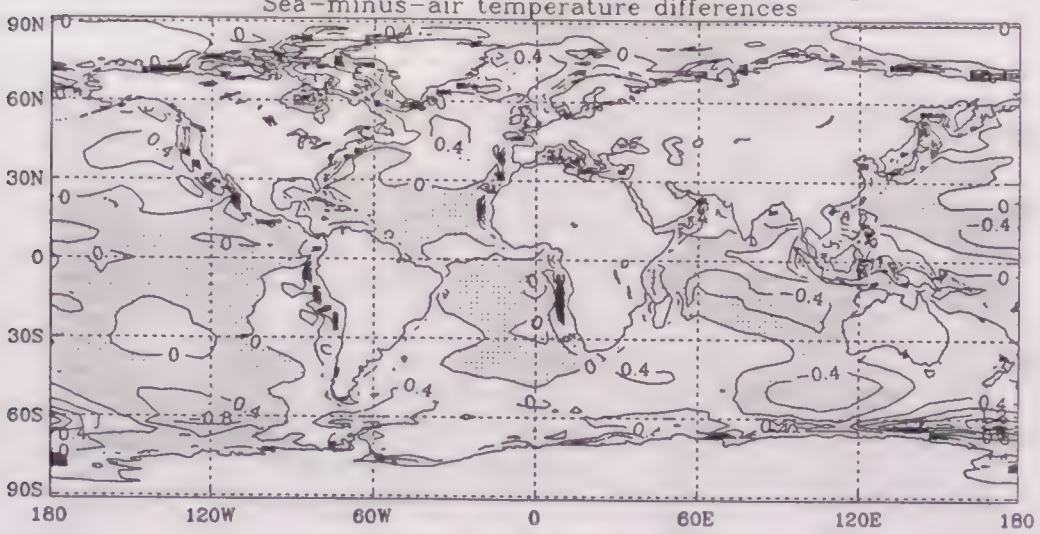

Contours every 0.4 K. Shading less than 0

(c) AMIP: 3rd Climate Version. 10-year Jun/Jul/Aug minus
GISST 5° x 5° climatology. Jun/Jul/Aug 1951-80. Night-time observations only
Sea-minus-air temperature differences

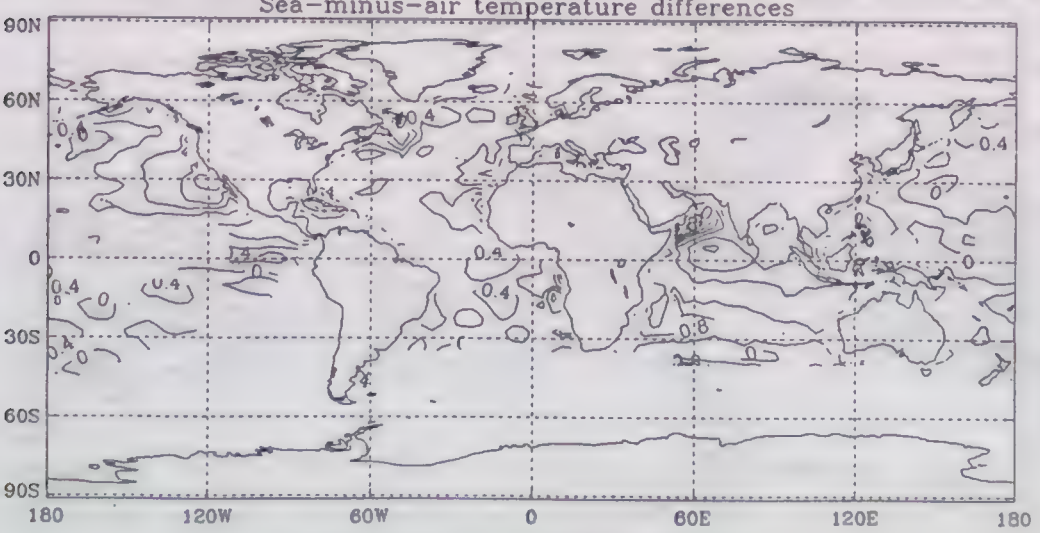

Contours every 0.4 K. Shading less than 0

Figure 27(a) AMIP: 3rd Climate Version. 10-year Dec/Jan/Feb
Vector wind and isotachs at 10 m
From 1/ 1/1979 to 1/ 1/1989

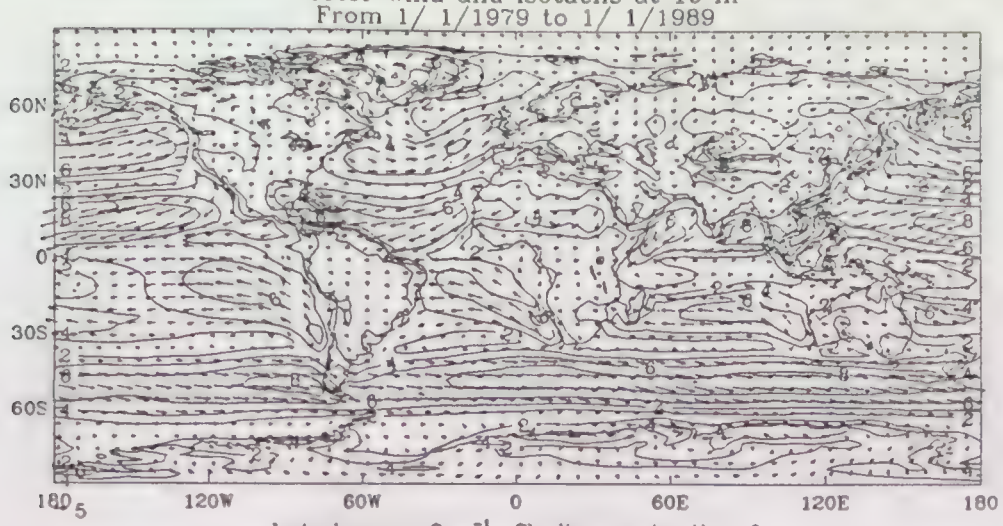

Isotachs every 2ms^{-1}. Shading greater than 6

(b) AMIP: 1st Climate Version. 10-year Dec/Jan/Feb
Vector wind and isotachs at 10 m
From 1/12/1978 to 1/ 3/1988

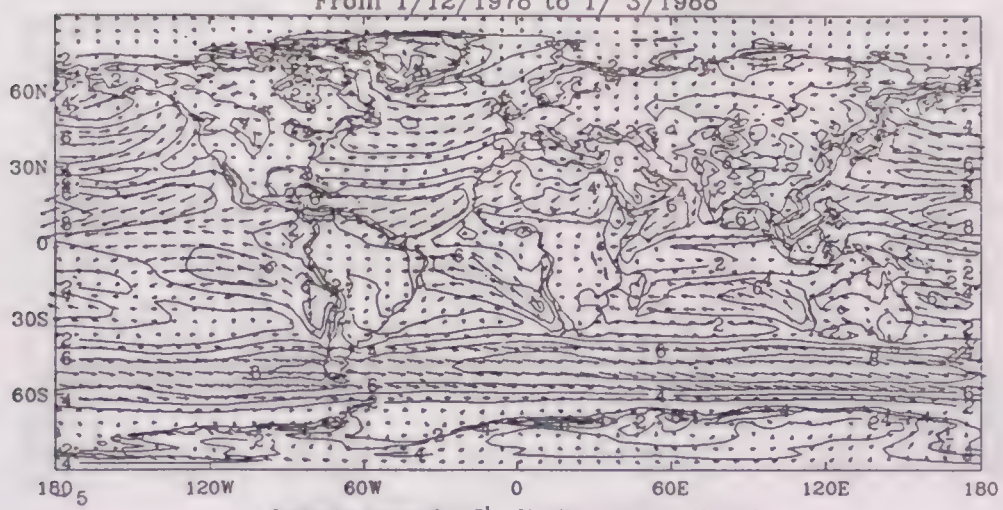

Isotachs every 2ms^{-1}. Shading greater than 6

(c) COADS ship wind climatology. Dec/Jan/Feb 1969-88
Vector wind and isotachs at 10 m
From 0/ 1/1969

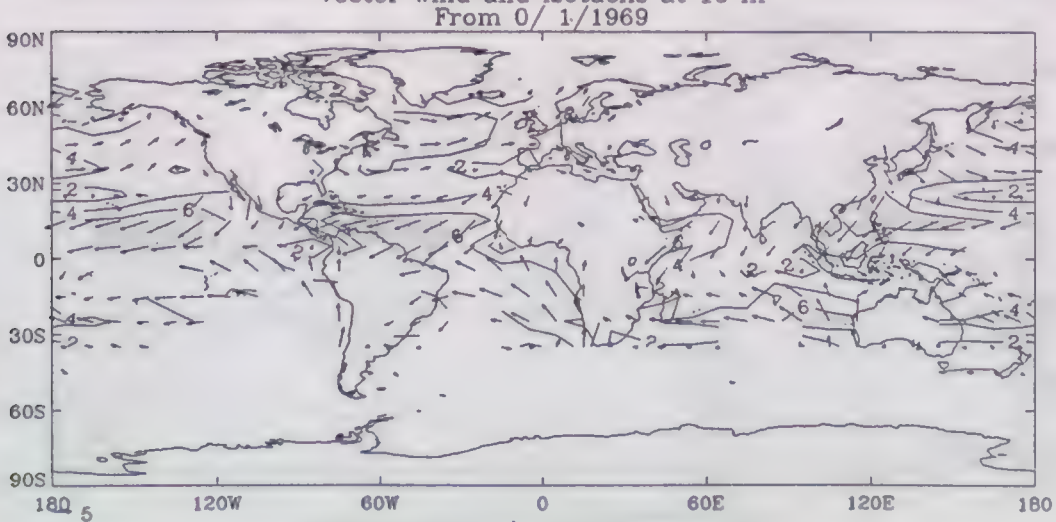

Isotachs every 2ms^{-1}. Shading greater than 6

Figure 28(a) AMIP: 3rd Climate Version. 10-year Jun/Jul/Aug
Vector wind and isotachs at 10 m
From 1/ 6/1979 to 1/ 9/1988

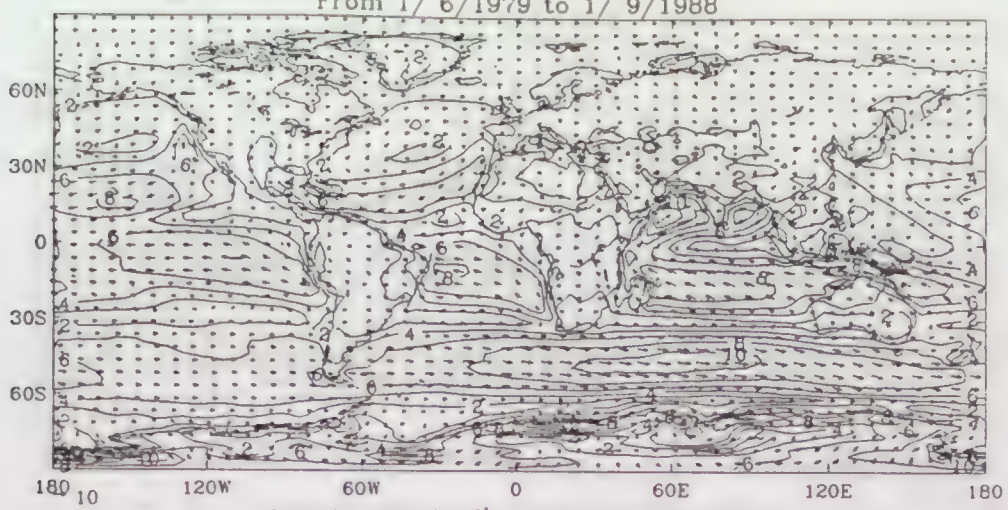

Isotachs every 2ms^{-1}. Shading greater than 6

(b) AMIP: 1st Climate Version. 10-year Jun/Jul/Aug
Vector wind and isotachs at 10 m
From 1/ 6/1979 to 1/ 9/1988

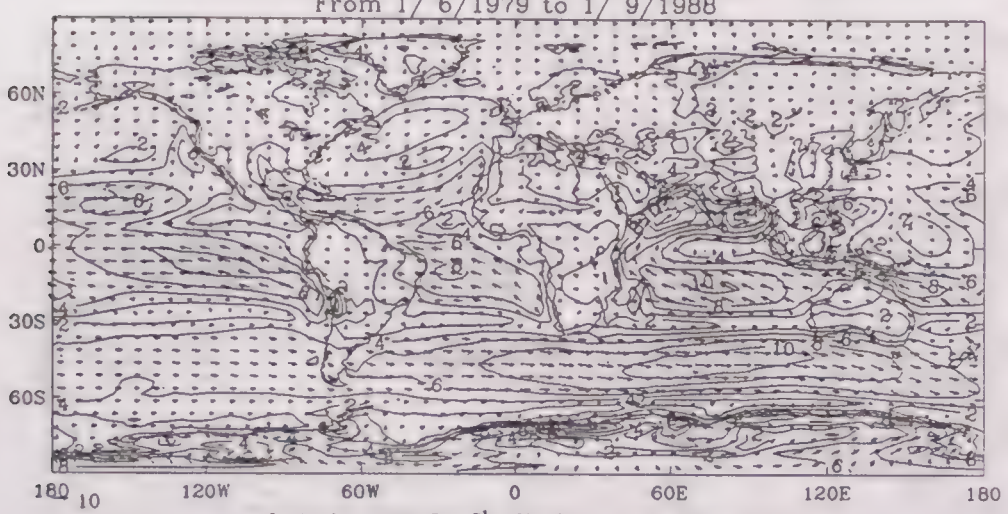

Isotachs every 2ms^{-1}. Shading greater than 6

(c) COADS ship wind climatology. Jun/Jul/Aug 1969-88
Vector wind and isotachs at 10 m
From 0/ 6/1969

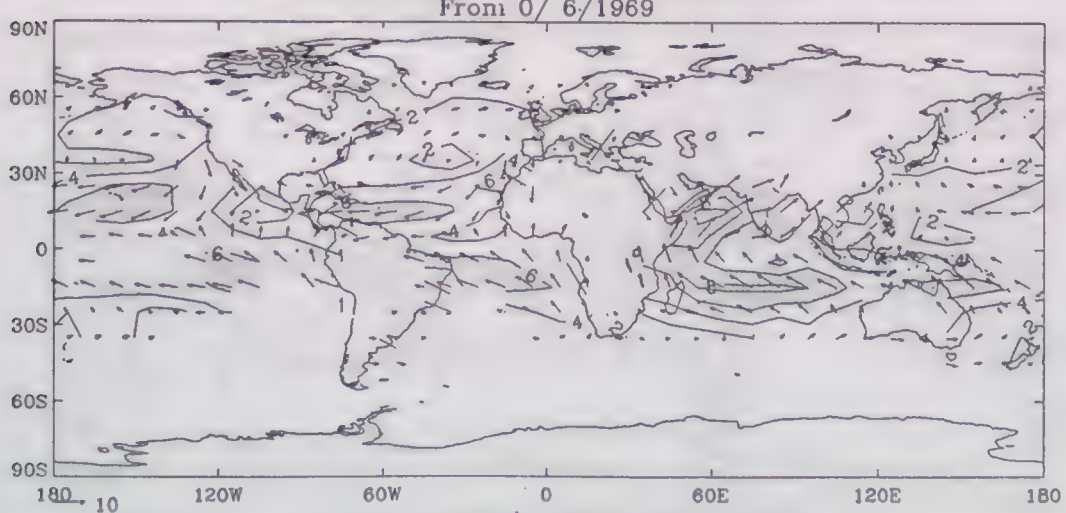

Isotachs every 2ms^{-1}. Shading greater than 6

Figure 29(a) AMIP: 3rd Climate Version. 10-year Dec/Jan/Feb
Surface latent heat flux
From 1/ 1/1979 to 1/ 1/1989

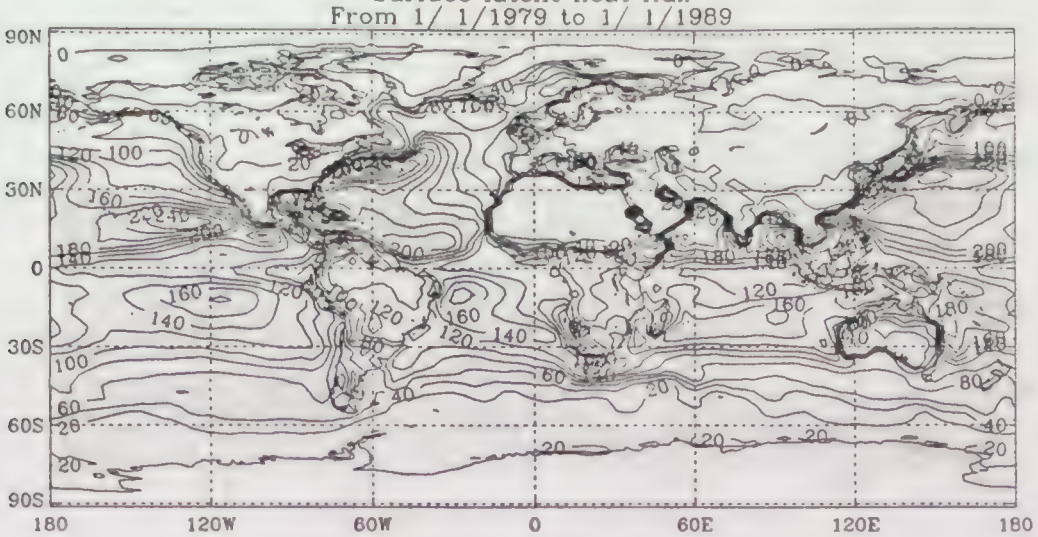

Contours every 20 Wm^{-2}. Shading greater than 160

(b) AMIP: 3rd Climate Version. 10-year Dec/Jan/Feb minus
AMIP: 1st Climate Version. 10-year Dec/Jan/Feb
Surface latent heat flux

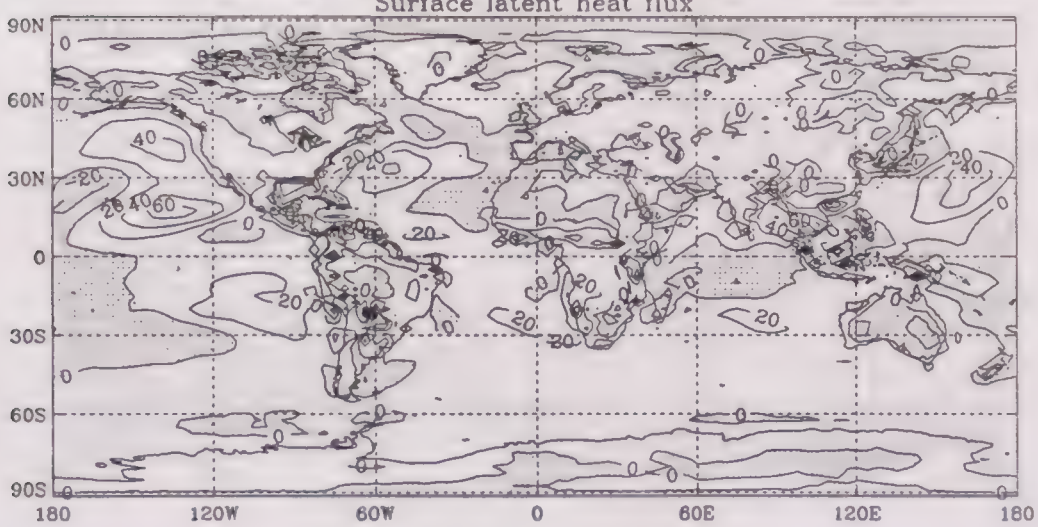

Contours every 20 Wm^{-2}. Shading less than 0

(c) AMIP: 3rd Climate Version. 10-year Dec/Jan/Feb minus
Oberhuber climatology. Dec/Jan/Feb
Surface latent heat flux

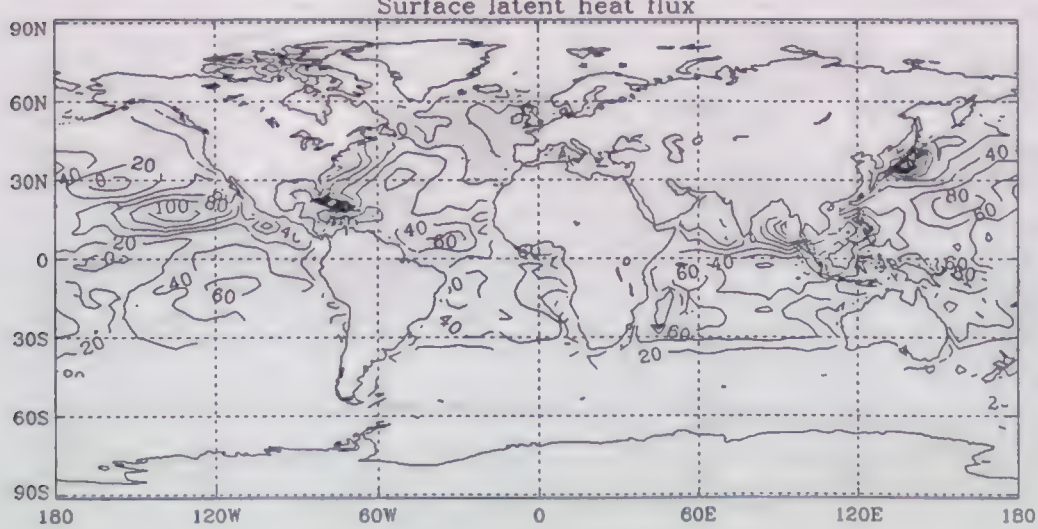

Contours every 20 Wm^{-2}. Shading less than 0

Figure 30(a) AMIP 3rd Climate Version 10-year Jun/Jul/Aug
Surface latent heat flux
From 1/ 6/1979 to 1/ 9/1988

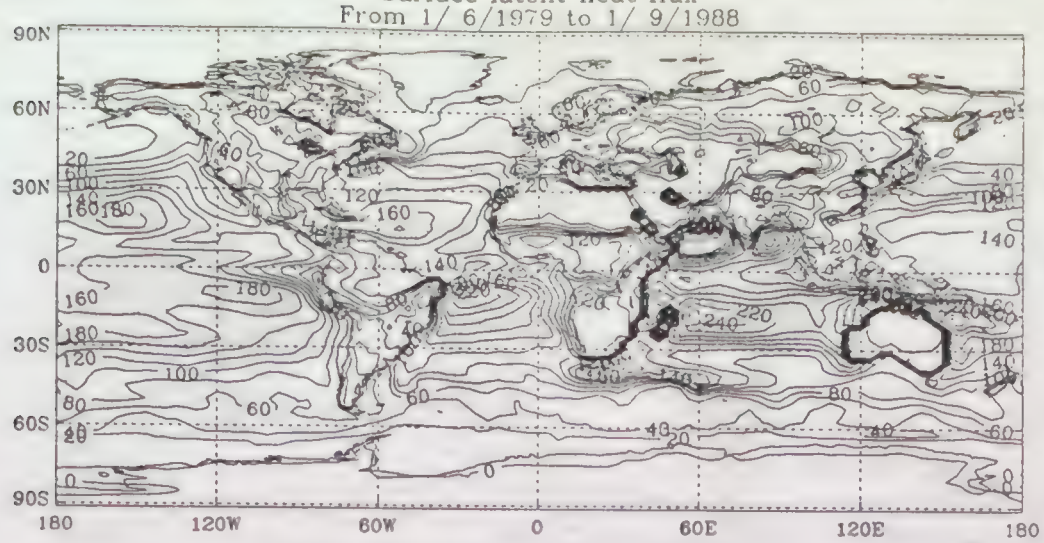

Contours every 20 Wm^{-2}. Shading greater than 160

(b) AMIP: 3rd Climate Version. 10-year Jun/Jul/Aug minus
AMIP: 1st Climate Version. 10-year Jun/Jul/Aug
Surface latent heat flux

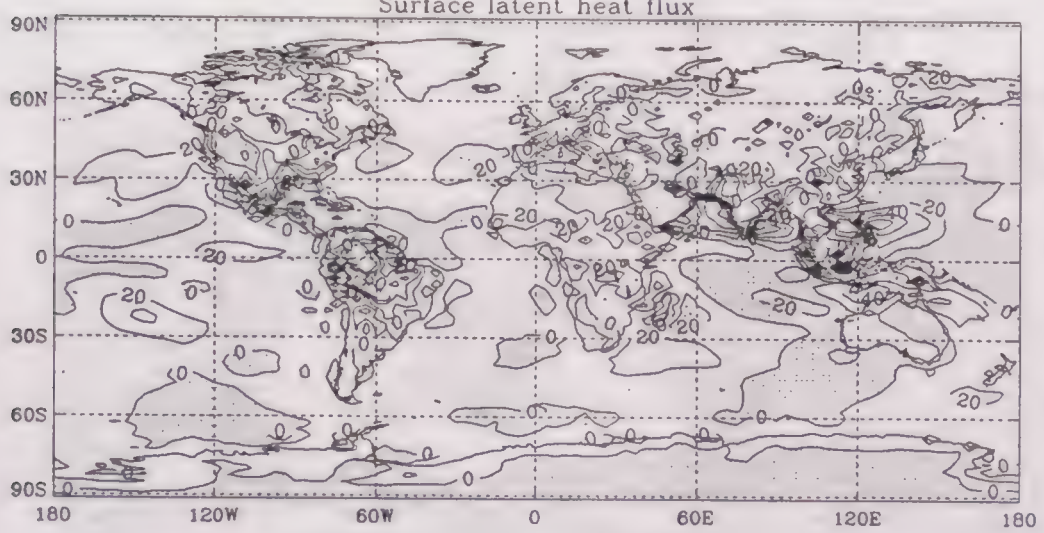

Contours every 20 Wm^{-2}. Shading less than 0

(c) AMIP: 3rd Climate Version. 10-year Jun/Jul/Aug minus
Oberhuber climatology. Jun/Jul/Aug
Surface latent heat flux

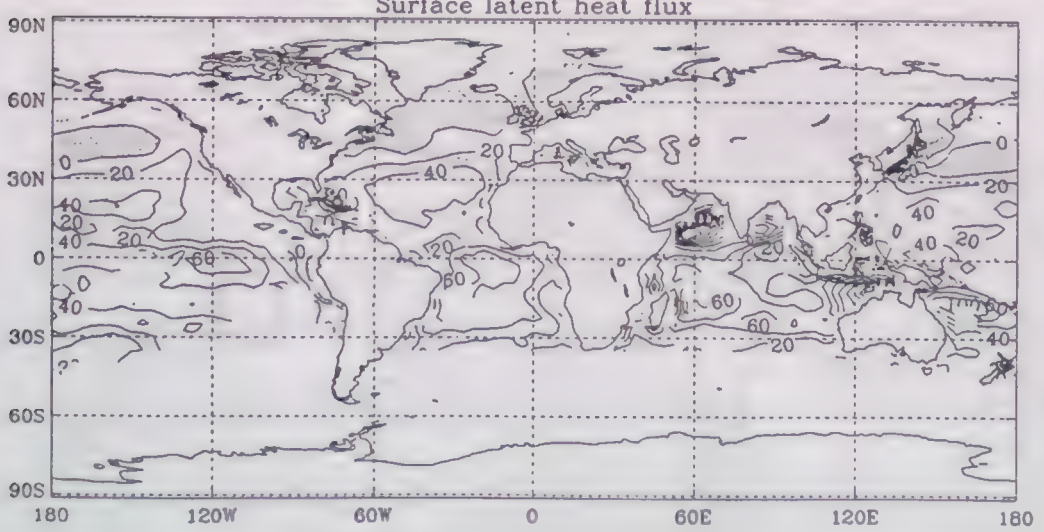

Contours every 20 Wm^{-2}. Shading less than 0

Figure 31(a) AMIP: 3rd Climate Version. 10-year Dec/Jan/Feb
Surface sensible heat flux
From 1/ 1/1979 to 1/ 1/1989

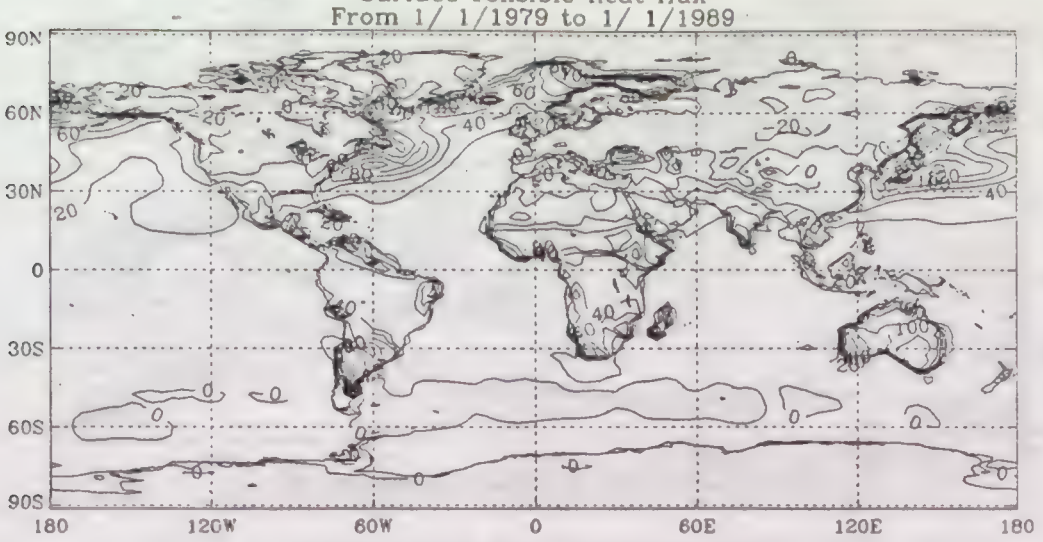

Contours every 20 Wm^{-2}. Shading less than 0

(b) AMIP: 3rd Climate Version. 10-year Dec/Jan/Feb minus
AMIP: 1st Climate Version. 10-year Dec/Jan/Feb
Surface sensible heat flux

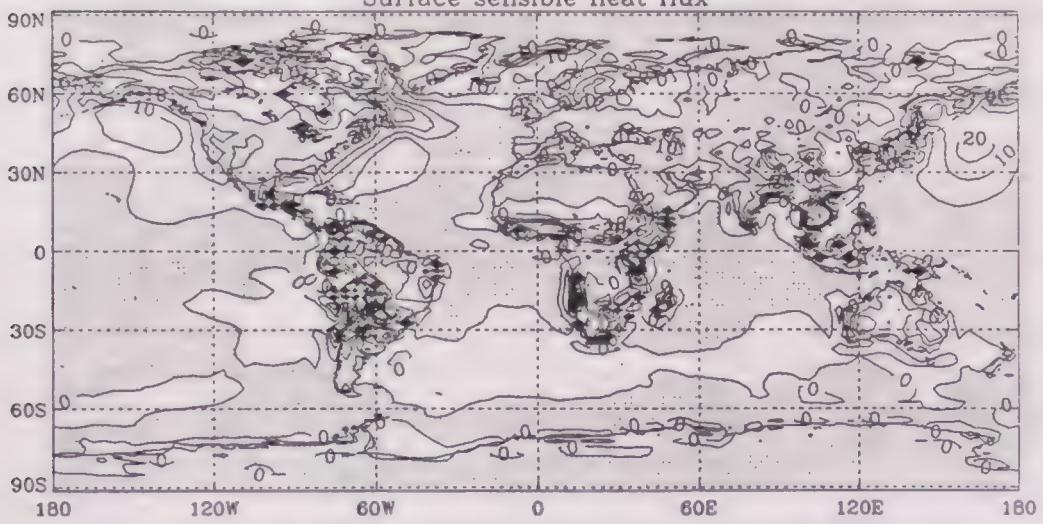

Contours every 10 Wm^{-2}. Shading less than 0

(c) AMIP: 3rd Climate Version. 10-year Dec/Jan/Feb minus
Oberhuber climatology. Dec/Jan/Feb
Surface sensible heat flux

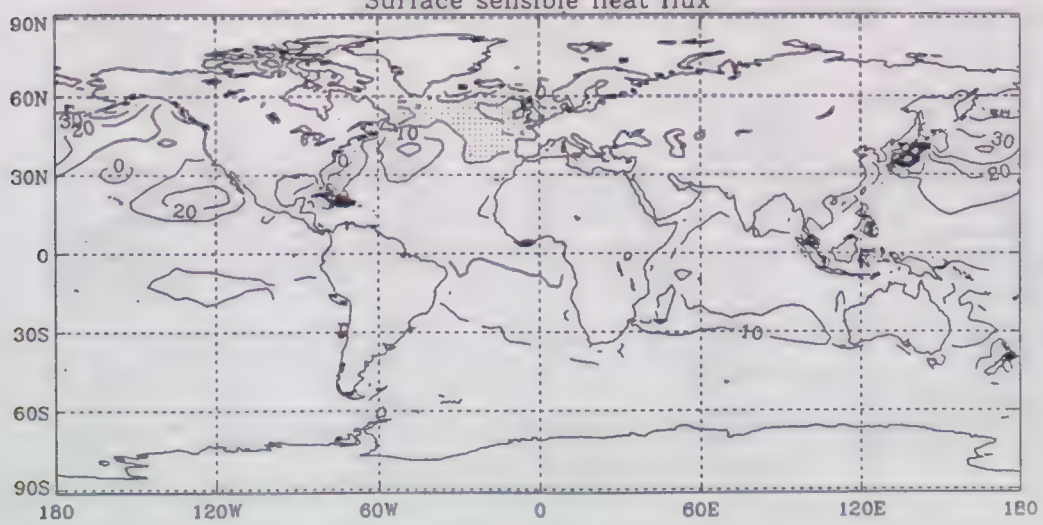

Contours every 10 Wm^{-2}. Shading less than 0

Figure 32(a) AMIP: 3rd Climate Version. 10-year Jun/Jul/Aug
Surface sensible heat flux
From 1/ 6/1979 to 1/ 9/1988

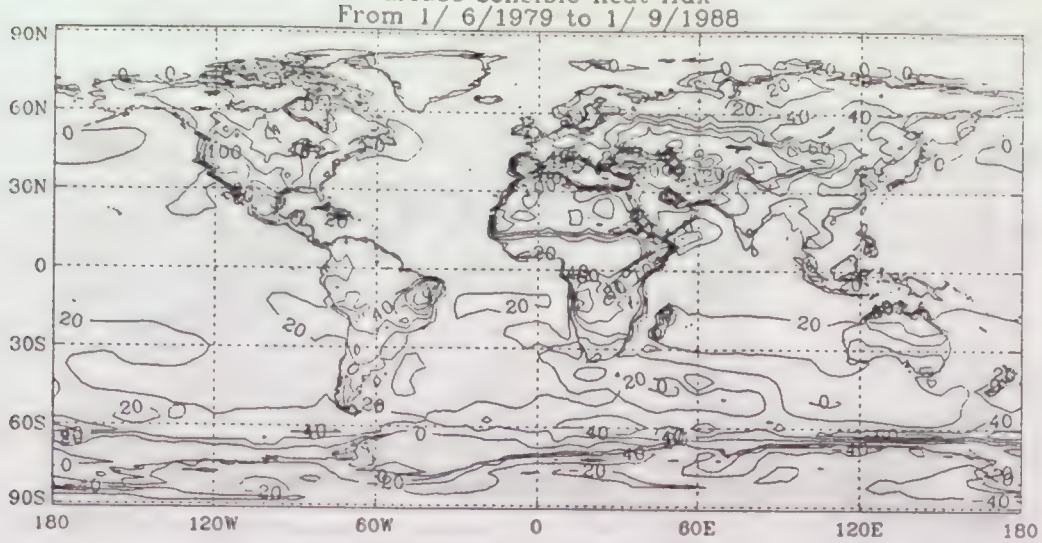

Contours every 20 Wm^{-2}. Shading less than 0

(b) AMIP: 3rd Climate Version. 10-year Jun/Jul/Aug minus
AMIP: 1st Climate Version. 10-year Jun/Jul/Aug
Surface sensible heat flux

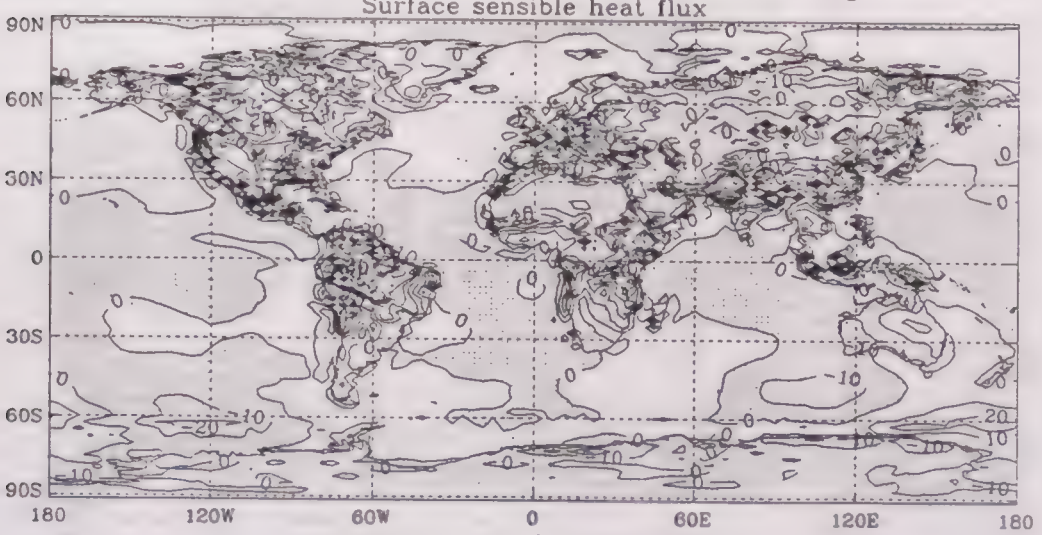

Contours every 10 Wm^{-2}. Shading less than 0

(c) AMIP: 3rd Climate Version. 10-year Jun/Jul/Aug minus
Oberhuber climatology. Jun/Jul/Aug
Surface sensible heat flux

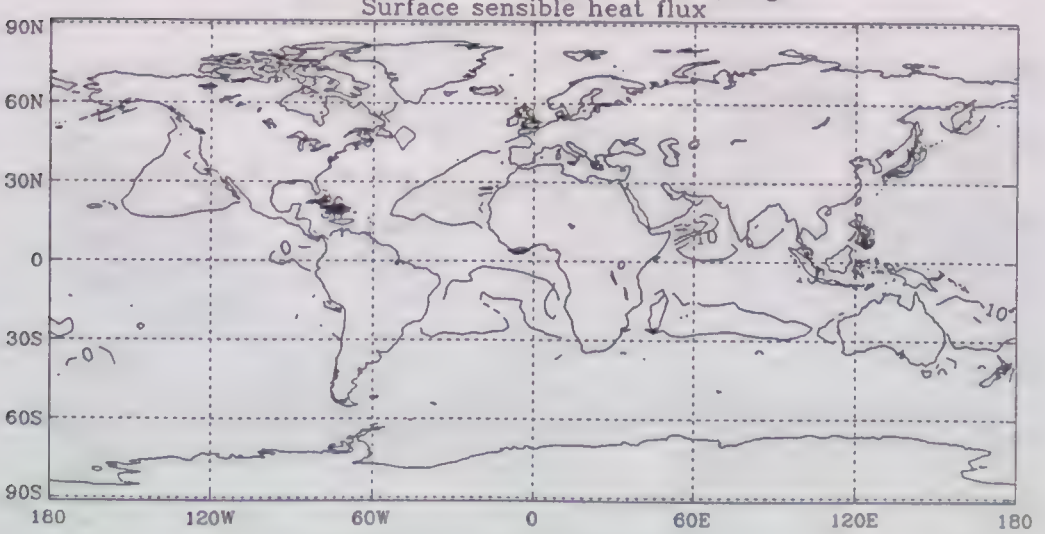

Contours every 10 Wm^{-2}. Shading less than 0

Figure 33(a) AMIP: 3rd Climate Version. 10-year Dec/Jan/Feb
Surface wind stress
From 1/ 1/1979 to 1/ 1/1989

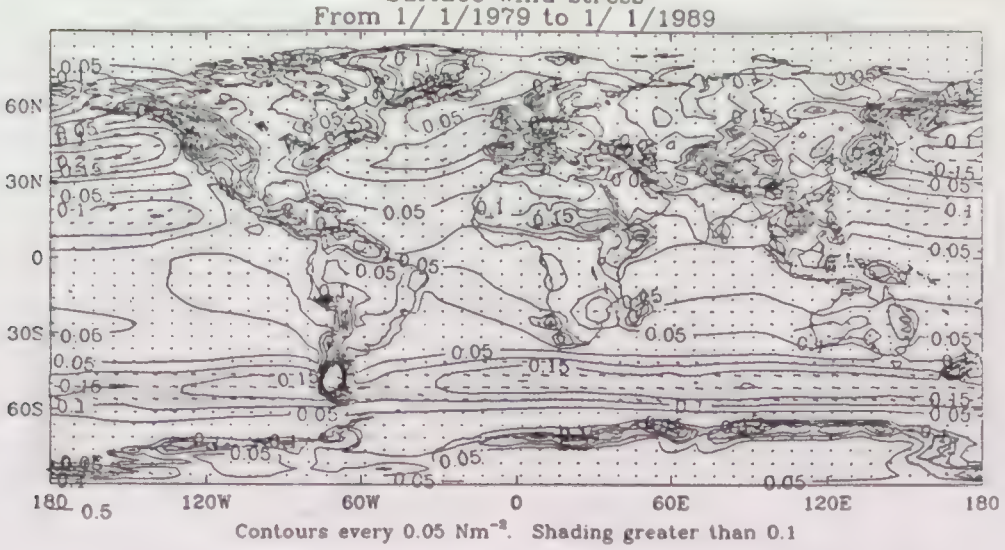

Contours every 0.05 Nm^{-2}. Shading greater than 0.1

(b)
AMIP: 1st Climate Version. 10-year Dec/Jan/Feb
Surface wind stress
From 1/12/1978 to 1/ 3/1988

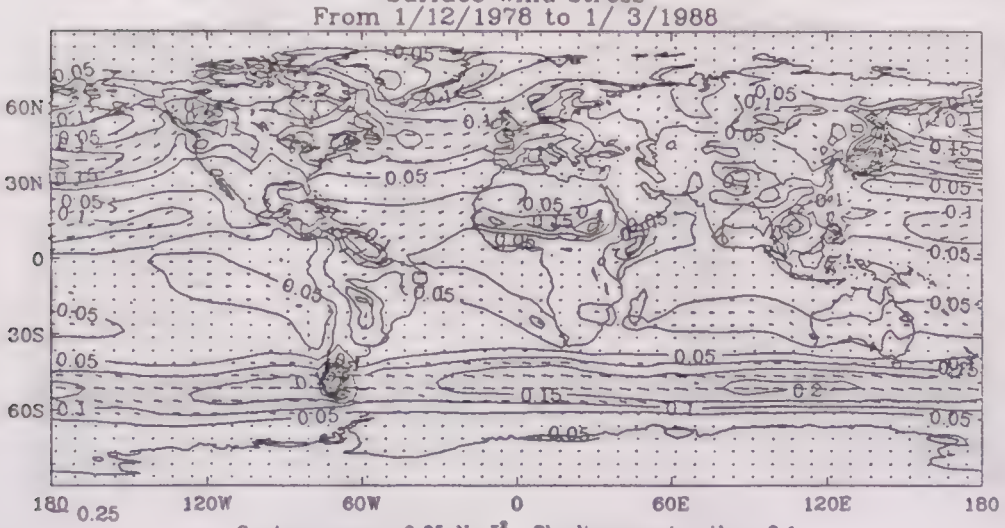

Contours every 0.05 Nm^{-2}. Shading greater than 0.1

(c)
Hellerman climatology. Dec/Jan/Feb
Surface wind stress
From 1/ 1/1870 to 31/12/1976

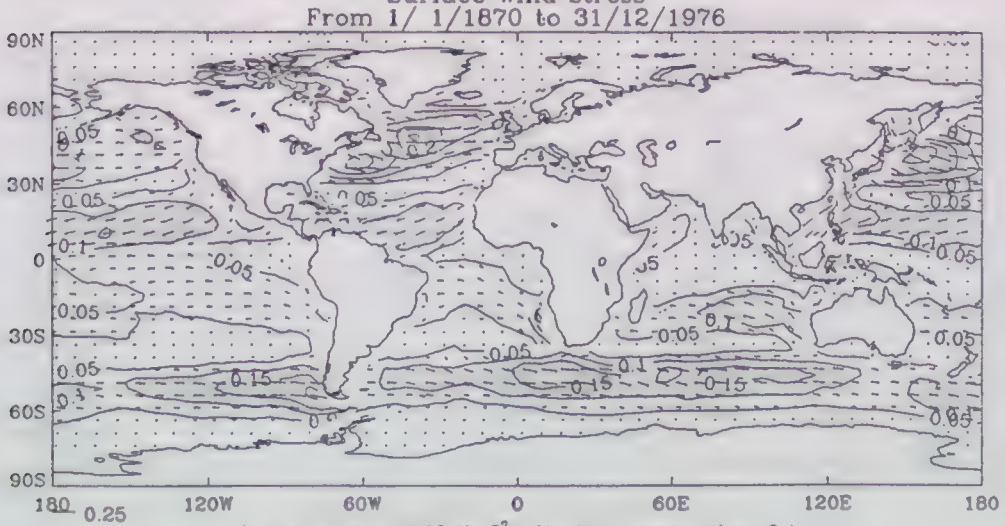

Contours every 0.05 Nm^{-2}. Shading greater than 0.1

Figure 34(a) AMIP: 3rd Climate Version. 10-year Jun/Jul/Aug
Surface wind stress
From 1/ 6/1979 to 1/ 9/1988

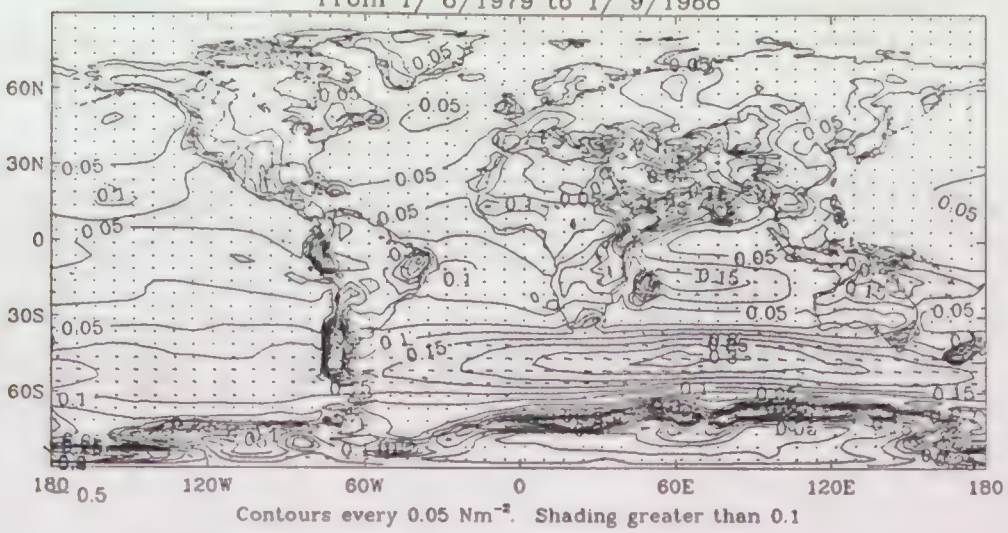

Contours every 0.05 Nm^{-2}. Shading greater than 0.1

(b)
AMIP: 1st Climate Version. 10-year Jun/Jul/Aug
Surface wind stress
From 1/ 6/1979 to 1/ 9/1988

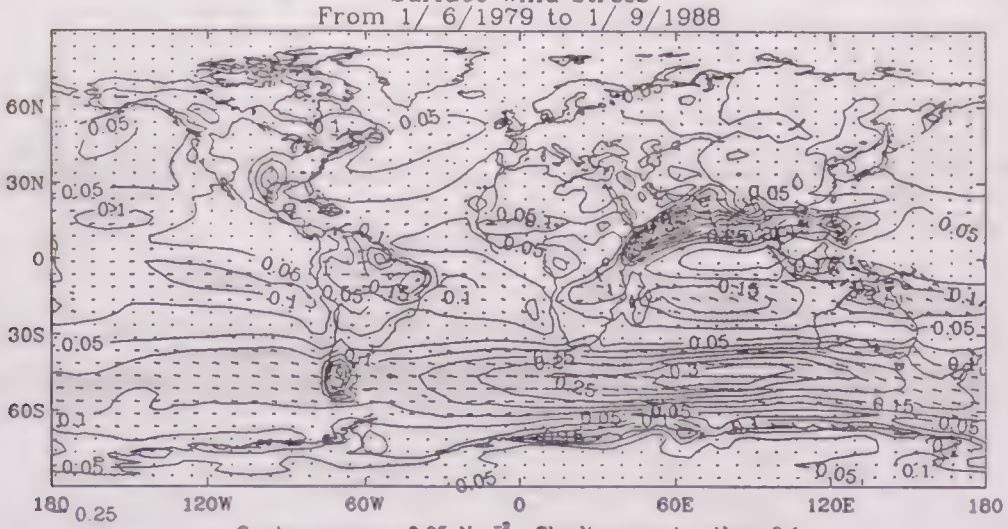

Contours every 0.05 Nm^{-2}. Shading greater than 0.1

(c)
Hellerman climatology. Jun/Jul/Aug
Surface wind stress
From 1/ 6/1870 to 31/ 8/1976

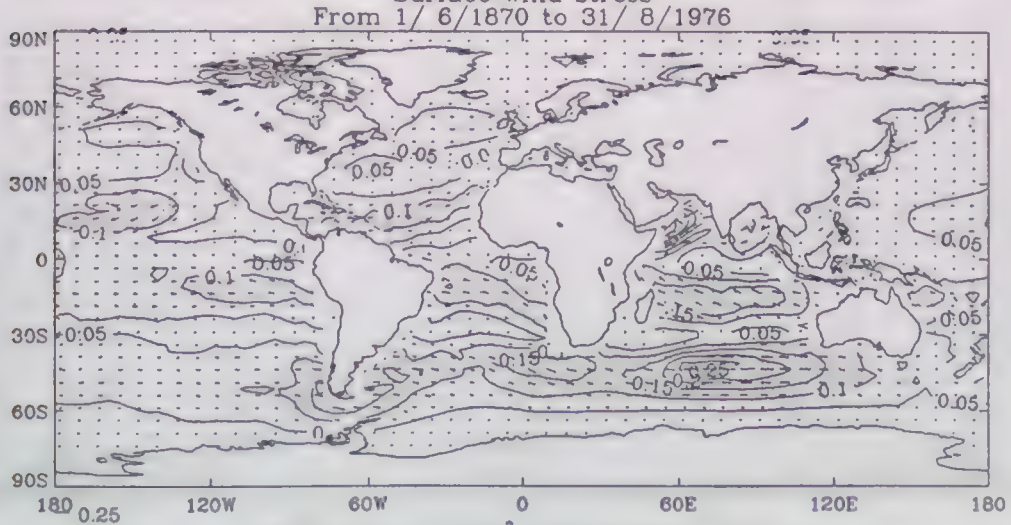

Contours every 0.05 Nm^{-2}. Shading greater than 0.1

Figure 35(a) AMIP: 3rd Climate Version. 10-year Dec/Jan/Feb
Zonal mean layer cloud
From 1/ 1/1979 to 1/ 1/1989

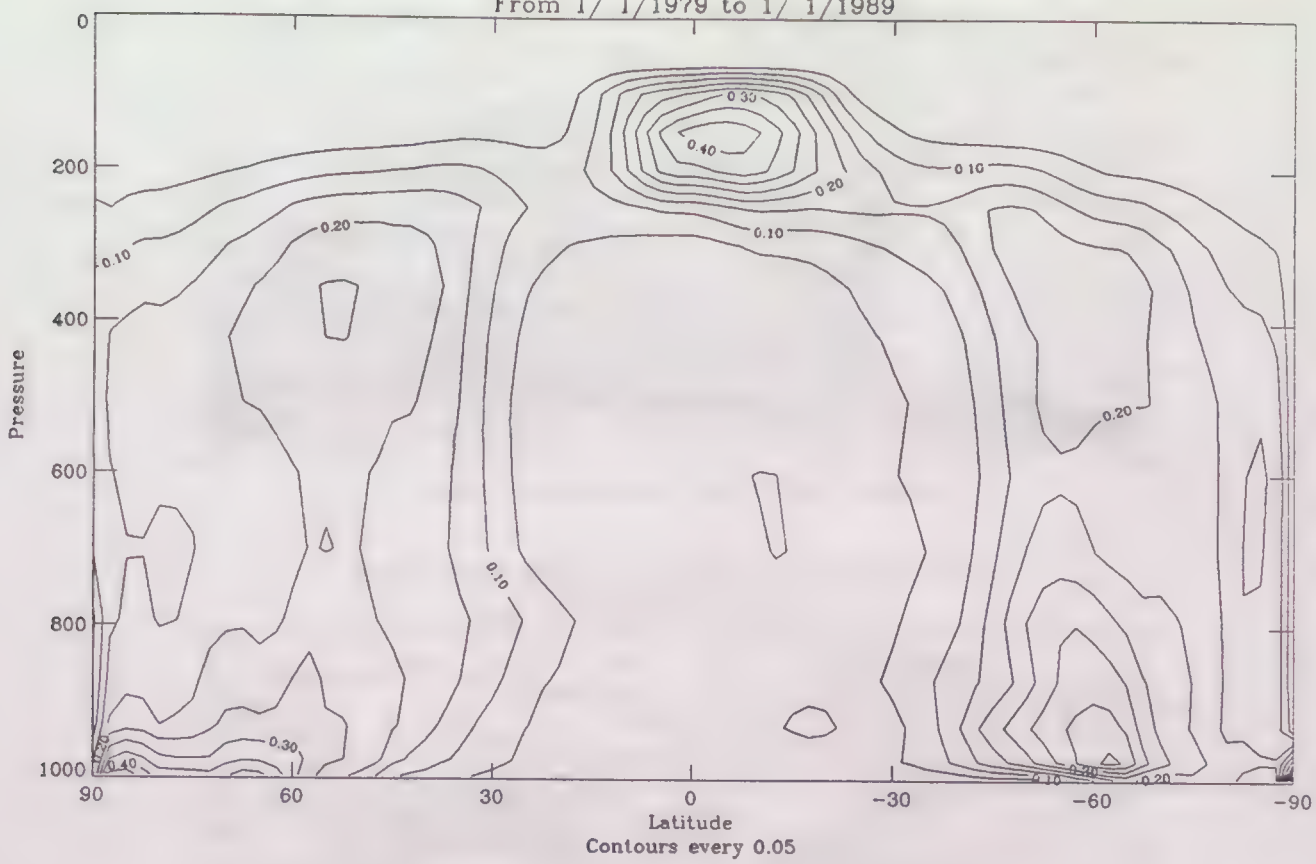

(b) AMIP: 3rd Climate Version. 10-year Dec/Jan/Feb minus
AMIP: 1st Climate Version. 10-year Dec/Jan/Feb
Zonal mean layer cloud

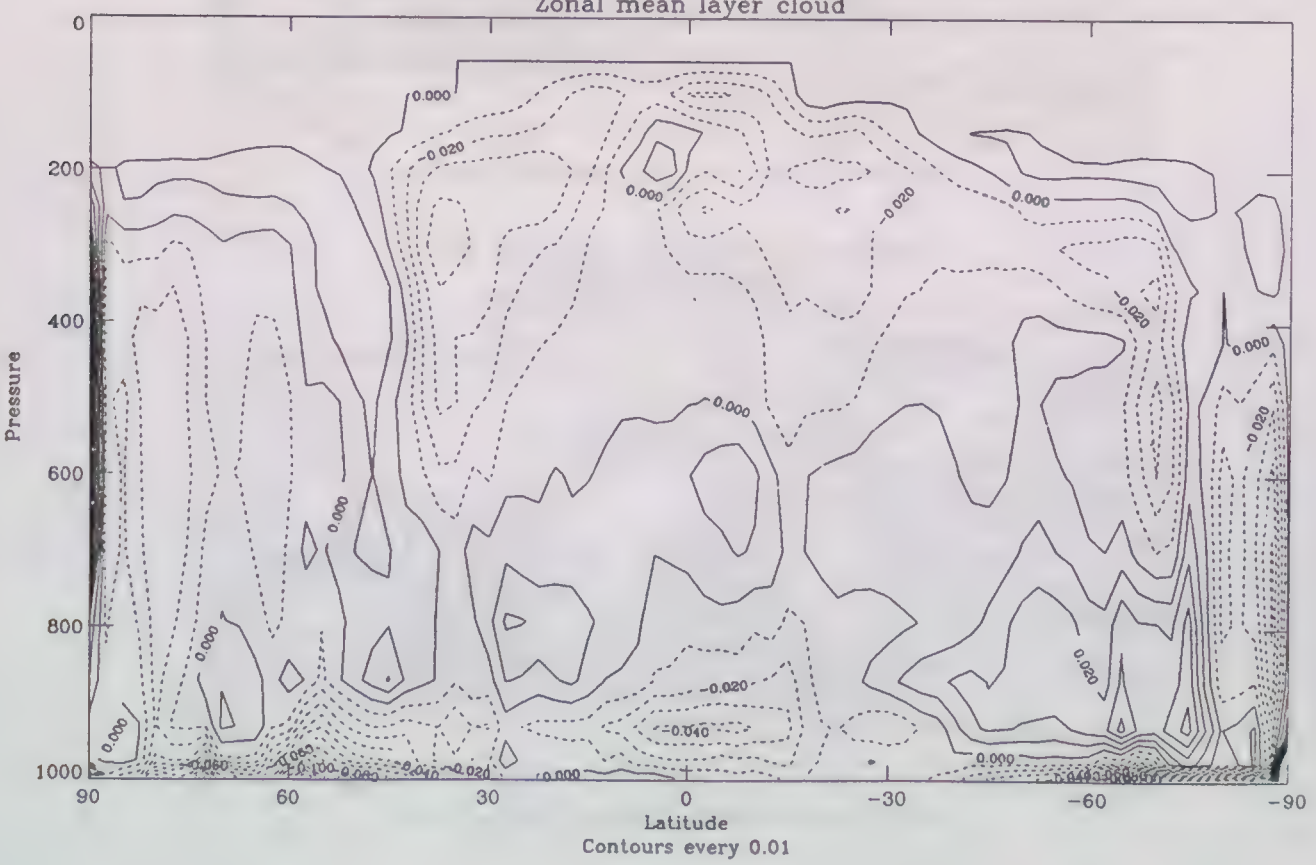

Figure 36(a) AMIP: 3rd Climate Version 10-year Jun/Jul/Aug
Zonal mean layer cloud
From 1/ 6/1979 to 1/ 9/1988

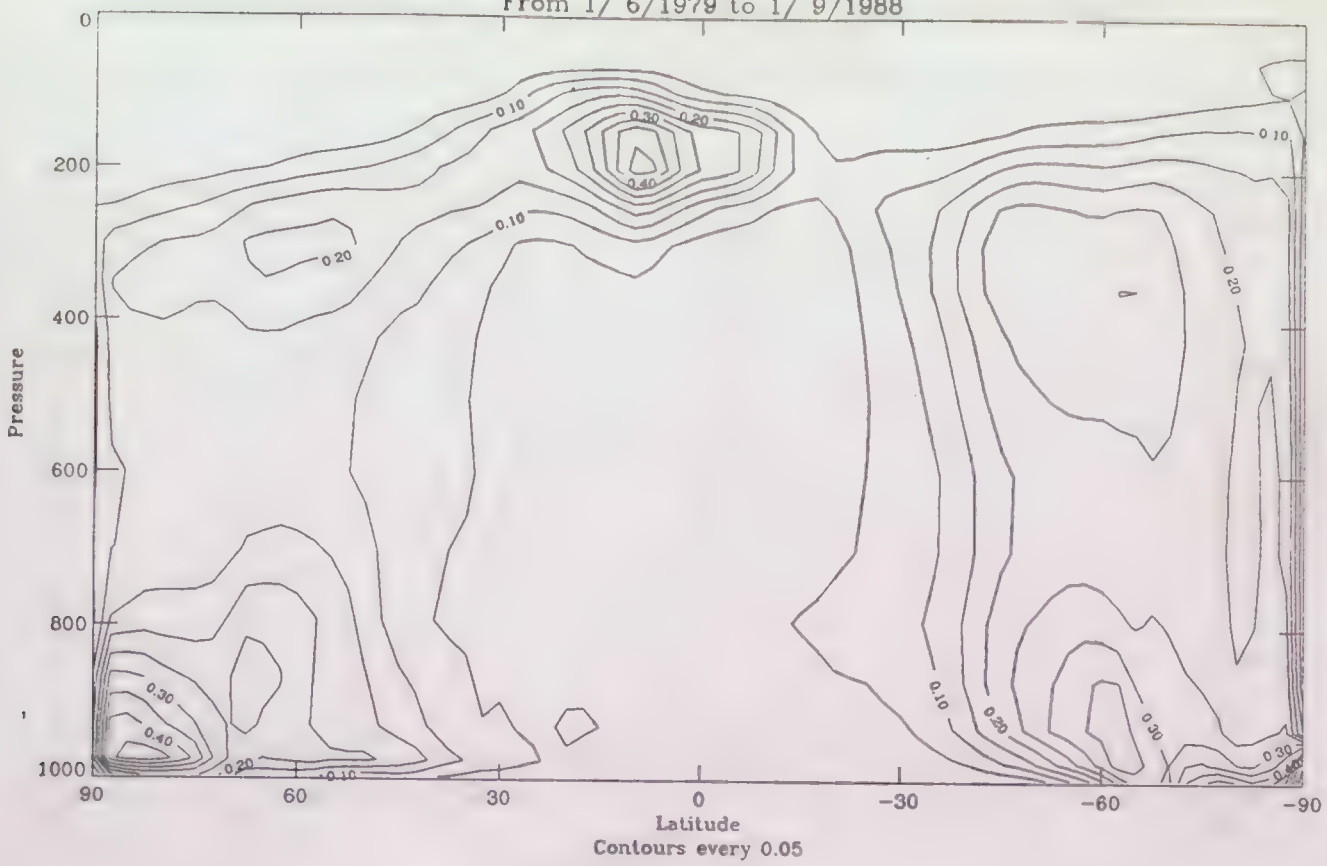

(b) AMIP: 3rd Climate Version. 10-year Jun/Jul/Aug minus
AMIP: 1st Climate Version. 10-year Jun/Jul/Aug
Zonal mean layer cloud

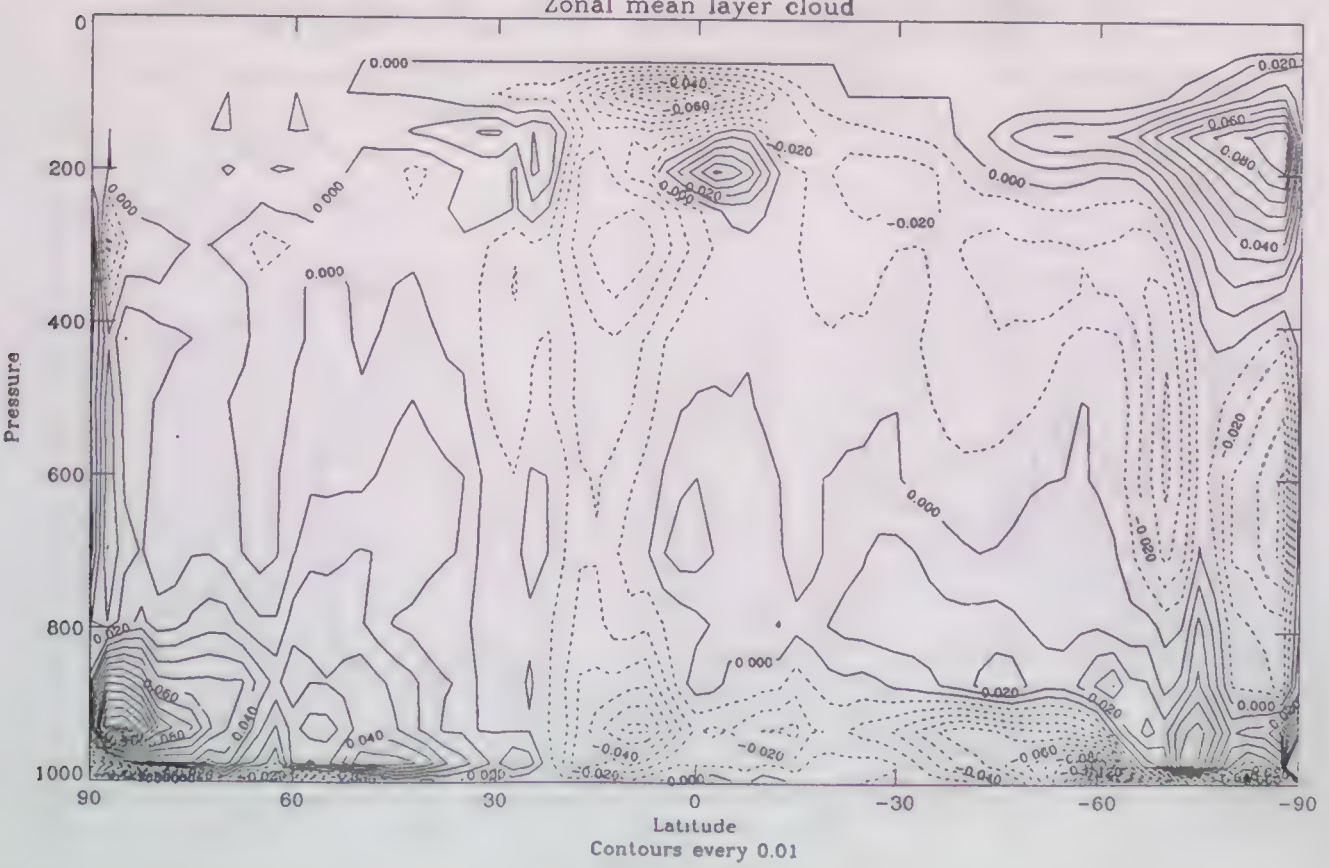

Figure 37(a) AMIP: 3rd Climate Version. 10-year Dec/Jan/Feb
Zonal mean convective cloud
From 1/ 1/1979 to 1/ 1/1989

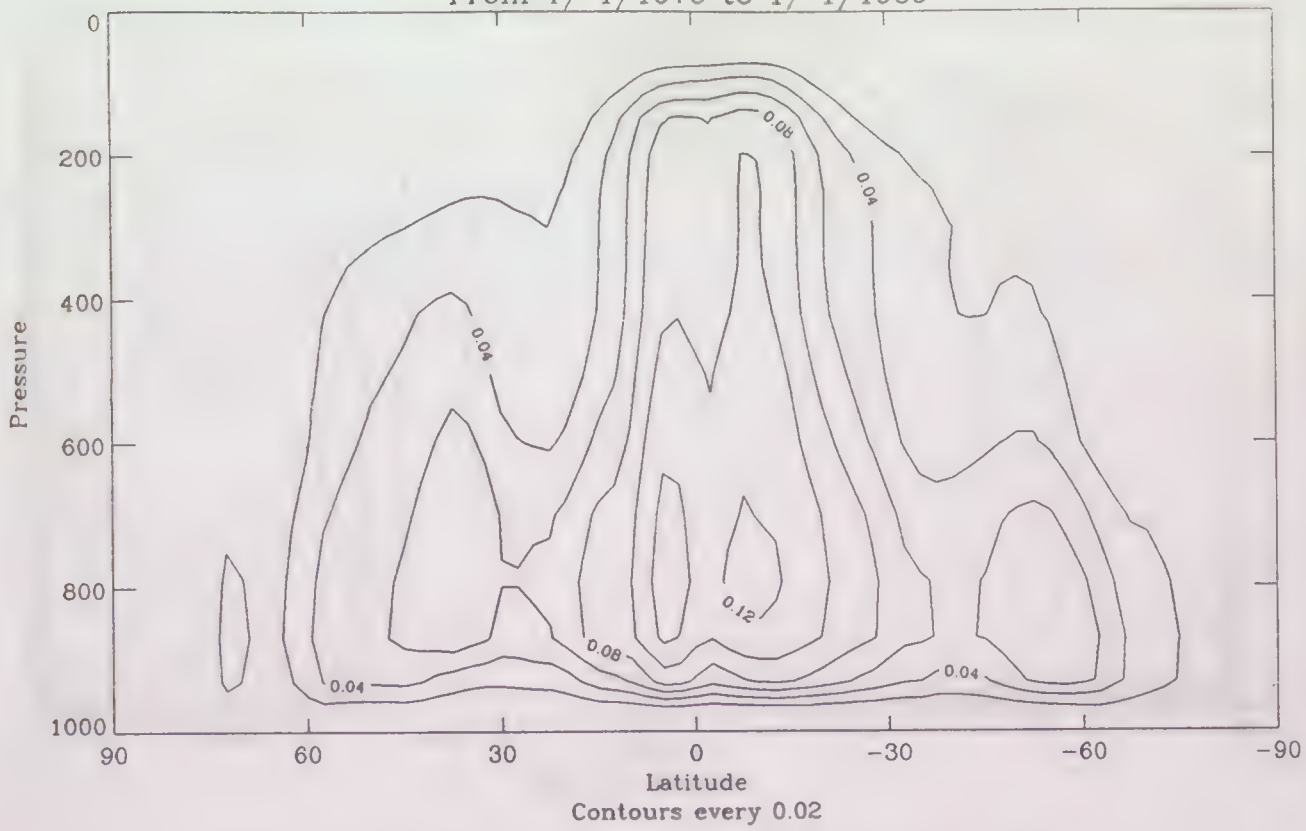

(b) AMIP: 3rd Climate Version. 10-year Dec/Jan/Feb minus
AMIP: 1st Climate Version. 10-year Dec/Jan/Feb
Zonal mean convective cloud

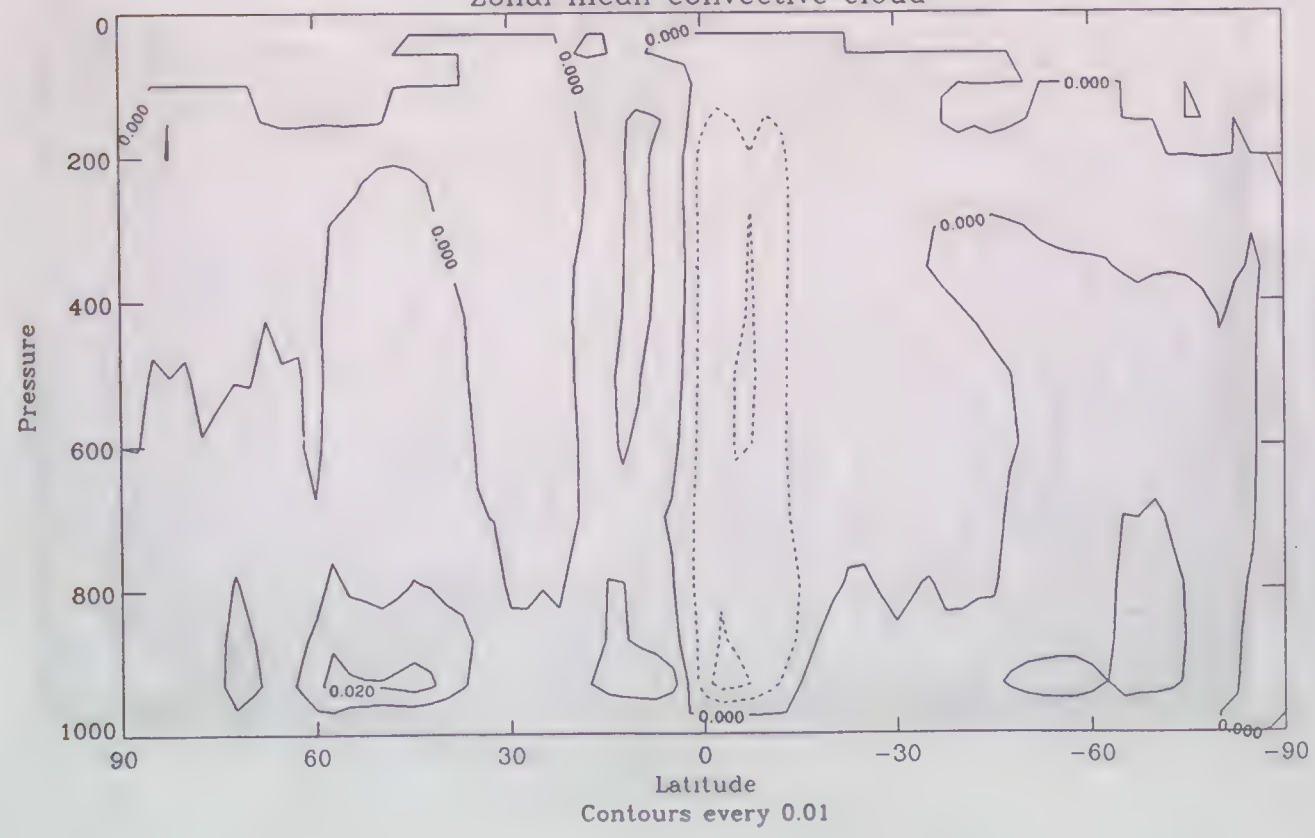

Figure 38(a) AMIP: 3rd Climate Version. 10-year Jun/Jul/Aug
Zonal mean convective cloud
From 1/ 6/1979 to 1/ 9/1988

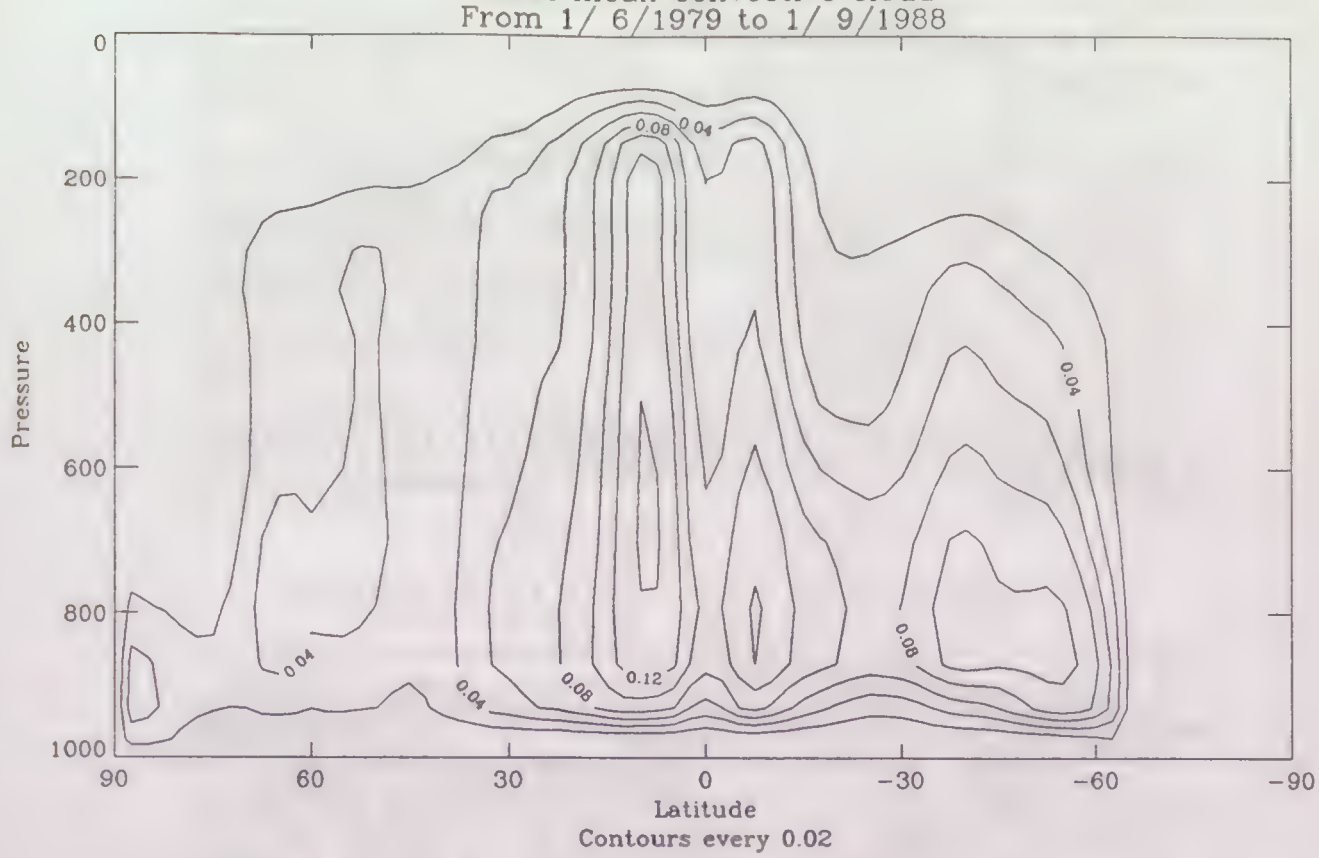

(b) AMIP: 3rd Climate Version. 10-year Jun/Jul/Aug minus
AMIP: 1st Climate Version. 10-year Jun/Jul/Aug
Zonal mean convective cloud

Figure 39(a) AMIP. 3rd Climate Version. 10-year Dec/Jan/Feb
Total cloud amount
From 1/ 1/1979 to 1/ 1/1989

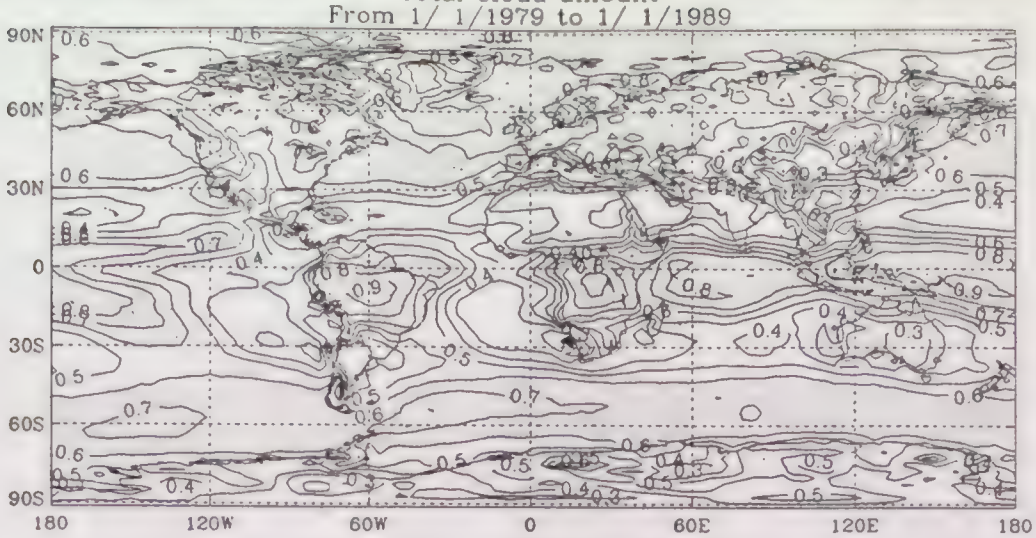

Contours every 0.1. Shading greater than 0.6
Area-weighted mean value = 0.55

(b) AMIP: 3rd Climate Version. 10-year Dec/Jan/Feb minus
AMIP: 1st Climate Version. 10-year Dec/Jan/Feb
Total cloud amount

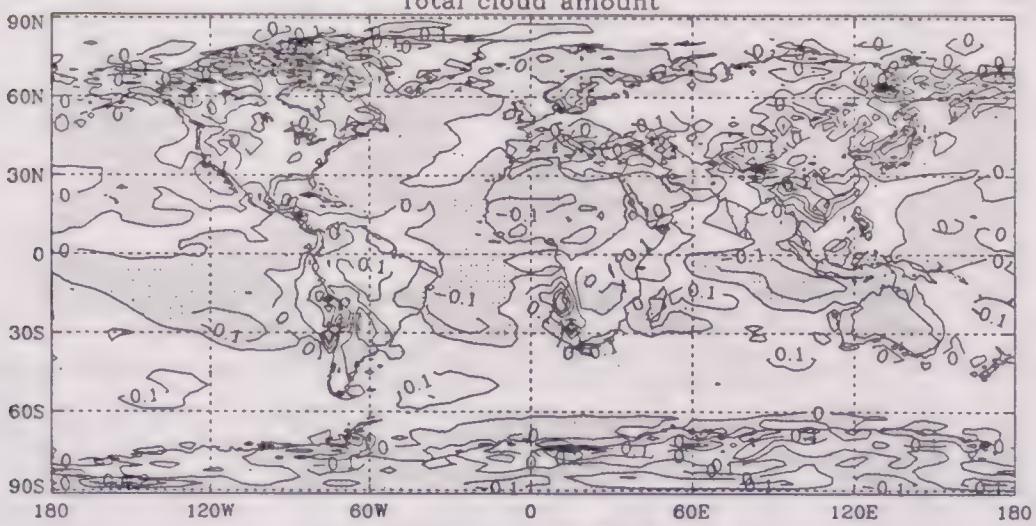

Contours every 0.1. Shading less than 0

(c) AMIP: 3rd Climate Version. 10-year Dec/Jan/Feb minus
ISCCP climatology. Dec/Jan/Feb 1984-90
Total cloud amount

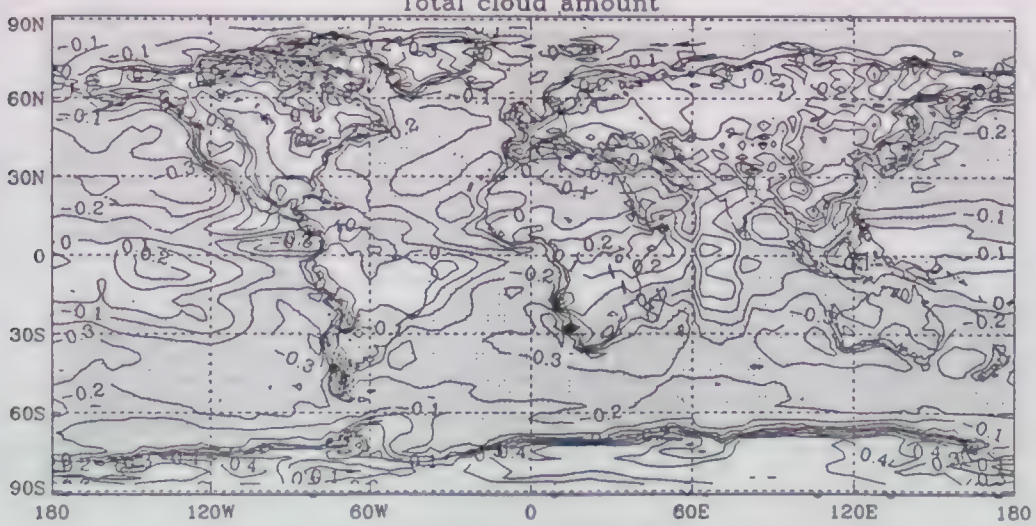

Contours every 0.1. Shading less than 0

Figure 40(a) AMIP: 3rd Climate Version. 10-year Jun/Jul/Aug
Total cloud amount
From 1/ 6/1979 to 1/ 9/1988

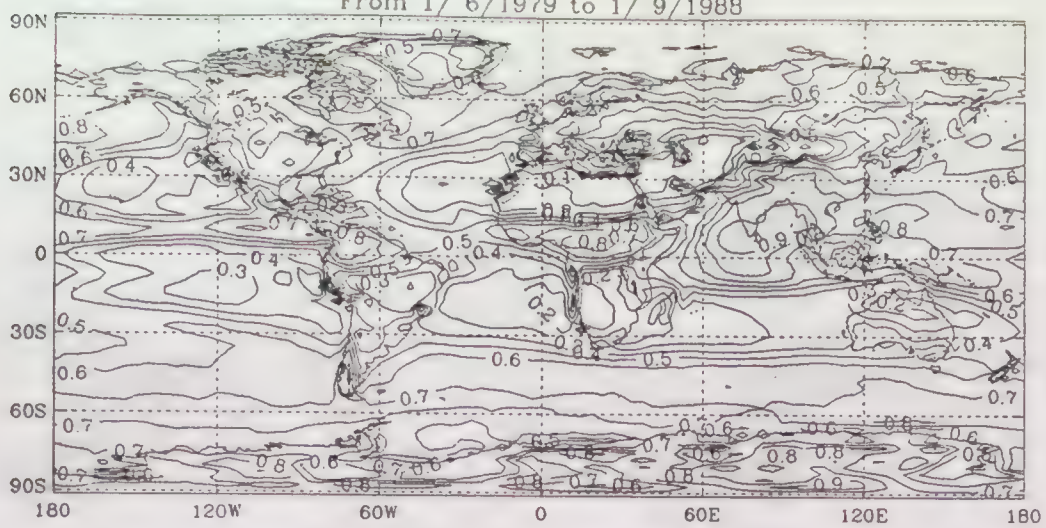

Contours every 0.1. Shading greater than 0.6
Area-weighted mean value = 0.53

(b) AMIP: 3rd Climate Version. 10-year Jun/Jul/Aug minus
AMIP: 1st Climate Version. 10-year Jun/Jul/Aug
Total cloud amount

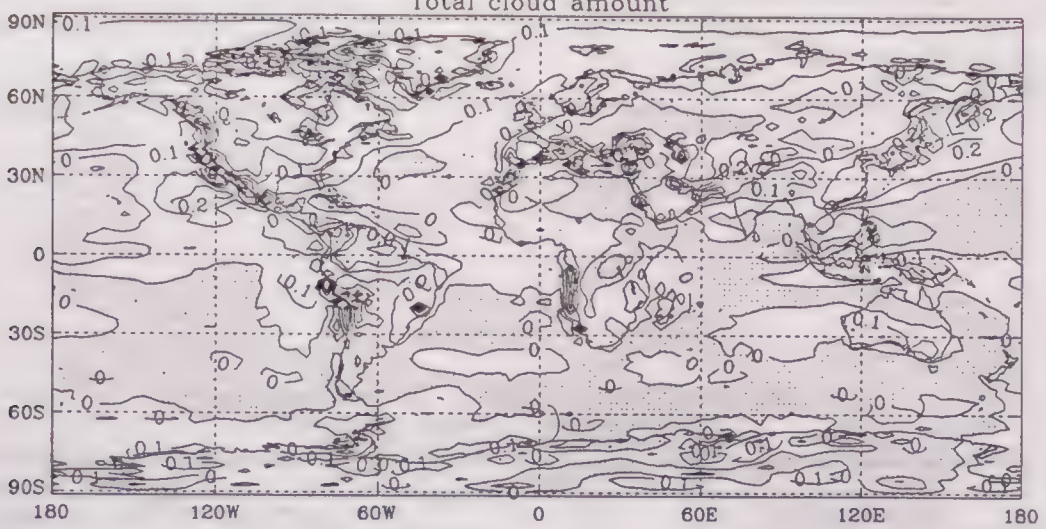

Contours every 0.1. Shading less than 0

(c) AMIP: 3rd Climate Version. 10-year Jun/Jul/Aug minus
ISCCP climatology. Jun/Jul/Aug 1984-90
Total cloud amount

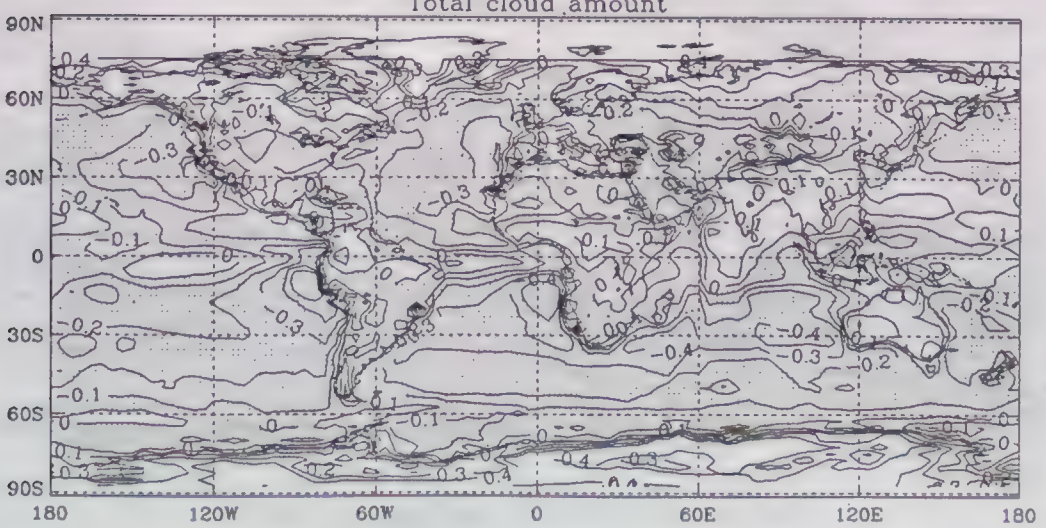

Contours every 0.1. Shading less than 0

Figure 41(a) AMIP: 3rd Climate Version. 10-year Dec/Jan/Feb
Vertically integrated cloud liquid water
From 1/ 1/1979 to 1/ 1/1989

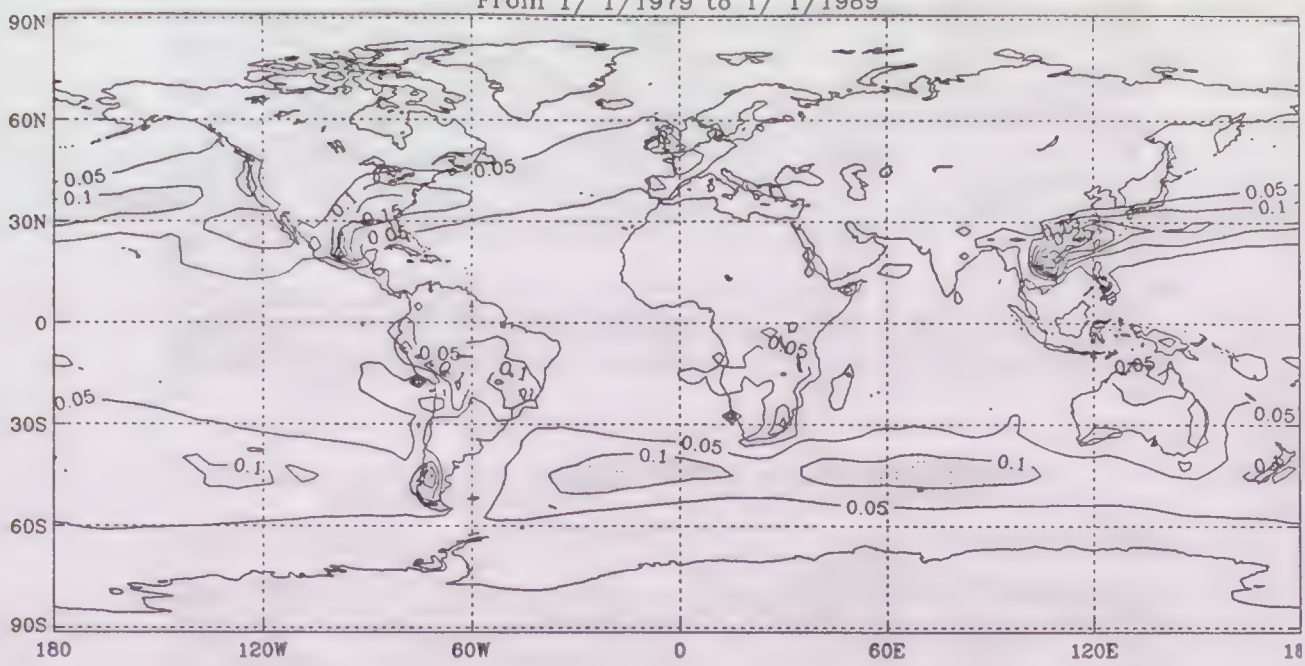

Contours every 0.05 Kg m^{-2}. Shading greater than 0.1

(b) AMIP: 1st Climate Version. 10-year Dec/Jan/Feb
Vertically integrated cloud liquid water
From 1/12/1978 to 1/ 3/1988

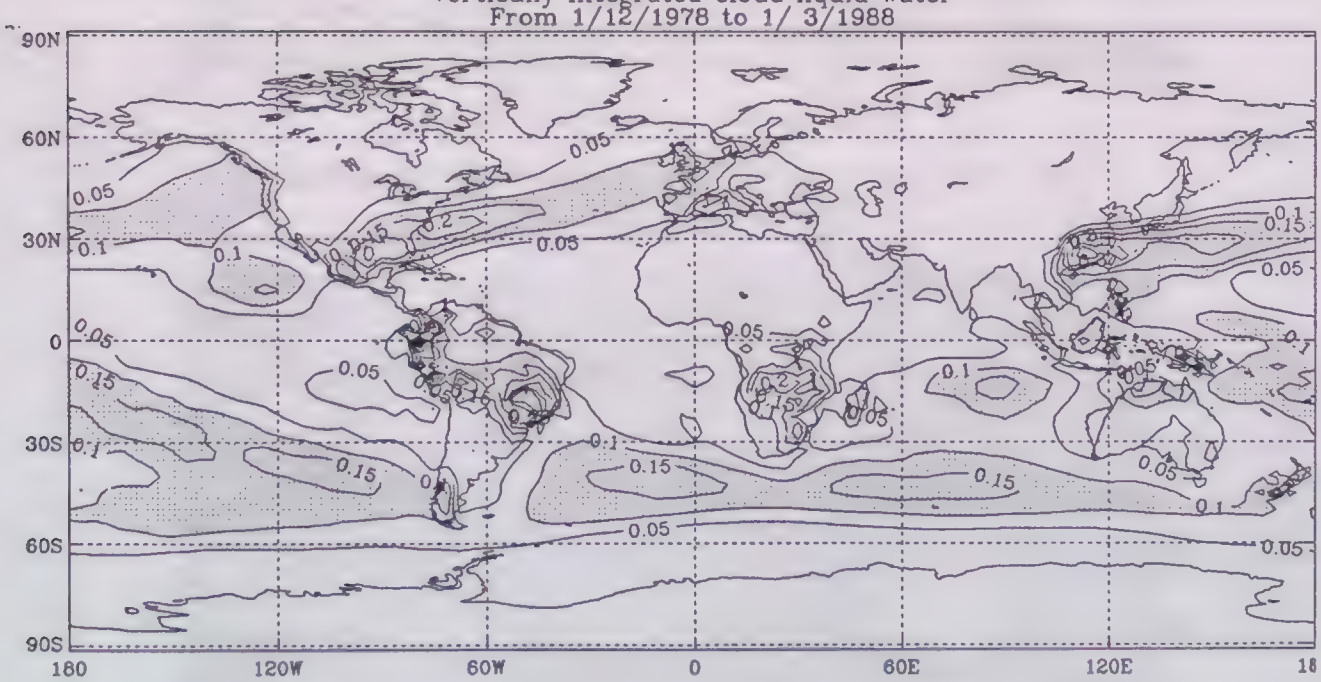

Contours every 0.05 Kg m^{-2}. Shading greater than 0.1

Figure 42(a) AMIP: 3rd Climate Version. 10-year Jun/Jul/Aug
Vertically integrated cloud liquid water
From 1/ 6/1979 to 1/ 9/1988

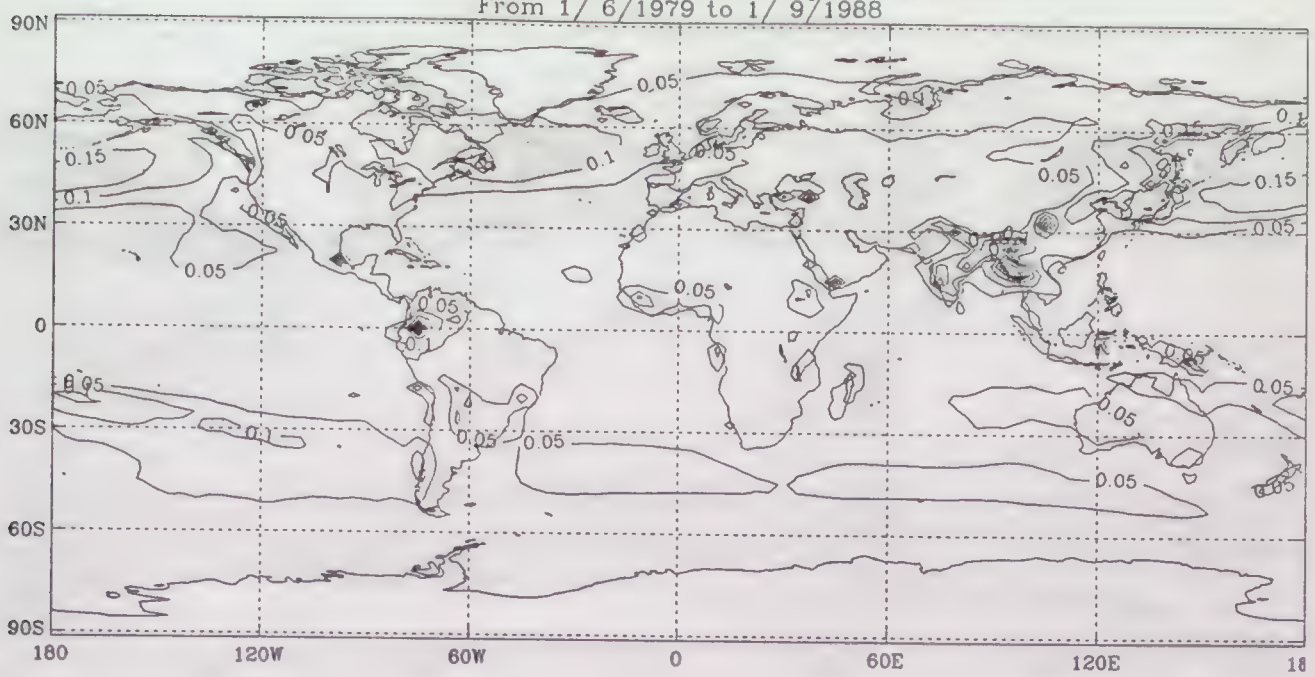

Contours every 0.05 Kg m^{-2}. Shading greater than 0.1

(b) AMIP: 1st Climate Version. 10-year Jun/Jul/Aug
Vertically integrated cloud liquid water
From 1/ 6/1979 to 1/ 9/1988

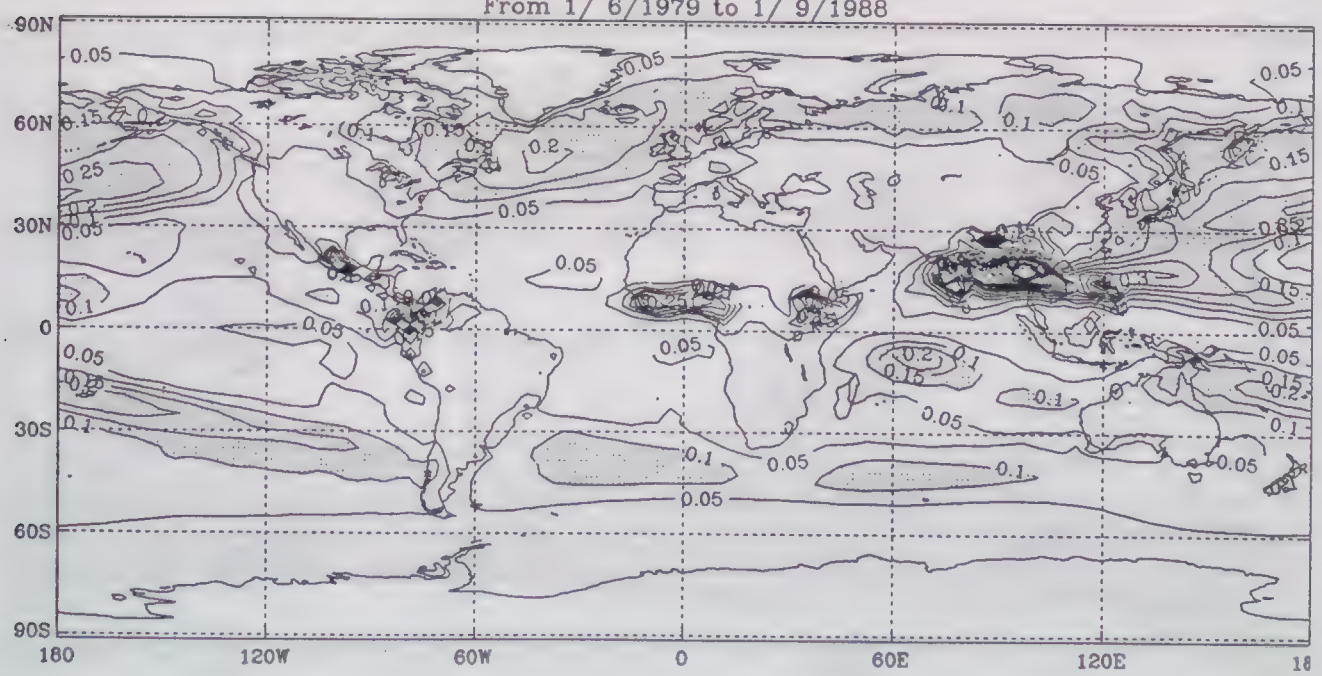

Contours every 0.05 Kg m^{-2}. Shading greater than 0.1

Figure 43(a) AMIP: 3rd Climate Version. 10-year Dec/Jan/Feb
Vertically integrated cloud ice
From 1/ 1/1979 to 1/ 1/1989

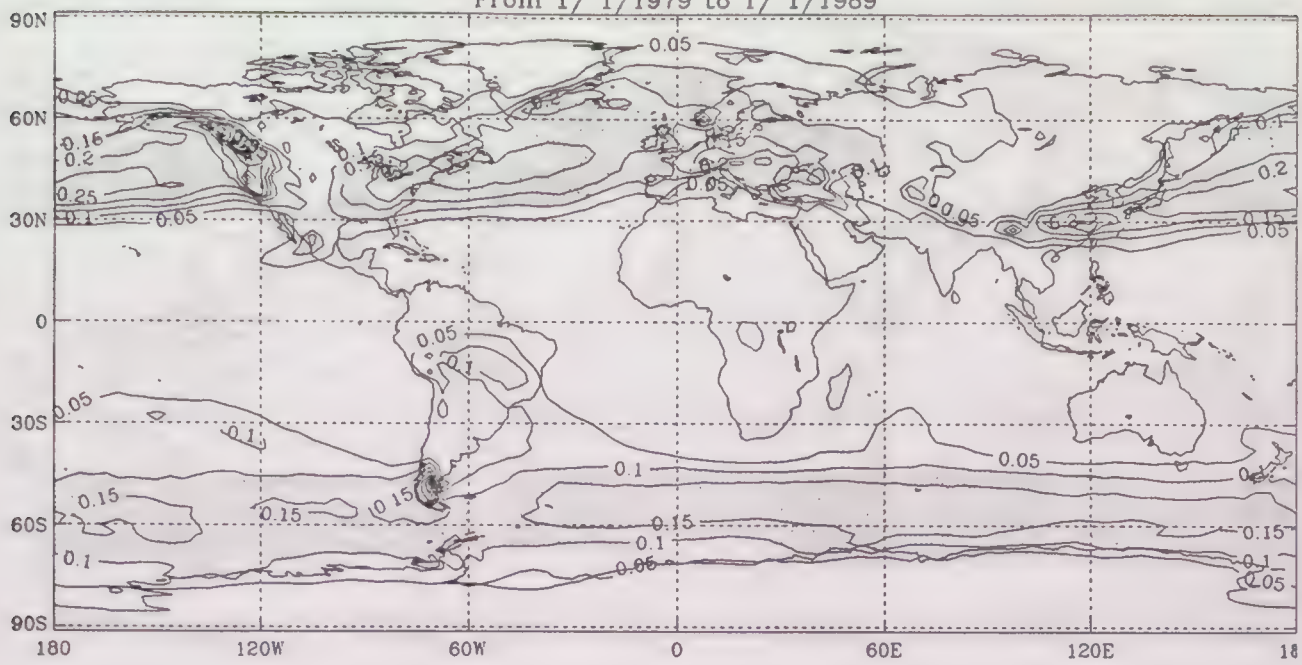

Contours every 0.05 Kg m^{-2}. Shading greater than 0.1

(b) AMIP: 1st Climate Version. 10-year Dec/Jan/Feb
Vertically integrated cloud ice
From 1/12/1978 to 1/ 3/1988

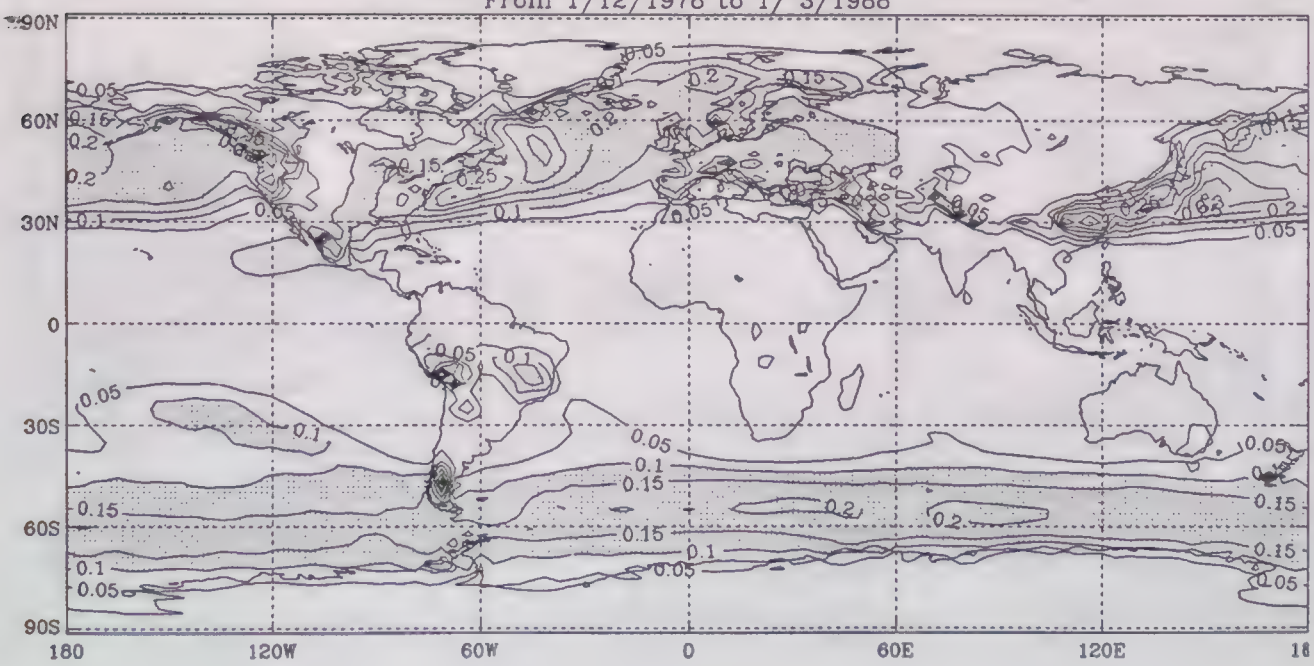

Contours every 0.05 Kg m^{-2}. Shading greater than 0.1

Figure 44(a) AMIP: 3rd Climate Version. 10-year Jun/Jul/Aug
Vertically integrated cloud ice
From 1/ 6/1979 to 1/ 9/1988

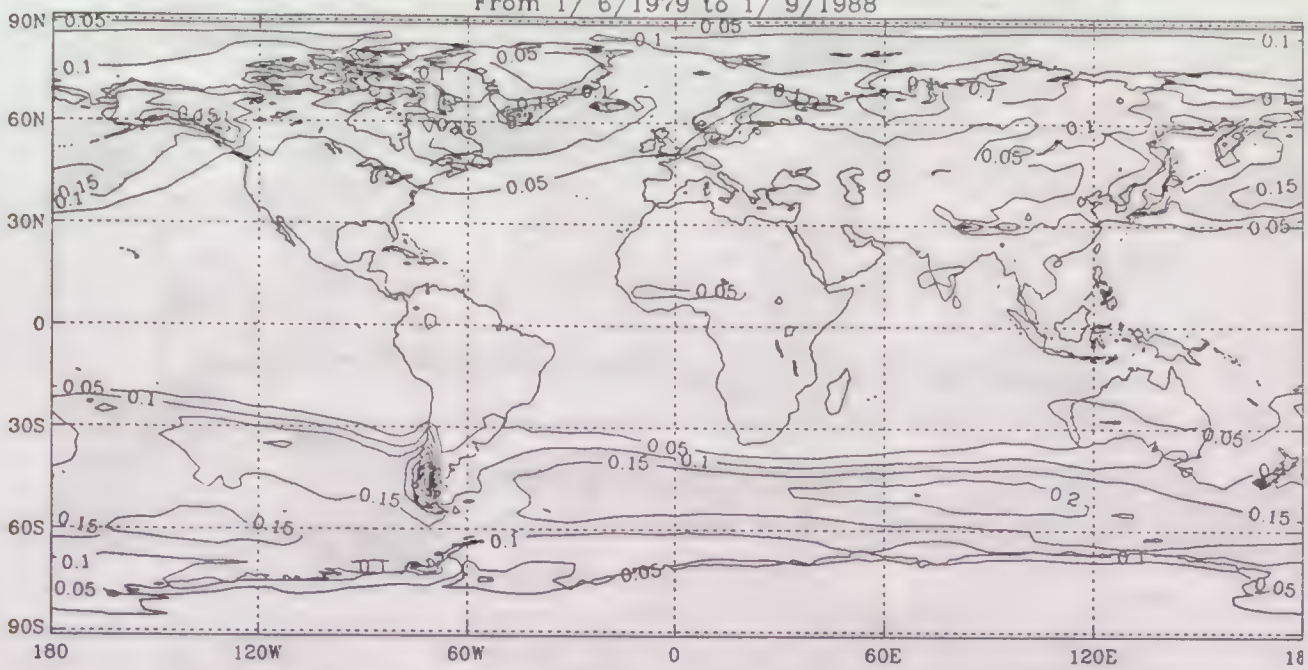

Contours every 0.05 Kg m^{-2}. Shading greater than 0.1

(b) AMIP: 1st Climate Version. 10-year Jun/Jul/Aug
Vertically integrated cloud ice
From 1/ 6/1979 to 1/ 9/1988

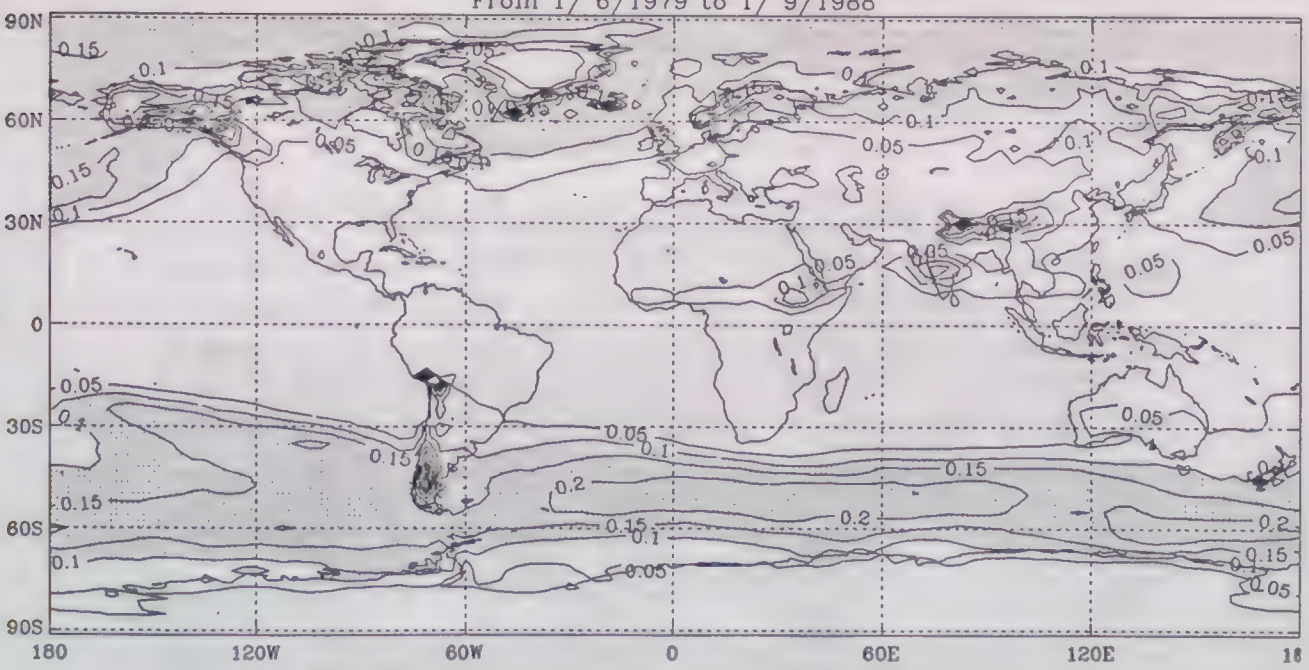

Contours every 0.05 Kg m^{-2}. Shading greater than 0.1

Figure 45(a) AMIP 3rd Climate Version. 10-year Dec/Jan/Feb
Albedo at top of atmosphere
From 1/ 1/1979 to 1/ 1/1989

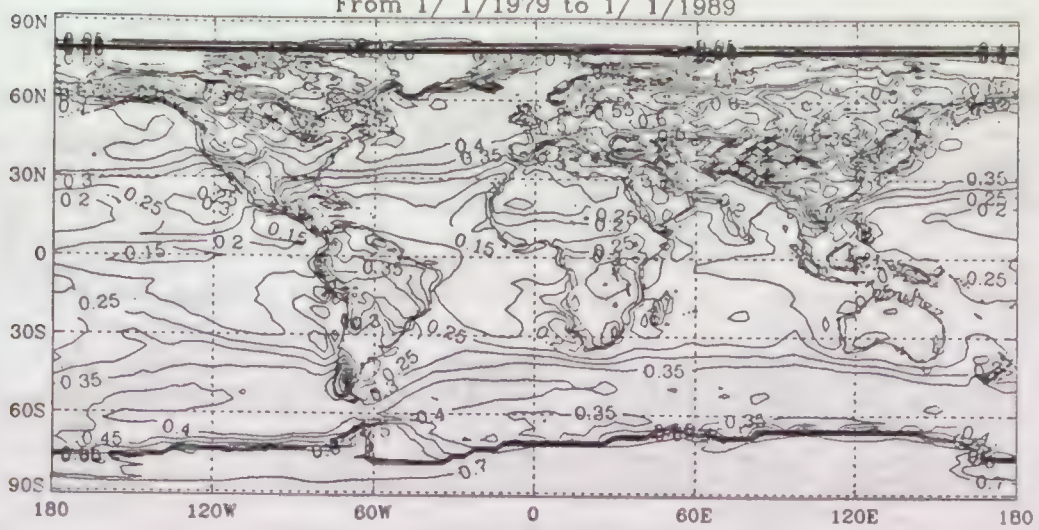

Contours every 0.05. Shading greater than 0.3
Area-weighted mean value = 0.32

(b) AMIP: 3rd Climate Version. 10-year Dec/Jan/Feb minus
AMIP: 1st Climate Version. 10-year Dec/Jan/Feb
Albedo at top of atmosphere

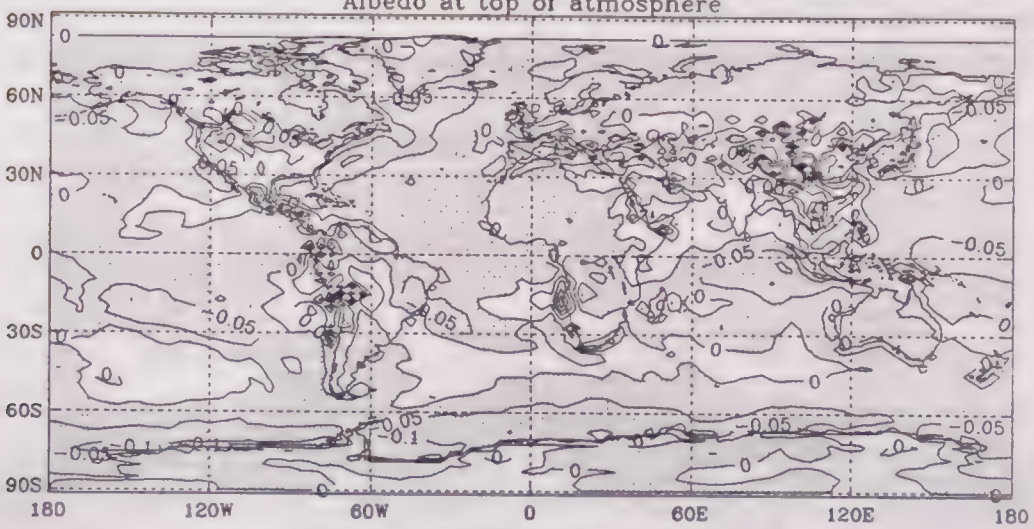

Contours every 0.05. Shading less than 0

(c) AMIP: 3rd Climate Version. 10-year Dec/Jan/Feb minus
ERBE climatology. Dec/Jan/Feb 1985-88
Albedo at top of atmosphere

Contours every 0.05. Shading less than 0

Figure 46(a) AMIP 3rd Climate Version 10-year Jun/Jul/Aug
Albedo at top of atmosphere
From 1/ 6/1979 to 1/ 9/1988

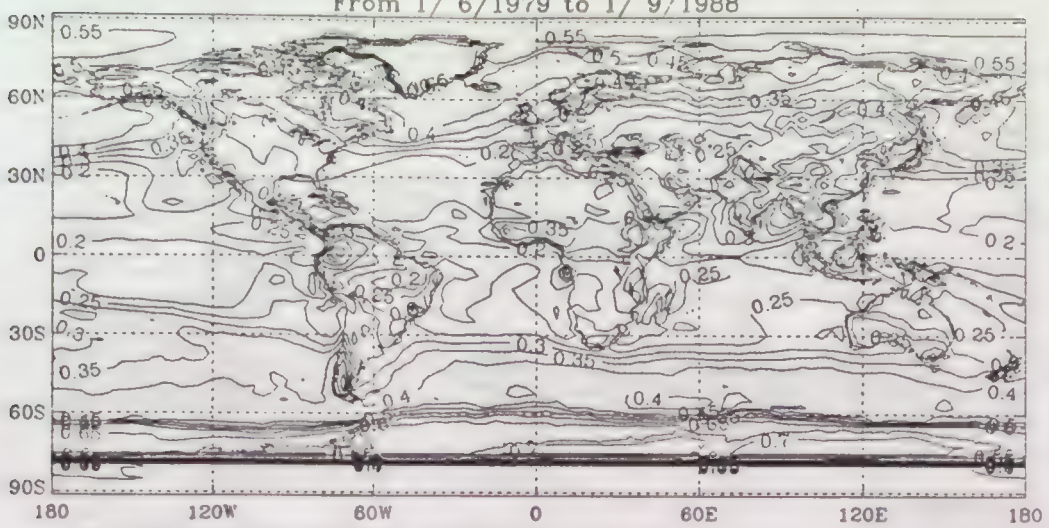

Contours every 0.05. Shading greater than 0.3
Area-weighted mean value = 0.31

(b) AMIP: 3rd Climate Version. 10-year Jun/Jul/Aug minus
AMIP: 1st Climate Version. 10-year Jun/Jul/Aug
Albedo at top of atmosphere

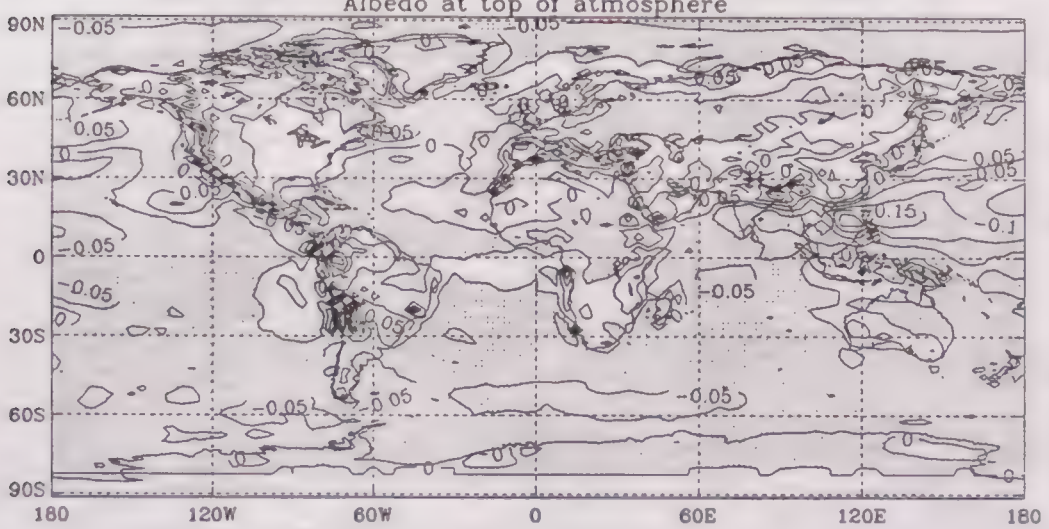

Contours every 0.05. Shading less than 0

(c) AMIP: 3rd Climate Version. 10-year Jun/Jul/Aug minus
ERBE climatology. Jun/Jul/Aug 1985-88
Albedo at top of atmosphere

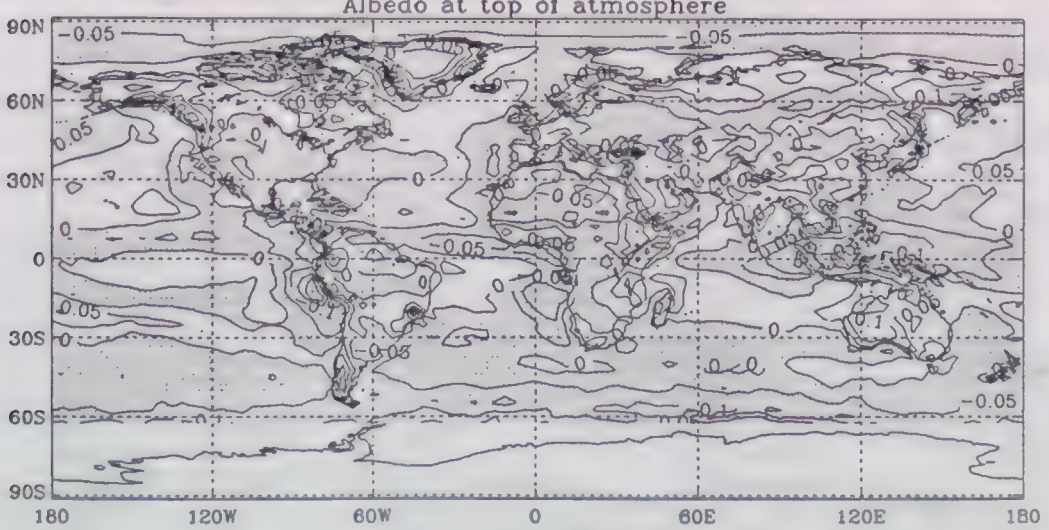

Contours every 0.05. Shading less than 0

Figure 47(a) AMIP. 3rd Climate Version. 10-year Dec/Jan/Feb
Outgoing longwave radiation at top of atmosphere
From 1/ 1/1979 to 1/ 1/1989

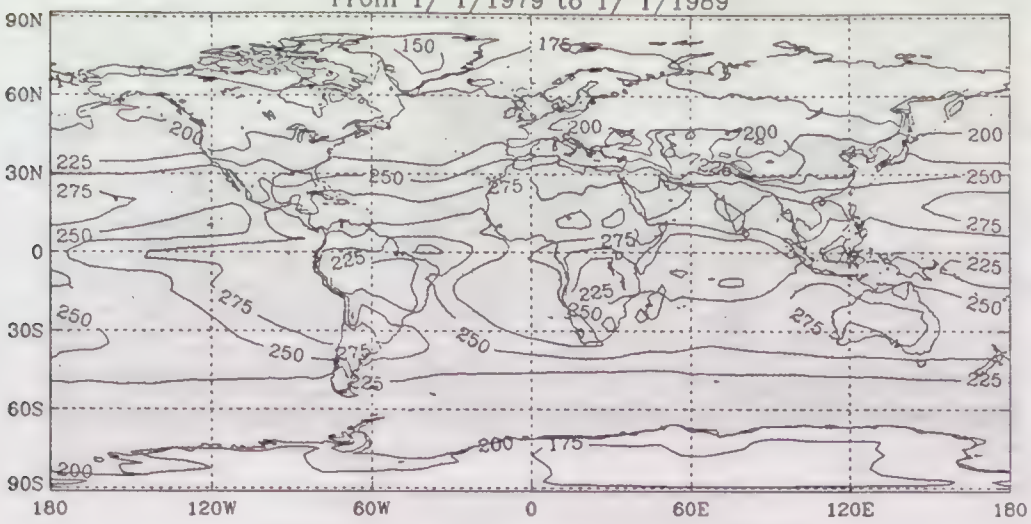

Contours every 25 Wm^{-2}. Shading greater than 200
Area-weighted mean value = 237.43

(b) AMIP: 3rd Climate Version. 10-year Dec/Jan/Feb minus
AMIP: 1st Climate Version. 10-year Dec/Jan/Feb
Outgoing longwave radiation at top of atmosphere

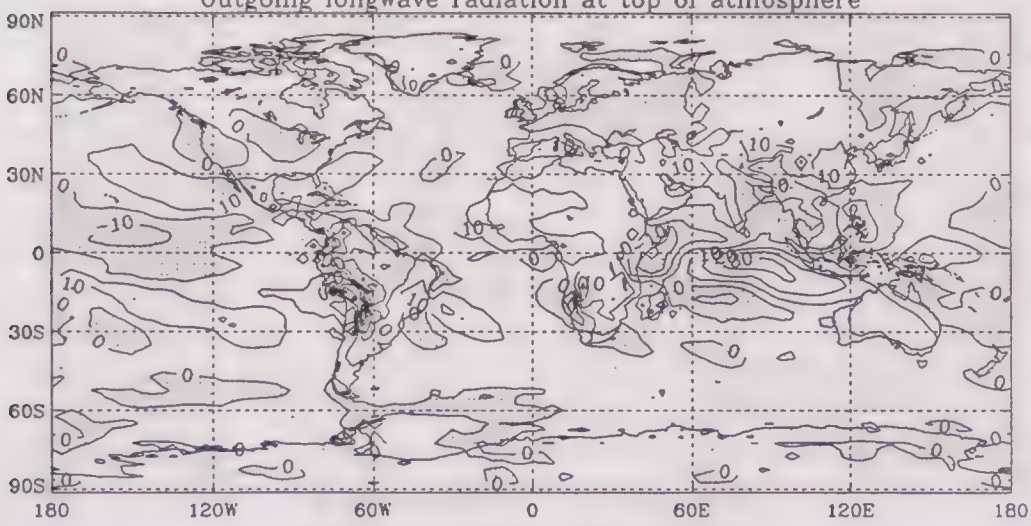

Contours every 10 Wm^{-2}. Shading less than 0

(c) AMIP: 3rd Climate Version. 10-year Dec/Jan/Feb minus
ERBE climatology. Dec/Jan/Feb 1985-88
Outgoing longwave radiation at top of atmosphere

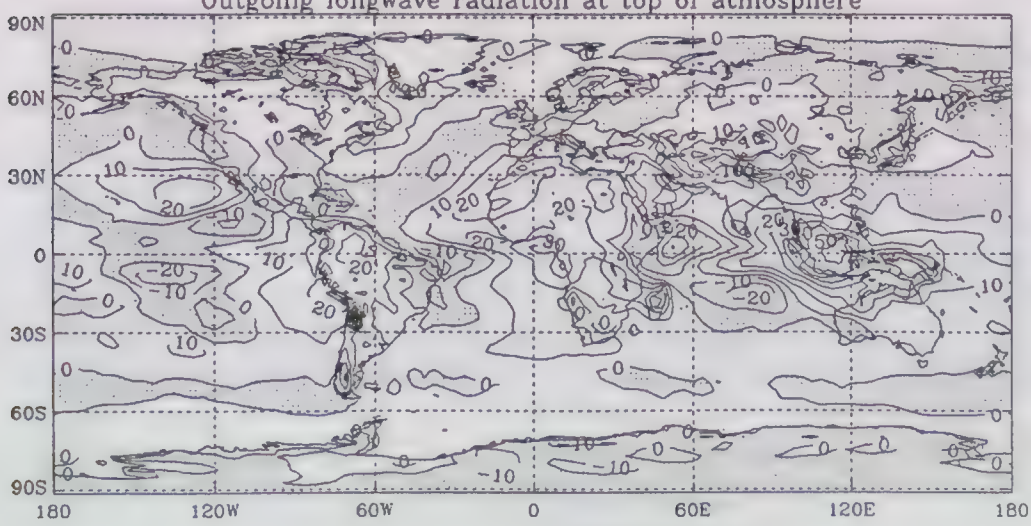

Contours every 10 Wm^{-2}. Shading less than 0

Figure 48(a) AMIP: 3rd Climate Version. 10-year Jun/Jul/Aug
Outgoing longwave radiation at top of atmosphere
From 1/ 6/1979 to 1/ 9/1988

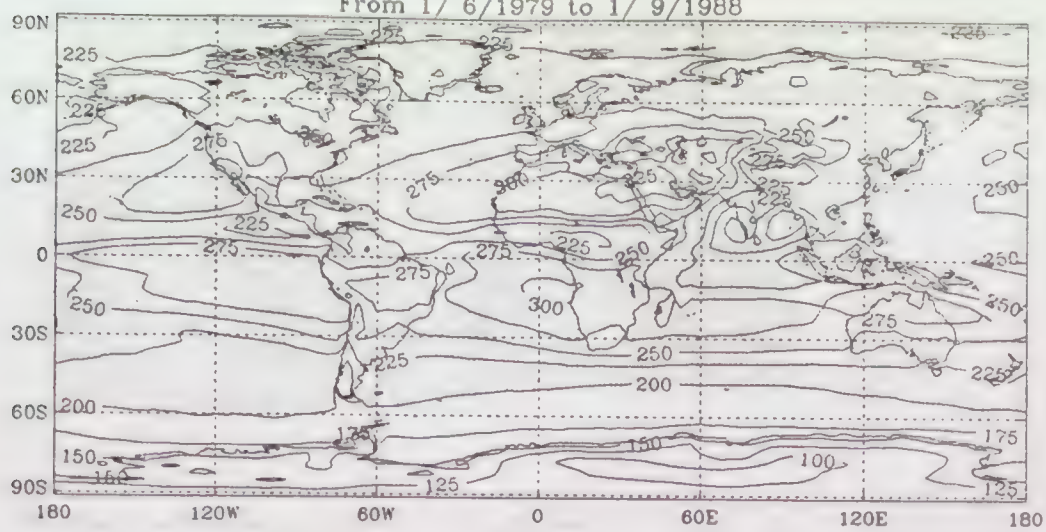

Contours every 25 Wm^{-2}. Shading greater than 200
Area-weighted mean value = 243.85

(b) AMIP: 3rd Climate Version. 10-year Jun/Jul/Aug minus
AMIP: 1st Climate Version. 10-year Jun/Jul/Aug
Outgoing longwave radiation at top of atmosphere

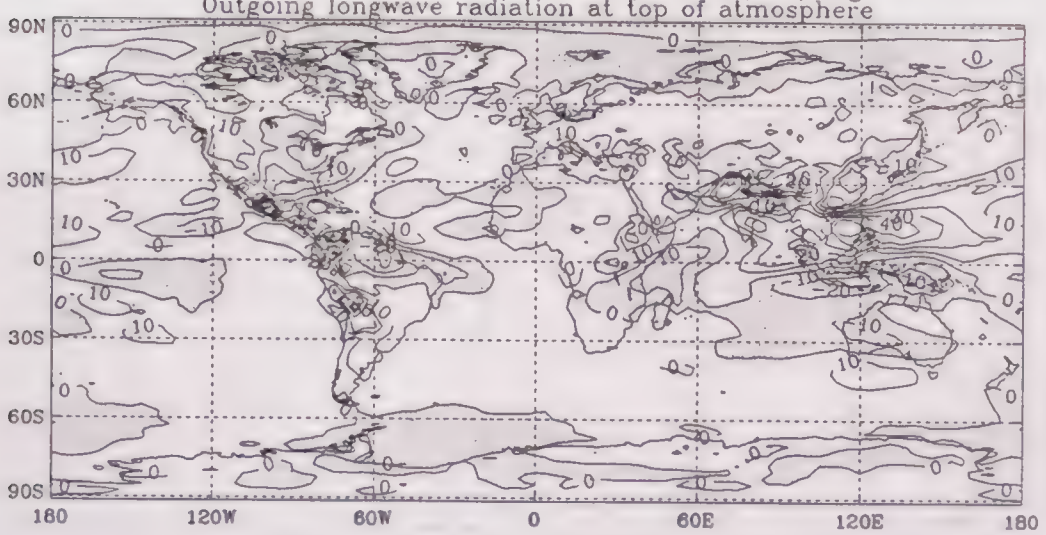

Contours every 10 Wm^{-2}. Shading less than 0

(c) AMIP: 3rd Climate Version. 10-year Jun/Jul/Aug minus
ERBE climatology. Jun/Jul/Aug 1985-88
Outgoing longwave radiation at top of atmosphere

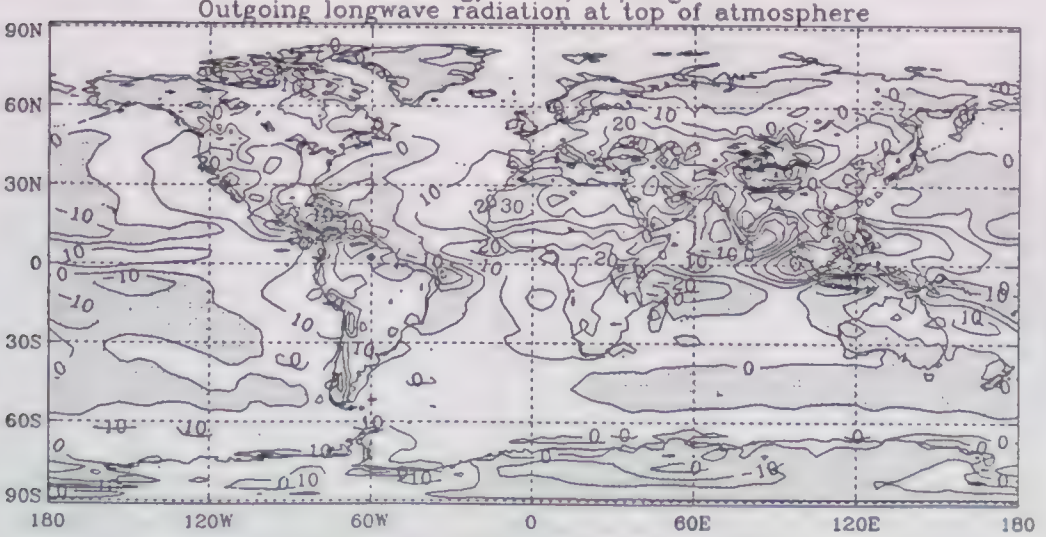

Contours every 10 Wm^{-2}. Shading less than 0

Figure 49(a) AMIP: 3rd Climate Version. 10-year Dec/Jan/Feb
Zonal mean northward flux of momentum by transient eddies
From 1/ 1/1979 to 1/ 1/1989

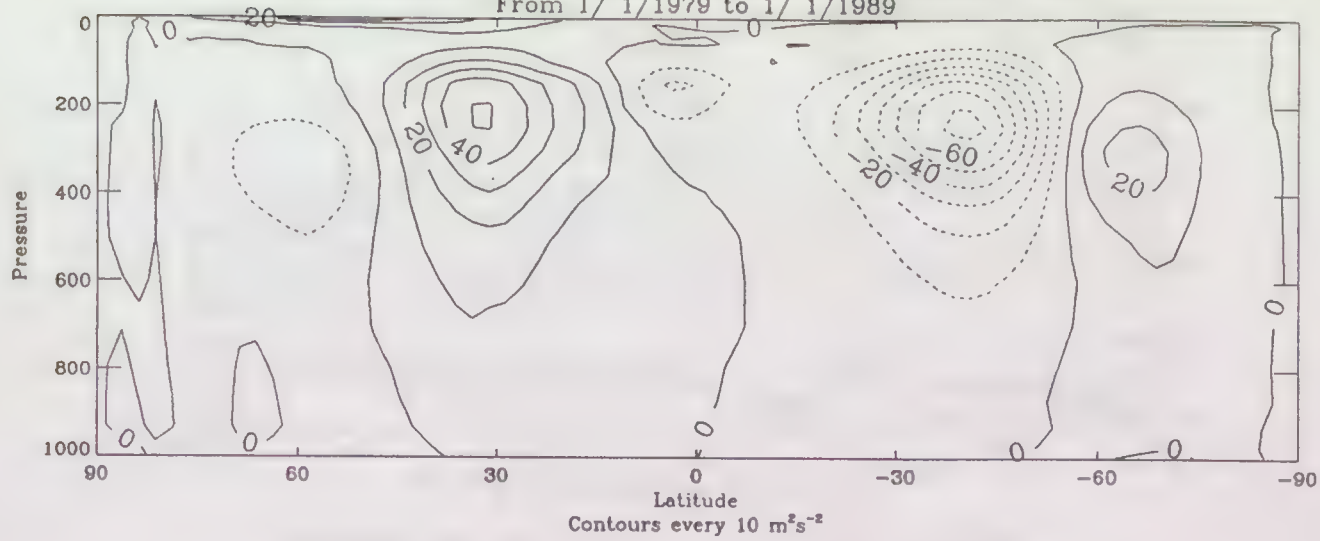

(b) AMIP: 1st Climate Version. 10-year Dec/Jan/Feb
Zonal mean northward flux of momentum by transient eddies
From 1/12/1978 to 1/ 3/1988

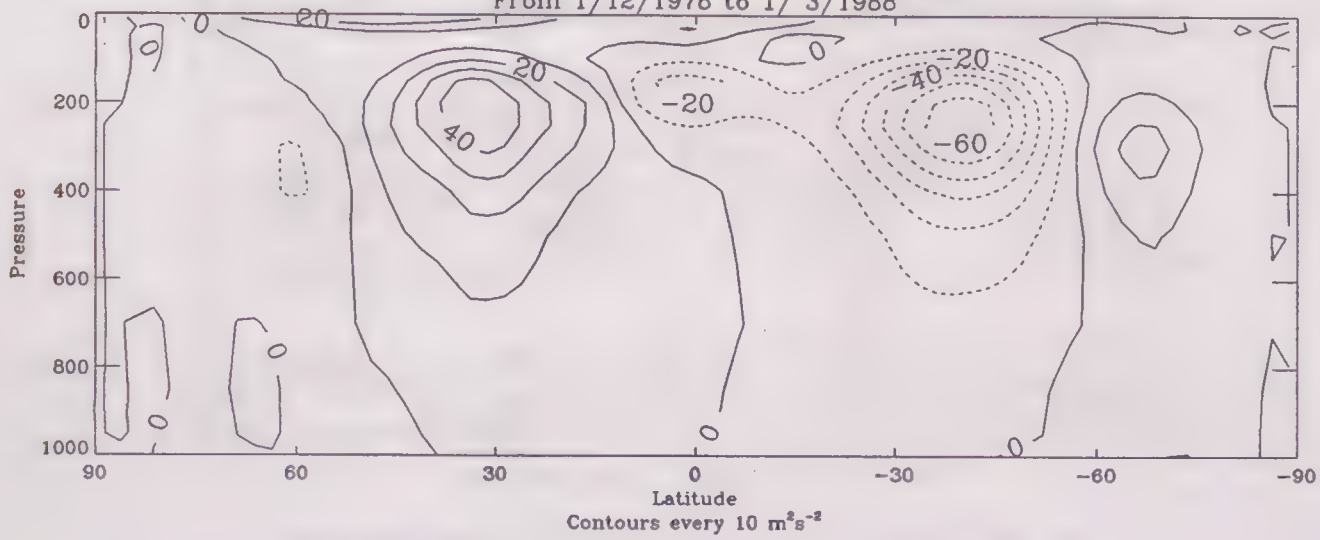

(c) ECMWF climatology. Dec/Jan/Feb 1979-88
Zonal mean northward flux of momentum by transient eddies

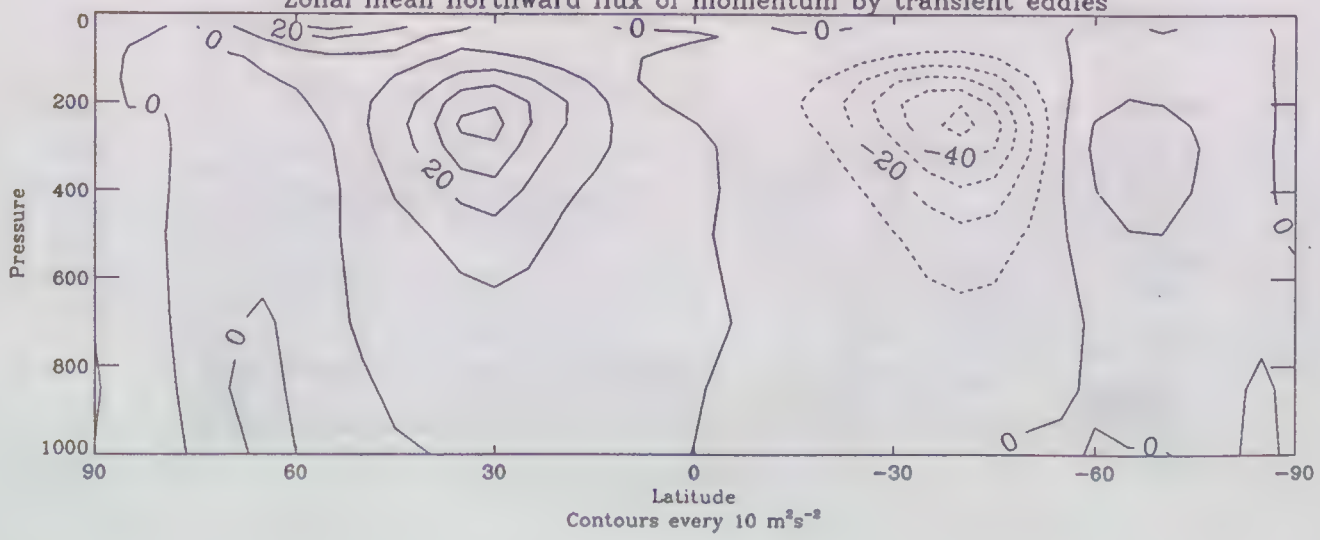

Figure 50(a) AMIP: 3rd Climate Version 10-year Jun/Jul/Aug
Zonal mean northward flux of momentum by transient eddies
From 1/ 6/1979 to 1/ 9/1988

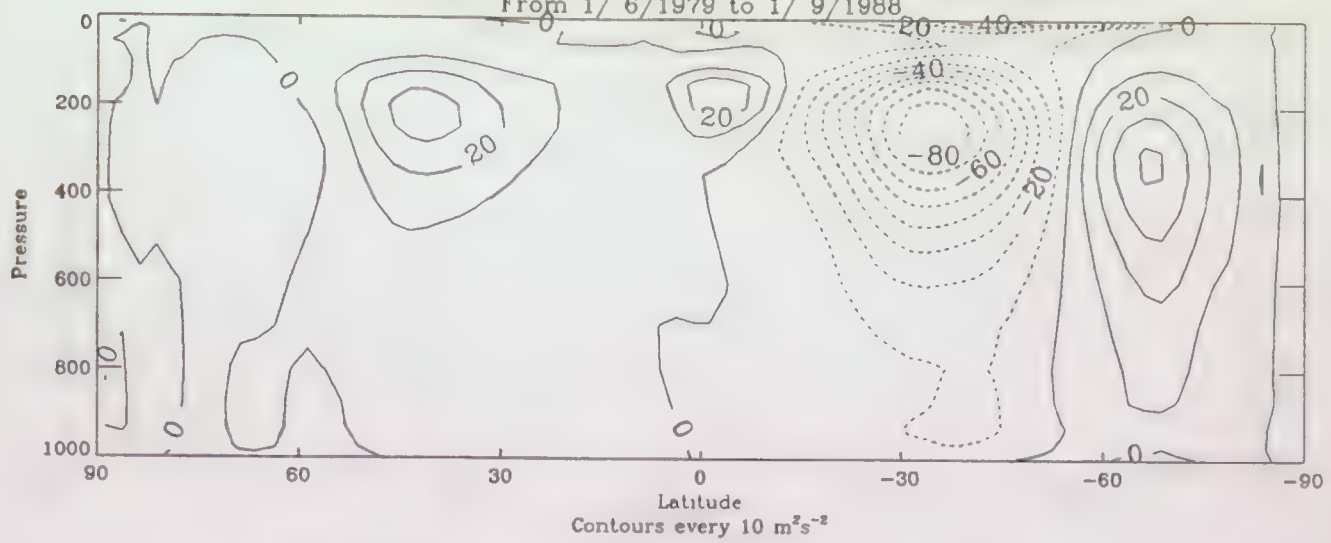

(b) AMIP: 1st Climate Version. 10-year Jun/Jul/Aug
Zonal mean northward flux of momentum by transient eddies
From 1/ 6/1979 to 1/ 9/1988

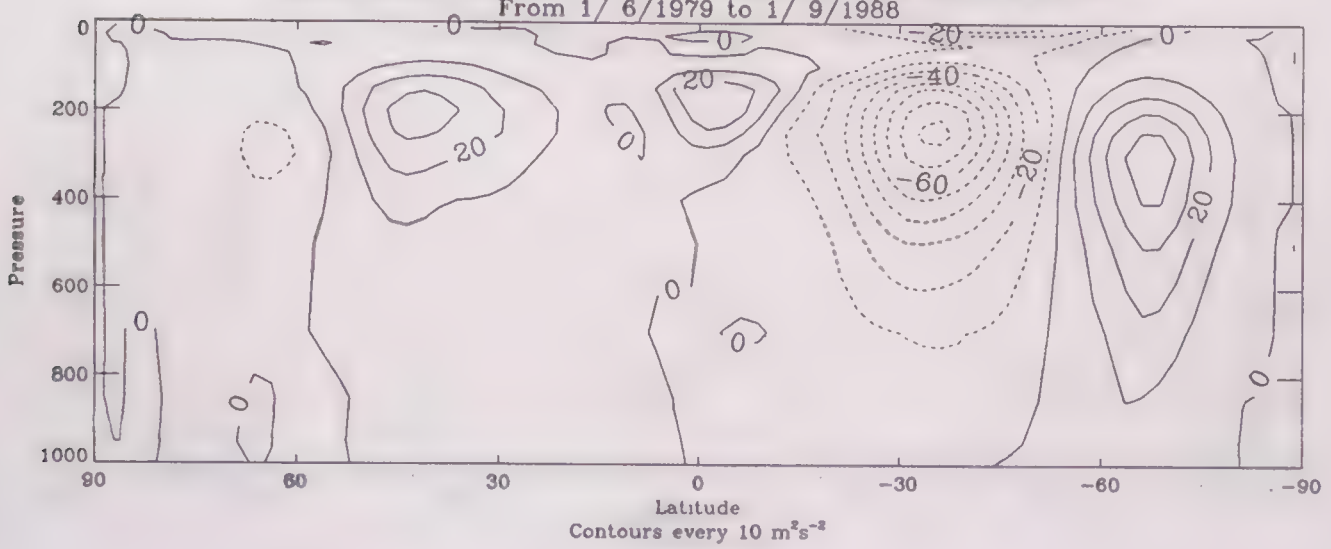

(c) ECMWF climatology. Jun/Jul/Aug 1979-88
Zonal mean northward flux of momentum by transient eddies

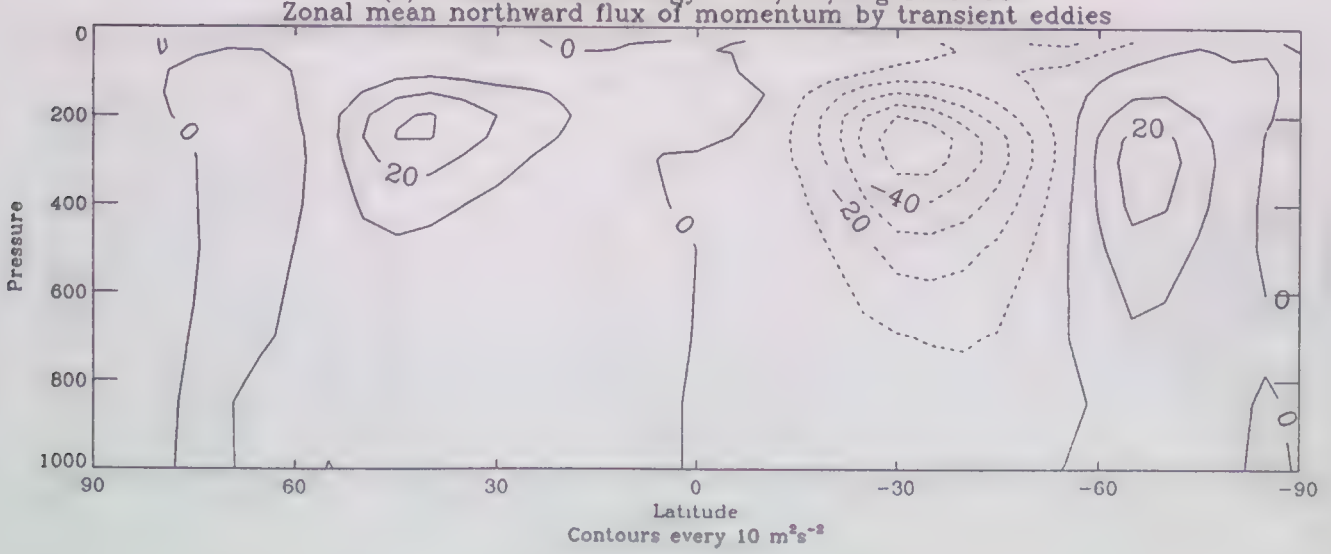

Figure 51(a) AMIP: 3rd Climate Version. 10-year Dec/Jan/Feb
Zonal mean northward flux of momentum by stationary eddies
From 1/ 1/1979 to 1/ 1/1989

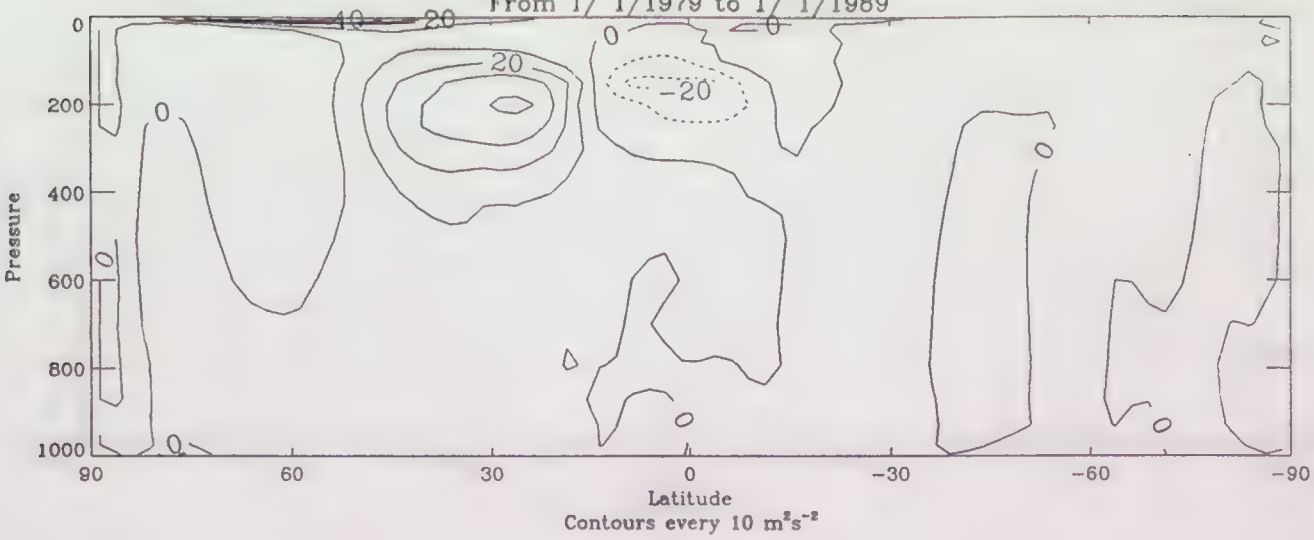

(b) AMIP: 1st Climate Version. 10-year Dec/Jan/Feb
Zonal mean northward flux of momentum by stationary eddies
From 1/12/1978 to 1/ 3/1988

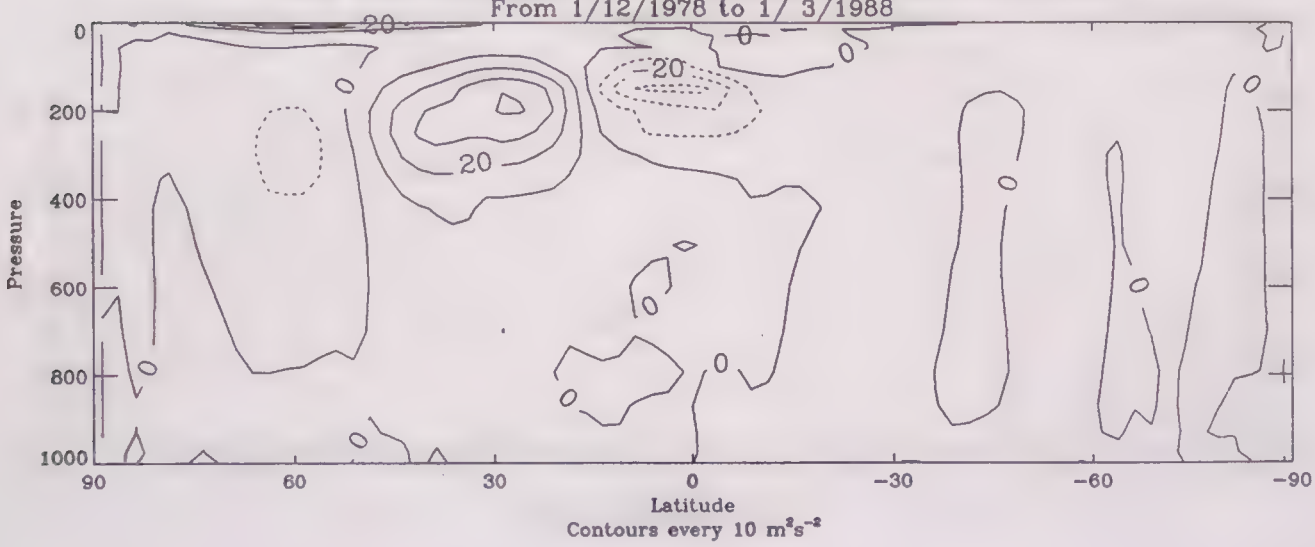

(c) ECMWF climatology. Dec/Jan/Feb 1979-88
Zonal mean northward flux of momentum by stationary eddies

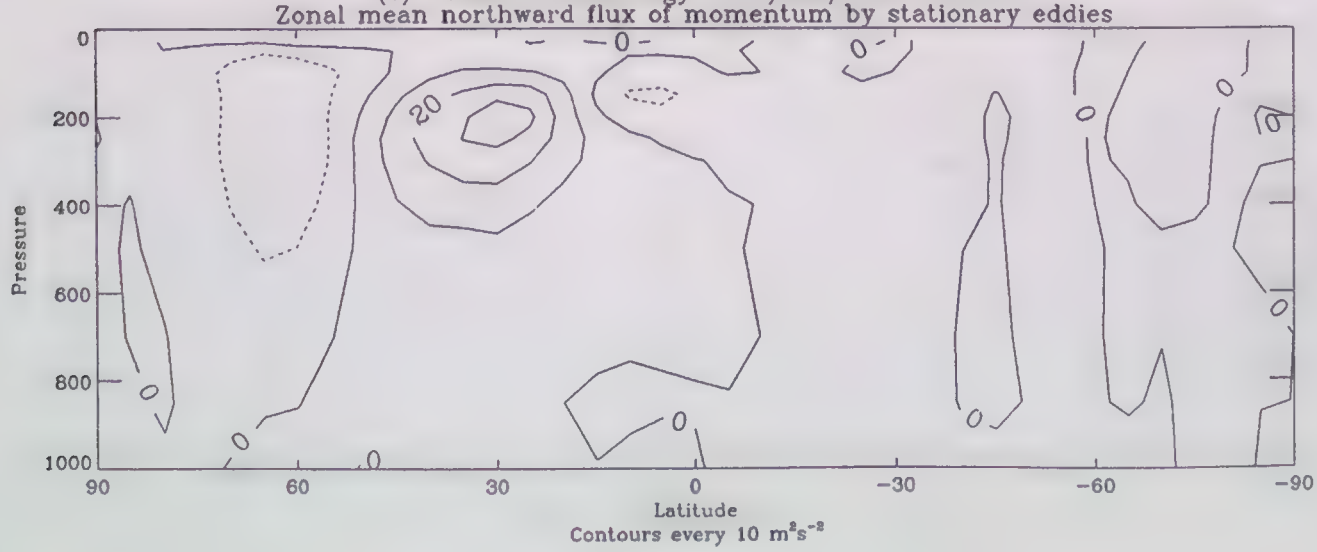

Figure 52(a) AMIP: 3rd Climate Version. 10-year Jun/Jul/Aug
Zonal mean northward flux of momentum by stationary eddies
From 1/ 6/1979 to 1/ 9/1988

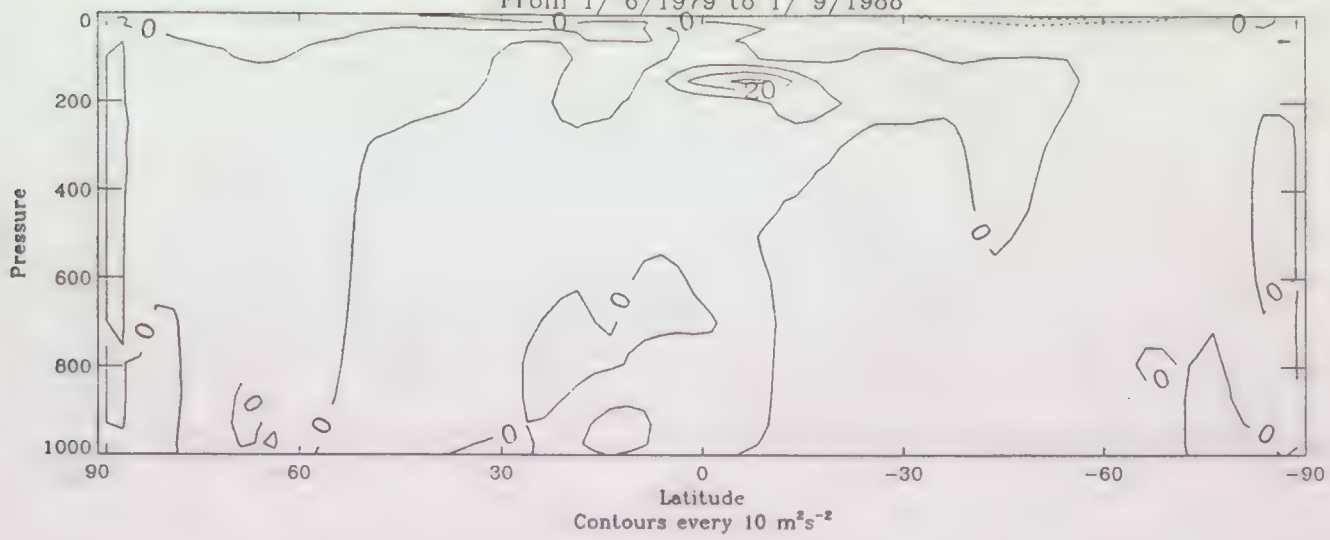

(b) AMIP: 1st Climate Version. 10-year Jun/Jul/Aug
Zonal mean northward flux of momentum by stationary eddies
From 1/ 6/1979 to 1/ 9/1988

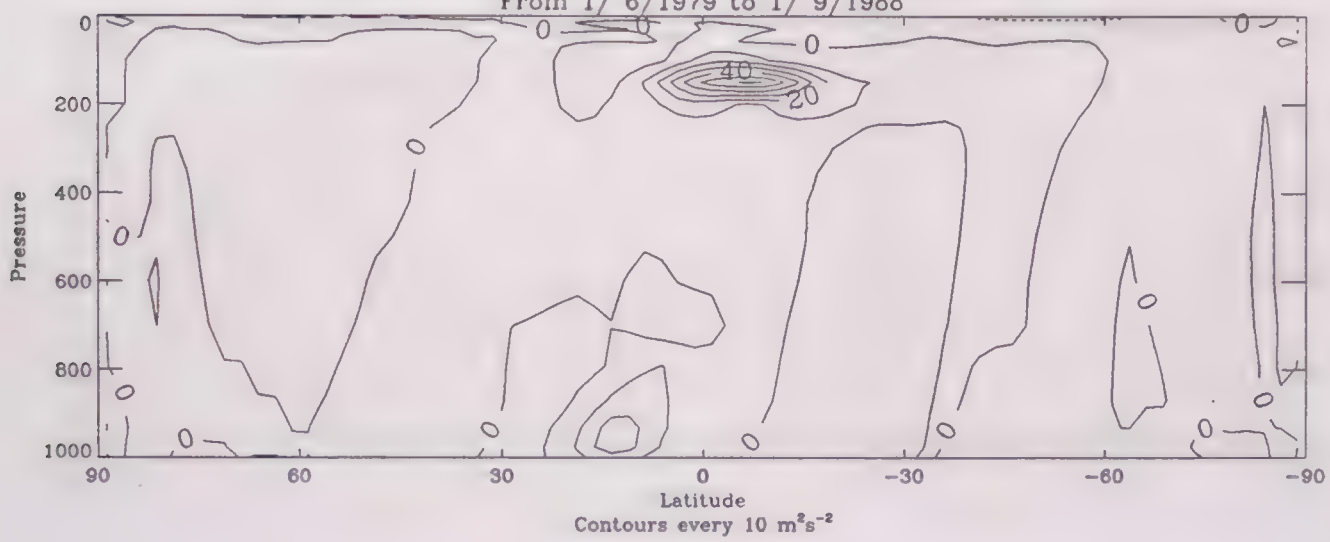

(c) ECMWF climatology. Jun/Jul/Aug 1979-88
Zonal mean northward flux of momentum by stationary eddies

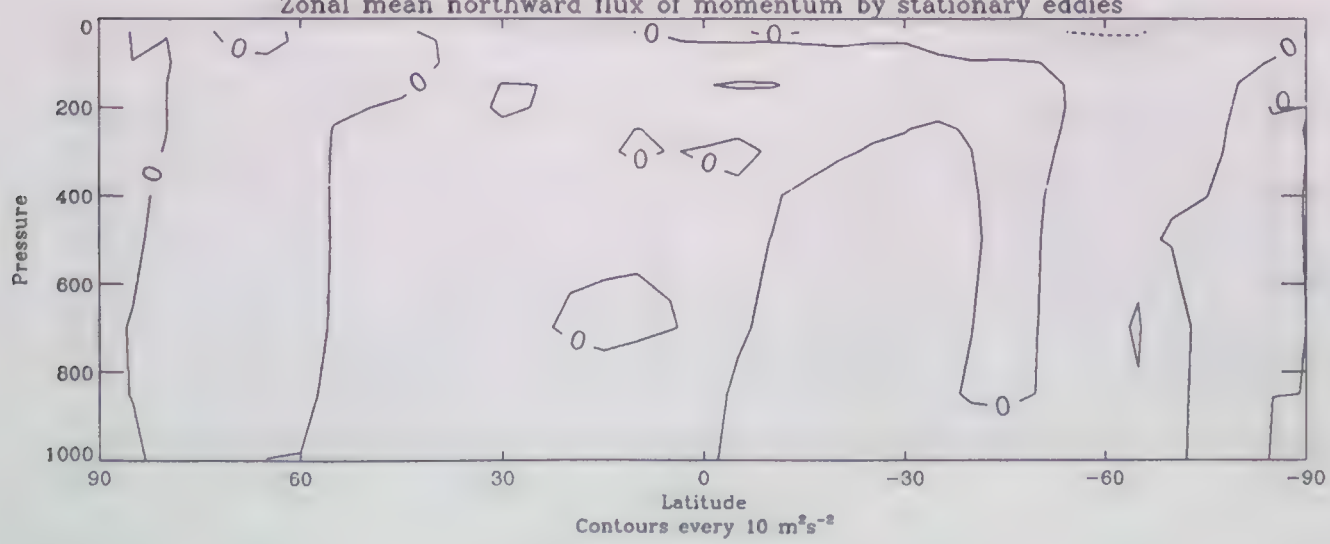

Figure 53(a) AMIP: 3rd Climate Version. 10-year Dec/Jan/Feb
Zonal mean northward flux of sensible heat by transient eddies
From 1/ 1/1979 to 1/ 1/1989

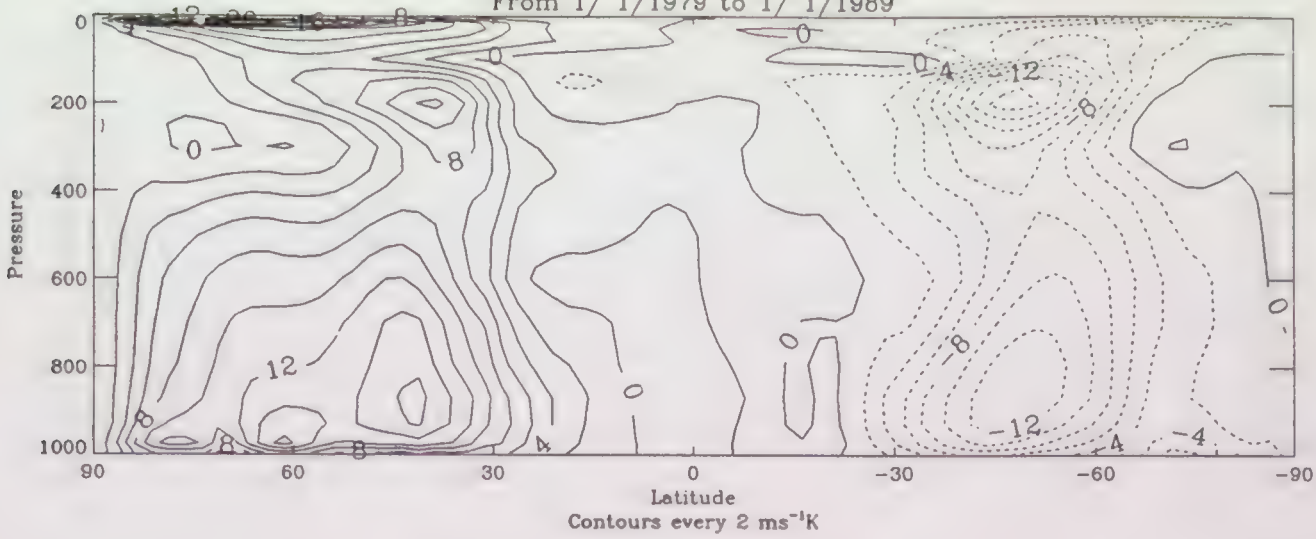

(b) AMIP: 1st Climate Version. 10-year Dec/Jan/Feb
Zonal mean northward flux of sensible heat by transient eddies
From 1/12/1978 to 1/ 3/1988

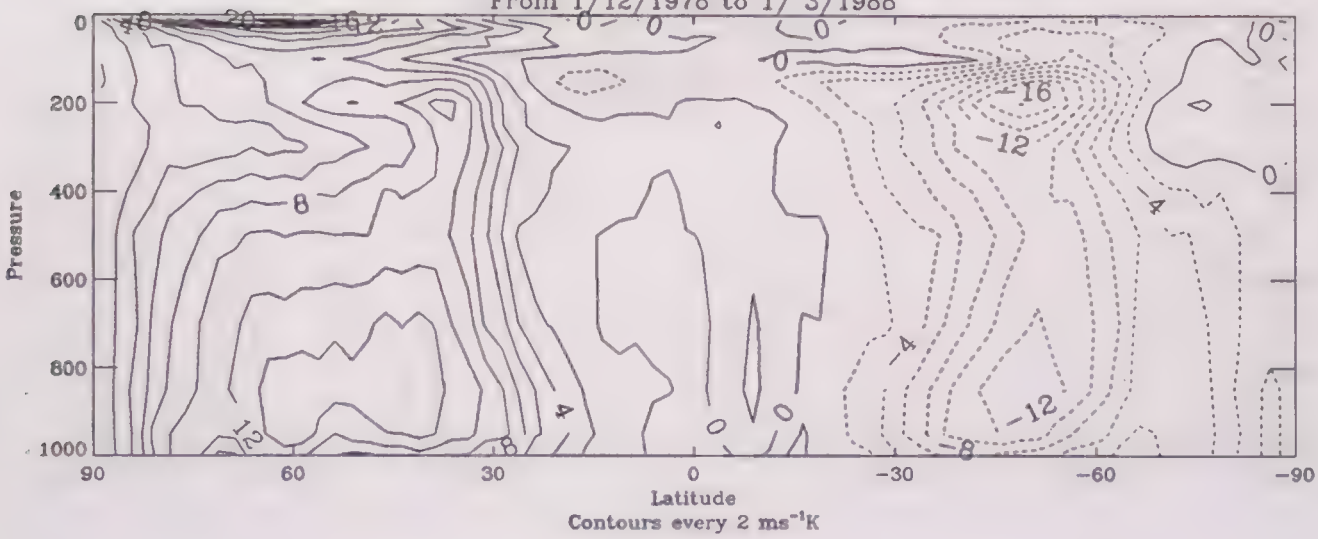

(c) ECMWF climatology. Dec/Jan/Feb 1979-88
Zonal mean northward flux of sensible heat by transient eddies

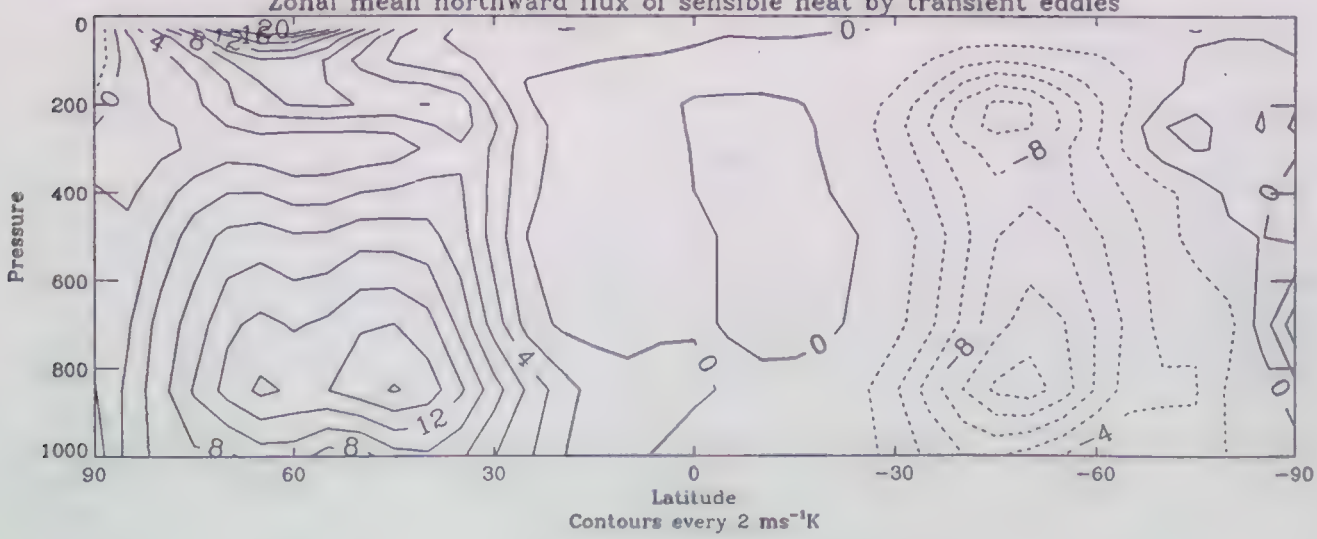

Figure 54(a) AMIP: 3rd Climate Version. 10-year Jun/Jul/Aug
Zonal mean northward flux of sensible heat by transient eddies
From 1/ 6/1979 to 1/ 9/1988

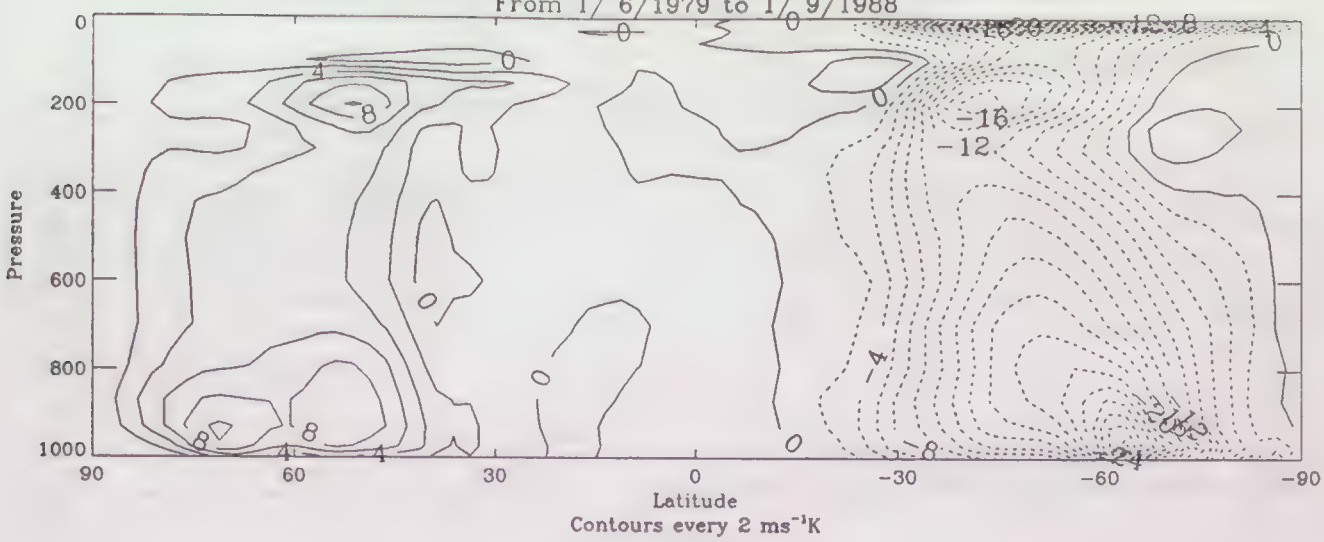

(b) AMIP: 1st Climate Version. 10-year Jun/Jul/Aug
Zonal mean northward flux of sensible heat by transient eddies
From 1/ 6/1979 to 1/ 9/1988

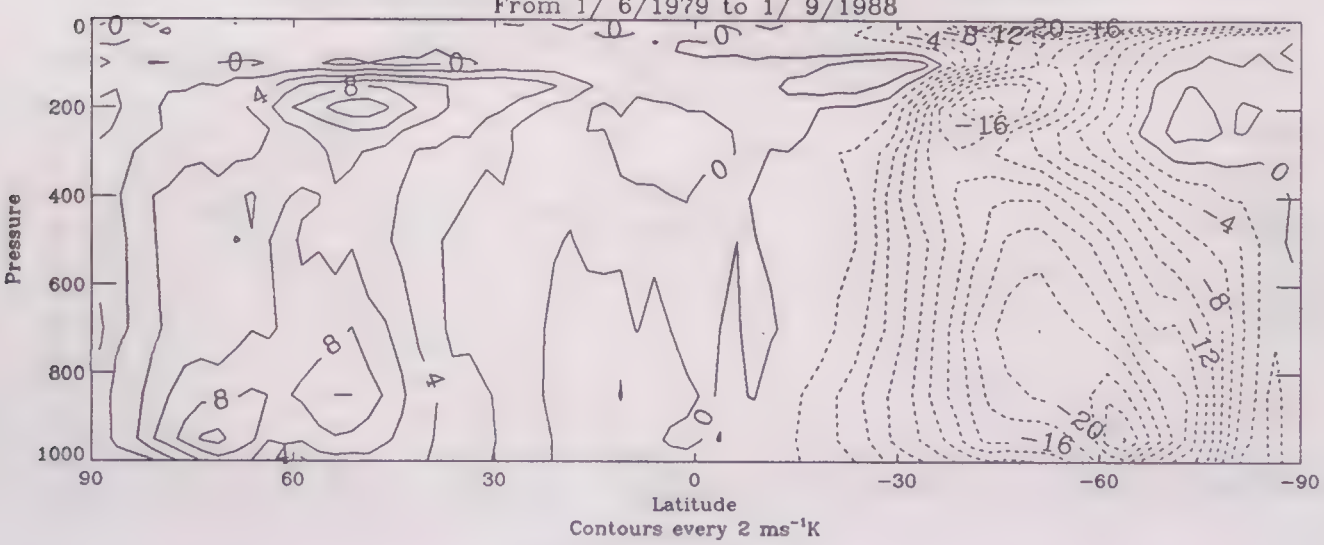

(c) ECMWF climatology: Jun/Jul/Aug 1979-88
Zonal mean northward flux of sensible heat by transient eddies

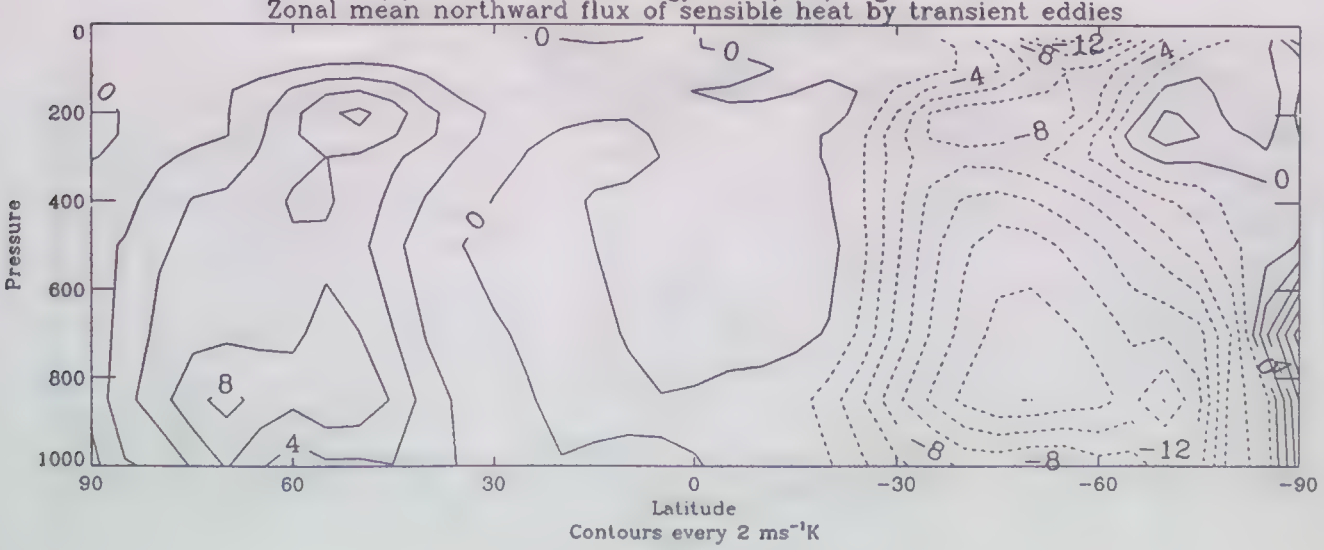

Figure 55(a) AMIP: 3rd Climate Version. 10-year Dec/Jan/Feb
Zonal mean transient eddy kinetic energy
From 1/ 1/1979 to 1/ 1/1989

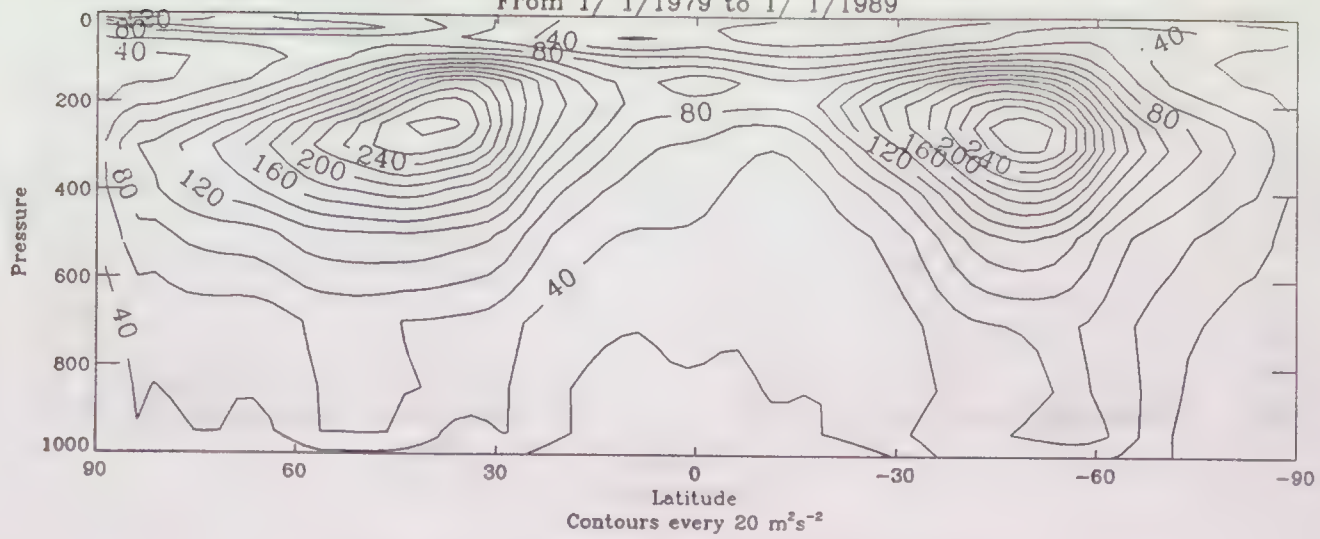

(b) AMIP: 3rd Climate Version. 10-year Dec/Jan/Feb minus
AMIP: 1st Climate Version. 10-year Dec/Jan/Feb
Zonal mean transient eddy kinetic energy

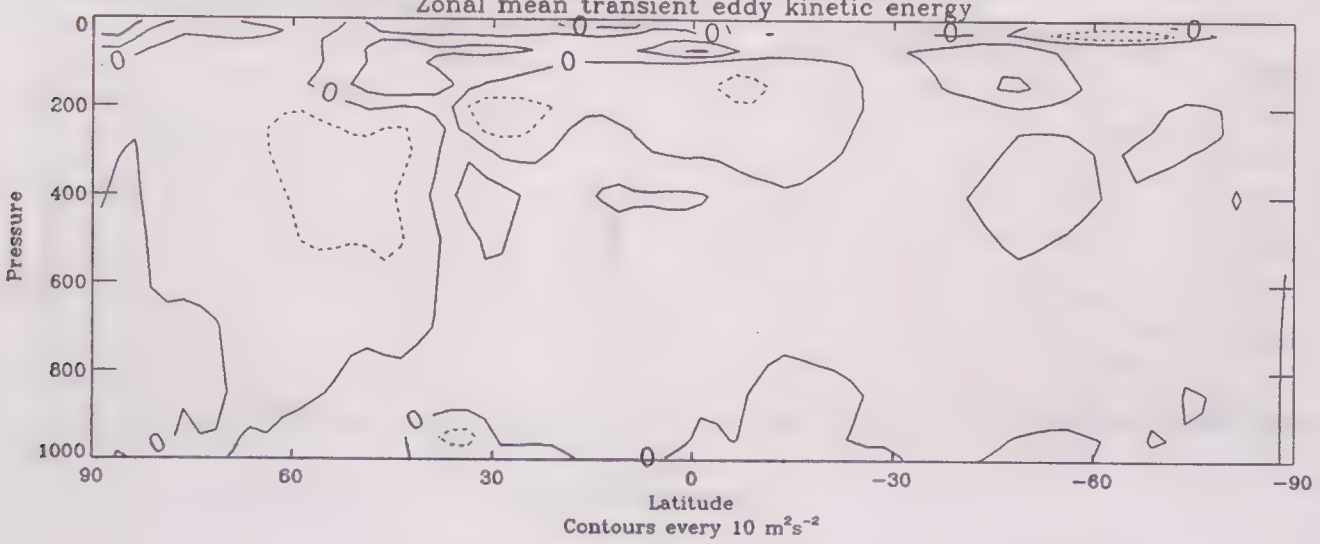

(c) AMIP: 3rd Climate Version. 10-year Dec/Jan/Feb minus
ECMWF climatology. Dec/Jan/Feb 1979-88
Zonal mean transient eddy kinetic energy

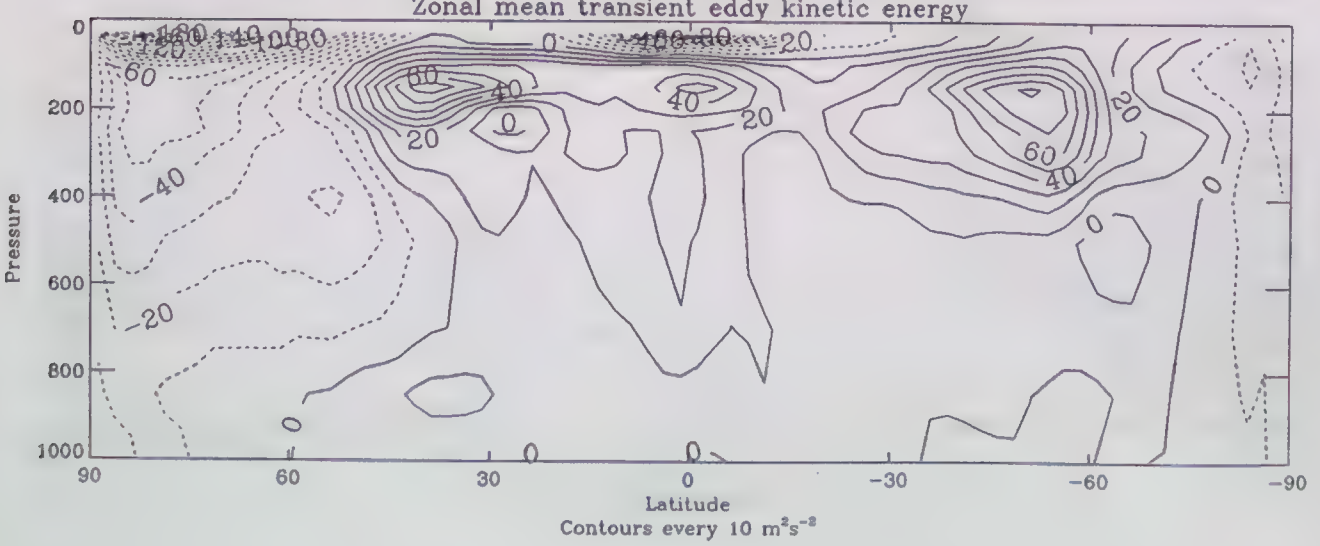

Figure 56(a) AMIP: 3rd Climate Version 10-year Jun/Jul/Aug
Zonal mean transient eddy kinetic energy
From 1/ 6/1979 to 1/ 9/1988

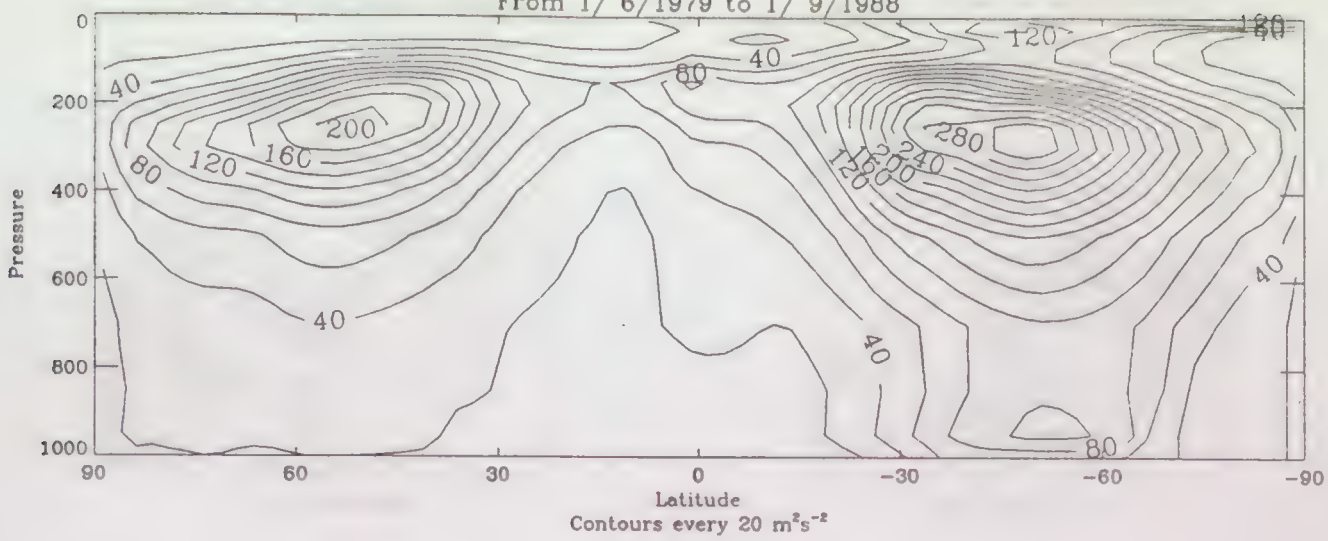

(b) AMIP: 3rd Climate Version. 10-year Jun/Jul/Aug minus
AMIP: 1st Climate Version. 10-year Jun/Jul/Aug
Zonal mean transient eddy kinetic energy

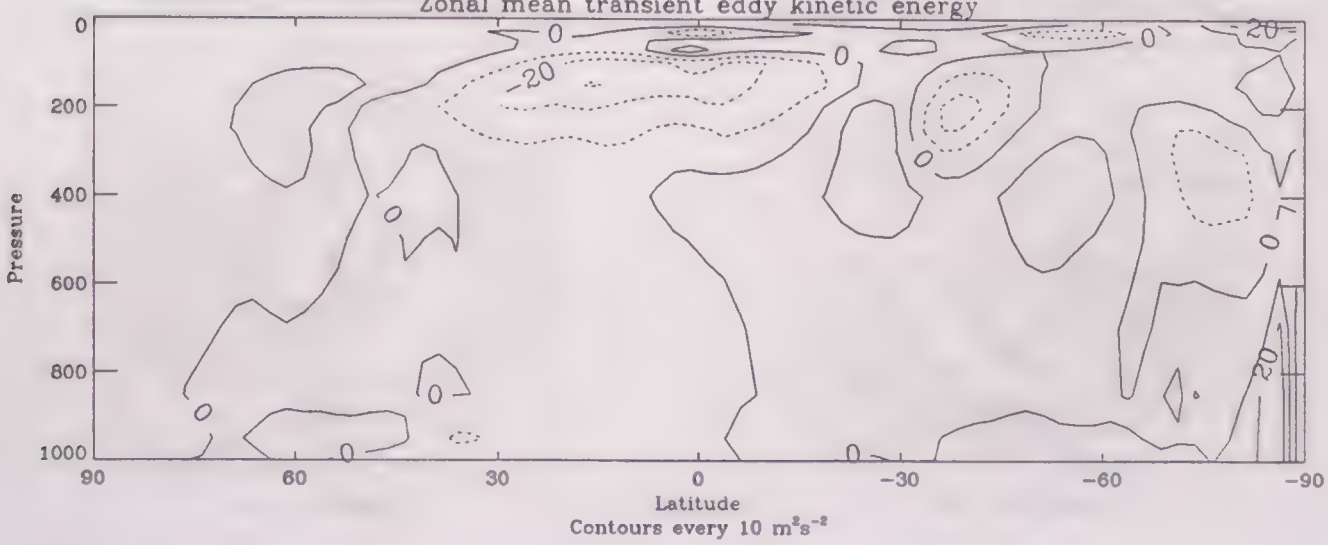

(c) AMIP: 3rd Climate Version. 10-year Jun/Jul/Aug minus
ECMWF climatology. Jun/Jul/Aug 1979-88
Zonal mean transient eddy kinetic energy

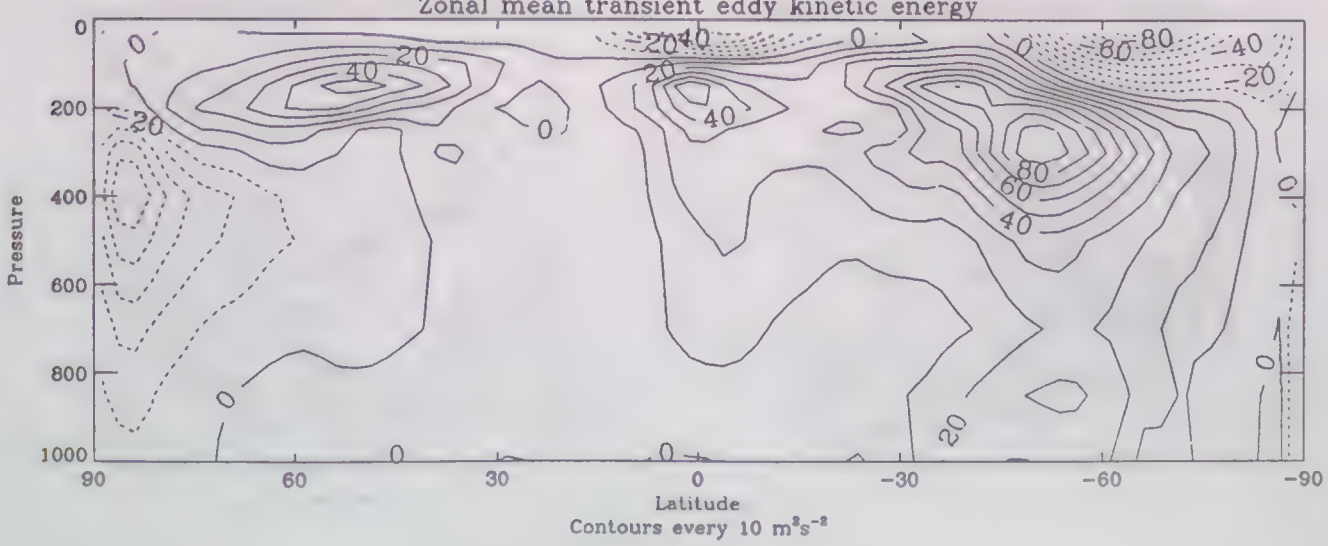

Figure 57

AMIP: 3rd climate version. Dec/Jan/Feb
standard deviation of band pass filtered 500mb heights

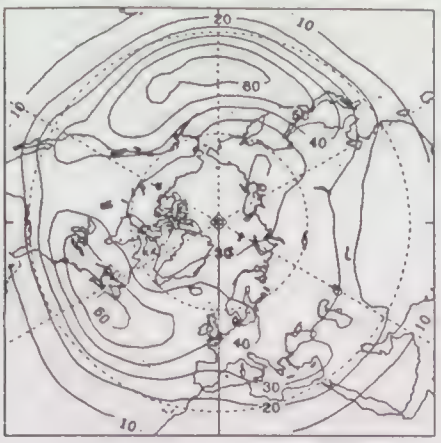

Contours every 10.m

AMIP: 3rd climate version. Dec/Jan/Feb
standard deviation of band pass filtered 500mb heights

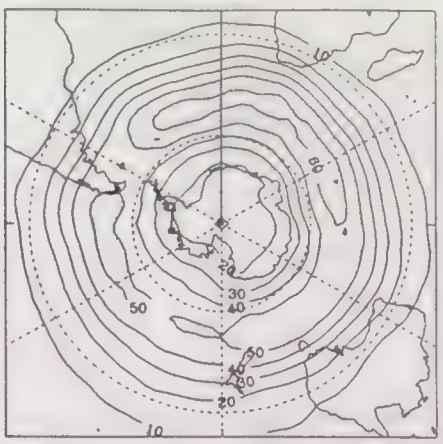

Contours every 10.m

AMIP: 1st climate version. Dec/Jan/Feb
standard deviation of band pass filtered 500mb heights

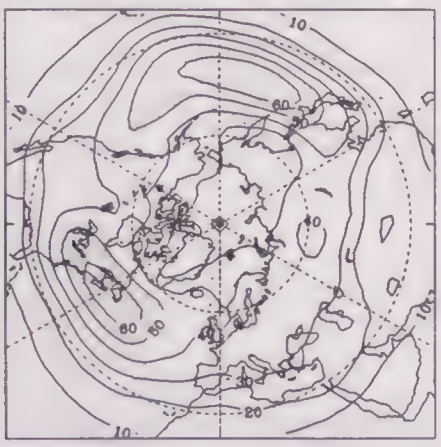

Contours every 10.m

AMIP: 1st climate version. Dec/Jan/Feb
standard deviation of band pass filtered 500mb heights

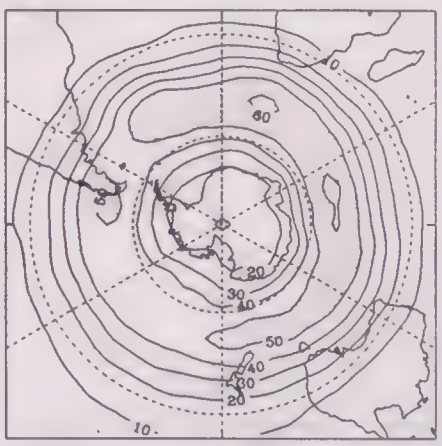

Contours every 10.m

UK climatology 1984–94. Dec/Jan/Feb
standard deviation of band pass filtered 500mb heights

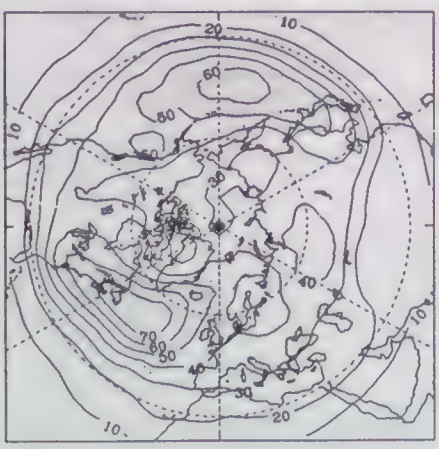

Contours every 10.m

UK climatology 1984–94. Dec/Jan/Feb
standard deviation of band pass filtered 500mb heights

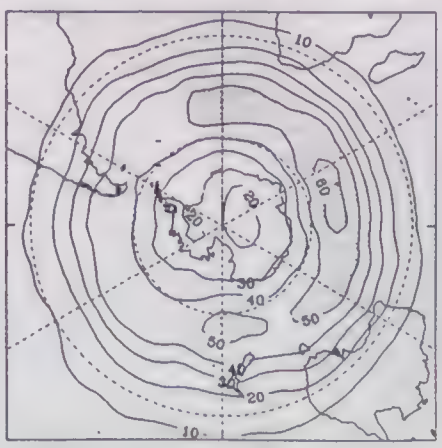

Contours every 10.m

Figure 58

AMIP. 3rd climate version Jun/Jul/Aug
standard deviation of band pass filtered 500mb heights

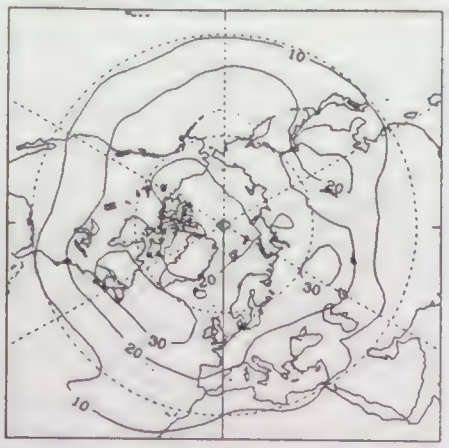

Contours every 10.m

AMIP. 3rd climate version. Jun/Jul/Aug
standard deviation of band pass filtered 500mb heights

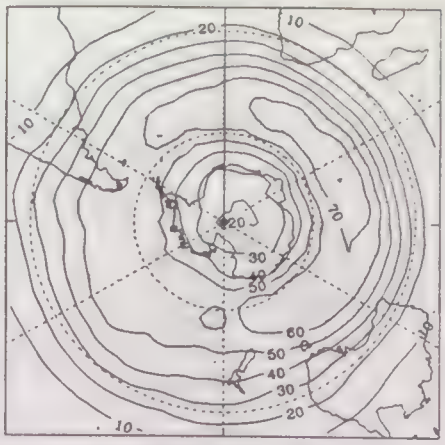

Contours every 10.m

AMIP. 1st climate version. Jun/Jul/Aug
standard deviation of band pass filtered 500mb heights

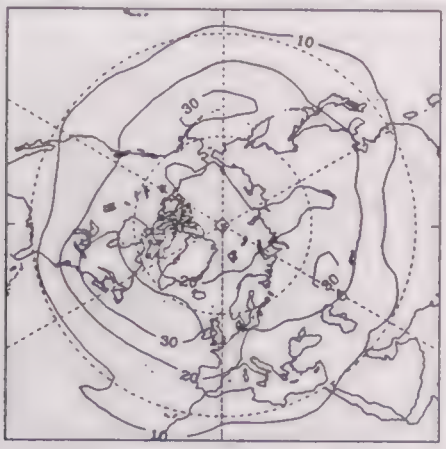

Contours every 10.m

AMIP. 1st climate version. Jun/Jul/Aug
standard deviation of band pass filtered 500mb heights

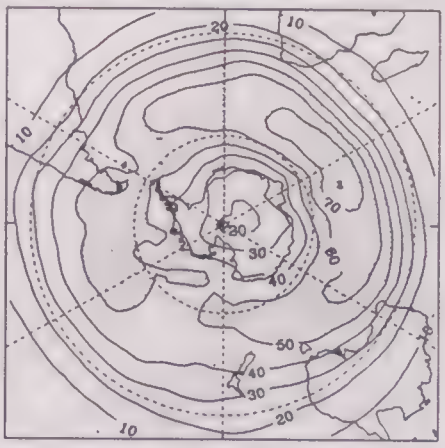

Contours every 10.m

UK climatology 1984-94. Jun/Jul/Aug
standard deviation of band pass filtered 500mb heights

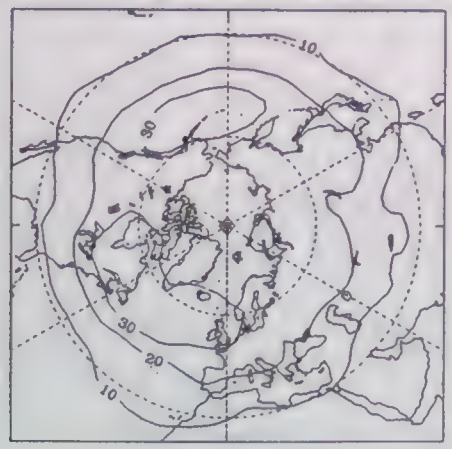

Contours every 10.m

UK climatology 1984-94. Jun/Jul/Aug
standard deviation of band pass filtered 500mb heights

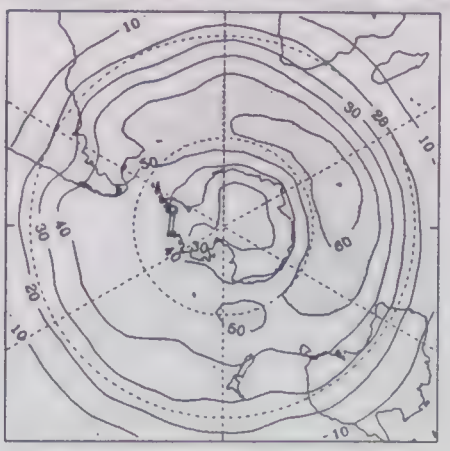

Contours every 10 m

Figure 59

AMIP: 3rd climate version. Dec/Jan/Feb
standard deviation of low pass filtered 500mb heights

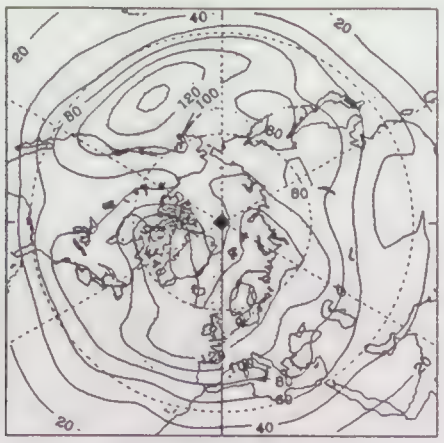

Contours every 20.m

AMIP: 3rd climate version. Dec/Jan/Feb
standard deviation of low pass filtered 500mb heights

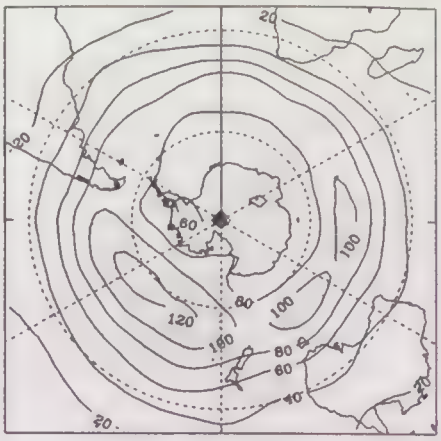

Contours every 20.m

AMIP: 1st climate version. Dec/Jan/Feb
standard deviation of low pass filtered 500mb heights

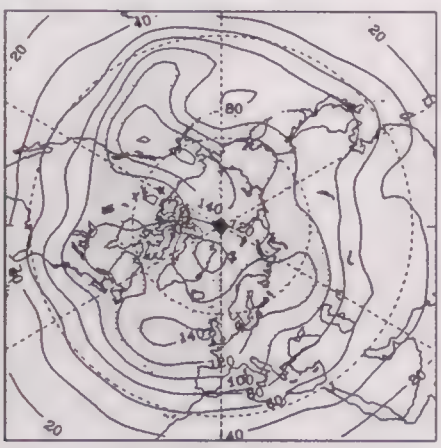

Contours every 20.m

AMIP: 1st climate version. Dec/Jan/Feb
standard deviation of low pass filtered 500mb heights

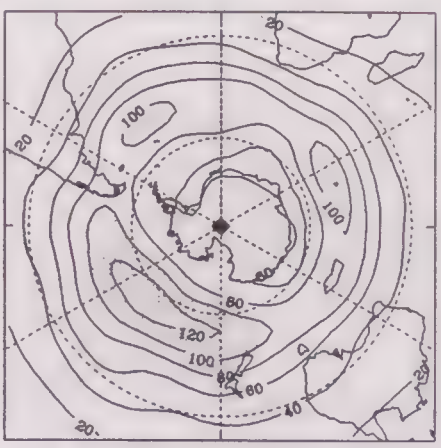

Contours every 20.m

UK climatology 1984–94. Dec/Jan/Feb
standard deviation of low pass filtered 500mb heights

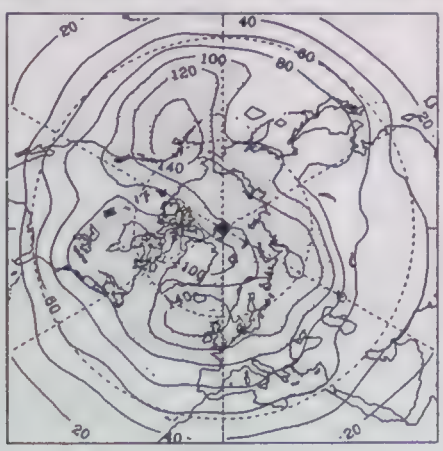

Contours every 20.m

UK climatology 1984–94. Dec/Jan/Feb
standard deviation of low pass filtered 500mb heights

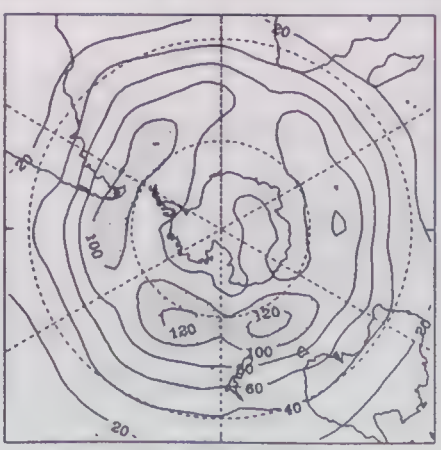

Contours every 20.m

Figure 60

AMIP. 3rd climate version. Jun/Jul/Aug
standard deviation of low pass filtered 500mb heights

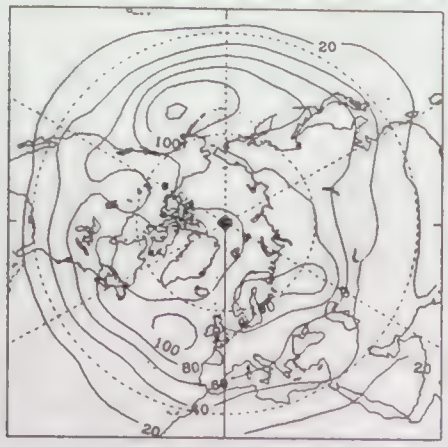

Contours every 20.m

AMIP. 3rd climate version. Jun/Jul/Aug
standard deviation of low pass filtered 500mb heights

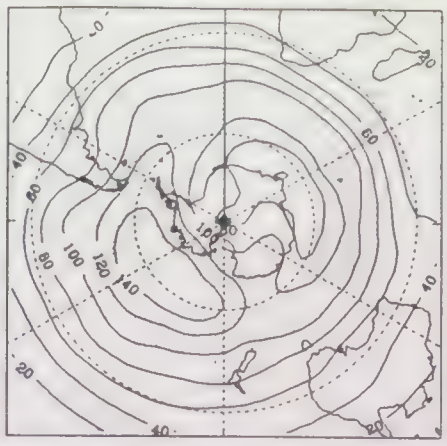

Contours every 20.m

AMIP. 1st climate version. Jun/Jul/Aug
standard deviation of low pass filtered 500mb heights

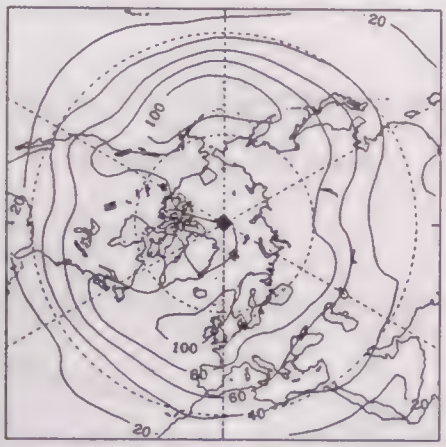

Contours every 20.m

AMIP. 1st climate version. Jun/Jul/Aug
standard deviation of low pass filtered 500mb heights

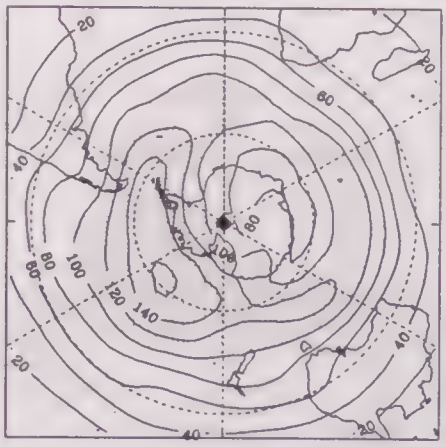

Contours every 20.m

UK climatology 1984-94. Jun/Jul/Aug
standard deviation of low pass filtered 500mb heights

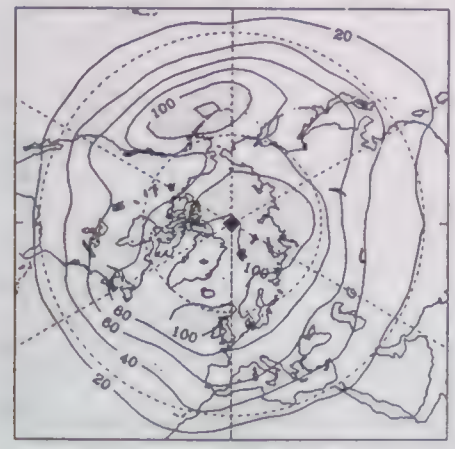

Contours every 20.m

UK climatology 1984-94. Jun/Jul/Aug
standard deviation of low pass filtered 500mb heights

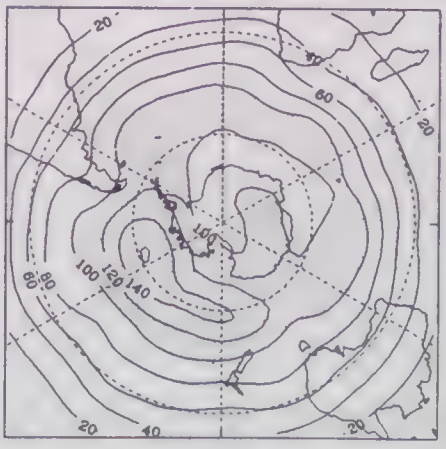

Contours every 20.m

Figure 61

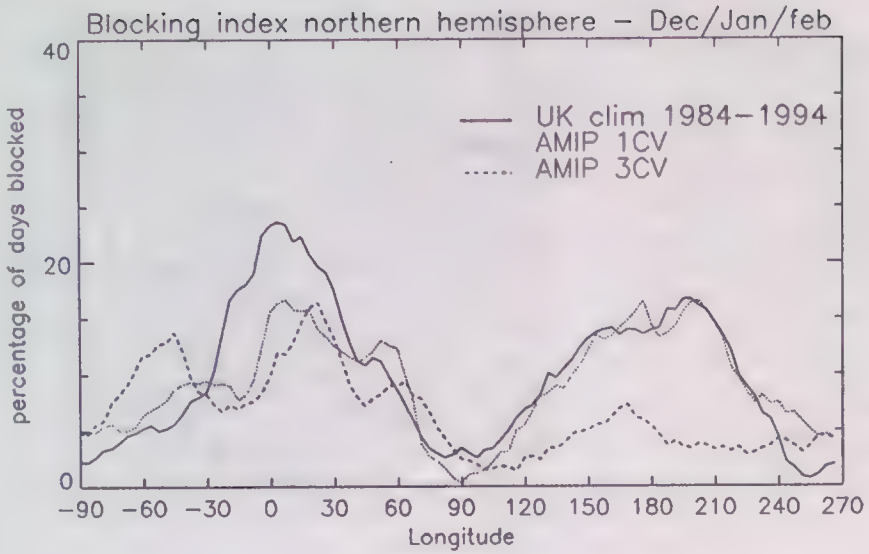
Blocking index northern hemisphere – Dec/Jan/feb
UK clim 1984–1994
AMIP 1CV
AMIP 3CV
percentage of days blocked
Longitude
0
20
40
–90 –60 –30 0 30 60 90 120 150 180 210 240 270

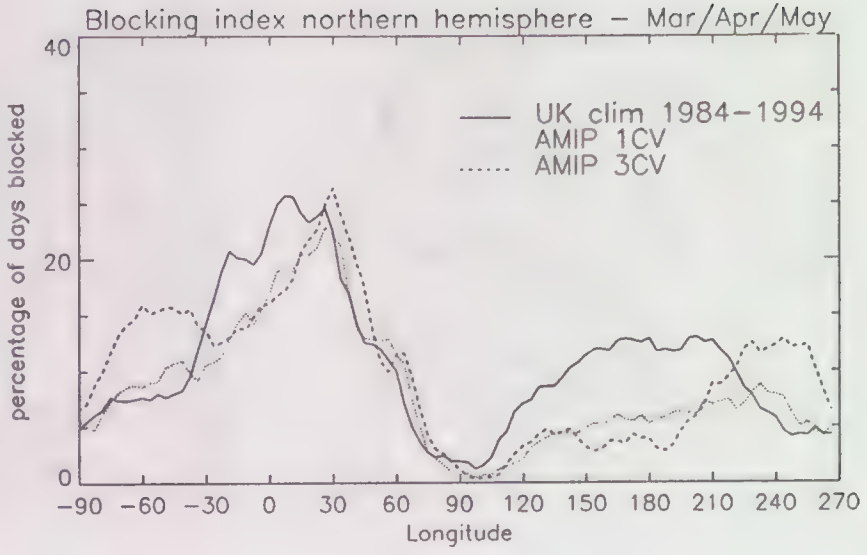
Blocking index northern hemisphere – Mar/Apr/May
UK clim 1984–1994
AMIP 1CV
AMIP 3CV
percentage of days blocked
Longitude
0
20
40
–90 –60 –30 0 30 60 90 120 150 180 210 240 270

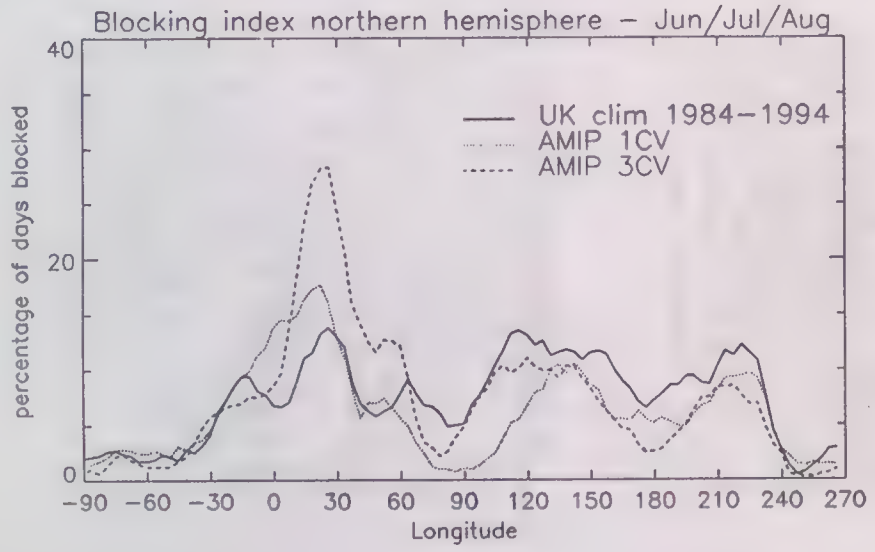
Blocking index northern hemisphere – Jun/Jul/Aug
UK clim 1984–1994
AMIP 1CV
AMIP 3CV
percentage of days blocked
Longitude
0
20
40
–90 –60 –30 0 30 60 90 120 150 180 210 240 270

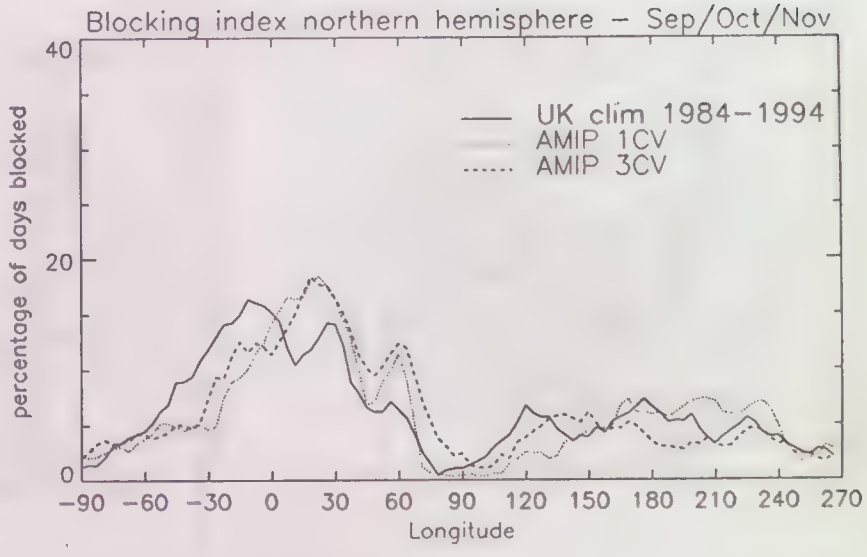
Blocking index northern hemisphere – Sep/Oct/Nov
UK clim 1984–1994
AMIP 1CV
AMIP 3CV
percentage of days blocked
Longitude
0
20
40
–90 –60 –30 0 30 60 90 120 150 180 210 240 270

Figure 62(a) AMIP: 3rd Climate Version. Dec/Jan/Feb 1979-88
Standard deviation of seasonal mean sea-level pressure
From 1/12/1978 to 1/ 3/1988

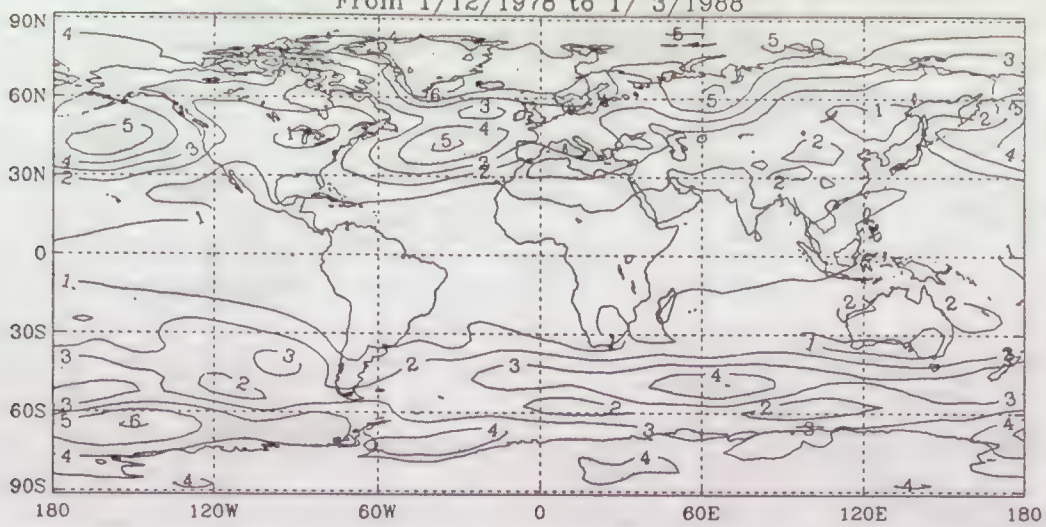

(b) AMIP: 1st Climate Version. Dec/Jan/Feb 1979-88
Standard deviation of seasonal mean sea-level pressure
From 1/12/1978 to 1/ 3/1988

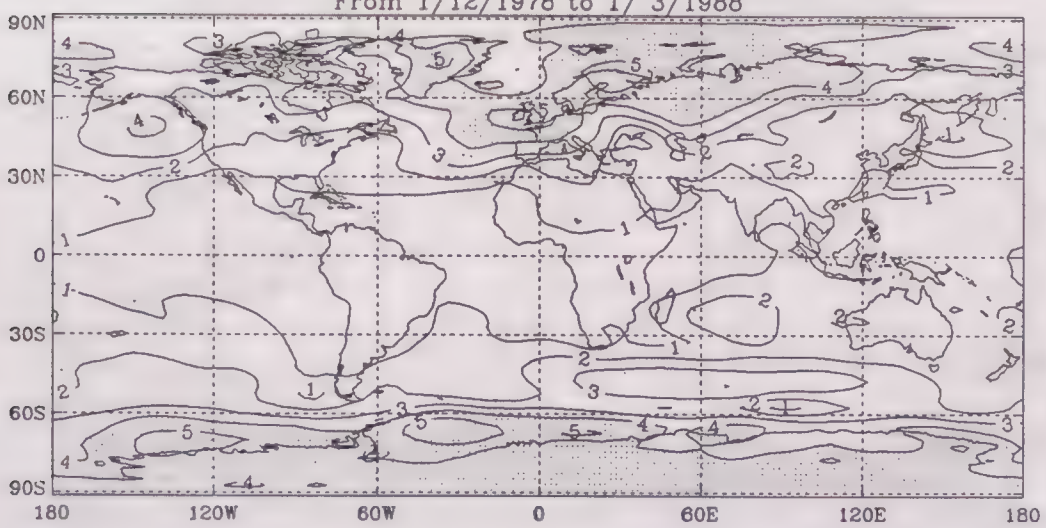

(c) UK Climatology Dec/Jan/Feb
Standard deviation of seasonal mean sea-level pressure
From 1/12/1983 to 28/ 2/1994

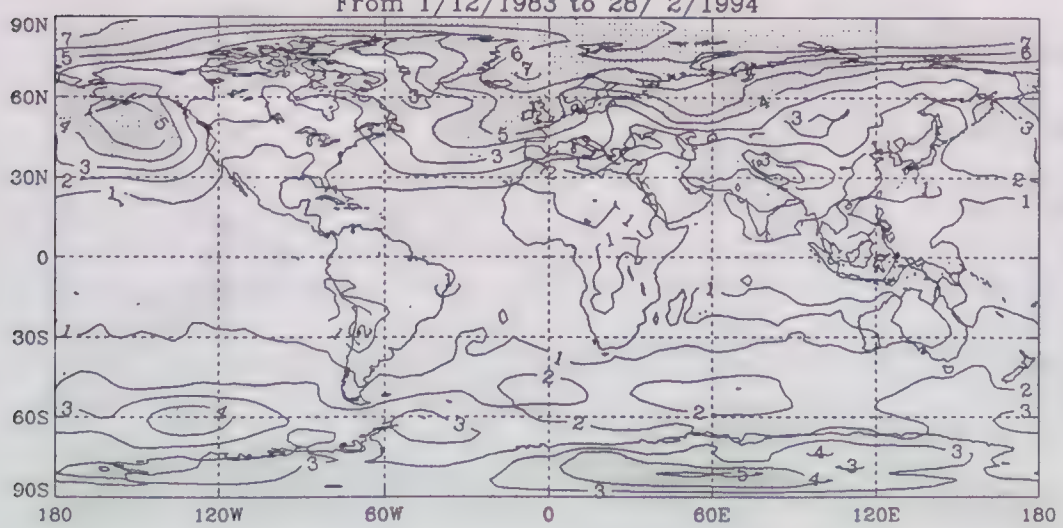

Figure 63(a) AMIP: 3rd Climate Version. Jun/Jul/Aug 1979–88
Standard deviation of seasonal mean sea-level pressure
From 1/ 6/1979 to 1/ 9/1988

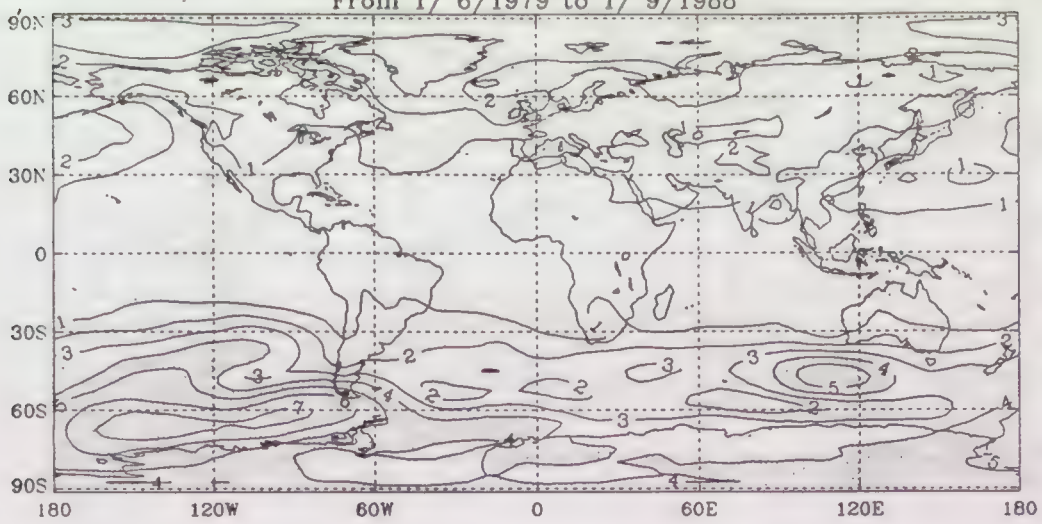

(b) AMIP: 1st Climate Version. Jun/Jul/Aug 1979–88
Standard deviation of seasonal mean sea-level pressure
From 1/ 6/1979 to 1/ 9/1988

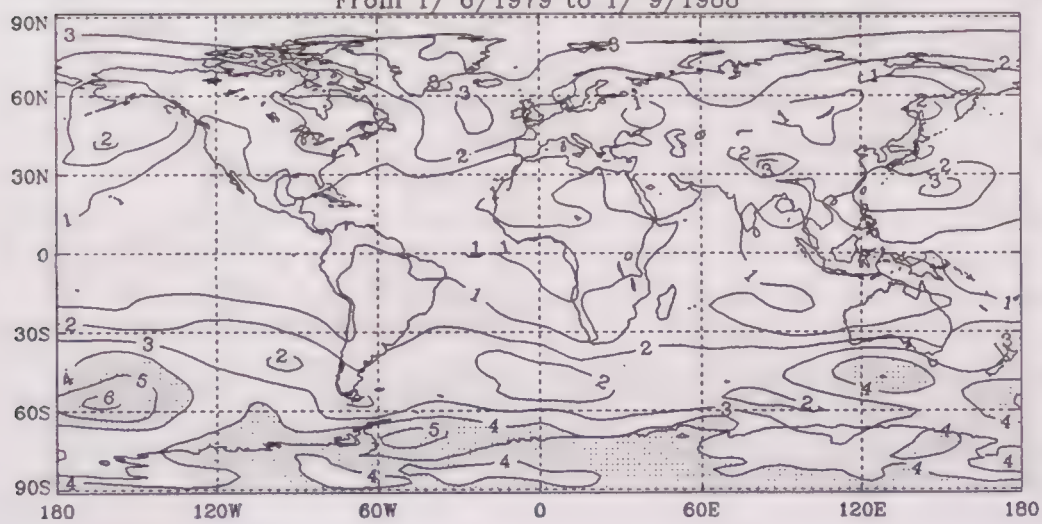

(c) UK Climatology Jun/Jul/Aug
Standard deviation of seasonal mean sea-level pressure
From 1/ 6/1983 to 31/ 8/1993

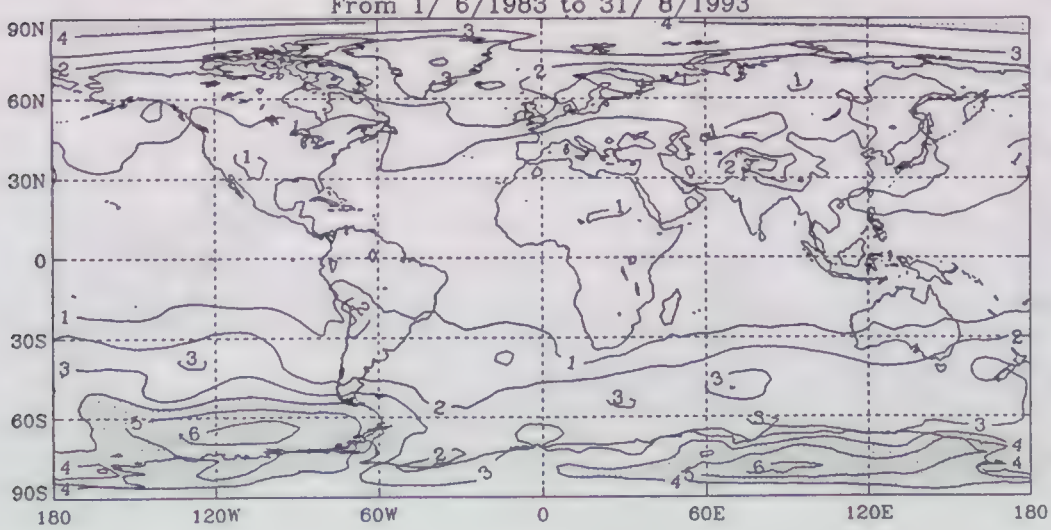

CLIMATE RESEARCH TECHNICAL NOTES

CRTN 1	Oct 1990	Estimates of the sensitivity of climate to vegetation changes using the Penman-Monteith equation. P R Rowntree
CRTN 2	Oct 1990	An ocean general circulation model of the Indian Ocean for hindcasting studies. D J Carrington
CRTN 3	Oct 1990	Simulation of the tropical diurnal cycle in a climate model. D P Rowell
CRTN 4	Oct 1990	Low frequency variability of the oceans. C K Folland, A Colman, D E Parker and A Bevan
CRTN 5	Dec 1990	A comparison of 11-level General Circulation Model Simulations with observations in the East Sahel. K Maskell
CRTN 6	Dec 1990	Climate Change Prediction. J F B Mitchell and Qing-cun Zeng
CRTN 7	Jan 1991	Deforestation of Amazonia - modelling the effects of albedo change. M F Mylne and P R Rowntree
CRTN 8	Jan 1991	The role of observations in climate prediction and research. D J Carson
CRTN 9	Mar 1991	The greenhouse effect and its likely consequences for climate change. D J Carson
CRTN 10	Apr 1991	Use of wind stresses from operational N.W.P. models to force an O.G.C.M. of the Indian Ocean. D J Carrington
CRTN 11	Jun 1991	A new daily Central England Temperature series, 1772-1991. D E Parker, T P Legg and C K Folland
CRTN 12	Jul 1991	Causes and predictability of Sahel rainfall variability. D P Rowell, C K Folland, K Maskell, J A Owen, M N Ward

CLIMATE RESEARCH TECHNICAL NOTES

CRTN 13	Jul 1991	Modelling changes in climate due to enhanced CO2, the role of atmospheric dynamics, cloud and moisture. C A Senior, J F B Mitchell, H Le Treut and Z-X Li
CRTN 14	Sep 1991	Sea temperature bucket models used to correct historical SST data in the Meteorological Office. C K Folland
CRTN 15	Aug 1991	Modelling climate change, and some potential effects on agriculture in the U.K. P R Rowntree, B A Callander and J Cochrane
CRTN 16	Aug 1991	The Boreal Forests and Climate G Thomas and P R Rowntree
CRTN 17	Aug 1991	Development of a Stratosphere-Troposphere Data Assimilation System. R Swinbank.
CRTN 18	Sep 1991	A study of asynchronous coupling using a simple climate model. M K Davey.
CRTN 19	Sep 1991	The Oceanic Carbon Cycle. N K Taylor
CRTN 20	Nov 1991	Worldwide ocean-atmosphere surface fields in Sahel wet and dry years using provisionally corrected surface wind data. M N Ward
CRTN 21	Dec 1991	Coupled tropical ocean global atmosphere models at the UKMO. M K Davey, C Gordon, S Ineson and S Lawrence
CRTN 22	Dec 1991	Empirical parameterisation of tropical ocean-atmosphere coupling. M Allen, M K Davey, D L T Anderson and P D Killworth
CRTN 23	Feb 1992	The temporal evolution of Equatorial Currents in the Indian Ocean D L T Anderson, D J Carrington, R A Corry and C Gordon
CRTN 24	Feb 1992	Stratospheric analyses provided by the U.K. Meteorological Office M J Bailey, A O'Neill and V D Pope

CLIMATE RESEARCH TECHNICAL NOTES

CRTN 25	Feb 1992	Modelling interannual variability in the Indian Ocean using momentum fluxes from the UKMO and ECMWF operational weather analyses. D L T Anderson and D J Carrington
CRTN 26	Mar 1992	A GCM simulation of the impact of Amazonian deforestation on climate using an improved canopy representation J Lean and P R Rowntree
CRTN 27	Mar 1992	The parameterization of rainfall interception in GCMs A J Dolman and D Gregory
CRTN 28	Jun 1992	Development of worldwide marine data eigenvectors since 1985 A W Colman
CRTN 29	Jun 1992	A tropical ocean model with reduced physics M K Davey
CRTN 30	Jun 1992	International Temperature Workshop, Boulder, Colorado, USA, 16 January 1992 Edited by D E Parker
CRTN 31	Jul 1992	Simulation of clear-sky outgoing longwave radiation over the oceans using operational analyses A Slingo and M J Webb
CRTN 32	Sep 1992	A prediction of the transient response of climate J M Murphy
CRTN 33	Nov 1992	LEPS scores for assessing climate model simulations and long-range forecasts. C K Folland
CRTN 34	Jan 1993	Stratospheric Data Assimilation System Guide Editer: R Swinbank
CRTN 35	Mar 1993	A Stratosphere-Troposphere Data Assimilation System R Swinbank and A O'Neill
CRTN 36	Mar 1993	Validation of hydrological schemes for climate models against catchment data. P R Rowntree and J Lean

CLIMATE RESEARCH TECHNICAL NOTES

CRTN 37	Apr 1993	Modelling of palaeoclimates: Examples from the recent past J F B Mitchell
CRTN 38	May 1993	A simulation of seasonality in ENSO forecast skill M K Davey, D L T Anderson and S Lawrence
CRTN 39	Jul 1993	ENSO Prediction experiments using a simple ocean-atmosphere model D-H Wu, D L T Anderson and M K Davey
CRTN 40	Sep 1993	Diagnosis of dynamic sea-surface and sea-level changes from the Cox ocean model J M Gregory
CRTN 41	Sep 1993	Seasonal variations of the clear-sky greenhouse effect: the role of changes in atmospheric temperatures and humidities M J Webb, A Slingo and G L Stephens
CRTN 42	Nov 1993	Sea-level changes under increasing atmospheric CO_2 in a transient coupled ocean-atmosphere GCM experiment. J M Gregory
CRTN 43	Dec 1993	Global and regional patterns of climate change: recent predictions for the Arctic P R Rowntree
CRTN 44	Feb 1994	The effect of changing horizontal diffusion in the atmospheric version of the unified climate model C D Hall and R A Stratton
CRTN 45	Mar 1994	Simulation of El-Niño/Southern Oscillation like variability in a global AOGCM and its response to CO_2 increase. S F B Tett
CRTN 46	Apr 1994	Global data required for monitoring climate change. D E Parker and C K Folland
CRTN 47	May 1994	Seasonal uptake of anthropogenic CO_2 in an ocean general circulation model. N K Taylor

CLIMATE RESEARCH TECHNICAL NOTES

CRTN 48	Jun 1994	A tropic-wide oscillation of boreal summer rainfall and patterns of sea-surface temperature. M N Ward, K Maskell, C K Folland, D P Rowell and R Washington
CRTN 49	Jun 1994	Simulation of the tropical Pacific using a simplified ocean model M A Balmaseda, D L T Anderson and M K Davey
CRTN 50	Sep 1994	Simulation of global mean temperature using a box-diffusion climate model P R Rowntree
CRTN 51	Sep 1994	Seasonal dependence of ENSO prediction skill M A Balmaseda, M K Davey and D L T Anderson
CRTN 52	Nov 1994	Simulation of the Indian Monsoon and Tropical Intraseasonal Variability by a General Circulation Model P M Inness and D Gregory
CRTN 53	Mar 1995	A comparison of modelled surface fluxes with climatological estimates. C Gordon and D K Wright
CRTN 54	Mar 1995	The representation of moist convection in atmospheric models. D Gregory
CRTN 55	Mar 1995	A consistent treatment of the evaporation of rain and snow for use in large-scale models D Gregory
CRTN 56	Apr 1995	Workshop on simulations of the Climate of the Twentieth Century using GISST, 28-30 November 1994, Hadley Centre, Bracknell, UK Edited by C K Folland and D P Rowell
CRTN 57	May 1995	Enhanced shortwave cloud radiative forcing due to anthropogenic aerosols. S E Swartz and A Slingo
CRTN 58	May 1995	The simulation of the tropical oceans in models of different horizontal resolution. C Gordon, D K Wright and C M Roberts
CRTN 59	Sep 1995	The water budget of middle latitude continental regions - a modelling and observational study P R Rowntree
CRTN 60	Sep 1995	Intraseasonal variability of the Indian summer monsoon simulated by the Hadley Centre climate model K Ashok, D Gregory and P M Inness

CLIMATE RESEARCH TECHNICAL NOTES

CRTN 61 Sep 1995 Climate simulations with the Unified Model: AMIP runs

C D Hall, R A Stratton and M L Gallani